



Picking apart a fibronectin receptor network:

How endothelial $\alpha v\beta 3$ -integrin, $\alpha 5\beta 1$ -integrin and neuropilin-1 regulate
angiogenesis.

James A. G. E. Taylor

A thesis submitted for the Doctor of Philosophy (Ph.D.) in Biomolecular Sciences

September 2023

University of East Anglia
School of Biological Sciences

Quadram Institute Bioscience
Gut Microbes and Health

Abstract

Angiogenesis, the growth of new blood vessels from pre-existing vessels, is crucial to both embryonic development and the maintenance of lifelong health, but also supports various pathological conditions. Its progression is complex, requiring the coordination of multiple signalling pathways and key regulators to deliver appropriate vascular expansion in response to pro-angiogenic stimuli. Some of its fundamental mechanisms have been characterised in great depth, revealing that angiogenesis relies heavily on the integrins $\alpha v\beta 3$ and $\alpha 5\beta 1$, as well as their principle extracellular matrix (ECM) ligand, fibronectin. Both integrins transmit signals bidirectionally between extracellular and intracellular compartments, sensing both ECM components and growth factor signals to regulate endothelial migration and proliferation. Therapeutic antagonism of these receptors was therefore assumed to provide anti-angiogenic benefit against pathological conditions where angiogenesis is dysregulated, namely solid tumours, where excessive vascular growth provides both nutrients and metastatic routes. Unfortunately, their mono-therapeutic blockade provided little clinical benefit and could even worsen prognosis by encouraging tumour vascularisation. Later findings attributed tumour angiogenic escape to endothelial VEGFR2 and neuropilin-1 (NRP1), one of a pair of pleiotropic co-receptors. NRP1 has since received great attention for its pairwise interactions with both $\alpha v\beta 3$ -integrin and $\alpha 5\beta 1$ -integrin. We believe these receptors operate within a complex trimeric network to orchestrate angiogenic processes, and that their intricate and off-time contradictory crosstalk is essential to our understanding of angiogenesis and the development of multi-target angiogenic therapies. To unpick this receptor network, we utilised genetically engineered mouse models in which our endothelial targets could be depleted either individually, or in combination, to study how they cooperate and compete to regulate developmental and pathological angiogenesis *in vivo* and *in vitro*. Our results indicate that whilst NRP1 plays a dominant role developmentally, integrin crosstalk regulates aspects of VEGFR2's lifecycle.

Access Condition and Agreement

Each deposit in UEA Digital Repository is protected by copyright and other intellectual property rights, and duplication or sale of all or part of any of the Data Collections is not permitted, except that material may be duplicated by you for your research use or for educational purposes in electronic or print form. You must obtain permission from the copyright holder, usually the author, for any other use. Exceptions only apply where a deposit may be explicitly provided under a stated licence, such as a Creative Commons licence or Open Government licence.

Electronic or print copies may not be offered, whether for sale or otherwise to anyone, unless explicitly stated under a Creative Commons or Open Government license. Unauthorised reproduction, editing or reformatting for resale purposes is explicitly prohibited (except where approved by the copyright holder themselves) and UEA reserves the right to take immediate 'take down' action on behalf of the copyright and/or rights holder if this Access condition of the UEA Digital Repository is breached. Any material in this database has been supplied on the understanding that it is copyright material and that no quotation from the material may be published without proper acknowledgement.

Contents

Abstract	2
Contents	3
List of figures	7
List of tables	9
Acknowledgements	10
1 Introduction	12
1.1 Preface.....	12
1.2 The vascular system.....	13
1.2.1 The cardiovascular system.....	13
1.3 The endothelial extracellular matrix.....	17
1.4 Blood vessel development.....	18
1.4.1 Vasculogenesis.....	18
1.4.2 Angiogenesis.....	18
1.4.3 The angiogenic cascade	19
1.4.3.1 Adopting an angiogenic-competent state	19
1.4.3.2 Tip cell selection & vessel elongation	20
1.4.3.3 Tubulogenesis, anastomosis & maturation	21
1.5 VEGFs and VEGFRs balance new vessel growth with vascular maintenance	23
1.5.1 VEGFs – key angiogenic & homeostatic regulators	23
1.5.2 VEGFR2 controls core angiogenic signalling pathways.....	25
1.5.3 VEGFR2 endosomal trafficking regulates signalling strength and receptor preservation	27
1.6 Neuropilin-1 – an essential VEGFR2 co-receptor.....	32
1.7 Integrins – integral cell-ECM links	35
1.7.1 Integrin adhesion complexes.....	38
1.7.2 Integrins in angiogenesis	41
1.8 Endothelial fibronectin receptors in angiogenesis	42
1.8.1 α v β 3-integrin.....	42
1.8.2 α v β 3-integrin functionality is context dependent.....	42
1.8.3 α 5 β 1-integrin.....	46
1.8.4 Neuropilin-1 – a rediscovered adhesion receptor	47

1.9	Neuropilin-1, $\alpha v\beta 3$ & $\alpha 5\beta 1$ – linking three angiogenic players.....	49
1.9.1	$\alpha v\beta 3$ & $\alpha 5\beta 1$ – interconnected Integrins.....	49
1.9.2	$\alpha v\beta 3$ -integrin & Neuropilin-1	51
1.9.3	$\alpha 5\beta 1$ -integrin & Neuropilin-1.....	52
1.10	Research aims.....	53
2	Methodologies	54
2.1	Chemicals & antibodies	54
2.2	Animals	56
2.3	Breeding	56
2.4	Genotyping	57
2.4.1	DNA preparation.....	57
2.4.2	PCR reactions.....	58
2.4.3	Agarose gel electrophoresis	59
2.5	Tamoxifen preparation.....	60
2.6	Retinal angiogenesis assay	60
2.6.1	Image acquisition & processing	61
2.6.2	Retinal morphometric analysis.....	61
2.6.2.1	Vascular extension.....	61
2.6.2.2	Vascular density & branching	61
2.6.2.3	Vessel regression	62
2.6.2.4	Sprout enumeration	62
2.6.2.5	Filopodial analysis.....	62
2.6.2.6	Corrected total cell fluorescence.....	63
2.7	Mouse lung microvascular endothelial cell isolation.....	63
2.8	Endothelial cell immortalisation.....	64
2.9	TAT-Cre recombinase nucleofection	64
2.10	Routine cell culture & experimental matrix flask coating	65
2.11	Western blotting.....	65
2.12	VEGF signalling assays	66
2.13	Cell surface biotinylation assay	66
2.14	Co-immunoprecipitation assays	67
2.15	Immunocytochemistry.....	68
2.16	MG-132 treatment	68
2.17	Chloroquine treatment.....	68

2.18	ATN-161 treatment.....	69
2.19	Adhesion assay	69
2.20	CMT19T tumour growth assays.....	69
2.21	Tumour section immunofluorescence & imaging.....	70
2.22	Statistical analysis.....	70
3	Developing, maintaining, and validating the tools required to investigate how $\alpha\beta3$-integrin, $\alpha5\beta1$-integrin and neuropilin-1 regulate angiogenesis.	72
3.1	Breeding strategy and best practise for the generation and maintenance of genetically engineered mouse models.....	73
3.2	Validating the Cre- <i>loxP</i> system as a suitable method by which to excise target genes in the postnatal mouse retina.	78
3.3	Generation and validation of immortalised endothelial knockout cell lines derived from genetically engineered mouse models using TAT-Cre-recombinase.	85
3.4	Endothelial responsiveness to VEGF is preserved following PyMT-induced immortalisation.	88
3.5	Discussion	91
4	Interplay between $\alpha\beta3$-integrin, $\alpha5\beta1$-integrin and neuropilin-1 coordinates developmental angiogenesis in the postnatal mouse retina through autonomous and combined vascular-bed specific functions.	93
4.1	Neuropilin-1 is the principle driving force for sprouting angiogenesis in the postnatal mouse retina, but candidate interactions with and between $\beta3$ -integrin and $\alpha5$ -integrin may be essential for the superficial plexus to fully vascularise.....	94
4.2	Neuropilin-1 is critical to the timely vascularisation of the mouse retina.....	102
4.3	Delaying target depletion to circumvent angiogenic compensation revealed the involvement of $\alpha5$ -integrin in deep plexus vascularisation.	111
4.4	Crosstalk between $\beta3$ -integrin, $\alpha5$ -integrin and NRP1 is context-dependent.	120
4.5	Endothelial $\beta3$ -integrin and $\alpha5$ -integrin are required for angiogenic sprout development <i>in vivo</i>	121
4.6	Endothelial $\beta3$ -integrin contributes to retinal vessel stability during vascular remodelling.	124
4.7	Endothelial $\beta3$ -integrin and $\alpha5$ -integrin control filopodial dynamics.	128
4.8	Discussion	136
5	Endothelial $\beta3$-integrin, $\alpha5$-integrin and NRP1 control VEGFR2 dynamics via distinct mechanisms <i>in vitro</i>.	140

5.1	β 3-integrin and NRP1 are essential for VEGFR2 signalling, but co-expression of β 3-integrin and α 5-integrin is required for VEGFR2 preservation.....	141
5.2	β 3-integrin depletion enhanced VEGFR2 trafficking to degrading machinery.	149
5.3	Lysosomal, but not proteasomal inhibition rescued the VEGFR2 downregulation induced by β 3-integrin depletion.	153
5.4	Co-inhibition of α v β 3-integrin and α 5 β 1-integrin reduced VEGFR2 protein levels without effecting its membrane shedding or endothelial adhesion to fibronectin.	158
5.5	Investigating the contribution of β 3-integrin and α 5-integrin to pathological angiogenesis <i>in vivo</i>	162
5.6	Co-targeting β 3-integrin and α 5-integrin prophylactically impaired tumorigenesis.	163
5.7	Discussion	169
6	Final discussion.....	172
	Abbreviations	176
	References.....	182

List of figures

Figure 1.1 The cardiovascular system and blood vessel architecture.	16
Figure 1.2 The angiogenic cascade.	22
Figure 1.3 VEGFR homo-/hetero-dimerization and VEGFR2 co-receptor/auxiliary protein complexes.	28
Figure 1.4 The VEGF-activated VEGFR2 PLC γ /Grb2-ERK pathway and Ca ²⁺ signalling.	29
Figure 1.5 VEGF-activated VEGFR2 SRC signalling.	30
Figure 1.6 VEGFR2 endosomal trafficking.	31
Figure 1.7 Neuropilin protein structure.	34
Figure 1.8 Mammalian α -integrin and β -integrin subunits, their heterodimeric combinations, and their respective ligands.	37
Figure 1.9 The spatial distribution of integrin adhesion complexes.	40
Figure 1.10 α v β 3-VEGFR2 crosstalk.	45
Figure 3.1 The mechanism of PDGFB.iCreER ^{T2} -mediated excision of floxed targets following tamoxifen administration.	75
Figure 3.2 Crossbreeding approach to the generation of each genetically engineered mouse line.	75
Figure 3.3 Confirmatory PCR analysis of each routinely analysed genetic modification.	76
Figure 3.4 Gender ratios of progeny born in each genetically engineered mouse line.	77
Figure 3.5 Characterization of vascular toxicity induced by PDGFB-driven Cre-recombinase in retinal vasculature at P6 and P12.	84
Figure 3.6 Nucleofection with TAT-Cre-recombinase was able to generate endothelial cells lines with long-lasting depletions of each target receptor.	87
Figure 3.7 The VEGF phosphorylation response of key angiogenic signalling pathways is maintained following PyMT-induced immortalisation.	90
Figure 4.1 Neuropilin-1 is the principle driving force for sprouting angiogenesis in the postnatal mouse retina, but candidate interactions with and between β 3-integrin and α 5-integrin may be essential for the superficial plexus to fully vascularise.	101
Figure 4.2 Neuropilin-1 is critical to the timely vascularization of the mouse retina.	110
Figure 4.3 Delaying target depletion to circumvent angiogenic compensation reveals the involvement of α 5-integrin in deep plexus vascularisation.	119
Figure 4.4 Endothelial β 3-integrin and α 5-integrin are required for angiogenic sprout development <i>in vivo</i>	123

Figure 4.5 Endothelial β 3-integrin contributes to retinal vessel stability during vascular remodelling.	127
Figure 4.6 Endothelial β 3-integrin and α 5-integrin control filopodial dynamics.	135
Figure 5.1 β 3-integrin and NRP1 are essential for VEGFR2 signalling, but β 3-integrin and α 5-integrin are collectively required for VEGFR2 preservation.	148
Figure 5.2 β 3-integrin depletion enhanced VEGFR2 trafficking to degrading machinery.	152
Figure 5.3 Lysosomal but not proteasomal inhibition rescued VEGFR2 downregulation induced by β 3-integrin depletion.	157
Figure 5.4 Co-inhibition of α v β 3-integrin and α 5 β 1-integrin reduces VEGFR2 protein levels without effecting its membrane shedding or endothelial adhesion to fibronectin.	161
Figure 5.5 Co-targeting β 3-integrin and α 5-integrin could prophylactically impair tumorigenesis.	168

List of tables

Table 2.1 List of primary antibodies.	54
Table 2.2 List of secondary antibodies	56
Table 2.3 Oligonucleotide primers and PCR reaction conditions used for each gene.....	59

Acknowledgements

There are countless people to whom I owe my thanks for their ideas, inspiration and encouragement not only throughout my PhD, but across all my endeavours over the last eight years that I have spent in Norwich. I can honestly say these years have been the best so far, so thank you to all those who shared them with me.

To my family – you are all crazy, but you're my kind of crazy. Whether it's getting up at 4 am to drive me to the start line of a triathlon, or simply lending an ear, I know you will always have my back in whatever endeavour I choose to pursue. Thank you for all that you do for me. Here's to more adventures.

To Dr Stephen Robinson, thank you for your kindness and belief in me over the last 5 years, I could not have wished for a more caring supervisor and friend. This PhD would certainly have been much more difficult without your care and attention (as well as your frequent provision of Kofra coffee). Dr Alistair McKee, Dr Chris Benwell, Dr Chris Price, and Dr Wesley Fowler (and your lovely little family), I fail to recall a day spent together in which we were not laughing head over heels. I shall miss our coffee breaks, our mischievous deeds in lab, our Thursday clubs, and our conversations interlaced with quotes from *The Lord of the Rings* and *Hot Fuzz* (perhaps, one day, we will catch those swans). Dr Chris Price, I wish you all the very best and look forward to visiting you in California as CEO of Pricey Ltd someday. Dr Chris Benwell (otherwise named CB, Benwell, Bruh, and Mr Legs), thank you for being so generous with your time and expertise. I simply cannot thank you enough for your calm counsel and sharp eyes over the last four years. To Dr Nancy Teng, thank you for making each day such a joy. Your infectious positivity, encouraging words, and freshly baked focaccia were always such a delight. Dr Aleks Gontarczyk, Dr Kate Makin, Dr Jordi Lambert and Dr Sally Dreger, thank you for helping me find my feet in the lab during my Masters and the early years of my PhD. As a Robinson Lab newbie, I welcomed your cheerful and light-hearted approach. To Alicia Nicklin, Luke Mitchell, Nilda Ilker, and Rhianna-lily Smith, cheers for the laughs, you all have a bright future ahead of you and I look forward to hearing about the path you choose to take! Finally, Dr Robert Johnson, thank you for intrusting me with this project. I truly appreciated your patience with me as a Masters student, getting my head round all the α s and β s took some time, but we got there in the end!

Throughout my PhD Professor Sam Fountain never failed to provide an uplifting word whilst applying a methodical and eagle-eyed critique to my work. This encouraged me to think outside the box and appraise my findings. Thank you for your consistent guidance and confidence in my abilities.

To my triathlon family, you're a wonderful bunch, thanks for introducing me to this amazing sport. Here's to more adventures, epic races, and long early morning rides! Jason Battle, thank you for your care and support as a coach. Perhaps entering a half-ironman as my first triathlon was somewhat foolhardy, but it certainly paved the way towards some truly unforgettable experiences. Without your guidance, racing for GB Age-Group Triathlon would have remained a dream.

1 Introduction

1.1 Preface

During organogenesis the cardiovascular system is the first functional organ system to develop (1). Its formation is owed to widespread angiogenic expansion of a rudimentary vascular tree that subsequently undergoes specification, remodelling and pruning to arrive at a functional circulatory system that enables post-natal and adult life. Unfortunately, angiogenesis is commonly dysregulated in pathology, with excessive or limited vascular growth contributing to the progression of numerous conditions such as arthritis, retinopathies, chronic wounds, atherosclerosis, and cancer (2). Here, we aimed to determine how three endothelial receptors were regulating angiogenic processes via complex crosstalk mechanisms. These receptors, namely $\alpha v\beta 3$ -integrin, $\alpha 5\beta 1$ -integrin and NRP1, have been documented to interact in duplicate, but the possibility that they function in triplicate as a receptor network had yet to be considered. The following review of available literature collates current knowledge of these receptors, their paired interactions, and their potential as anti-angiogenic targets.

1.2 The vascular system

Blood vascular systems evolved to accommodate the growing nutritional demand of multicellular organisms. Only through such a system can our volume and surface area lack parity, our metabolic demands be satisfied, and cellular homeostasis be maintained (3).

In humans the vascular system encompasses two discrete networks: namely the lymphatic and cardiovascular systems. Though lymphatic circulation is essential for multicellular life and is intricately linked with the cardiovascular system, this report is solely focused on the latter. Cardiovascular circulation fundamentally refers to the heart, its associated vessels, the blood housed within these vessels, and its cellular residents (erythrocytes, immune cells and platelets) (4). Its development progresses in tandem with embryogenesis such that our growing nutritional requirements can be met. Testifying to just how densely this system pervades our tissues, oxygen diffusion from vasculature is limited to just 100 μm and as such, an overwhelming majority of our constituent cells must lie within this threshold distance to receive satisfactory oxygen delivery. Even the outer walls of large blood vessels possess their own blood supply (the vasa vasorum) to overcome this limitation. It is therefore unsurprising that successful embryogenesis is critically tied to coordinated cardiovascular expansion, and that when vascular development goes awry, so too does our development (5).

1.2.1 The cardiovascular system

Driven by rhythmic cardiac contractions, blood continuously flows through its housing vasculature within a closed loop. This loop, which both begins and ends at the heart, is divided into two circulatory forms: pulmonary and systemic (Fig 1.1).

Following a circuit of the body, deoxygenated blood is shunted to the lungs where it is re-saturated with oxygen. Upon its return to the heart, marking the end of pulmonary circulation, blood is propelled into the systemic system where it flows through progressively smaller vasculature to eventually reach microcirculation. Here, capillaries pervade intricately through tissues and organs to enable systemic exchange of metabolic substrates for by-products (4). Both larger calibre vessels

and their connected downstream vasculature may adapt their tone in response to vasomotor signals, thereby elevating or reducing local blood flow (vasodilation and vasoconstriction) to match tissue perfusion with metabolic demand (6). At the periphery of microcirculation capillaries connect with venules which in turn converge with veins, large diameter vessels carrying deoxygenated blood back to the heart to be recirculated (4).

Analogous to the heterogeneity of different tissues and organs, different branches of the vascular system adopt equally variable morphological and functional traits to account for the needs of their resident niche (7). Still, most blood vessels share three discrete histological layers: the tunica adventitia, tunica media and tunica intima (Fig 1.1). The tunica adventitia is the outermost layer and performs a structurally supportive role by virtue of its elastic and collagenous composition. Similarly, the tunica media also provides mechanical support. Its composition of vascular smooth muscle cells (VSMCs) embedded within an elastin and collagen-rich ECM bestows the characteristic elasticity of arterial vessels, though the exact composition of these two layers will differ depending on the specific vessel in question. Common to all vessels is the tunica intima, a single layer of endothelial cells continuous throughout all vasculature. This cellular membrane, or endothelium, is supported by a basement membrane (BM), a fibro-elastic sub-endothelial layer, and a covering of mesenchymal perivascular cells (4, 8). Capillaries, however, do not conform to this regular structural arrangement. Instead, they possess only an endothelium and an associated BM within which a sparse population of mural cells (VSMCs and pericytes) are embedded. Within these microvessels, oxygen, metabolite, and macromolecule filtration is a continuous, tightly regulated process by virtue of their thin endothelial wall (4, 9).

For a time the endothelium was thought of as an inert monolayer merely providing a ubiquitous semi-permeable membrane for metabolic exchange and a robust, streamlined surface for efficient fluid flow (9). Whilst this is largely true for the higher calibre micro-vessels (venules and arterioles), more recent research has recognised capillary endothelial cells as a remarkably heterogenous population. In addition to the long-established variety of organ specific barrier phenotypes governing the endothelium's macromolecular porosity (continuous, discontinuous, and fenestrated), endothelial cells also possess organotypic expression signatures uniquely adapted to their local niche. For example, high through-put gene expression analysis of tissue-specific endothelial translomes revealed amplified expression of glucose transporter 1 in brain endothelial cells and fatty acid metabolism genes in cardiac endothelial cells. These are likely

mechanisms by which microvasculature can preferentially filter its metabolic cargo to account for organotypic diversity in metabolite penchant (10). Crucially, endothelial heterogeneity is not limited to nutrient exchange mechanisms and barrier phenotypes. Different microvascular endothelial populations reportedly possess a range of metabolic rates and angiogenic aptitudes (11). The latter of these differentials refers to the ability of endothelial cells to undergo structural remodelling in response to appropriate stimulatory cues. This process, termed angiogenesis, is more strictly defined as the growth of new vasculature from parent blood vessels.

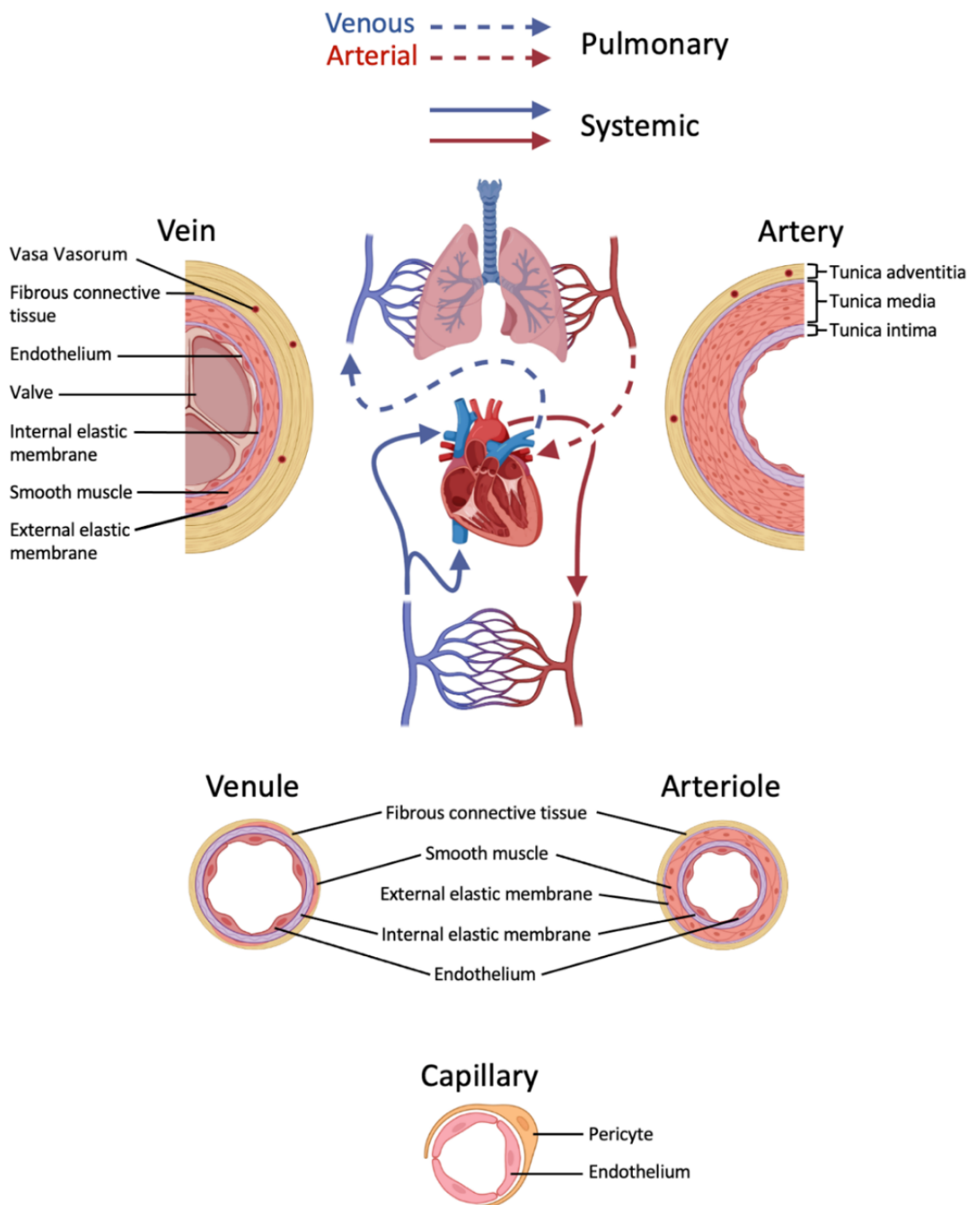


Figure 1.1 The cardiovascular system and blood vessel architecture. Pulmonary circulation is responsible for re-oxygenating blood in the lungs before returning it to the heart. Systemic circulation then perfuses oxygenated blood throughout the body via arterial vessels and capillary microvasculature before returning to the heart once more via the venous system. The three architectural layers of blood vessels: the tunica adventitia, tunica media, and tunica intima, change in composition and thickness throughout the vascular tree, whilst capillaries only possess a thin endothelial wall and a BM to which a population of pericytes adhere to. Figure generated using BioRender.

1.3 The endothelial extracellular matrix

Non-cellular ECM components provide mechanical support for the vascular endothelium and can be grouped into two morphologically distinct matrices: the extracellular BM and the interstitial matrix. The BM underlies the quiescent endothelium and is organised into matrix sheets primarily composed of fibronectin, laminins, collagen IV, entactin and heparan sulfate proteoglycans (HSPGs), whilst the interstitial matrix is comprised of collagens (both fibrillar and non-fibrillar), fibronectin, elastin and glycosaminoglycans containing non-collagenous glycoproteins (12, 13, 14). Upon receipt of pro-angiogenic signals the endothelium becomes activated and its underlying BM undergoes enzymatic degradation. Activated endothelial cells are then able to migrate towards the interstitial matrix. Concurrent increases in vascular permeability allow soluble plasma proteins such as fibronectin and fibrinogen to extravasate from the activated vasculature and form new deposits of provisional, angiogenic-competent ECM scaffolds for the protruding endothelial cell to migrate over. Continued remodelling of the interstitial matrix is mediated by the direct actions of endothelial cells secreting fibronectin and vitronectin as well as that of secreted proteases which help liberate angiogenic factors trapped within the interstitial matrix to enhance the surrounding pro-angiogenic milieu. Upon conclusion of angiogenesis the secretion of protease inhibitors halts further matrix remodelling, encourages deposition of a structurally supportive interstitial matrix as well as the re-acquisition of a BM and vascular quiescence (13).

The fibronectin component of this angiogenic-competent matrix is essential for embryonic vascular development. Evidencing this, its global genetic depletion in mice causes embryonic lethality due to a variety of cardiovascular abnormalities, and its upregulation is mirrored by that of endothelial adhesion receptors during angiogenesis (15, 16, 17). Its precise structure varies according to alternative splicing, but this modular glycoprotein falls within 230-270 kDa, consists of type I, II and III repeating units, and exists as a dimer linked by two disulphide bonds. Fibronectin may be synthesised as a soluble plasma protein or an insoluble cellular protein, the latter of which is secreted locally and assembled into meshworks of interconnected fibrils (14).

1.4 Blood vessel development

We have previously determined the importance of angiogenesis during our development and the preservation of life-long health. The subsequent sections will outline how this process unfolds, from the initial activation of the vascular endothelium through to the eventual re-establishment of quiescence in the newly formed vessel. Development of the vascular system by angiogenesis primarily takes place *in utero* following the events of vasculogenesis (1). Both processes must be stringently controlled, with life-threatening consequences resulting from their improper execution during development or their manipulation under pathological scenarios during post-natal and adult life (18, 19, 20, 21).

1.4.1 Vasculogenesis

The vascular system owes its initial formation to vasculogenesis, a term denoting *de novo* blood vessel development. This process begins as extra-embryonic mesodermal cells termed hemangioblasts aggregate and differentiate into endothelial progenitor cells which in turn give rise to mature endothelial cells (1, 22). These cells subsequently amalgamate and undergo morphogenic changes to generate endothelial tube-like structures which, following arteriovenous specification, constitute the primary vascular plexus of the developing embryo, a vascular blueprint that is later expanded upon by angiogenesis (23).

1.4.2 Angiogenesis

Angiogenesis is a strictly defined process. However, it may proceed via one of two distinct processes: sprouting or intussusceptive angiogenesis. The latter denotes the formation of an intussusceptive pillar that traverses the lumen of mature vessels and results in vessel duplication, doubling the available vascular space (24). Sprouting angiogenesis instead refers to the development, elongation and subsequent stabilisation of an endothelial sprout emanating from a pre-existing vessel. As well as being the focus of this thesis, sprouting angiogenesis is by far the more common and well-investigated mechanism of the two (25).

Following its expansion and remodelling of the vasculogenic primordia initially developed *in utero*, angiogenesis functions more selectively to accommodate scenarios such as tissue growth and wound healing. Continued endothelial receptiveness to angiogenic cues therefore remains essential for organismal health throughout life. Predictably, angiogenic dysregulation is common to numerous pathologies, with excessive angiogenesis contributing to cancer and age-related macular degeneration, and insufficient angiogenesis affiliating with atherosclerosis and chronic wound healing (21, 26). Deciphering the molecular events that coordinate angiogenesis whilst determining how these events differ under pathological scenarios therefore bears significant therapeutic relevance. However, making any meaningful leaps in our understanding of this process first necessitates a firm grasp of the wealth of literature outlining the cascade of sequential events driving this process.

1.4.3 The angiogenic cascade

1.4.3.1 Adopting an angiogenic-competent state

In contrast to angiogenic vasculature, unstimulated vascular endothelial cells exhibit a sedentary, phalanx phenotype typified by a reduced migratory and proliferative response to growth factors and tight intercellular junctions maintained by the barrier proteins occludins, claudins, VE-cadherin and N-cadherin, the last of which mediates intercellular contact between endothelial cells and pericytes (27). Intimately connected mural cells provide autocrine maintenance cues such as vascular endothelial growth factors (VEGFs), angiopoietin-1 (ANG1) and low levels of fibroblast growth factors (FGFs) to the dormant endothelium to induce continued pericyte attachment, endothelial survival, and intercellular junction strength. This quiescent phenotype must first be abolished before angiogenesis can proceed (28).

Hypoxia, relative oxygen deficiency, drives the expression of pro-angiogenic transcription factors such as the hypoxia inducible factor (HIF) family. These heterodimeric molecules possess an α - and complementary β -subunit, the former of which is continually ubiquitinated and proteolytically degraded under normoxic conditions (29). During hypoxia oxygen deficiency allows HIF- α to escape degradation and heterodimerise with HIF-1 β to establish a functional transcription factor complex (30). Its target genes encode various pro-angiogenic cytokines including VEGF, FGF and angiopoietin-2 (ANG2), the secretion of which establishes an angiogenic gradient that stimulates

nearby vessels to revert from their quiescent phenotype and adopt an angiogenic-competent state (29, 30). More specifically, these factors stimulate coordinated disassembly of the vessel wall through inducement of mural cell detachment, inter-endothelial cell junction loosening, increased nitric-oxide (NO) dependent vascular permeability, and secretion of A disintegrin and metalloproteinases (ADAMs) and matrix metalloproteinases (MMPs) to degrade the BM and begin remodelling the surrounding ECM. This newly restructured, fibronectin-rich environment provides a physical growth substrate for the now activated endothelial cells to migrate over, a process primarily mediated by cell-adhesion receptors termed integrins (13). In particular, $\alpha v\beta 3$ -integrin and $\alpha 5\beta 1$ -integrin are dramatically upregulated on angiogenic endothelial cells relative to their quiescent counterparts and are the principal facilitators of endothelial adhesion to fibronectin (16, 31).

1.4.3.2 Tip cell selection & vessel elongation

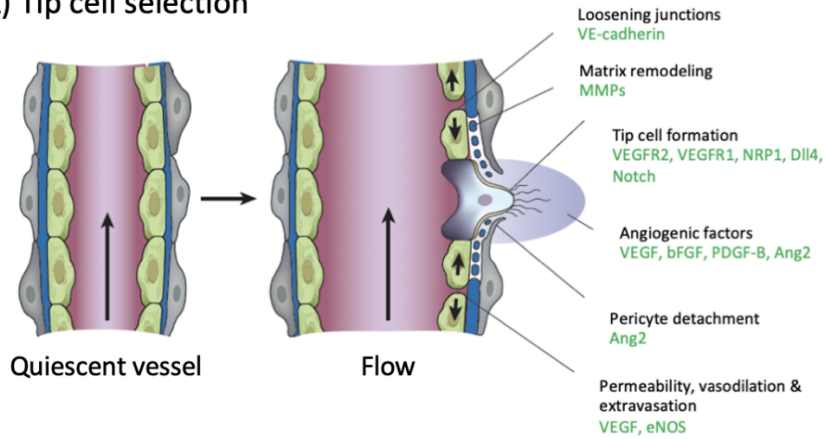
Once liberated from its constraints, a single endothelial cell becomes selected to guide the developing vessel along an angiogenic gradient (Fig 1.2A). These specialised endothelial cells, known as tip cells, prevent the development of numerous sprouts which would otherwise establish a chaotic capillary network. During this selective process the endothelial cells neighbouring the filopodia-rich tip cell become stalk cells which, in contrast, are less migratory and more proliferative. Tip/stalk cell specification begins with a competition for tip cell status (13). Briefly, VEGF released from the hypoxic parenchyma activates its cognate receptor, VEGF receptor 2 (VEGFR2), stimulating the upregulation of Delta-like-ligand 4 (Dll4), a cell surface ligand of the Notch receptor. *Trans* Dll4/Notch interactions between neighbouring endothelial cells induces successive proteolytic cleavage of Notch to release the Notch-intracellular domain (NICD) (32). NICD acts as a transcriptional regulator in the nucleus, inducing a new expression profile that diminishes endothelial responsiveness to VEGF by reducing their expression of VEGFR2 and its co-receptor NRP1 whilst also upregulating Jagged1 (33). Jagged1 subsequently antagonises Dll4 to suppress Notch activation in adjacent cells, thereby encouraging a tip cell phenotype in its neighbour (34). Cumulatively, these pathways dictate that the cell expressing most VEGFR2 will most potently suppress its neighbours via lateral inhibition and eventually assume tip cell status whilst its neighbours will adopt a stalk cell phenotype (35). Even after this initial selective process, endothelial cells at the forefront of the growing sprout continually compete for tip cell status (36). To prevent this continued competition from interrupting vessel growth, tip cell proliferation occurs

asymmetrically, thereby preventing generated daughter cells from immediately assuming a tip cell phenotype (37).

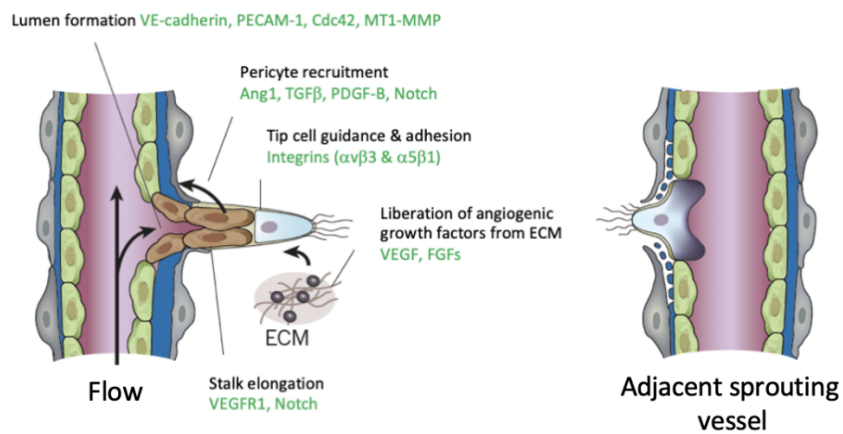
1.4.3.3 Tubulogenesis, anastomosis & maturation

With the leading tip cell providing guidance and the trailing stalk cells mediating vessel elongation, the nascent sprout traverses the interstitial space towards the source of angiogenic signals (Fig 1.2B). During extension the trailing stalk cells undergo tubulogenesis to generate a lumen and begin perfusion. Once fully extended into the avascular region the neo-vessel must then anastomose with existing vasculature to establish a functionally perfused loop, a process spatially regulated by VEGF-A/VEGFR1 signalling and encouraged by resident macrophages (38, 39). If the new vessel is to sustain blood flow and avoid regression, it must subsequently mature and regain quiescence (Fig 1.2C) (13). Induced by platelet derived growth factor-B (PDGF-B), ANG1, transforming growth factor- β (TGF- β) and Notch, mural cells re-associate with the neovessel and engage in *trans* ANG1-Tie2 interactions with underlying endothelial cells to strengthen inter-endothelial junctions (40). These factors also stimulate the deposition of a new BM which is further facilitated by the secretion of protease inhibitors such as tissue inhibitors of metalloproteinases (TIMPs) and plasminogen activator inhibitor-1 (PAI-1) to stop continued matrix degradation and remodelling (13, 41, 42). Together, these events resolve the angiogenic cascade, leaving a mature vessel that rebalances nutrient provision and demand in the previously hypoxic microenvironment.

A) Tip cell selection



B) Tip cell guidance & sprout elongation



C) Anastomosis & maturation

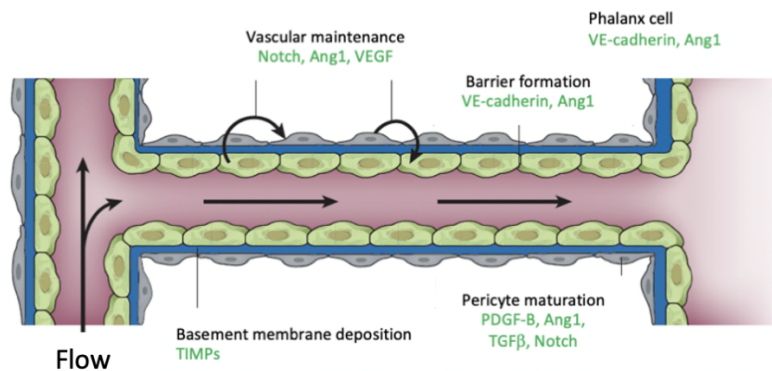


Figure 1.2 The angiogenic cascade. A) Pro-angiogenic factors released in response to hypoxia relieve endothelial quiescence by stimulating mural cell detachment, inter-endothelial cell junction loosening, BM degradation, ECM remodelling and tip cell selection. **B)** Once selected, the tip cell leads sprout development towards the source of its activating stimuli. Neighbouring stalk cells proliferate to extend the growing sprout whilst undergoing tubulogenesis. **C)** Macrophages (not shown) facilitate anastomosis whilst endothelial cells begin mural cell recruitment and BM deposition to encourage quiescence and avoid regression. Adapted from (13).

1.5 VEGFs and VEGFRs balance new vessel growth with vascular maintenance

VEGFs (vertebrate VEGFs A-D, parapoxvirus VEGF-E, snake venom VEGF-F, and placental growth factor (PlGF)) and their cognate receptors, the receptor tyrosine kinases (RTKs) VEGFR1-3, are vital for the orchestration of angiogenesis and for continual vascular maintenance, but also conduct a variety of roles in the development and function of multiple organs (43). VEGF signalling output is impressively diverse, and predictably influences various tranches of endothelial behaviour. This functional diversity is in part due to the homo- or hetero-dimerisation of VEGF receptors, thus forming an array of receptor complexes each with biological nuances as well as the added influences of co-receptors to which VEGF also binds with high affinity, namely neuropilins and HSPGs. Further still, VEGF/VEGFR complexes are liable to recruit non-VEGF-binding auxiliary proteins such as integrins, VE-cadherin and ephrin-B2 that also play their part in the regulation of VEGF signalling. The composition of these multi-protein transmembrane complexes, as well as the identity of the VEGF isoform stimulating it, represent some of the variables influencing endothelial responses to VEGF signals (Fig 1.3) (43, 44).

1.5.1 VEGFs – key angiogenic & homeostatic regulators

Though vertebrate VEGF ligands (VEGFs A-D) share comparable dimeric structures, VEGF-A (herein referred to as VEGF) represents the most prominent player in angiogenesis. Its governing authority over other pro-angiogenic growth factors is shown not only through its evolutionary conservation from fish to mammals, but also the severe vascular defects and embryonically lethal phenotype that arises in mice when just one of its two encoding alleles is depleted (18, 21). Moreover, depletion of either of its cognate receptors, VEGFR1 or VEGFR2, results in hyper- and hypo-vascularisation respectively, likewise causing embryonic lethality (20, 45, 46). The importance of VEGF/VEGFR signalling cannot, therefore, be understated in the development of vascular systems.

Within the VEGF family are numerous variants resulting from alternative splicing of its 8-exon gene that can exist in soluble, membrane-bound, and/or matrix-bound states (47, 48). These are VEGF₁₂₁, VEGF_{121b}, VEGF₁₄₅, VEGF_{145b}, VEGF₁₆₅, VEGF_{165b}, VEGF₁₈₃, VEGF₁₈₉, and VEGF₂₀₆. Notably, VEGF_{xxx}b variants are weaker VEGFR2 agonists due to their inability to bind with either NRP1 or HSPGs, but their natural occurrence remains questioned with some attributing their initial identification to

unreliable cloning methods (44, 49, 50). The abundance of these isoforms varies, with VEGF₁₄₅ and VEGF₂₀₆ being expressed to a lesser degree, but irrespective of this variability, VEGF₁₆₅ is regarded as the most potent VEGFR2 agonist due to its specific inducement of VEGFR2-NRP1 complexation and its unique ability to both freely diffuse through tissues whilst also binding with cell-surface HSPGs (44, 51, 52). The heparin-binding properties of these isoforms determines their solubility. VEGF₁₈₉ and VEGF₂₀₆ bind with HSPGs via two heparin-binding domains and are therefore largely immobilised within the ECM, whereas VEGF₁₂₁ lacks ECM-interaction domains and is consequently the most freely diffusible variant with the greatest spatial range (52, 53). The spectrum in affinity for HSPGs across these variants is essential for vascular patterning, as the sole expression of non-heparin-binding or only heparin-binding isoforms induced opposing vascular defects. An appropriate ratio of both diffusible and immobilised VEGFs is therefore required to achieve normal angiogenic growth (54). Despite this, VEGF₁₆₅ remains the most dominant pro-angiogenic driving force of these growth factors. Attesting to this, mice solely expressing VEGF₁₆₄ (the mouse homologue of human VEGF₁₆₅) are viable, whilst those individually expressing other variants such as VEGF₁₂₀ (VEGF₁₂₁ in humans) or VEGF₁₈₈ (VEGF₁₈₉ in humans) show significantly less favourable survival after birth (55).

In contrast to the embryonically lethal phenotype arising from the global depletion of a single VEGF-A allele, the global absence of murine VEGF-B prompted no change in overall survival despite their reduced heart size and abnormal atrial conduction. Though required for appropriate cardiac function then, broader cardiovascular development and function appeared independent of this VEGF isoform (18, 56, 57). The remaining two vertebrate VEGFs, VEGF-C and VEGF-D, are the primary ligands of VEGFR3 and are most functionally relevant in lymphomagenesis, though they can bind to VEGFR2 with low-affinity following their proteolytic processing in humans (52). Haiko *et al* found that individual or combined global genetic depletion of these ligands conferred no detriment to blood vascular development or indeed the overall development of these mice (58). These findings provided clear evidence as to the importance of different VEGFs in cardiovascular development and function, but isolate VEGF-A, and more specifically VEGF-A₁₆₅, as the key player amongst them. Distinct from their well characterised role in stimulating neovascular growth, VEGFs are also utilised by quiescent microvasculature as autocrine homeostatic signals. This was determined following evidence that dormant endothelial cells could synthesize their own VEGF supply (59). Subsequent endothelial-specific murine VEGF-knockout studies through use of VE-cadherin-driven Cre-recombinase documented severe haemorrhaging, mature endothelial cell rupture and cardiovascular failure in these mice, a phenotype that was lost when only one

endothelial VEGF allele was depleted. This directly contrasted the embryonically lethal phenotype resultant of a constitutive single allele-knockout (18, 53). When looking at the autocrine effects of specific VEGF isoforms, only endothelial cells individually expressing VEGF₁₆₄ possessed long-term viability such that they could maintain a stable endothelial monolayer *in vitro* (60). These findings provide yet further testimony as to the functional dominance of this variant.

1.5.2 VEGFR2 controls core angiogenic signalling pathways

According to canonical VEGFR activation, VEGF binds with one of its cognate receptors to induce receptor homodimerization or heterodimerization and trans-autophosphorylation of its cytoplasmic tyrosine residues. In combination with their adjacent amino-acid sequences these phospho-tyrosine residues act as docking sites for the recruitment of adaptor molecules, intermediaries that subsequently flux through a convoluted network of interconnected signalling pathways to influence different aspects of endothelial cell behaviour (61). Of the three VEGF RTKs, VEGFR2 is renowned as the principal pro-angiogenic receptor in endothelial cells and is therefore the primary focus of this section, though the angiogenic involvement of VEGFR1 and VEGFR3 will be briefly touched upon (43).

Originally identified as Fms-like tyrosine kinase-1 (Flt-1), VEGFR1 is abundantly expressed in the vascular endothelium and is the cognate receptor of VEGF-A, VEGF-B and PlGF (62). Despite possessing a strong affinity for VEGF-A, an affinity 10-fold higher than that of VEGFR2 in fact, its kinase activity is only weakly activated upon ligand binding (63). This receptor therefore functions as a VEGF-sink, acting to sequester VEGF from VEGFR2 which would otherwise robustly stimulate downstream pro-angiogenic signalling cascades. This negative angiogenic regulator also exists as a soluble isoform (sVEGFR1) due to alternative *Vegfr-1* splicing which further enables its occlusion of VEGF (64). The overall angiogenic influence of this decoy receptor has been documented as essential for vascular development and function, as the global depletion of VEGFR1 caused embryonic lethality by E8.5-9.0 due to abnormal vascular patterning and excessive endothelial proliferation. The absence of its kinase domains alone, however, conferred no vascular detriment (46, 65, 66). Its extracellular sequestration of VEGF, and not its cytoplasmic kinase activity, was therefore necessary for normal angiogenesis and appropriate vascular development. That said,

close monitoring of VEGFR1 expression is necessary, as an overabundance of sVEGFR1 expression is associated with pre-eclampsia and peripartum cardiomyopathy (67, 68).

VEGFR3 is the canonical receptor of VEGF-C and VEGF-D. Whilst primarily expressed on lymphatic endothelial cells this receptor also plays critical roles during cardiovascular development as its global depletion in mice is embryonically lethal by E9.5 due to cardiovascular failure prior to the development of the lymphatic system (69). Although expressed more strongly in lymphatic endothelial cells, VEGFR3 retains functionality in the blood vascular endothelium during adulthood. Its long-term, endothelial-specific depletion in adult mice resulted in an elevated baseline permeability that was exacerbated in response to VEGF. The authors attributed these effects to elevated VEGFR2 expression, indicating that VEGFR3 would normally suppress this over-expression (70). VEGFR3 is also a known regulator of sprouting angiogenesis in the retina, where its upregulation in tip cells aids their conversation to stalk cells during vascular maturation (71). Nevertheless, angiogenesis could proceed normally in its endothelial absence due to the compensatory effects of VEGFR2 (72).

VEGFR2, like VEGFR1 and VEGFR3, is comprised of seven extracellular immunoglobulin (Ig)-like domains, a transmembrane domain, and a cytoplasmic domain encompassing a juxtamembrane region, a tyrosine kinase domain, and a C-terminal tail (61). Akin to VEGFR1, its Ig-like domains 2 and 3 are responsible for VEGF binding and it may also be expressed in a soluble form (sVEGFR2) capable of binding and sequestering VEGF-C (73). Ligand binding has historically been thought to induce receptor dimerization, but phosphorylated, un-ligated VEGFR2 dimers exist as a result of inter-monomer contacts between extracellular and transmembrane domains. Still, ligand transduction enables the appropriate conformation of its transmembrane region required for full kinase domain activation (74). In turn, various tyrosine residues are trans-auto-phosphorylated including: Y949, Y1052, Y1057, Y1173, and Y1212 (Y951, Y1054, Y1059, Y1175, and Y1214 in humans). These phospho-tyrosine residues then act as docking sites for adaptor molecules which in turn activate various signalling pathways that ultimately regulate endothelial migration, permeability, proliferation, and survival (Fig 1.4 & 1.5) (61). Of these tyrosine residues, Y1173 is arguably one of the most important. Evidencing this, substitution of this tyrosine residue for phenylalanine (Y1173F) confers the same embryonically lethal phenotype as the global depletion of VEGFR2 itself, each owing to severe vascular defects (20, 75).

1.5.3 VEGFR2 endosomal trafficking regulates signalling strength and receptor preservation

Like other RTKs, VEGFR2 must be present at the plasma membrane to become fully activated, but translating cell surface stimulation into activation of intracellular signalling pathways and ultimately targeted changes in gene transcription requires receptor internalisation. This was previously thought of solely as a method by which to terminate signalling responses, but its internalisation and endosomal trafficking is now recognised as essential for appropriate activation of its downstream signalling effectors such as ERK and Akt (76). Furthermore, un-ligated VEGFR2 exists in endosomal stores awaiting VEGF stimulation to trigger its recycling to the cell surface (77). As such, its various trafficking routes are indispensable to its broader function as a pro-angiogenic receptor. Notably, the GTPases encompassed within the Rab family mark trafficking vesicles and can be used to distinguish between various intracellular trafficking routes (78). In its un-ligated state, VEGFR2 undergoes constitutive, rapid recycling via Rab4-positive endosomes (Fig 1.6). This recycling pathway protects the receptor from ectodomain cleavage at the plasma membrane, thereby preserving it in its mature form whilst also maintaining endothelial receptiveness to VEGF signals (43, 79). Upon VEGF stimulation, VEGFR2 is internalised in a Rab5-dependent manner before proceeding via one of three possible endosomal routes: Rab4-dependent fast recycling, Rab11-dependent slow recycling, or Rab7-dependent endosomal traffic destined for lysosomal degradation (80). The latter of these routes ultimately concludes the endothelial VEGF response by reducing VEGFR2 abundance, though various phosphotyrosine phosphatases (PTP1B, VE-PTP) also control VEGF signalling by de-phosphorylating specific VEGFR2 phospho-residues (43). Crucially however, VEGF/VEGFR signalling is regulated by a multitude of co-receptors such as neuropilins and integrins (81).

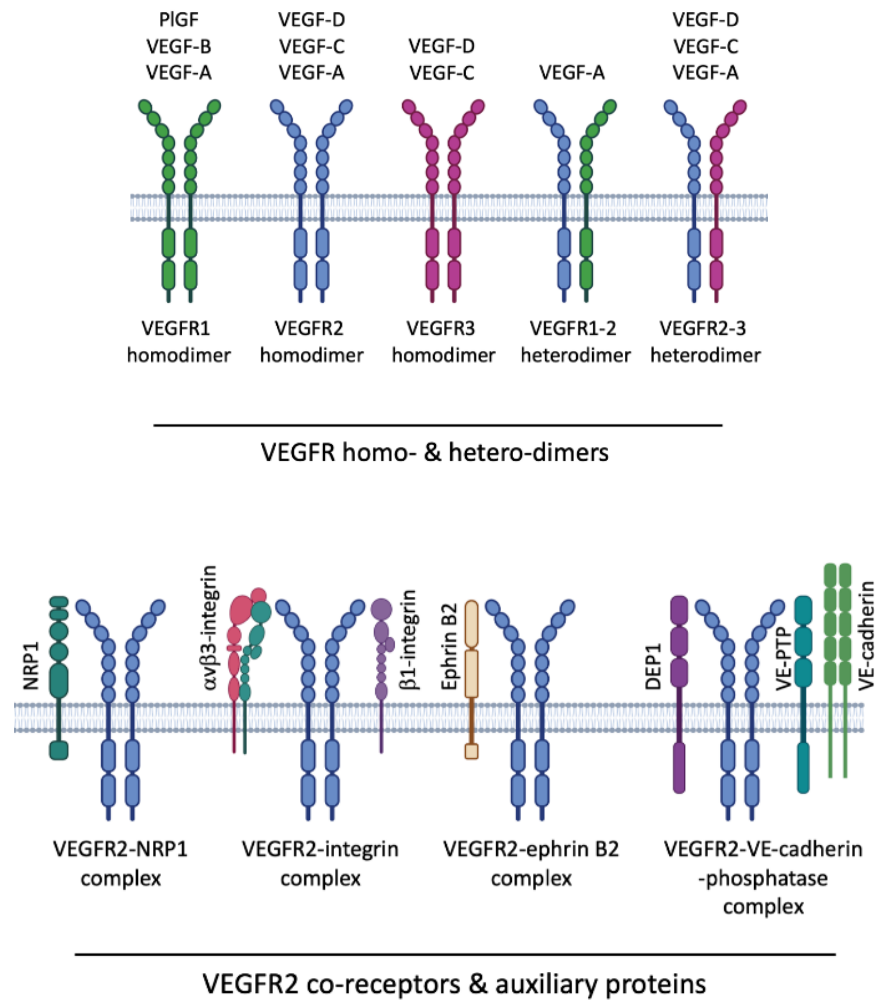


Figure 1.3 VEGFR homo-/hetero-dimerization and VEGFR2 co-receptor/auxiliary protein complexes. VEGF ligands A-D bind with their cognate VEGF receptors in their homo- or hetero-dimeric forms. The activity of VEGFR2 homodimers is regulated by a variety of VEGF-binding co-receptors and auxiliary proteins, some of which are depicted here: NRP1, $\alpha\beta3$ -integrin, $\beta1$ -integrin, ephrin B2, density enhanced phosphatase-1 (DEP1), vascular endothelial-protein tyrosine phosphatase (VE-PTP) and VE-cadherin. Figure adapted from (43) and generated using Biorender.

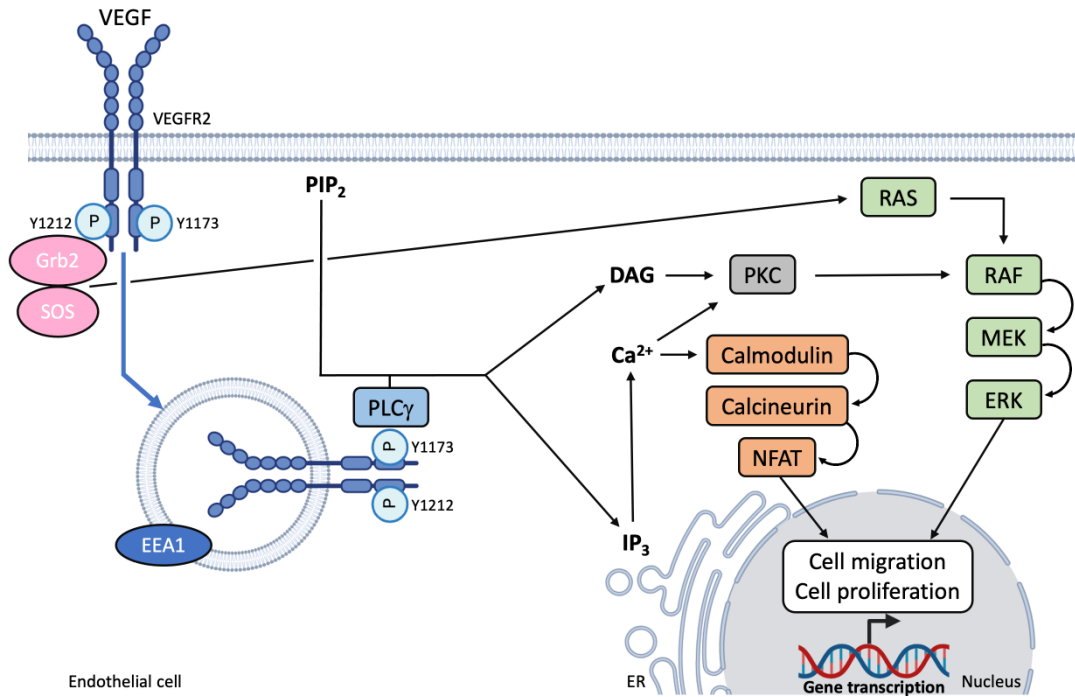


Figure 1.4 The VEGF-activated VEGFR2 PLC γ /Grb2-ERK pathway and Ca²⁺ signalling. VEGFR2 activation and phosphorylation at Y1173 induces its internalisation. Now housed in early endosome antigen 1 (EEA1)-positive endosomes, VEGFR2 phospho-Y1173 is responsible for the recruitment and activation of phospholipase C γ (PLC γ) which in turn hydrolyses phosphatidylinositol 4, 5-biphosphate (PIP₂) to generate the secondary messengers inositol 1, 4, 5-triphosphate (IP₃) and diacylglycerol (DAG). IP₃ releases Ca²⁺ from the endoplasmic reticulum (ER) which, in tandem with DAG, activates Ca²⁺-dependent protein kinase C (PKC). PKC then stimulates the RAF-MEK-ERK signalling cascade. ERK's nuclear translocation and activation of various transcription factors influences endothelial gene expression and ultimately cellular functions such as proliferation and migration. Ca²⁺ released from the ER also promotes VEGF-signalling through an alternative mechanism. Calmodulin is a Ca²⁺ sensor that, once activated in the presence of these cations, triggers the Ca²⁺-dependent serine/threonine phosphatase calcineurin to de-phosphorylate the nuclear factor of activated T cell (NFAT) family. These transcription factors promote VEGF signalling by reducing VEGFR1 expression to increase VEGF bioavailability (43). Src-homology 2 (SH2) domain containing adaptor proteins such as growth factor receptor-bound protein 2 (Grb2) are recruited to and activated by VEGFR2 phospho-Y1212. In combination with Son of Sevenless (SOS), active Grb2 stimulates RAS which in turn helps drive the RAF-MEK-ERK signalling cascade (82). Figure adapted from (43) using Biorender.

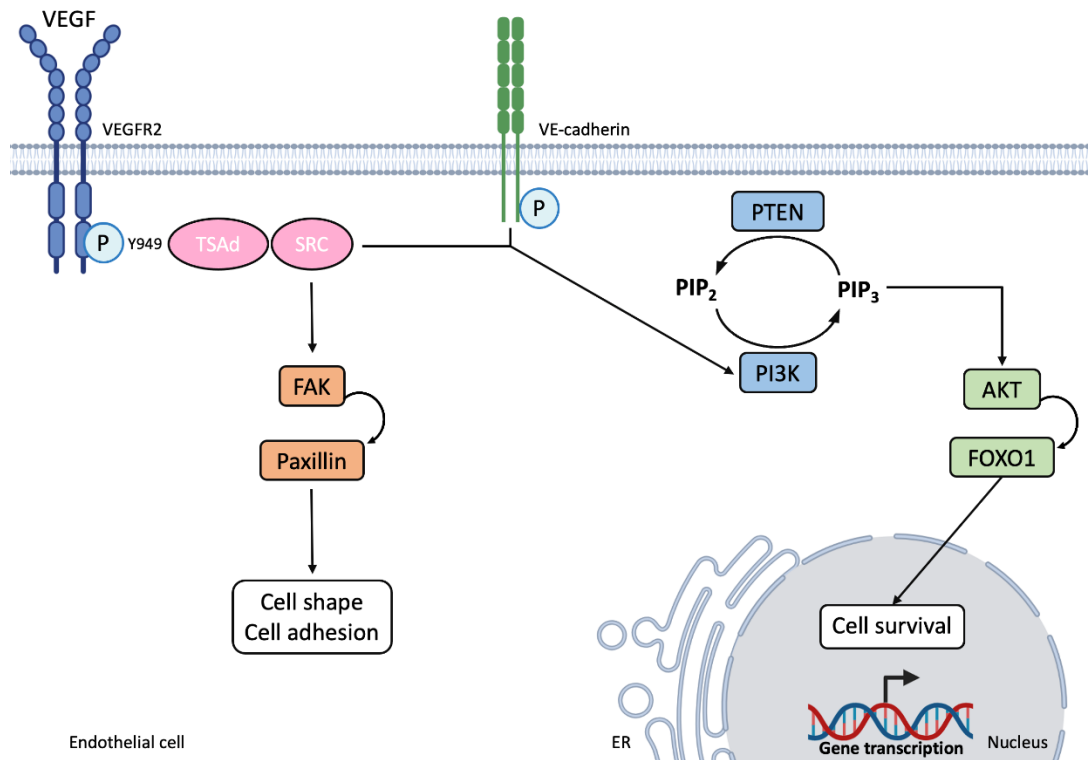


Figure 1.5 VEGF-activated VEGFR2 SRC signalling. Activation of the SRC family of cytoplasmic tyrosine kinases is reliant on phospho-Y949. This residue acts as a docking site for T cell-specific adaptor (TSAd) via its SH2 domain. Activated TSAd subsequently binds with SRC through its SH3 domain resulting in its activation. This is necessary for the activation of phosphoinositide 3-kinase (PI3K) as VEGFR2 is unable to bind with this kinase directly. SRC, in tandem with VE-cadherin, activates PI3K to enable its generation of phosphatidylinositol 3, 4, 5-triphosphate (PIP₃), a secondary messenger responsible for the activation of Akt via binding with its plextrin homology domain. Importantly, phosphatase and tensin homolog (PTEN) catalyses PIP₃ hydrolysis to downregulate this pathway when necessary. Active Akt then phosphorylates forkhead box protein O1 (FOXO1) resulting in its cytoplasmic sequestration and the downregulation of cell death associated genes (43, 83). An additional SRC substrate is focal adhesion kinase (FAK) which, through activation of its substrate paxillin, influences endothelial cell adhesion and shape in response to VEGF. Figure adapted from (43) using Biorender.

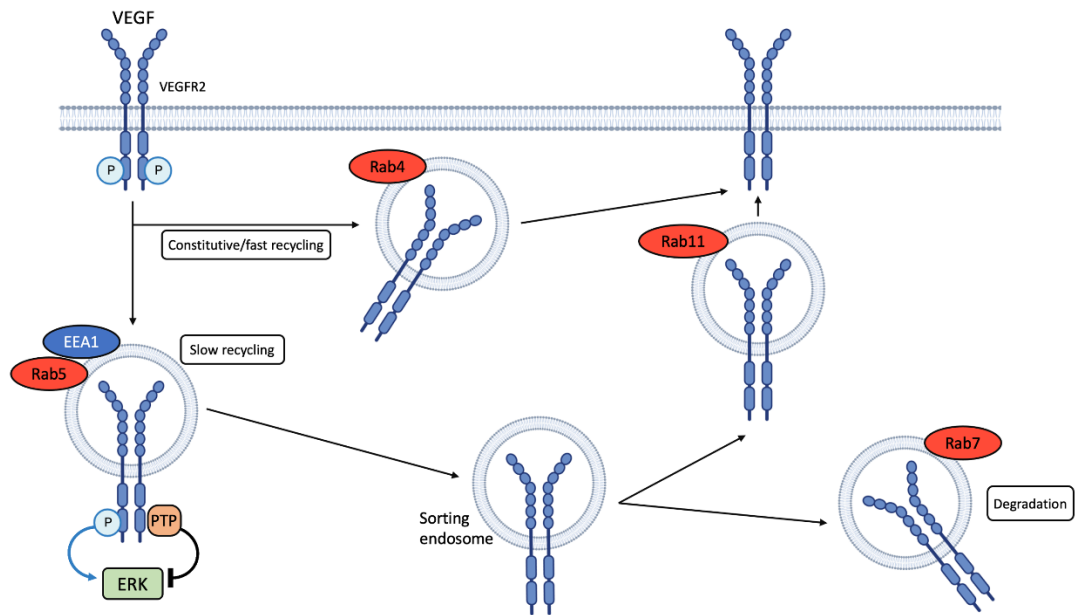


Figure 1.6 VEGFR2 endosomal trafficking. In the absence of ligand, VEGFR2 is constitutively recycled via Rab4-positive endosomes. This pathway is relatively fast when compared with the alternative Rab-11-dependent recycling route. VEGFR2 endosomal traffic is directed down this pathway following ligand binding and receptor activation. It is first internalised to Rab5-positive and EEA1-positive early endosomes where its phospho-tyrosine residues continue to stimulate pro-angiogenic signalling cascades until their PTP-mediated de-phosphorylation. VEGFR2 is then either shuttled to lysosomes for degradation by Rab7-positive late endosomes or recycled back to the plasma membrane by Rab11-positive endosomes. Figure adapted from (43) using Biorender.

1.6 Neuropilin-1 – an essential VEGFR2 co-receptor

Following its discovery in *Xenopus* some 30 years ago, NRP1 was soon identified as a receptor for axonal guidance signals and therefore implicated in neurodevelopment (84, 85, 86). Shortly thereafter, this novel receptor was re-discovered in both tumour cells and endothelial cells as an isoform-specific VEGF receptor (87, 88). In addition to the commonality between nerve and blood vessel development, linking endothelial NRP1 with this potent pro-angiogenic growth factor immediately suggested its involvement in the field of angiogenesis (89). Indeed, NRP1 is now richly documented for its roles in vascular biology, particularly for its function as a VEGFR2 co-receptor.

The neuropilin family encompasses two type-1 transmembrane glycoproteins, namely NRP1 and neuropilin-2 (NRP2) (Fig 1.7). In vertebrates these receptors are highly conserved, sharing a matching domain architecture with 44% amino-acid homology (90). Typical of type I transmembrane molecules, both NRP1 and NRP2 possess an extracellular N-terminal ligand binding domain, a single transmembrane helix, and a short cytoplasmic C-terminal region. Encompassed within its extracellular moiety are five domains that collectively enable NRP1's diverse array of extracellular ligands including class III semaphorins and VEGFs (Fig 1.6) (90, 91). To convert transduction of these ligands into intracellular responses NRP1 must recruit adaptor molecules to its C-terminal tail due its lack of intrinsic catalytic functionality. To accomplish this, its C-terminus houses an SEA-motif capable of interacting with PDZ-domain containing proteins including GIPC1 (GAIP interacting protein C terminus member 1, also known as synectin) and NIP1 (neuropilin-interacting protein-1) to link extracellular signals with intracellular signalling machinery (90, 92). Much like VEGFRs, NRP1 also encompasses several splice variants including the mature membrane bound isoform, the NRP1(Δ exon16) isoform, and four soluble isoforms: s_{III} NRP1, s_{IV} NRP1, s_{11} NRP1 and s_{12} NRP1. These soluble isoforms lack the cytoplasmic and transmembrane domains of the fully transcribed protein, but maintain affinity for both semaphorins and VEGFs and are therefore capable of sequestering these factors (93, 94, 95).

Early studies linking NRPs to vascular development did so via an assortment of mutant mouse studies. Unexpectedly, NRP2-null mice are viable and fertile, presenting no observable cardiovascular abnormalities (96). In contrast, the global depletion or over-expression of NRP1 in transgenic mice resulted in an embryonically lethal phenotype characterised by deficient neural

vascularisation when depleted and extensive microvascular expansion and haemorrhaging when over-expressed (97, 98). Similarly, constitutive endothelial-specific NRP1 depletion caused late gestational lethality due to systemic vascular dearth and disorganisation, leaving only a primitive vascular plexus in these embryos (99). Suitable angiogenic development is therefore reliant on endothelial NRP1 expression. Interestingly, the vascular defects resulting from global depletion of both NRPs caused embryonic lethality earlier than that caused by NRP1 depletion alone, indicating NRP1 and NRP2 may engage in crosstalk to regulate vascular morphogenesis (100). The Robinson lab has since evidenced further their collective angiogenic involvement, reporting a significantly greater anti-tumorigenic effect following their endothelial co-depletion than that induced when either was targeted individually. Importantly this effect was owed to a more substantial reduction in tumour vascularity (101). Moreover, the aforementioned lethal phenotype prompted by global NRP1/2 co-depletion mimicked that of VEGF and VEGFR2 knockout mice, prompting investigation of this receptor in VEGF-induced angiogenesis (20, 46, 100).

To this end, Soker *et al* reported that when co-expressed with VEGFR2, NRP1 enhanced VEGF-VEGFR2 interactions. This augmentation was notably VEGF₁₆₅ specific, with VEGF₁₂₁ conferring no such enhancement despite still being capable of binding with NRP1 (87, 102). Notably, like NRP1, NRP2 also binds with VEGF₁₆₅ but does so with a 50-fold weaker affinity (103). It was postulated that NRP1 may act as an affinity modulator, actively shuttling VEGF₁₆₅ to its cognate receptor to strengthen its bioavailability and downstream signalling (88). Indeed, enhanced VEGFR2 activity was later owed to complexation of NRP1 with VEGFR2 in *cis* via a VEGF₁₆₅ bridge, establishing a trimeric complex that facilitated VEGF₁₆₅-VEGFR2 interactions. VEGF₁₆₅-VEGFR2 binding affinity, however, remained unaltered. The observed elevation in VEGFR2 activity was instead proposed to emanate from complex clustering, whereby VEGFR2/VEGF₁₆₅/NRP1 complexes would amalgamate and thereby enhance VEGF-induced signalling through receptor clustering (51). Formation of such complexes was later confirmed, though the resulting amplification of VEGF-induced signalling was attributed to an increase in binding affinity between VEGF₁₆₅ and VEGFR2 (104). Regardless, the cytoplasmic domains of both VEGFR2 and NRP1 are essential for their clustering, as reduced VEGFR2 phosphorylation impaired assembly with NRP1 independently of ligand binding, and truncated NRP1 lacking its PDZ-binding domain equally decreased their complexation. Endothelial cells deficient in GIPC1 mirrored these findings, further evidencing a cytoplasmic link between VEGFR2 and NRP1 during receptor clustering (105). Some discrepancy therefore exists as to the mechanism of signalling enhancement, but the role of NRP1 as a VEGFR2 co-receptor was

established alongside an understanding that its endothelial expression is vital for appropriate vascular developmental.

The function of NRP1 as a VEGFR2 co-receptor extends beyond their interactions at the cell surface. Ballmer-Hofer *et al* reported that, following VEGF₁₆₅ stimulation, NRP1/VEGFR2 complexes co-trafficked preferentially through Rab5, Rab4 and Rab11-positive vesicles before returning to the plasma membrane in a de-phosphorylated state. By limiting Rab7-directed traffic these receptors were preserved and the VEGF response prolonged (80). Its guidance of VEGFR2 intracellular cargo was deemed essential for both p38 MAPK and ERK activation, but these effects are reliant on NRP1 binding with VEGFR2 is *cis* (80, 106). The alternative complex conformation in *trans*, where NRP1 and VEGFR2 present on the cell surface of adjacent cells form a trimeric complex with VEGF₁₆₅, has the opposite effect, limiting the receptor's internalisation and associated amplification of downstream signalling cascades (107).

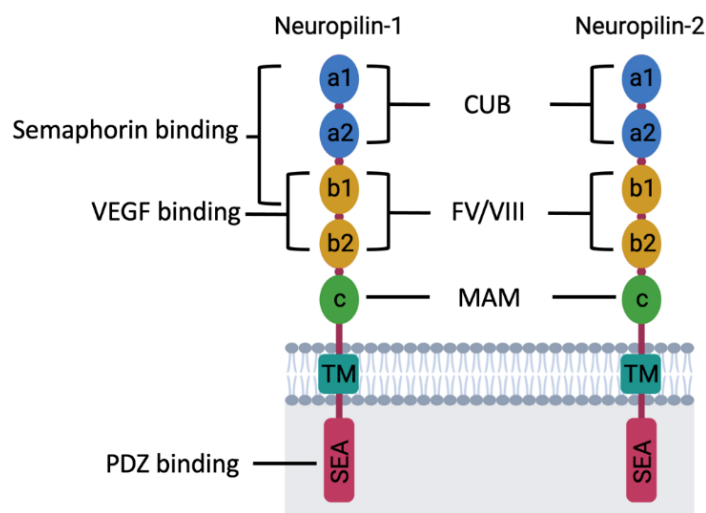


Figure 1.7 Neuropilin protein structure. NRP1 and NRP2 are each comprised of a cytoplasmic domain with a C-terminal PDZ-binding motif (the amino-acids SEA), a transmembrane domain (TM), a MAM (c) domain which is implicated in NRP1 oligomerisation, two factor V/VIII domains (b1 and b2) responsible for VEGF binding, and two CUB domains (a1 and a2) which, together with b1/b2, are necessary for semaphorin binding. Adapted from (108) using BioRender.

1.7 Integrins – integral cell-ECM links

Metazoan cell-matrix adhesion is principally mediated by integrins, a family of transmembrane receptors that establish cellular connections to ECM constituents and members of the immunoglobulin superfamily (109). Named for their integral role in the generation of dynamic intracellular-extracellular contacts and their integration of signals from either side of the plasma membrane, these receptors gained significant attention for their regulatory role in endothelial migration (109, 110). Angiogenesis is critically reliant upon the appropriate orchestration of this cellular process and as such, the involvement of integrins within angiogenesis has been widely researched.

Encompassed within the integrin family are 24 distinct heterodimeric membrane-spanning receptors individually composed of one α and one β subunit. The specific identity of the α and β subunits, of which there are 18 and 8 respectively, determines ligand specificity (Fig 1.8) (109). Structurally, each subunit is a type I transmembrane glycoprotein classically composed of an extracellular ligand binding domain, a transmembrane hydrophobic region and, akin with NRPs, a non-catalytic cytoplasmic tail. These subunits associate non-covalently to form functional heterodimers that are heterogeneously expressed on nearly every cell type (111, 112). The range of different integrin heterodimers accommodates cell adhesion to different substrates but despite this, there is a degree of functional overlap (113). For example, numerous integrins share the tripeptide Arginine-Glycine-Aspartic acid (RGD) motif as a ligand recognition sequence, enabling collective adhesion to fibronectin and many other matrix components (114). Shared ligand recognition sequences however do not discount the unique binding properties and discrete functions of each integrin, as evidenced by the range of phenotypes observed when different integrin genes are manipulated in mouse models (109).

Integrins are classically known for their ability to ligate with ECM constituents to enable cell adhesion and migration. However, integrins are in fact vital bidirectional signalling receptors, capable of both transmitting and receiving extracellular and intracellular signals. Signals received from the intracellular compartment regulate integrin-ligand affinity and integrin avidity (i.e overall adhesive strength influenced by individual receptor-ligand affinities and the frequency of these interactions) at the cell surface via 'inside-out' signalling, whilst signals derived from their

extracellular ligands ultimately feed into a variety of intracellular signalling cascades via 'outside-in' signalling (109). Considering the former, integrins are not constitutively active and will exist in one of three possible conformations: bent closed, extended closed, and extended open. Most cell surface integrins remain in the inactive, bent closed conformation with their extracellular stalk domains curled towards the plasma membrane and their ligand-binding headpiece obscured from available substrates due to the energy demands of shifting to an extended form, though the willingness of integrins to undertake this transition varies between heterodimers. Some, such as $\alpha 5 \beta 1$ -integrin and $\alpha v \beta 1$ -integrin, are relatively activatable due to their heterodimeric instability (i.e. their lower intra-heterodimer affinity). This lowers the energy barrier separating bent and extended conformations and enables them to adopt the latter more freely. Consequently, the extended form of these integrins is less stable than integrins with greater intra-heterodimer affinity, such as $\alpha v \beta 3$, $\alpha v \beta 5$, and $\alpha v \beta 6$. The conformational transition of these receptors is more taxing on cellular energy but provides a more substantial increase to cellular avidity due to their greater cell surface retention once extended. In this state integrins can ligate with their specific substrates and outside-in signalling may proceed. Notably however, integrins lack intrinsic signalling capabilities, so must recruit adaptor molecules for received signals to materialise as intracellular responses (115, 116).

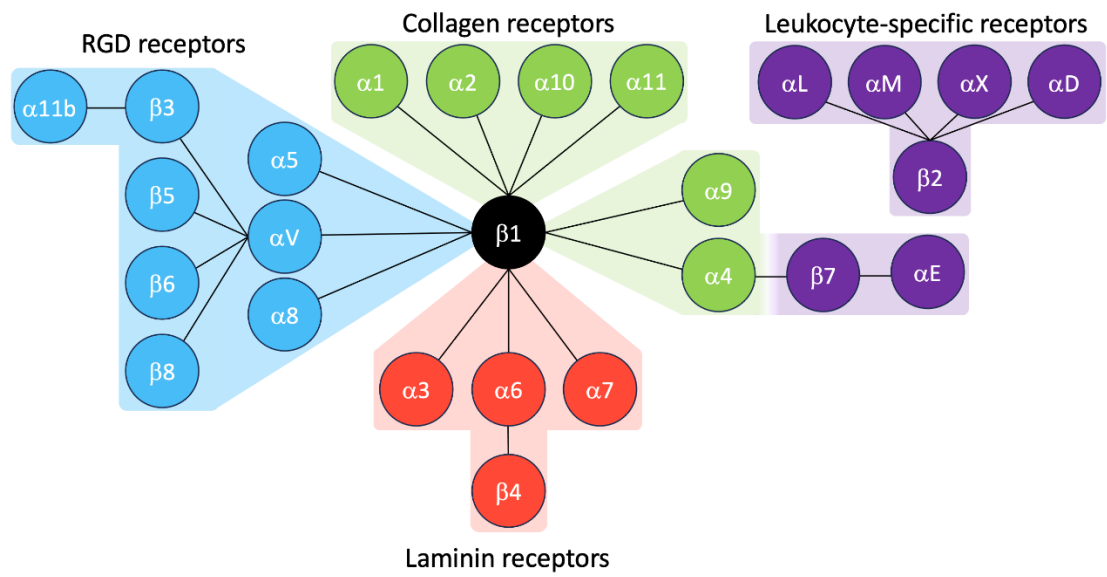


Figure 1.8 Mammalian α -integrin and β -integrin subunits, their heterodimeric combinations, and their respective ligands. The 18 α - and 8 β -subunits establish 24 distinct integrin heterodimers. Each of their respective ligands are illustrated. Figure adapted from (109).

1.7.1 Integrin adhesion complexes

Cell-ECM links mediated by integrins connect extracellular substrates with the cell's cytoskeletal scaffolding through a host of intermediary adaptors. Connection to the actomyosin contractility apparatus then enables force generation that drives the maturation of integrin adhesion complexes (IACs), coordinated cell shape changes, directional migration, and ECM remodelling (117).

IACs are heterogenous aggregates categorised according to composition, size, longevity, cellular distribution, and function (Fig 1.9). The first, smallest, and most transient IACs to form are filopodial tip adhesions. Filopodia, membrane protrusions emanating from lamellipodia at the migratory front of the cell, are composed linear F-actin bundles sheathed by the plasma membrane and possess un-ligated integrins necessary to form these initial adhesive outposts. Once ligated, these integrins recruit adaptor molecules such as vinculin, talin and kindlin to tether filopodial tip adhesions to the actin cytoskeleton before Rho GTPase mediated actin-myosin contractile forces drive stress fibre formation and adhesion maturation (118, 119). Filopodial tip adhesions grow into nascent adhesions (< 0.5 μm in diameter) as the lamellipodia extends and facilitate cell locomotion by translocating centripetally whilst contracting peripherally (120). These adhesions are typically littered across the leading edge of the cell and, like their predecessors, are equally prone to disassembly. Assuming they continue to mature, nascent adhesions recruit more integrin heterodimers and a further assortment of adaptor molecules such as kindlin, Src family kinases, paxillin and FAK, which collectively drive continued actin polymerisation and actomyosin contractility to drive the continued maturation of these adhesive clusters into dot-like focal complexes (< 1 μm in diameter) and elongated focal adhesions (FAs) (< 2-5 μm in diameter) (117). These adhesions witness both spatial and temporal changes in integrin composition, with $\alpha 5 \beta 1$ -integrin predominating in smaller, earlier-forming nano-adhesions to form transient cell-ECM links, whilst $\alpha v \beta 3$ -integrin primarily resides in older, larger adhesive clusters to provide more stable mechanical links to the ECM (121). Continued maturation over a longer period (~48 hours) enables FAs to lengthen into fibrillar adhesions (1-10 μm) enriched in $\alpha 5 \beta 1$ -integrin, a primary site of fibronectin fibrillogenesis, and is accompanied by their centripetal translocation towards the cell body (117, 122).

Of the protein kinases recruited to activated integrins, FAK is perhaps one of the most well investigated. This non-receptor protein tyrosine kinase possesses an N-terminal FERM domain, a C-terminal focal adhesion targeting domain, and interspaced between the two, a central tyrosine kinase domain (123). The FERM domain auto-inhibits the kinase domain as well as the autophosphorylation site at Y397 to prevent constitutive FAK activation (124). Recruitment to active integrins via the adaptor proteins talin and paxillin relieves this auto-inhibition, activating FAK and prompting its rapid autophosphorylation at Y397 (125). This phospho-residue then acts as docking site for Src, establishing a dual kinase FAK-Src complex that phosphorylates additional FAK residues and thereby enables the recruitment and activation of SH2-domain containing Grb2 and PI3K. These activated proteins subsequently flux through their respective signalling cascades to influence cell survival, proliferation and migration. Moreover, the high concentration of signalling intermediaries present within these aggregates enables efficient and rapid broadcasting of these signals (126, 127). Active FAK also facilitates actin polymerisation in lamellipodia and filopodia through augmentation of the Rho GTPase family, namely Rac1 and Cdc42 (128). Ultimately, FAK is an essential signalling apparatus and a core component of cell adhesions. This importance is clearly evidenced through its targeted genetic depletion, as mice deficient in FAK die by E8.5 due to stunted vascular development (129). Further evidencing the critical role of this non-RTK in angiogenesis, though survival is prolonged, endothelial murine depletion of FAK is also embryonically lethal by E10.5-11.5 due to irregular vascular growth and extensive haemorrhaging (130, 131).

Integrin-based adhesion is therefore not only essential for cellular adhesion and migration, but also for ECM remodelling, proliferation, differentiation, and survival. In fact, the absence of integrin-mediated adhesion induces anoikis, a form of controlled cell death resultant of inadequate adherence, far faster than a deficiency of growth factors does apoptosis (132, 133, 134). Subsequent sections will discuss the importance of these bidirectional signalling receptors within angiogenesis (115).

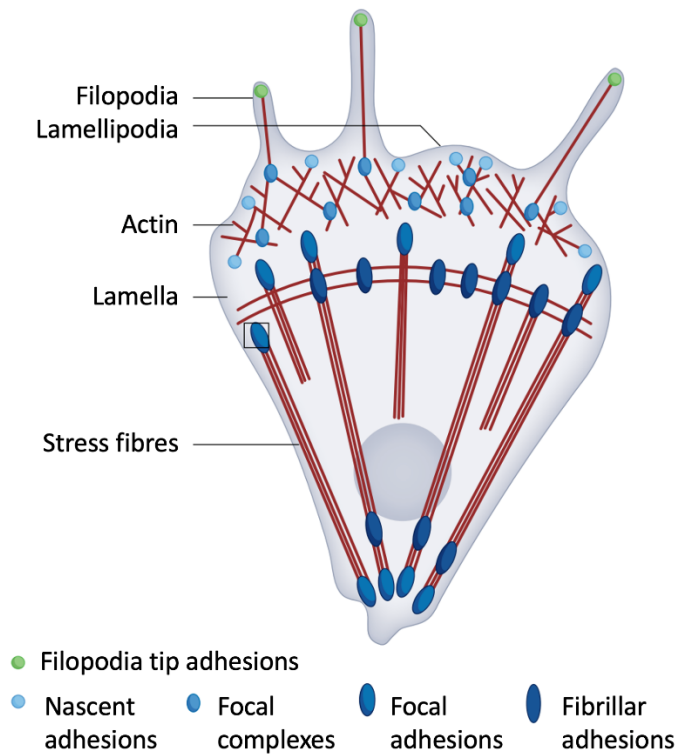


Figure 1.9 The spatial distribution of integrin adhesion complexes. Five classical IACs are recognised which, in order of increasing size, are: filopodia tip adhesions, nascent adhesions, focal complexes, focal adhesions and fibrillar adhesions. Illustrated here is the spatial distribution of these adhesions. Figure from (117).

1.7.2 Integrins in angiogenesis

Angiogenesis is driven, in part, by the coordinated migration and proliferation of endothelial cells in response to environmental cues. Integrins conduct crucial roles in the regulation of these processes and are key drivers of embryonic and post-natal vascularisation (135). Endothelial cells express a discrete collection of integrins, namely: the collagen receptors $\alpha1\beta1$ and $\alpha2\beta1$; the fibronectin receptors $\alpha4\beta1$, $\alpha5\beta1$ and $\alpha v\beta3$; the laminin receptors $\alpha6\beta1$ and $\alpha6\beta4$; the osteopontin receptor $\alpha9\beta1$; and the vitronectin receptors $\alpha v\beta3$ and $\alpha v\beta5$ (135, 136). During angiogenesis the endothelial expression of many of these integrins is downregulated whilst that of others is elevated, establishing a unique integrin expression profile in which both $\alpha v\beta3$ -integrin and $\alpha5\beta1$ -integrin are enriched relative to quiescent endothelial counterparts. Evidence of their endothelial upregulation upon receipt of a pro-angiogenic signal was indicative of the important neovascular functions that these receptors conduct (16, 31).

Upregulation of these integrins coincides with the deposition of fibronectin, a principal ECM constituent of angiogenic microenvironments as evidenced by the lethal cardiovascular defects that result from its genetic ablation in mice (15, 137). $\alpha v\beta3$ - and $\alpha5\beta1$ -integrin are the major endothelial receptors for this matrix substrate and are responsible for translating endothelial-fibronectin adherence into survival, proliferative and migratory cues (138). These integrins therefore perform vital functions during angiogenesis by establishing crucial links with the fibronectin-rich ECM. Discussed below are some of the discrete and overlapping functions that these fibronectin-binding integrins conduct during angiogenesis, and although integrins $\alpha1\beta1$, $\alpha2\beta1$, $\alpha v\beta5$ and $\alpha4\beta1$ are all upregulated in response to pro-angiogenic cues, they do not ligate with fibronectin and are therefore not the focus of this thesis (136).

1.8 Endothelial fibronectin receptors in angiogenesis

1.8.1 $\alpha v\beta 3$ -integrin

$\alpha v\beta 3$ -integrin is a promiscuous receptor, capable of ligating with numerous ECM substrates including fibrinogen, osteopontin, angiostatin, vitronectin and fibronectin (136). Its elevated expression on angiogenic endothelial cells was initially reported over two decades ago by Brooks *et al* (31). As a novel neovascular marker the therapeutic potential of $\alpha v\beta 3$ -integrin antagonists to selectively target pathological angiogenesis was quickly realised (139).

Prior to continuing, it is important to remark upon the methods used to genetically target this integrin and thereby model its physiological functions. αv -integrin is capable of heterodimerising with multiple β -subunits, namely $\beta 3$, $\beta 5$, $\beta 6$ and $\beta 8$. As such, manipulation of the *ITGAV* gene yields heterogenous biological effects that cannot be attributed to the ablation of $\alpha v\beta 3$ -integrin alone (140). Moreover, genetic deletion of αv -integrin was frequently embryonically lethal in murine models (141). Endothelial $\beta 3$ -integrin however, complexes solely with αv -integrin, thereby establishing this monomer as a suitable candidate for the selective endothelial manipulation of $\alpha v\beta 3$ -integrin (109).

1.8.2 $\alpha v\beta 3$ -integrin functionality is context dependent

Based on prior findings that $\alpha v\beta 3$ -integrin represented a novel neovascular marker, many groups attempted to pharmacologically antagonise this receptor to suppress pathological angiogenesis. In pre-clinical models, $\alpha v\beta 3$ -integrin inhibition successfully disrupted tumour growth and associated pathological angiogenesis by instigating apoptosis selectively in angiogenic endothelial cells (139, 140, 141, 142). Numerous disorders characterised by pathological neovascularisation have since been associated with elevated levels of this integrin including brain, lung, and breast cancers, but also ocular neovascular disorders such as retinopathy of prematurity (136, 143, 144, 145). These early findings highlighted both the pro-angiogenic nature of $\alpha v\beta 3$ -integrin, as well as its clinical potential for the development of more selective anti-angiogenic therapeutics that might surpass VEGF-targeted therapies that are commonly associated with excessive toxicity and treatment resistance (146).

Complementing this developing narrative portraying $\alpha v\beta 3$ -integrin as an indispensable driver of angiogenesis, this integrin was demonstrated to function synergistically with VEGFR2. More specifically, Soldi *et al* reported that phosphorylated VEGFR2 co-immunoprecipitated with $\beta 3$ -integrin following VEGF stimulation, and that this interaction was augmented by plating cells on $\alpha v\beta 3$ -integrin's canonical ligand vitronectin (147). It was later shown that VEGF-induced clustering of this integrin at the cell surface, and phosphorylation of $\beta 3$ -integrin's cytoplasmic tail were prerequisites of this synergistic interaction (147, 148). The latter was established using 'DiYF' mice in which the cytoplasmic domain of mutated $\beta 3$ -integrin was unable to be phosphorylated. VEGF-induced angiogenesis in these mice was significantly impaired both *in vivo* and *in vitro* using endothelial cells isolated from the lungs. These cells were less adhesive and less motile than their wild-type (WT) counterparts and demonstrated defective VEGF-induced VEGFR2 phosphorylation. Pathological angiogenesis was also hindered such that subcutaneous tumours grew two-fold smaller than their WT equivalents (149). The established crosstalk between these receptors was later shown to be mediated by c-Src, a non-RTK that, following its VEGF-induced recruitment to adhesions and subsequent activation, directly phosphorylated $\beta 3$ -integrin at Y747 and Y759 to promote a high-avidity confirmation that could then engage with VEGFR2 (Fig 1.10) (150).

The overwhelming evidence depicting $\alpha v\beta 3$ -integrin as a pro-angiogenic molecule and selective neovascular marker established it as an ideal therapeutic target. Pharmacological agents that could selectively antagonise this integrin were soon developed. Of note, the RGD peptide mimetic Cilengitide (EMD-121974) was engineered to obstruct $\beta 3$ -integrin. Despite showing initial promise in pre-clinical models, managing to potently and selectively antagonise angiogenesis both *in vitro* and *in vivo*, Cilengitide failed to improve the overall survival of patients with aggressive glioblastoma, resulting in its failure of phase III clinical trials (151, 152).

The failure of Cilengitide was unexpected considering prior findings explicitly demonstrating $\alpha v\beta 3$ -integrin as a fundamental pro-angiogenic molecule abundantly expressed on angiogenic vasculature. The true angiogenic nature of this receptor was therefore queried. Contradicting past literature, both αv - and $\beta 3$ -null mice still underwent significant developmental angiogenesis, and the latter were viable and fertile (141, 153). Moreover, $\beta 3$ -integrin depletion was shown to enhance the micro-vessel density and growth of subcutaneous human melanoma and lung carcinoma

implants beyond that observed in WT mice (154). This integrin therefore appeared to conduct either redundant pro-angiogenic functions, or actively performed previously unseen anti-angiogenic roles under developmental and pathological scenarios. Importantly, the latter study also reported the expression of other integrins was unchanged in these mice, but that of VEGFR2 was upregulated (154). This upregulation was later determined to be a requirement for the enhanced pathological angiogenesis observed in β 3-null mice (155). Together these studies determined that β 3-integrin could regulate neovascular development by restricting the over-expression of endothelial VEGFR2. Co-targeting both β 3-integrin and VEGFR2 *in vivo* therefore inhibited angiogenesis more potently than when either was targeted individually (156). Atkinson *et al* evidenced a further anti-angiogenic role of this integrin. They determined that Rac1, a member of the Rho GTPase family and an important driver of endothelial migration, was sequestered within α v β 3-integrin containing mature FAs as a Rcc2/Anxa2/Rac1 complex, either preventing its involvement in microtubule stabilisation that would normally facilitate migration, or actively destabilising microtubules. Atkinson *et al* were unable to determine between these two possibilities. In either scenario, β 3-integrin depletion facilitated the preferential association of Rac1 and α 5 β 1-integrin, an interaction that enhanced microtubule stability and associated endothelial migration (157). This mechanism provided an explanation as to the sensitivity of tumours in β 3-null mice to Rac1 inhibition (158). Worth *et al* documented an additional mechanism by which β 3-integrin could limit α 5 β 1-integrin's enhancement of cell migration speed. They reported that by enabling the phosphorylation of vasodilator-stimulated phosphoprotein (VASP), β 3-integrin prevented association of VASP with Rap1-GTP-interacting adaptor molecule (RIAM) in FAs, a complex that would otherwise enhance β 1-integrin/talin interactions and its associated effects on migration speed (159). Further contradicting its traditional pro-angiogenic function, Cilengitide was even shown to enhance VEGF-induced pathological angiogenesis and exacerbate tumour growth when used at nanomolar concentrations. Mechanistically, these low concentrations were reported to promote recycling of both VEGFR2 and α v β 3-integrin to the plasma membrane (160).

α v β 3-integrin was therefore shown to conduct either pro- or anti-angiogenic functions depending upon the context in which it was present. Understanding when and why this integrin performed these differential roles would plausibly re-establish its therapeutic potential. To isolate the endothelial-autonomous contribution of α v β 3-integrin to angiogenesis, Steri *et al* utilised two endothelial-specific β 3-knockout mouse models. In one model endothelial β 3-integrin was constitutively depleted. Here, pathological angiogenesis was not enhanced by β 3-integrin depletion

(161). The increased neovascularisation observed by Reynolds *et al* in mice globally depleted of β 3-integrin must therefore have occurred independently of its endothelial function (154, 155). In the second model, endothelial β 3-integrin expression was temporally controlled using the PDGFb.iCreER^{T2} promoter. Its depletion immediately prior to tumour engraftment successfully inhibited tumour vascularisation and growth, though only transiently. In time, rescue mechanisms could compensate for its absence and drive angiogenesis and tumour expansion once more (161). In summary, α v β 3 appeared to conduct pharmacologically targetable pro-angiogenic functions and thus antagonising or depleting this integrin bestowed reproducible anti-angiogenic effects in tumour growth assays. However, provided sufficient time, compensatory mechanisms could account for the absence of this integrin resulting in only transient therapeutic efficacy of α v β 3-integrin antagonists.

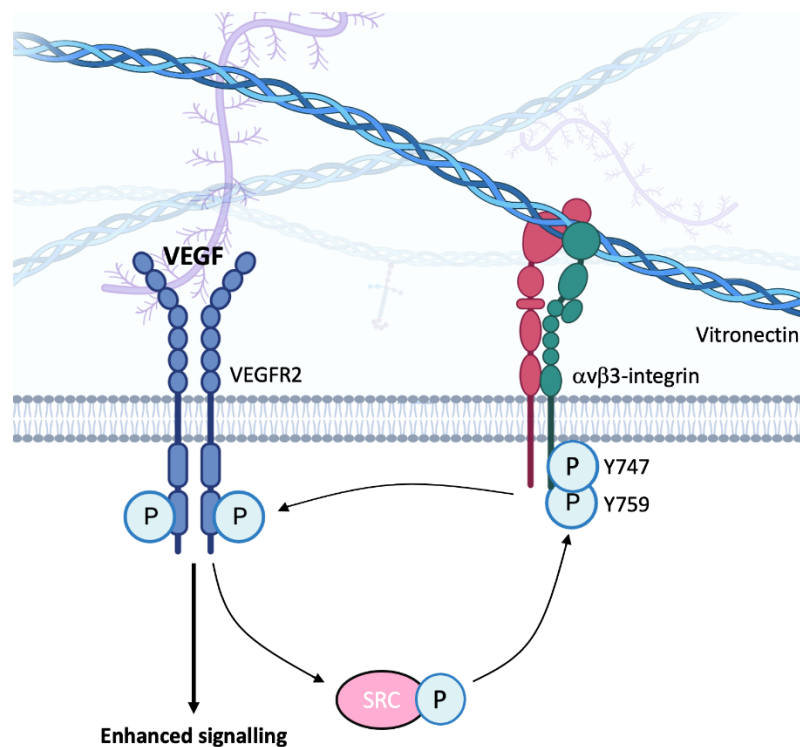


Figure 1.10 α v β 3-VEGFR2 crosstalk. VEGF-induced VEGFR2 trans-autophosphorylation of cytoplasmic tyrosine residues enables recruitment and activation of c-Src. Once active, c-Src subsequently phosphorylates the cytoplasmic tail of α v β 3-integrin at Y747 and Y759 in a vitronectin-dependent manner. Active α v β 3-integrin then forms a complex with VEGFR2, enhancing its trans-autophosphorylation and associated downstream signalling. Figure adapted from (162) using Biorender.

1.8.3 $\alpha 5\beta 1$ -integrin

Analogous to $\alpha v\beta 3$ -integrin, expression of the fibronectin receptor $\alpha 5\beta 1$ -integrin is markedly amplified on angiogenic endothelial cells and thus it was likewise assumed to conduct essential angiogenic functions (16, 163, 164). Careful consideration must also be given to its genetic manipulation. $\beta 1$ -null mouse embryos exhibit peri-implantation lethality at E4.5, not even reaching the beginning of vasculogenesis (165, 166). This severe phenotype was likely due to the wide array of α -subunits that $\beta 1$ -integrin heterodimerises with ($\alpha 1-11$ & αv) (109). Associating solely with $\beta 1$ -integrin, however, $\alpha 5$ -integrin is an ideal target for selective $\alpha 5\beta 1$ -integrin ablation. $\alpha 5$ -null mice also die during embryogenesis, though they present a significantly less severe phenotype, reaching E10-11 before cardiovascular failure (167, 168).

To isolate its endothelial-specific angiogenic involvement, conditional manipulation of $\alpha 5\beta 1$ -integrin in the endothelium was required. Predictably, constitutive endothelial-specific knockout of $\beta 1$ -integrin remained embryonically lethal, but that of $\alpha 5$ -integrin caused no observable vascular or developmental defects (169, 170). Whilst this does not refute endothelial $\alpha 5\beta 1$ -integrin's pro-angiogenic nature, it does oppose its importance to embryonic vasculogenesis and angiogenesis as previously observed in the aforementioned global knockout studies. Non-endothelial $\alpha 5\beta 1$ -integrin may instead perform crucial roles during these processes. Potentially accounting for this developmentally normal phenotype, the authors documented a redistribution of αv -integrin from its usual dissemination across the plasma membrane to FAs where $\alpha 5$ -integrin would normally be present (169). Considering endothelial $\alpha 5$ -integrin depletion had a negligible impact on endothelial cell migration or motogenic signalling pathways, αv -integrin may have been able to sustain endothelial migration through its re-distribution. Notably though, $\alpha 5$ -null endothelial cells were found to adhere poorly to fibronectin matrices resulting in reduced post-natal retinal vascularisation in mouse models, and more still, dual depletion of both $\alpha 5$ - and αv -integrin caused embryonic lethality due to defective remodelling of major vessels (169, 171). As such, αv -integrin appeared to compensate for some of $\alpha 5$ -integrin's endothelial functions to accommodate murine development, but regardless, $\alpha 5\beta 1$ -integrin retained autonomous angiogenic functions through its selective ligation with fibronectin.

More outstanding effects were observed on endothelial proliferation in the absence of $\alpha 5$ -integrin. Following hypoxia, cerebral vessels dramatically upregulate expression of both $\alpha 5\beta 1$ -integrin and fibronectin, and immunofluorescence imaging localised this upregulation to proliferative endothelial cells, circumstantially alluding to its pro-proliferative functionality (16, 172). Upregulation of this integrin also coincided with enhanced proliferation in $\beta 3$ -null brain endothelial cells, a phenomenon augmented by plating these cells on fibronectin, a matrix component previously shown to promote endothelial cell-cycle progression (138, 173, 174). This proliferative enhancement appeared to be unidirectional, as $\alpha 5$ -null brain endothelial cells showed no reciprocal increase in endothelial $\beta 3$ -integrin and presented impaired proliferation *in vitro* (175). $\alpha 5\beta 1$ -integrin therefore appeared to contribute autonomously to angiogenesis via its selective ligation with fibronectin. From a pathological perspective, its pro-angiogenic involvement was therapeutically targetable, as antibody and peptide antagonists directed against this integrin could suppress the growth of HT29 colon carcinomas (163). Despite this promising result, conditional endothelial depletion of $\alpha 5$ -integrin bestowed no beneficial effect on the growth of subcutaneously implanted lung carcinomas, even when depleted alongside αv -integrin (176). Like $\alpha v\beta 3$ -integrin, the angiogenic function(s) of endothelial $\alpha 5\beta 1$ -integrin therefore remained questioned.

1.8.4 Neuropilin-1 – a rediscovered adhesion receptor

Selective genetic manipulation of NRP1 has time and again demonstrated its function as an essential regulator of vascular morphogenesis (97, 98, 99, 100). However, these studies focused on NRP1's function as a co-receptor, with little consideration given to its originally identified role as an adhesion receptor (177).

The adhesive capabilities of NRP1 have since been investigated. Its siRNA-mediated knockdown impaired endothelial adhesion to a variety of matrices including fibronectin *in vitro*, and significantly perturbed endothelial migration in response to chemotactic signals (178). The additional roles this receptor plays as an adhesion receptor may help explain why mice depleted of VEGF₁₆₅ present less severe vascular defects than those ablated of NRP1 (179). Furthermore, knock-in mice expressing NRP1 with a mutated VEGF-binding pocket to attenuate its enhancement of VEGF signalling were viable and exhibited normal mendelian ratios at birth without any developmental vascular defects, starkly contrasting the severe vascular abnormalities and lethal

phenotype resultant of endothelial specific NRP1 ablation. This indicated that developmental angiogenesis could proceed independently of NRP1's role as a VEGFR2 co-receptor. During their post-natal development however, these mice did present with delayed retinal angiogenesis and exhibited impaired recovery following hind-limb ischaemia (99, 180). Aside from the pleiotropic functional aptitude of NRP1 as a co-receptor, its function as an endothelial adhesion receptor was gaining ground.

When investigating the endothelial-autonomous contribution of NRP1 to angiogenesis, Fantin *et al* recognised that the Cre-loxP recombination system used to ablate NRP1 left a mosaic expression pattern in which some endothelial cells were successfully ablated whilst others managed to escape recombination. Utilising this inefficiency, they revealed that any remaining NRP1-expressing endothelial cells preferentially assumed tip cell status (181). They later reported NRP1 as an essential mediator of filopodia formation in these leading cells, specifically by mediating ECM-induced activation of Cdc42. Utilising the mouse retina as a physiological model of angiogenesis, they determined that Cdc42 inhibition generated a deformed retinal vascular network analogous to that produced following NRP1 inhibition, concluding that NRP1 performed essential pro-migratory functions in endothelial cells by mediating crucial links to the ECM (182).

Raimondi *et al* later reported a novel motogenic mechanism of NRP1 independent of VEGF/VEGFR2 signalling. Specifically, NRP1 was documented to complex with the non-receptor tyrosine kinase ABL1 in a fibronectin-dependent fashion, a complex that in turn phosphorylated and activated the integrin associate paxillin. Paxillin was then able to mediate actin cytoskeletal remodelling and coordinate endothelial migration. Importantly, antagonising ABL1 inhibited both physiological and pathological retinal angiogenesis (183). NRP1 was therefore recognised as a critical regulator of endothelial adhesion and motility during angiogenesis independently of its function as a VEGFR2 co-receptor. Importantly, these newly identified adhesive and motogenic functions occurred indirectly, likely via modulation of integrin activity.

1.9 Neuropilin-1, $\alpha v\beta 3$ & $\alpha 5\beta 1$ – linking three angiogenic players

Thus far, a majority of that discussed has revolved around the independent functions of our three receptors of interest whilst occasionally alluding to some overlapping and interconnected functions during vascular formation. Mounting evidence indicated these receptors may form an angiogenic regulatory network in which both competitive and cooperative interactions occur. These interactions are outlined below and represent the base knowledge upon which this project aims to build.

1.9.1 $\alpha v\beta 3$ & $\alpha 5\beta 1$ – interconnected Integrins

Though both $\alpha v\beta 3$ - and $\alpha 5\beta 1$ -integrin conduct their own discrete functions during angiogenesis, their parallel upregulation on angiogenic endothelial cells and shared substrate mean their ligation and subsequent downstream influences on cell signalling frequently overlap (184). As such, a compensatory relationship between these two receptors seemed logical, whereby the anti-angiogenic effects resulting from antagonism or genetic targeting of one could be offset by the activity of the other and vice versa. Selective inhibition of either integrin, however, could successfully impair angiogenesis (139, 163, 185). Despite this, crosstalk mechanisms occurring between these integrins have since been elucidated.

Blystone *et al* initially reported crosstalk between these integrins. They demonstrated that antibody-mediated inhibition of $\alpha v\beta 3$ -integrin repressed the ability of leukaemia cells to perform phagocytosis, an $\alpha 5\beta 1$ -dependent process. Considering $\alpha 5\beta 1$ -mediated fibronectin adhesion remained unaffected, they postulated that $\alpha v\beta 3$ -integrin's cytoplasmic domain could modulate $\alpha 5\beta 1$ -integrin functionality (186). They later reported that $\alpha v\beta 3$ -integrin mediated this crosstalk unidirectionally via the cytoplasmic tail of its β -subunit, specifically suppressing $\alpha 5\beta 1$ -integrin's activation of calcium/calmodulin-dependent protein kinase II (187, 188). In a similar study, $\alpha v\beta 3$ -integrin antagonism inhibited the $\alpha 5\beta 1$ -mediated motility of human embryonic kidney cells towards a fibronectin stimulus (189). These early studies therefore established $\alpha v\beta 3$ -integrin as an inhibitory modulator of $\alpha 5\beta 1$ -integrin.

In contrast, Ly *et al* reported a similar, but opposite regulatory mechanism. They noted that the *de novo* expression of $\alpha 5\beta 1$ -integrin in Chinese hamster ovary (CHO) cells inhibited $\alpha v\beta 3$ -mediated adhesion and migration independently of $\alpha 5\beta 1$ -fibronectin ligation, an antagonistic effect that was ablated when $\alpha 5$ -integrin's cytoplasmic tail was replaced with that of $\alpha 4$ -integrin. Moreover, CHO cells expressing $\beta 3$ -integrin with a mutated cytoplasmic tail exhibited normal adhesion and migration even in the presence of $\alpha 5\beta 1$ -integrin (190). This study elegantly substantiated the existence of crosstalk between these integrins, establishing $\alpha 5\beta 1$ -integrin as a regulator of $\alpha v\beta 3$ -integrin affinity via a cytoplasmic interaction. As such, though the directionality of this interaction juxtaposed that found by Blystone *et al*, its mediation appeared to be similarly orchestrated by a cytosolic mechanism.

In a study more relevant to angiogenesis, $\alpha v\beta 3$ -mediated endothelial adhesion and migration on both fibronectin and vitronectin was suppressed following antagonism of $\alpha 5\beta 1$ -integrin. Considering $\alpha 5\beta 1$ -integrin can only adhere with fibronectin, the impaired endothelial motility on vitronectin indicated $\alpha 5\beta 1$ -fibronectin ligation was required for appropriate $\alpha v\beta 3$ -mediated adhesion. The authors documented an increase in protein kinase A (PKA) activity in tandem with $\alpha 5\beta 1$ -integrin antagonism, an increase that if inhibited restored $\alpha v\beta 3$ -integrin functionality (191). $\alpha 5\beta 1$ -integrin therefore appeared to enact trans-dominant effects, either antagonising $\alpha v\beta 3$ -integrin when unligated with fibronectin, or promoting it when ligated by suppressing PKA activity, the latter of which has been previously reported by Kim *et al* (192). It has since been determined that when plating cells on $\alpha 5\beta 1$ -integrin selective substrates FAs actively recruit $\alpha v\beta 3$ -integrin despite its inability to engage with the ECM, a relationship that was not mirrored on $\alpha v\beta 3$ -integrin selective substrates (193). The study by Atkinson *et al* (detailed in section 1.8.2) evidenced a further endothelial crosstalk mechanism occurring between these integrins in which the activity of Rac1 was potentiated in $\beta 3$ -null endothelial cells by engaging with $\alpha 5$ -integrin instead (157). These data indicated that $\beta 3$ -integrin would normally suppress $\alpha 5$ -integrin's engagement with Rac1 which may have contributed towards the enhanced growth of tumours and their associated vasculature in $\beta 3$ -null mice (154, 158).

1.9.2 α v β 3-integrin & Neuropilin-1

Considering the interactions between NRP1 and VEGFR2 as well as those between VEGFR2 and β 3-integrin, Robinson *et al* postulated that NRP1 may act as a junction between these two pathways. They documented that NRP1 antagonism inhibited angiogenesis more prominently when β 3-integrin was depleted. In addition, abolishing the activity of β 3-integrin's cytoplasmic tail, which mediates α v β 3/VEGFR2 interactions, resulted in enhanced VEGFR2/NRP1 association. Angiogenesis therefore appeared to become NRP1-dependent in the absence of β 3-integrin, suggesting that this integrin may negatively regulate VEGFR2/NRP1 complexation via a cytoplasmic interaction. Subsequent co-immunoprecipitation of α v β 3-integrin and NRP1 confirmed their interaction, together establishing β 3-integrin as a negative regulator of VEGFR2/NRP1 association (194).

Utilising β 3-heterozygous (het) mice which, in comparison to β 3-null mice, exhibit relatively normal levels of VEGFR2, Ellison *et al* reported that depletion of endothelial NRP1 in these heterozygous animals significantly perturbed pathological angiogenesis and tumour growth. Importantly, this confirmed that pathological angiogenesis does indeed become NRP1-dependent in the absence of β 3-integrin, but additionally suggested that even slight alterations in β 3-integrin expression could alter NRP1 functionality. Furthermore, VEGF-induced migration of β 3-het endothelial cells was also dependent upon NRP1, specifically its cytoplasmic tail. This NRP1-dependent motility was reported as a product of VEGF-induced NRP1 translocation distal from mature FAs. Once away from these sites, NRP1 was able to activate paxillin-1 which in turn promoted cytoskeletal remodelling and endothelial migration (183, 195). As such, β 3-integrin was proposed to inhibit NRP1 by mediating its retention within FAs. Coupled with findings that NRP1 and α v β 3-integrin were upregulated on numerous tumours and associated with worsened prognosis, these data indicated that β 3-integrin antagonism could sensitise angiogenesis to NRP1 inhibition. Indeed, co-targeting of these molecules was able to significantly suppress pathological angiogenesis in established tumours (195). These findings have gained weight in recent years, with NRP1/ β 3-integrin overexpression in breast cancer having been proposed as a predictive biomarker of chemotherapeutic resistance and as a potential targeting strategy (196).

1.9.3 $\alpha 5\beta 1$ -integrin & Neuropilin-1

Considering NRP1 knockdown impaired endothelial adhesion to fibronectin, crosstalk between NRP1 and the canonical fibronectin receptor seemed likely (178). Indeed, NRP1 has since been documented to directly interact with both $\alpha 5$ - and $\beta 1$ -integrin (179, 197).

The importance of these interactions for integrin-mediated matrix remodelling was demonstrated by Valdembri *et al.* Following confirmation that NRP1 interacted with $\alpha 5\beta 1$ -integrin via its cytoplasmic SEA-motif at adhesion sites via FRET analysis, they determined that NRP1 was required for $\alpha 5\beta 1$ -mediated endothelial adhesion on fibronectin as well as the fibrillogenesis of this matrix component in a VEGF-independent manner. They additionally revealed that NRP1 drove $\alpha 5\beta 1$ -integrin endocytosis and subsequent recycling to newly forming adhesive sites at the plasma membrane. Mechanistically, NRP1 stimulated integrin internalisation via recruitment of GIPC1. $\alpha 5\beta 1$ -integrin containing Rab5-positive vesicles were then recycled quickly to the plasma membrane via a GIPC1/myosin VI-mediated mechanism. siRNA-mediated knockdown of each of the molecules, namely NRP1, GIPC1 and myosin VI, impaired the ability of endothelial cells to generate a fibronectin fibrillar network (179).

Fantin and Lanahan *et al.*, however, disputed the involvement of NRP1's cytoplasmic domain in angiogenesis, demonstrating that its ablation caused no developmental cardiovascular defects (106, 198). Furthermore, Ellison and colleagues reported that depletion of NRP1's cytoplasmic tail had no detrimental angiogenic effects in a pathological setting unless $\beta 3$ -integrin was additionally depleted (195). The crosstalk mechanism outlined by Valdembri *et al.*, however, agreed with findings that endothelial NRP1 depletion compromised endothelial tip cell guidance (106, 198). Moreover, its cytoplasmic tail was linked with arteriovenous patterning (198), as mice expressing just NRP1's extracellular and transmembrane domains ($\text{NRP1}^{\text{cyto}\Delta/\Delta}$) show an abnormally high frequency of arterial-venous crossings in retinal vasculature, a phenomenon associated with branch retinal vein occlusion in humans (198). Some discrepancy therefore exists regarding the functional importance of NRP1's cytoplasmic tail to angiogenesis. Nevertheless, crosstalk between NRP1 and $\alpha 5\beta 1$ -integrin influenced endothelial interactions with fibronectin matrices which, as discussed, are vital for the appropriate progression of angiogenesis.

1.10 Research aims

To date, studies have overlooked the possibility that a trimeric receptor network may exist between $\alpha5\beta1$ -integrin, $\alpha v\beta3$ -integrin and NRP1 despite considerable effort to document paired receptor interactions. From the aforementioned literature we inferred that such a concerted network may well exist. To this end, we aimed to decipher how these receptors function in tandem or as a trio, predicting cooperative, competitive, or compensatory mechanisms occurring between them may help coordinate the complex, multi-stage process of angiogenesis.

More specifically, the aims of this project are to:

- Characterise the cellular and molecular consequences of genetically manipulating $\alpha v\beta3$ -integrin, $\alpha5\beta1$ -integrin and NRP1 in cultured endothelial cells.
- Examine the contribution of the three molecules to developmental angiogenesis.
- Test the individual and combined contributions of these receptors to pathological angiogenesis.

2 Methodologies

2.1 Chemicals & antibodies

All chemicals, unless otherwise stated, were purchased from ThermoFisher Scientific (Loughborough, UK). Details of all primary and conjugated secondary antibodies used in this thesis are listed below in tables 2.1 and 2.2.

Table 2.1 List of primary antibodies.

Antigen	Conjugate	Host	Reactivity	Supplier	Cat#/Clone#	Application
β 3-integrin	-	Rabbit	Mouse	CST	4702	WB
β 3-integrin	-	Rabbit	Mouse	Abcam	Ab75872	IF
α 5-integrin	-	Rabbit	Mouse	CST	4705S	WB
α 5-integrin	-	Rat	Mouse	Abcam	Ab25251	IF
α 5-integrin	-	Rabbit	Mouse	Abcam	Ab150361	IF
Neuropilin-1	-	Rabbit	Mouse	CST	3725	WB
Endomucin	-	Rat	Mouse	SCB	Sc-65495	WB/ECS
VE-cadherin	-	Rabbit	Mouse	Abcam	Ab205336	WB
PECAM-1	-	Rabbit	Mouse	eBioscience	48-0311-80	WB
ERG	-	Rabbit	Mouse	Abcam	Ab92513	WB
Claudin-5	-	Rabbit	Mouse	Abcam	Ab131259	WB
Prox-1	-	Rabbit	Mouse	Abcam	Ab11941	WB
Lyve-1	-	Rabbit	Mouse	abcam	Ab14917	WB
VEGFR2	-	Rabbit	Mouse	CST	2479	WB, IF
pVEGFR2 Y1173	-	Rabbit	Mouse	CST	2478	WB

FAK	-	Rabbit	Mouse	CST	3285	WB
pFAK Y397	-	Rabbit	Mouse	CST	3283	WB
Paxillin	-	Rabbit	Mouse	CST	2542	WB
pPaxillin Y118	-	Rabbit	Mouse	CST	2521	WB
Akt	-	Rabbit	Mouse	CST	9272	WB
pAkt T308	-	Rabbit	Mouse	CST	9275	WB
ERK1/2	-	Rabbit	Mouse	CST	4695	WB
pERK1/2 T202/Y204	-	Rabbit	Mouse	CST	9101	WB
HSC-70	-	Mouse	Mouse	SCB	Sc-7298	WB
β -actin	-	Rabbit	Mouse	CST	4970	WB
Rab7	-	Rabbit	Mouse	CST	2094S	IP
Rab7	Alexa-555	Rabbit	Mouse	CST	D95F2	IF
Vasculature	FITC	BS1- lectin	-	SA	L9381	IF
Collagen IV	-	Rabbit	Mouse	Abcam	Ab1908	IF
pFAK Y407	-	Rabbit	Mouse	Abcam	Ab4814	IF
Ter-119	-	Rat	Mouse	R&D	MAB1125	IF

Application key: **WB** – western blot, **ECS** – endothelial cell sorting, **IP** – immunoprecipitation, **IF** – immunofluorescence.

Supplier key: **CST** – Cell Signalling Technology, **SCB** – Santa Cruz Biotechnology, **SA** – Sigma Aldrich.

Table 2.2 List of secondary antibodies

Host	Anti-	Conjugate	Supplier	Cat#/Clone#	Application
Goat	Rabbit	HRP	Dako	P 0448	WB
Rabbit	Mouse	HRP	Dako	P 0260	WB
Donkey	Rabbit	Alexa-488	Invitrogen	A21206	IF
	Rat	Alexa-555	Invitrogen		IF
Donkey	Rabbit	Alexa-555	Invitrogen	A31572	IF
Goat	Rat	Alexa-594	Invitrogen	A11007	IF
Donkey	Rabbit	Alexa-647	Invitrogen	A31573	IF
Sheep	Rat	Dynabeads	Invitrogen	A-21100	ECS
Mouse	Biotin	-	JIL	200-002-211	CSB

Application key: **WB** – western blot, **ECS** – endothelial cell sorting, **IF** – immunofluorescence, **CSB** – cell surface biotinylation.

Supplier key: **JIL** – Jackson ImmunoResearch Laboratories Inc

2.2 Animals

The animals used were on a mixed C57/BL6;129sv background. All experiments performed were carried out in accordance with the UK Home Office regulations and the European Legal Framework for the Protection of Animals used for Scientific Purposes (European Directive 86/609/EEC). The Animal Welfare and Ethical Review Board (AWERB) committee at the University of East Anglia, School of Biological Sciences approved this study.

2.3 Breeding

PDGFb.iCreER^{T2} mice, provided by Marcus Fruttiger (UCL, London, UK), were crossed with mice floxed at our genes of interest to achieve inducible, endothelial specific depletion of our targets (199). This cross was initially performed between PDGFb.iCreER^{T2} mice and those with a single floxed target, whether it be: α 5-integrin floxed mice (169) (loxP sites flanking exon 1 of ITGA5) provided by Professor Richard Hynes (MIT), β 3-integrin floxed mice (200) (loxP sites flanking exon 1 of the ITGB3 gene) provided by Professor Kathy Weilbaecher (Washington University), or NRP1-

floxed mice (99) (loxP sites flanking exon 2 of the NRP1 gene) purchased from The Jackson Laboratory (Bar Harbor, Maine, USA). These single endothelial inducible knockout mice ($\beta 3^{fl/fl}$.PDGFb.iCreER^{T2}, $\alpha 5^{fl/fl}$.PDGFb.iCreER^{T2} and NRP1^{fl/fl}.PDGFb.iCreER^{T2}) were then crossed to obtain each double and triple combinatory floxed line ($\beta 3/\alpha 5^{fl/fl}$.PDGFb.iCreER^{T2}, $\beta 3/NRP1^{fl/fl}$.PDGFb.iCreER^{T2}, $\alpha 5/NRP1^{fl/fl}$.PDGFb.iCreER^{T2} and $\beta 3/\alpha 5/NRP1^{fl/fl}$.PDGFb.iCreER^{T2}). Expression of PDGFb.iCreER^{T2} was limited to breeding males to ensure that both Cre-positive and Cre-negative littermates were obtained. This was essential as Cre-negative offspring were used as the littermate controls for *in vivo* experiments to avoid bias due to the precise age or genetic background of each mouse.

2.4 Genotyping

To confirm the genetic status of each animal line within the colony (both floxing and PDGFb.iCreER^{T2} status), and to circumvent any unintentional crossbreeding between lines, all new breeding pairs and their first litters were subject to DNA genotyping from ear biopsies (this included genotyping for every allele carried in the Robinson Lab). Likewise, the genetic status of experimental animals was also confirmed from tail biopsies following their experimental endpoint.

2.4.1 DNA preparation

Ear/tail biopsies from mice were digested overnight at 56°C in lysis buffer (100 μ l) (Tris-HCl (50 mM, pH 8.5), EDTA (10 mM, pH 8.0), NaCl (100 mM) and SDS (0.2%)) containing proteinase K (100 μ g/ml – Sigma Aldrich) in separate wells of a 96-well PCR plate (Fisher Scientific). DNA was subsequently precipitated by adding isopropanol (100 μ l) to each well, agitating the plate, and centrifuging it at 1400 \times g for 30 minutes. Following careful removal of isopropanol by plate inversion, the DNA pellet was dried at 37°C. TE buffer (200 μ l) (Tris-HCl (10 mM, pH 7.5) and EDTA (1 mM)) was subsequently added to each well to resuspend the DNA. The PCR reactions described below were later performed in a 96-well block thermal cycler PCR machine (Bioer Technology, Binjiang, China).

2.4.2 PCR reactions

To analyse the floxed alleles of our three receptors of interest (β 3-integrin, α 5-integrin and NRP1) and that of the PDGFB-driven Cre-recombinase allele (PDGFB.iCreER^{T2}) via PCR, the following were combined and loaded into 96-well plates: DNA (0.5 μ l), MegaMix-Blue (10 μ l) (Microzone – Client Life Sciences: 1.1X reaction buffer containing Taq polymerase, 2.75 mM MgCl₂, 220 μ M dNTPs, and blue agarose loading dye), and 0.08 μ l of forward (F) and reverse (R) primers at a final concentration of 0.8 μ M from a 100 μ M stock. After loading the reaction mixes into 96-well PCR plates, 96-well block thermal cycler PCR machines were used to perform the PCR reactions. The specific oligonucleotide primers, thermal cycler reaction conditions required for amplification of β 3-integrin, α 5-integrin, NRP1 and PDGFB.iCreER^{T2} alleles as well as the PCR products of each reaction are detailed in table 2.3.

Table 2.3 Oligonucleotide primers and PCR reaction conditions used for each gene.

Gene	Oligonucleotide Primers		Amplification Programme	PCR Products
β3-integrin	F:	5' – TTGTTGGAGGTGAGCGAGTC – 3'	95°C 2mins 95°C 30secs 56°C 35x { 90secs 72°C 1min 72°C 8mins 4°C Indefinitely	Floxed: 182-bp Wildtype: 272-bp
	R:	5' – GCCCAGCGGATCTCCATCT – 3'		
α5-integrin	HT030:	5' –GCAGGATTTTACTCTGTGGGC– 3'	95°C 5mins 94°C 30secs 60°C 35x { 90secs 72°C 1min 72°C 10mins 16°C Indefinitely	Floxed: 821-bp Wildtype: 694-bp Excised: 501-bp
	HT0311:	5' –TCCTCTGGCGTCCGGCCAA– 3'		
	HT032:	5' –GAGGTTCTTCCACTGCCTCCTA– 3'		
Neuropilin-1	F:	5' –AGGTTAGGCTTCAGGCCAAT– 3'	94°C 3mins 94°C 30secs 65°C 35x { 1min 72°C 1min 72°C 10mins 16°C Indefinitely	Floxed: 738-bp Wildtype: 550-bp
	R:	5' –GGTACCCTGGGTTTTTCGATT– 3'		
Neuropilin-2	F (WT) a:	5' –CAGGTGACTGGGGATAGGGTA– 3'	94°C 2mins 94°C 20secs 65°C (-0.5°C) 10x touch down { 15secs 68°C 10secs 94°C 15secs 60°C 28x { 15secs 72°C 10secs 72°C 2mins 16°C Indefinitely	Floxed: 700-bp Wildtype: 400-bp
	R (common)	5' –AGCTTTTGCCTCAGGACCCA– 3'		
	a+b:			
	F (fl/fl) b:	5' –CCTGACTACTCCCAGTCATAGT– 3'		
PDGFβ.iCreER ^{T2} &	F:	5' –GCCGCCGGGATCACTCTC– 3'	94°C 4mins 94°C 30sec 57.5°C 34x { 45sec 72°C 1min 72°C 10mins 4°C Indefinitely	PDGFβ Positive: 443-bp β2-M: 300-bp
	R:	5' –CCAGCCGCCGTCGCAACT– 3'		
β2-Microglobulin (Internal control)	F:	5' – CACCGGAGAATGGGAAGCCGAA – 3'	72°C 1min 72°C 10mins 4°C Indefinitely	
	R:	5' – TCCACACAGATGGAGCGTCCAG – 3'		

Primer key: **F** – Forward, **R** – Reverse

2.4.3 Agarose gel electrophoresis

The PCR products for each reaction mentioned above were separated on a 1.8% agarose gel made via the following method: agarose (5.4g) (Fisher Scientific, Loughborough, UK) was dissolved in

dH₂O (250 ml) by microwaving for 2-3 minutes. More dH₂O (44 ml) was subsequently added to the dissolved agarose to cool the solution. This was supplemented with 50X TAE buffer (6 ml) (Tris (0.5 M), acetic acid (1 M) and EDTA (50 mM, pH 8.0)) and ethidium bromide (8 µl) (Fisher Scientific). This solution was then poured into a gel tank (Alpha Laboratories, Eastleigh, UK) containing the well forming combs appropriate for the number of PCR samples to be run. Once set, each PCR sample (~10 µl) was loaded into the wells and separated at 90V for 1 hour, or 90V for 90 minutes when running the α 5-integrin reaction. Images of the separated DNA bands captured using a BioDoc-It Transilluminator (UVP, Cambridge, UK) under UV light.

2.5 Tamoxifen preparation

Tamoxifen (Sigma-Aldrich) to be used for *in vivo* administration was dissolved in ethanol (200 mg/ml). It was subsequently mixed with corn oil (to provide a final concentration of 20 mg/ml) and shaken at ~180 rpm at 55°C for 6 hours. Once fully dissolved, aliquots were stored in light-blocking Eppendorfs at -20°C.

2.6 Retinal angiogenesis assay

Tamoxifen (20 mg/ml) was diluted in corn oil (2 mg/ml) and administered via one of two possible regimes. One entails two subcutaneous injections (50 µl) at P2 and P3 followed by two intraperitoneal injections (50 µl) at P4 and P5. Mice were then sacrificed at either P6 or P18. The second tamoxifen administration regime was delayed until P7 when the first of four daily intraperitoneal injections (50 µl) was administered, concluding on P10 before subsequent sacrifice and retina harvest on P12. The type of regime used is specified where appropriate. Under either regime both Cre-negative and Cre-positive littermates received tamoxifen. Following enucleation, eyes were fixed in 4% PFA for 1 hour at 4°C, washed in 2X PBS for 30 minutes at 4°C before retinal dissection. Once removed, each retina was partially cut into four leaflets, allowing it to be flattened before MeOH (100%) fixation for 20 minutes at -20°C. Retinas were subsequently permeabilised in 0.25% triton X-100/PBS for 30 minutes, washed in PBLEC (1X PBS, 1% Twene-20, CaCl₂ (0.1 mM), MgCl₂ (0.1 mM), MnCl₂ (0.1 mM)) for a further 30 minutes and then blocked in DAKO protein block (Agilent, X090930-2) for 1 hour. Retinas were then incubated overnight at 4°C in PBLEC with the appropriate primary antibody diluted in PBS: FITC-BS1-Lectin (Sigma Aldrich, L2895, 1:250),

endocan/ESM-1 (R&D, AF1999, 1:1000), collagen IV (Abcam, ab19808, 1:500), pFAK Y407 (Ab4814, 1:200), α 5-integrin (Ab25251, 1:250). Following two 20-minute washes in 0.1% triton X-100/PBS retinas were incubated with the appropriate Alexa[®] fluor secondary antibody diluted 1:500 in PBLEC for 2 hours at room temperature (RT). Retinas were subsequently flat mounted onto positively charged coloFrost[™] glass slides and coated with Fluoromount-G[™].

2.6.1 Image acquisition & processing

All retinal flat mounts were imaged with a Zeiss LSM880 Airyscan confocal microscope with ZEN Black software (Zeiss). FIJI-ImageJ[™] and Angiotool[™] (201) were used for image processing.

2.6.2 Retinal morphometric analysis

2.6.2.1 Vascular extension

High resolution images (1.204 pixels per micron) of FITC-BS1-lectin labelled retinal flat mounts were acquired at 10X magnification using ZEN Black's tile scan function. Radial outgrowth of retinal vasculature at P6, P12 and P18 was quantified by measuring the distance from the optic nerve head to the vascular periphery thrice per leaflet. Leaflet means were then averaged to give the mean radial outgrowth per retina before being presented as a relative percentage of the outgrowth quantified from Cre-negative control littermates.

2.6.2.2 Vascular density & branching

Retinal vascular density at P6 was measured from FITC-BS1-lectin-stained retinal flat mounts using Angiotool[™]. Three 450 μ m x 450 μ m fields were imaged at both the vascular periphery and vascular interior. These images were taken between an artery and a vein and 100 μ m from the vascular front and 400 μ m from the central retinal artery respectively. Vascular quantification was subsequently performed using Angiotool[™]. Vascular density values (FITC-BS1-lectin-positive area/total measured area) and the number of branching points were averaged before being presented as a relative percentage of that measured from Cre-negative control littermates. Vascular branching values were then made relative to their respective vascular density values to account for any

mirrored changes between the two. At P12 and P18, 850 μm x 850 μm z-sections were taken using ZEN Black's Z-stack function at 10X magnification in the centre of three leaflets per retina between an artery and a vein and equidistant from the vascular front and central retinal artery. Using the Z-projection function in FIJI-ImageJ™, images of the superficial, intermediate, and deep plexuses were isolated from these z-sections and analysed using Angiotool™. Measurements from each respective plexus were averaged across the three z-sections to give the average vessel density of each plexus per retina. As before, vascular density was then presented as a relative percentage of Cre-negative control littermates.

2.6.2.3 Vessel regression

Vessel regression was measured at P6 in FITC-BS1-lectin and collagen IV co-stained retinal flat mounts. Regressed vessels (FITC-BS1-lectin-negative and collagen IV-positive) were enumerated manually from three 200 μm x 200 μm fields per retinal leaf, taken between an artery and a vein and 100 μm from the vascular periphery. Leaflet means were then averaged to give the average number of regressed vessels per retina. Vessel regression was then presented as a relative percentage of Cre-negative control littermates.

2.6.2.4 Sprout enumeration

Endothelial sprouts, defined as morphological tip/stalk cell structures protruding from the retinal vascular front, were enumerated across each retinal leaflet before being divided by their respective leaflet vascular perimeter to account for varying vascular extension between groups. Leaflet values were subsequently averaged to arrive at retina means before being made relative to that calculated in their Cre-negative control littermates.

2.6.2.5 Filopodial analysis

Filopodia projections from 100 sprouts across 5 retinas per group (20 sprouts per retina) were enumerated manually, quantified from 200 μm x 200 μm fields imaged at 40X magnification at the retinal vascular periphery. These values were averaged per sprout, and subsequently per retina. To

perform the appropriate statistical analysis these data were not relativised to Cre-negative control littermates, but instead visualised alongside their respective controls as raw values. Filopodia tortuosity was calculated using FIJI-ImageJ™ by dividing the linear base-end distance of filopodia projections by their true length. For this analysis, 150 filopodia were measured from sprouts across 5 retinas per group. These data, which revealed both filopodial length and tortuosity, were again presented as raw values.

2.6.2.6 Corrected total cell fluorescence

pFAK Y407 and α 5-integrin intensity was calculated using FIJI-ImageJ™ within protruding sprouts by measuring corrected total cell fluorescence (CTCF), which was calculated via the following formula: (IntDen-Area) x background IntDen (QBI, The University of Queensland, Australia). Protruding sprout CTCF values were then normalised to that of their trailing perpendicular vasculature. A total of 25 sprouts were analysed across 5 retinas per group.

2.7 Mouse lung microvascular endothelial cell isolation

Primary lung endothelial cells were isolated from mice 3 to 6 weeks of age as described previously (202). Mice were sacrificed by cervical dislocation before their lungs were aseptically removed and collected in Mouse Lung Endothelial Cell media (MLEC – 1:1 Ham's F12:DMEM (low-glucose) (Invitrogen) supplemented with 20% foetal bovine serum (FBS); penicillin/streptomycin (100 units/ml) (Invitrogen), L-glutamine (2 mM) (Sigma-Aldrich), heparin (50 μ g/ml), endothelial mitogen (25 mg) (AbD Serotech)). Following extraction and a single rinse in 70% ethanol, lungs were returned to fresh MLEC media and homogenised with scalpels before digestion for 1 hour at 37°C in PBS supplemented with the following: Ca^{2+} and Mg^{2+} (1 mM), 0.1% Collagenase I (Gibco), 0.01% DNase I (Sigma-Aldrich). The digestion solution was agitated every 15 minutes. Following this the digests were aspirated three times through a 19G needle (Medisave) and once through a 21G needle (Medisave) before filtration through a 70 μ m sterile strainer. Subsequent centrifugation of filtrates at 260 x g for three minutes generated a pellet that was resuspended in MLEC media and seeded into a T75 flask pre-coated with the following solution: 0.1% gelatin containing fibronectin (10 μ g/ml) and collagen (COL I) (10 μ g/ml), and incubated at 37 °C, 5% CO₂, 95% humidity. Two PBS washes were performed the following day to remove erythrocytes and cellular debris. The cells

were then left in fresh MLEC media until reaching ~80% confluency before positively sorting for endomucin expression using Magnetic-Activated Cell Sorting (MACS) as described previously (202). Briefly, flasks were pre-cooled at 4°C for 20 minutes before incubation with rat-anti-mouse endomucin (1:1000 in PBS) (Santa Cruz) for 30 minutes at 4°C. Following a single PBS wash the cells underwent a further incubation in sheep-anti-rat IgG coated magnetic beads (1:1000 in MLEC) (Invitrogen) for 30 minutes at 4°C. After three PBS washes, the cells were detached using 0.25% trypsin-EDTA, resuspended in MLEC media and placed into a magnetic rack for 3 minutes. The supernatant was then discarded, and the endothelial cells bound to the magnetic beads were resuspended in MLEC media before being seeded into T25 flask pre-coated as described previously. Once confluent a second positive sort for endomucin was performed to ensure a pure endothelial isolation.

2.8 Endothelial cell immortalisation

Transfection of primary endothelial cells with polyoma-middle-T-antigen (PyMT) retrovirus was employed to override cellular senescence, thereby enabling greater cellular expansion and reduce the need for repeated re-isolation of primary endothelial cell cultures. As described previously by Robinson *et al*, newly isolated primary endothelial cell cultures were treated with PyMT conditioned media supplemented with polybrene for 6 hours at 37°C, 5% CO₂ and 95% humidity before returning to MLEC media overnight (194). Treatment with PyMT conditioned media was repeated the next day, but cells were instead kept in Immortalised Mouse Lung Endothelial Cell media (IMMLEC – 1:1 Ham's F12:DMEM (low glucose) supplemented with 10% FBS; penicillin/streptomycin (100 units/ml), L-glutamine (2 mM), heparin (50 µg/ml)). Immortalised endothelial cells were then expanded and frozen down for later use.

2.9 TAT-Cre recombinase nucleofection

To excise our target genes of interest from the immortalised lung microvascular endothelial cells described, 1.5×10^6 cells were resuspended in homemade nucleofection buffer (100 µl) (HEPES (200 mM), NaCl (137 mM), KCl (5 mM), D-glucose (6 mM) and Na₂HPO₄ (7 mM)) and nucleofected with TAT-Cre recombinase (70 units) (Sigma-Aldrich) using the Amaxa Nucleofector II (Amaxa Biosystems) according to nucleofection programme T-005. Nucleofected cells then entered a 10-

minute recovery period in pre-warmed IMMLC media prior to seeding into T25 flasks pre-coated with 0.1% gelatin containing fibronectin (10 µg/ml) and collagen (COL I) (10 µg/ml) before being incubated overnight at 37°C, 5% CO₂, 95% humidity. This nucleofection protocol was repeated the following day on the surviving cells and seeded once again into T25 flasks pre-coated as before. Once these cells had been successfully expanded, some cells were frozen down for later use whilst others were used to acquire lysate for confirmation of endothelial identity and target depletion.

2.10 Routine cell culture & experimental matrix flask coating

Following their isolation, immortalised, TAT-Cre nucleofected cell cultures were incubated at 37°C, 5% CO₂ and 95% humidity on plates pre-coated with 0.1% gelatin (Porcine skin type A – Sigma-Aldrich) made up in dH₂O for 20 minutes at 37°C. Flask coatings used for primary endothelial cell culture were additionally supplemented with PureCol (10 µg/ml – Nutacon B.V.) and human plasma fibronectin (10 µg/ml – Sigma-Aldrich). Human plasma fibronectin diluted in PBS (10 µg/ml) was used to coat experimental plates as indicated in the relevant sub-sections below unless an alternative concentration is otherwise stated. Coating was achieved by incubating the dishes for 1 hour at 37°C, 5% CO₂, 95% humidity. Cell detachment for routine sub-culturing was achieved using 0.25% Trypsin-EDTA solution (Sigma-Aldrich).

2.11 Western blotting

To obtain lysates, cells were lysed in electrophoresis sample buffer (ESB – Tris-HCl (65 mM, pH 7.5), sucrose (60 mM) and SDS (3%)) using an Eppendorf tip to scrape the cells from the surface of the plate. Once transferred to safe-lock Eppendorf tubes containing acid-washed glass beads (Sigma) the lysates were homogenised in a tissue lyser (Qiagen) at 50 Hz for 2 minutes before centrifugation at 16,500 x g for 10 minutes. Protein concentration was quantified using the BioRad DC protein assay and each sample (30 µg) was then reduced by addition of appropriate volumes of NuPAGE 10X sample reducing agent and 4X LD sample buffer (Life Technologies) to reach a final concentration of 1X. Prior to gel loading alongside molecular mass protein markers, samples were heated at 95°C for 5 minutes. Once loaded into 8% polyacrylamide gels, made in-house, they underwent 1.5 hours of SDS-PAGE at 100 volts in 1X running buffer (dH₂O (90%), 10X running buffer (10%) (glycine (1.92 M), Tris-Base (250 mM) and SDS (1%) in dH₂O (1 L)). Following separation,

proteins were transferred to a 0.45 μm Amersham Protran nitrocellulose membrane (GE Healthcare, Amersham) for 3 hours at 30 volts in 1X transfer buffer ((dH₂O (70%), methanol (20%) and 10X transfer buffer (10%) (glycine (1.92 M) and Tris-Base (250 mM) in dH₂O (1 L)). Following transfer, the membrane was blocked for 1 hour in 5% milk powder prepared in 0.1% Tween-20/PBS (PBST 0.1%) before incubation with the primary antibody (diluted 1:1000 in 5% milk blocking solution except for Heat Shock Protein-70 (HSC-70) and β -actin, which were diluted 1:2000) overnight at 4°C. After three 5-minute washes in PBST 0.1% the membranes were incubated in the appropriate horseradish peroxidase (HRP)-conjugated secondary antibody (diluted 1:2000 in 5% milk blocking solution) for 2 hours at RT in the dark. Following a further three 5-minute washes in PBST 0.1% a 1:1 solution of Pierce ECL Western Blotting Substrates was applied to the membranes and chemiluminescence was detected using a ChemiDoc XRS+ (Bio-Rad). Densitometric readings were quantified using FIJI-ImageJ™.

2.12 VEGF signalling assays

To investigate endothelial responses to VEGF challenge, endothelial cells were seeded onto 10 cm dishes (1.5×10^6 cells per dish) pre-coated with fibronectin in PBS (10 $\mu\text{g}/\text{ml}$). After 24 hours, cells were washed once with pre-warmed PBS and incubated for 3 hours in serum-free medium (Opti-MEM™ – Invitrogen). Following starvation, the endothelial cells were incubated with VEGF-A₁₆₄ (the murine equivalent of VEGF-A₁₆₅) (30 ng/ml), made in-house as previously described by Krilleke *et al* (203), for the specified durations. The plates were put on ice at the designated time point, the endothelial cells washed twice with PBS, lysed in ESB and subjected to western blotting analysis.

2.13 Cell surface biotinylation assay

Endothelial cells were seeded onto two 10 cm dishes (1.5×10^6 per dish) pre-coated with fibronectin in PBS (10 $\mu\text{g}/\text{ml}$). After 24 hours the endothelial cells were incubated for 3 hours in serum-free medium (Opti-MEM™ – Invitrogen) after which they were placed on ice for 5 minutes and moved to the cold storage room (4°C). Following two washes with ice-cold Soerensen buffer (SBS – KH₂PO₄ (14.7 mM), Na₂HPO₄ (2 mM) and Sorbitol (120 mM)) pH 7.8 the endothelial cells were labelled with 0.3 mg/ml biotin (Thermo Scientific) prepared in SBS pH 7.8 for 30 minutes at 4°C. Glycine (100 mM) was subsequently used to quench unreacted biotin for 10 minutes at 4°C. All dishes were then

washed with ice-cold SBS pH 8.2 before a single control dish from each genotype was incubated with mercaptoethanesulfonate (100 mM) (Sigma) prepared in strip buffer (Tris-HCl (50 mM), NaCl (100 mM)) for 75 minutes at 4°C. Remaining dishes were left in SBS pH 8.2 on ice. Excess mercaptoethanesulfonate was quenched with Iodoacetamide (100 mM) (Sigma) prepared in strip buffer for 10 minutes at 4°C before two further washes with SBS pH 8.2. All dishes were then lysed in biotinylation lysis buffer (Tris-HCl pH 7.4 (25 mM), NaCl (100 mM), MgCl₂ (2 mM), Na₃VO₄ (1 mM), EGTA (0.5 mM), Triton X-100 (1%), glycerol (5%), and 100X Halt protease inhibitor cocktail (1X)). Lysates were cleared by centrifugation at 12,000 x g for 20 minutes at 4°C and the supernatant protein concentration then quantified using the BioRad DC protein assay before subsequent immunoprecipitation with Dynabeads™ Protein G (Invitrogen) coupled to mouse anti-biotin antibody overnight at 4°C. The immunoprecipitated biotin-labelled cell surface proteins were then prepared for western blotting analysis in NuPAGE 10X sample reducing agent and 4X LD sample buffer at a final concentration of 1X as described previously (Methods – 2.11).

2.14 Co-immunoprecipitation assays

Endothelial cells were seeded onto 10cm dishes (2x10⁶ per dish) pre-coated with fibronectin in PBS (10 µg/ml) and incubated for 24 hours. These dishes were then placed on ice and the endothelial cells were subsequently lysed with biotinylation lysis buffer described above (Methods – 2.13) before protein was quantified using the DC BioRad assay. 500 µg of protein per sample was incubated with protein-G coupled Dynabeads® (Invitrogen) resuspended in 0.02% Tween-20/PBS (PBST 0.02%) that had been coupled with the appropriate primary antibody. To couple Dynabeads® with primary antibodies, Dynabead® solution was first removed using a magnetic tube stand (20 µl per sample in separate Eppendorf tubes) before resuspending them in PBST 0.02% (200 µl) and adding the primary antibody (3 µl per Eppendorf). The solution was then gently agitated via continuous inversion for 10 minutes at RT. Using the magnetic tube stand to isolate the antibody coupled Dynabeads® they were subsequently resuspended in biotinylation lysis buffer (20 µl per Eppendorf) ready for incubation with each lysate. Lysates were then incubated overnight at 4°C on a rotator. Three washes in the aforementioned lysis buffer (0.5 ml per wash per sample) were performed by gentle pipetting before pelleting the magnetic beads with a magnetic tube stand. One wash in PBS eluted any immunoprecipitated complexes. Samples were then prepared for western blotting analysis in NuPAGE 10X sample reducing agent and 4X LD sample buffer at a final concentration of 1X as described previously (Methods – 2.11).

2.15 Immunocytochemistry

Endothelial cells were seeded onto acid-washed, oven-sterilised coverslips (2.5×10^4 cells per coverslip) pre-coated with fibronectin in PBS (10 $\mu\text{g}/\text{ml}$) and incubated for 3 hours in serum-free media (Opti-MEM™ – Invitrogen). Following two PBS washes the cells were fixed in 4% PFA for 10 minutes at RT. Two additional PBS washes were then performed to remove excess fixative. Coverslips were then blocked in 0.3% triton X-100/PBS supplemented with 10% goat serum for one hour at RT before overnight incubation at 4°C in the appropriate primary antibody diluted in PBS: VEGFR2 (CST, 2479, 1:100), Rab7 (CST, D59F2, 1:250). The following day three PBS washes were performed before incubation in the suitable secondary antibody (1:200 in PBS) for two hours at RT in the dark. After an additional three washes in PBS the coverslips were mounted onto cover-slides with Fluoromount-G™ containing DAPI (Invitrogen). DAPI was not shown in representative images because it can obscure peri-nuclear endosomes. For image acquisition the Zeiss AxioImager M2 microscope (AxioCamMRm Camera) at 63X magnification with oil immersion.

2.16 MG-132 treatment

Endothelial cells were seeded onto 6 cm dishes (1×10^6 cells per dish) pre-coated with fibronectin in PBS (10 $\mu\text{g}/\text{ml}$). After 24 hours, cells were washed once with pre-warmed PBS and incubated for 3 hours at 37°C, 5% CO₂ and 95% humidity in serum-free medium (Opti-MEM™ – Invitrogen) supplemented with MG-132 (ab141003 – Abcam) (10 $\mu\text{mol}/\text{L}$). VEGF-A₁₆₄ (30 ng/ml) was then added to the media for the indicated durations before the plates were put on ice, the endothelial cells washed twice with PBS, lysed in ESB and subjected to western blotting analysis as described previously (Methods – 2.11).

2.17 Chloroquine treatment

Endothelial cells were seeded onto 6 cm dishes (1×10^6 cells per dish) pre-coated with fibronectin (10 $\mu\text{g}/\text{ml}$) in PBS. After 24 hours, cells were washed once with PBS and incubated at 37°C, 5% CO₂ and 95% humidity in serum-free medium (Opti-MEM™ – Invitrogen) supplemented with

chloroquine diphosphate salt (Sigma – C6628-25G) (50 $\mu\text{mol/L}$) for the specified durations before the plates were put on ice, the endothelial cells washed twice with PBS, lysed in ESB and subjected to western blotting analysis as described previously (Methods – 2.11).

2.18 ATN-161 treatment

Endothelial cells were seeded onto 6 cm dishes (1×10^6 cells per dish) pre-coated with fibronectin in PBS (10 $\mu\text{g/ml}$). After 24 hours, cells were washed once with PBS and incubated at 37°C, 5% CO_2 and 95% humidity in serum-free medium (Opti-MEM™ – Invitrogen) supplemented with ATN-161 at the indicated concentrations and in the presence or absence of MnCl_2 (2 mM) for 1 hour before the plates were put on ice, the endothelial cells washed twice with PBS, lysed in ESB and subjected to western blotting analysis as described previously (Methods – 2.11).

2.19 Adhesion assay

Endothelial cells were seeded into 96-well plates (3×10^4 per well) that had previously been pre-coated with fibronectin in PBS (2 $\mu\text{g/ml}$) and blocked in 1% BSA/PBS for 1 hour. They were left to adhere for 3 hours in serum-free medium (Opti-MEM™ – Invitrogen) supplemented with ATN-161 (10 mM). Three PBS washes were then performed to remove unattached cells. Adhered cells were then fixed used 4% PFA for 10 minutes. A single PBS wash was used to remove excess fixative before staining adhered cells with methylene blue (methylene blue (1%), borate (10 mM), MeOH (50%), pH 8.5). To remove excess methylene blue the plates were agitated under dH_2O . Following an air-drying period of 20 minutes wells were incubated for 10 minutes in de-stain solution (100 $\mu\text{l/well}$) (50% EtOH, 50% 0.1 M HCl). Absorbance at 630 nm was then read using the VersaMax spectrophotometer (Molecular Devices).

2.20 CMT19T tumour growth assays

Intraperitoneal injections of tamoxifen (75 mg/kg bodyweight, 20 mg/ml stock) (Jackson Laboratory Protocol, Bar Harbor, Maine, USA) were administered thrice weekly for the duration of each experiment from day (D) -4 (i.e 4 days prior to tumour cell implantation) to D 18. CMT19T lung

carcinoma cells (CR-UK Cell Production) were cultured in DMEM (high glucose, supplemented with 10% FBS, pen/strep (100 unit/ml)) prepared in PBS (1×10^6 per 100 μ l) and implanted into the flanks of animals subcutaneously at D0. Tumour growth was tracked using clipper measurements from D10 until the end of the experiment on D18 when they were removed, their volume calculated ($\text{length} \times \text{width}^2 \times 0.52$), and subsequently snap frozen in liquid nitrogen before being stored at -20°C for later analysis (204).

2.21 Tumour section immunofluorescence & imaging

Using the Cryostat HM-560 (Microm) frozen tumours were sectioned into 6 μm sections and mounted onto positively charged coloFrostTM glass slides. These slides were then air dried at RT for 10 minutes before being fixed in 4% PFA for a further 10 minutes at RT and subsequently washed twice in 0.3% Triton X-100/PBS and twice in PBLEC (1X PBS, 1% Tween-20, CaCl_2 (0.1 mM), MgCl_2 (0.1 mM), MnCl_2 (0.1 mM)). Sections were then blocked in DAKO serum-free protein block (Aligent) for 30 minutes before overnight incubation at 4°C with the appropriate primary antibody diluted in PBS: Endomucin (Santa-Cruz, Sc-65495, 1:500), VEGFR2 (CST, D95F2, 1:250) Sections were washed in 0.3% Triton X-100/PBS and PBLEC the following day before incubation in the appropriate Alexa fluor secondary antibody for 2 hours at RT in the dark. Sections were then blocked using Sudan Black (0.1 % in 70 % EtOH) for 5 minutes to quench auto-fluorescence and rinsed with dH_2O before being mounted with Fluoromount-GTM with DAPI (Invitrogen).

All tumour microscopy was then performed using a Zeiss AxioImager M2 microscope (AxioCamMRm Camera) at 20X magnification. Blood vascular density was measured by enumerating endomucin-positive vessels per mm^2 from three representative ROIs per section averaged over 2 sections per tumour. Values were then normalised to that calculated in their Cre-negative control tumours.

2.22 Statistical analysis

With the exception of filopodial number, length and tortuosity as well as $\alpha 5$ -integrin CTCF retinal analysis, analysis of Cre-positive mutants was performed by expressing data values relative to the

average value of their Cre-negative control littermates, which were normalised to 100%. The exceptions were presented as raw values alongside that of their respective Cre-negative control. Statistical significance between mutants and their respective Cre-negative controls was determined using a Student's t-test. Statistical significance between each Cre-positive mutant line was achieved using an ordinary one-way ANOVA with post-hoc Tukey multiple comparison test. All analysis was performed using GraphPad Prism 9. All data is presented using 'superplots' (205), where individual technical replicates (dots) are displayed and colour correlated with their overall mean, or biological replicate (triangles/squares). Bars represent the mean of biological replicates, with error bars displayed as standard error of the mean (SEM). Asterisks represent P values as follows: *=P<0.05, **=P<0.002, ***=P<0.0005, ****=P<0.0001.

3 Developing, maintaining, and validating the tools required to investigate how $\alpha v\beta 3$ -integrin, $\alpha 5\beta 1$ -integrin and neuropilin-1 regulate angiogenesis.

The involvement of $\alpha v\beta 3$ -integrin, $\alpha 5\beta 1$ -integrin and NRP1 in angiogenesis has been widely researched and revealed both cell-type and context specific angiogenic functions of each individual receptor (163, 206, 207). Previously we have discussed studies focussing on the pairwise receptor interactions which identified various crosstalk mechanisms essential to their functionality (179, 188, 195). We believe that to fully resolve the angiogenic function of these receptors, the interactions occurring between them must be considered as integral to their overall angiogenic contribution. We hypothesise that $\alpha v\beta 3$ -integrin, $\alpha 5\beta 1$ -integrin and NRP1 interact as a trio, and that the interactions occurring between them can be cooperative, competitive, and compensatory in nature depending on the angiogenic scenario in question.

To pick apart when and how these receptors interact to govern angiogenic processes we required suitable *in vivo* and *in vitro* model systems. We took a classical genetic approach to dissecting our proposed receptor network, using a spatiotemporal method of target depletion through which we could deplete our targets individually, in duplicate and in triplicate to assess the effects of each receptor combination on various aspects of sprouting angiogenesis.

3.1 Breeding strategy and best practise for the generation and maintenance of genetically engineered mouse models.

Genetically engineered mice are a favoured model for investigating both human physiology and pathology by virtue of their genetic and physiological similarities. Amongst the catalogue of tools that now exist for mammalian gene editing, we have utilised the Cre-*loxP* system to investigate our proposed receptor network. In addition to its provision of efficient recombination, this system may deliver spatial and/or temporal control over Cre-recombinase activity (Fig 3.1). Each of our three receptors of interest have been targeted previously via this method using endothelial promoters of Cre-recombinase to confer tissue specificity (99, 161, 169). However, despite restricting target deletion to the endothelium, constitutive depletion of NRP1 yields mid-to-late embryonic lethality and as such, we and others have also temporally restricted Cre-recombinase activation using an oestrogen receptor fused Cre model (CreER), the PDGFB.iCreER^{T2} system (99, 199). Using this method, target depletion is dependent upon post-natal tamoxifen administration, thereby allowing NRP1-sensitive embryonic development to occur unimpeded. When considering non-endothelial specific recombination, the PDGFB promoter is expressed in both keratinocytes and megakaryocytes (208). Although keratinocytes have been shown to partially recombine following tamoxifen treatment, they are limited to the skin epithelium and therefore unlikely to influence any of the *in vivo* models used in this thesis (199). Megakaryocytes, however, likely contribute to angiogenic processes and further still, have been shown to express each of our candidate receptors (206, 209, 210). Despite this, previous studies have not detected any recombination of our target receptors in this population (161).

Each of the genetically engineered lines used in this thesis were generated and used by previous members of the lab (161, 195, 211). In their generation, mice in which one of our three target genes was flanked by *loxP* sites were crossed with PDGFB.iCreER^{T2} expressing mice to arrive at the following three single inducible knockout lines: $\beta3^{fl/fl};PDGFB.iCreER^{T2}$ ($\beta3.EC^{KO}$), $\alpha5^{fl/fl};PDGFB.iCreER^{T2}$ ($\alpha5.EC^{KO}$), and $NRP1^{fl/fl};PDGFB.iCreER^{T2}$ ($NRP1.EC^{KO}$). These lines were then inter-crossed to establish each of the three possible double inducible knockout combinations: $\beta3/\alpha5^{fl/fl};PDGFB.iCreER^{T2}$ ($\beta3/\alpha5.EC^{KO}$), $\beta3/NRP1^{fl/fl};PDGFB.iCreER^{T2}$ ($\beta3/NRP1.EC^{KO}$), and $\alpha5/NRP1^{fl/fl};PDGFB.iCreER^{T2}$ ($\alpha5/NRP1.EC^{KO}$). The final combinatory inducible knockout

line, $\beta3/\alpha5/NRP1^{fl/fl};PDGFB.iCreER^{T2}$ ($\beta3/\alpha5/NRP1.EC^{KO}$), was generated by inter-crossing the first two double knockout lines to be established (Fig 3.2). This approach provided the seven possible permutations of our three targets in spatiotemporally controlled *in vivo* models, as confirmed by PCR analysis of each line (Fig 3.3). The progeny from each line also demonstrated normal male:female ratios (Fig 3.4). Notably, we have targeted just one subunit from both $\alpha v\beta3$ - and $\alpha5\beta1$ -integrin, namely $\beta3$ -integrin and $\alpha5$ -integrin respectively, to avoid the knock-on effects of depleting their heterodimeric partners. Whilst $\beta3$ - and $\alpha5$ -integrin heterodimerise exclusively with αv - and $\beta1$ -integrin, their partner integrins are promiscuous, capable of forming heterodimers with numerous other endothelial integrins (109). To avoid these complications $\beta3$ - and $\alpha5$ -integrin have been manipulated alone, though these modifications should be thought of as a method by which to functionally assess these integrins in their heterodimeric state.

Throughout the generation of these lines and in their maintenance thereafter, $PDGFB.iCreER^{T2}$ expression has been restricted to breeding males to ensure their progenies contained both Cre-negative, those mice that lack $PDGFB.iCreER^{T2}$ expression, and Cre-positive mice. This allowed Cre-negative animals to be used as internal controls for their Cre-positive littermates and thereby account for any experimental variability caused by genetic background. In addition, confining Cre-recombinase expression to the male germline prevented its expression and activity in oocytes which might otherwise enable recombination in the fertilized egg, potentially generating a global knockout of the floxed target(s) (212). To circumvent the accidental introduction of any unintended floxed sequences, Dr Johnson established a rigorous genetic profiling procedure for this colony. The genetic status of any mouse entering a breeding pair was verified via PCR for each genetic modification in use within the lab ($\beta3$ -integrin (200), $\alpha5$ -integrin (169), NRP1 (99), and NRP2 (213)). This had previously been limited to the genes that were expected to be modified, thereby allowing unintended modifications to go unnoticed. By verifying each breeding pair, their first litter, as well as any animal used for *in vivo* experiments following their experimental endpoint, any inadvertent genetic modifications would be detected. Following the first litter any subsequent litters were only analysed for $PDGFB.iCreER^{T2}$ expression, the PCR reaction of which gives a yes/no result. $\beta2$ -microglobulin was therefore used as an internal positive control for monitoring reaction success to exclude the possibility of false negative results.

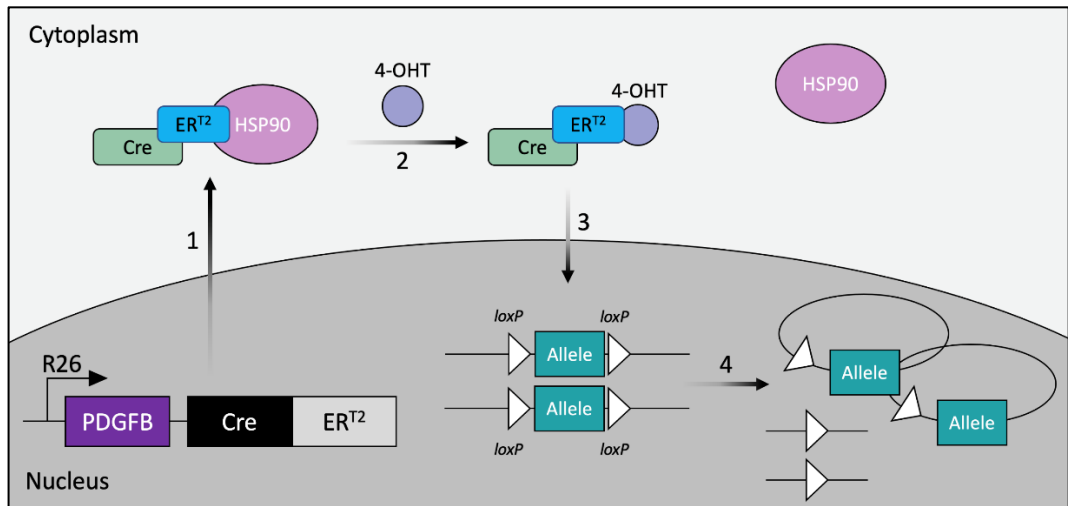


Figure 3.1 The mechanism of PDGFB.iCreER^{T2}-mediated excision of floxed targets following tamoxifen administration. 1) Before tamoxifen administration the oestrogen fusion protein CreER^{T2} is expressed under the PDGFB promoter at the Rosa26 (R26) locus and retained in the cytoplasm, sequestered by heat shock protein 90 (HSP90). 2 & 3) Once administered, tamoxifen is metabolized to 4-hydroxy tamoxifen (4-OHT) which then displaces HSP90 from CreER^{T2}, enabling its nuclear translocation. 4) CreER is then able to recognize loxP sites and induce their recombination, excising and inactivating floxed sequences. Figure adapted from (214).

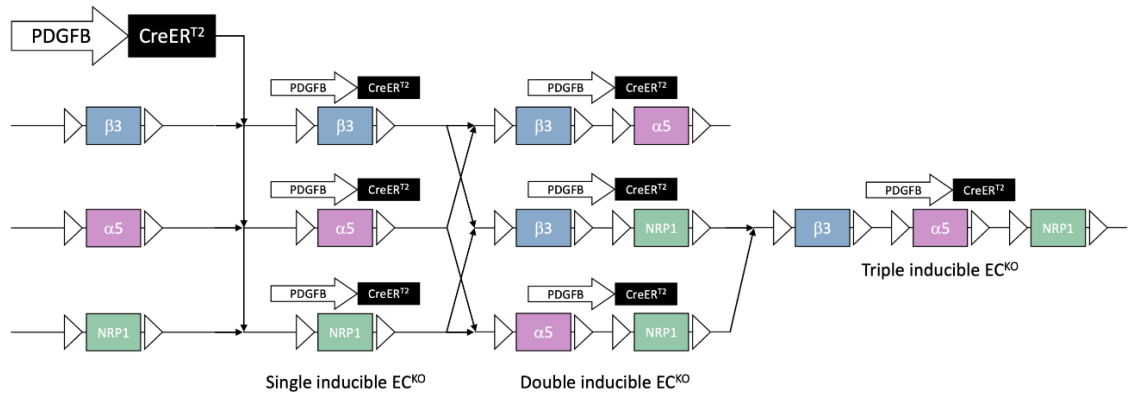


Figure 3.2 Crossbreeding approach to the generation of each genetically engineered mouse line. To establish each endothelial-specific, tamoxifen-inducible floxed mouse model, the displayed breeding strategy was employed. PDGFB.iCreER^{T2} expressing mice were crossed with those individually floxed at ITGA5 (α 5-integrin), ITGB3 (β 3-integrin) and NRP1. Consecutive rounds of crossbreeding then enabled the generation of the double and triple inducible knockout lines.

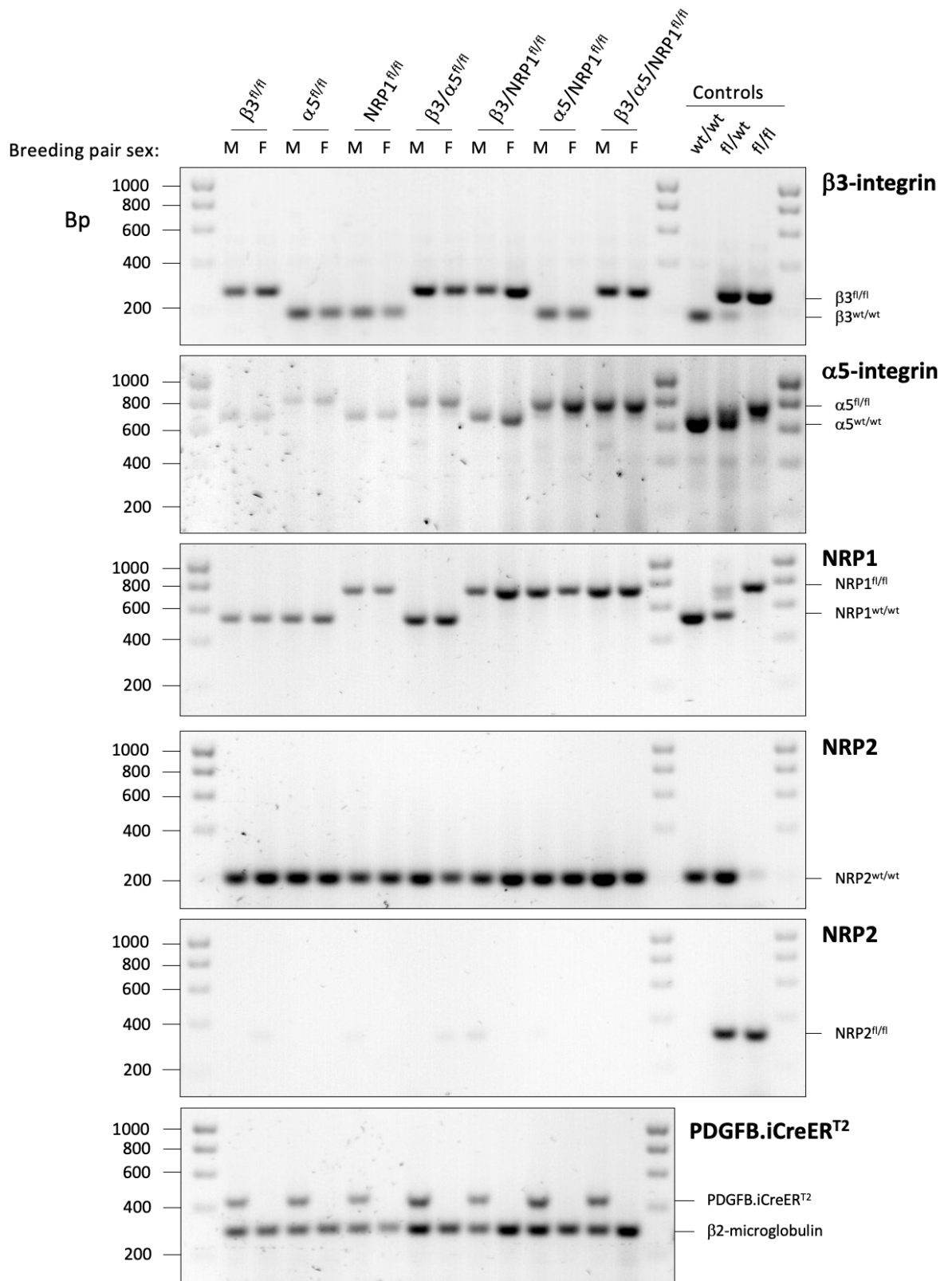


Figure 3.3 Confirmatory PCR analysis of each routinely analysed genetic modification. DNA from breeding pair ear biopsies (M – male, F – female) taken from each floxed line were analysed via PCR for each genetic modification routinely examined throughout the duration of this project ($\beta 3$ -integrin, $\alpha 5$ -integrin, NRP1, NRP2, and PDGFB.iCreER^{T2}). Samples were run on a 1.8% agarose gel. NRP2 WT and floxed PCR reactions are performed separately due to the equal height of the bands.

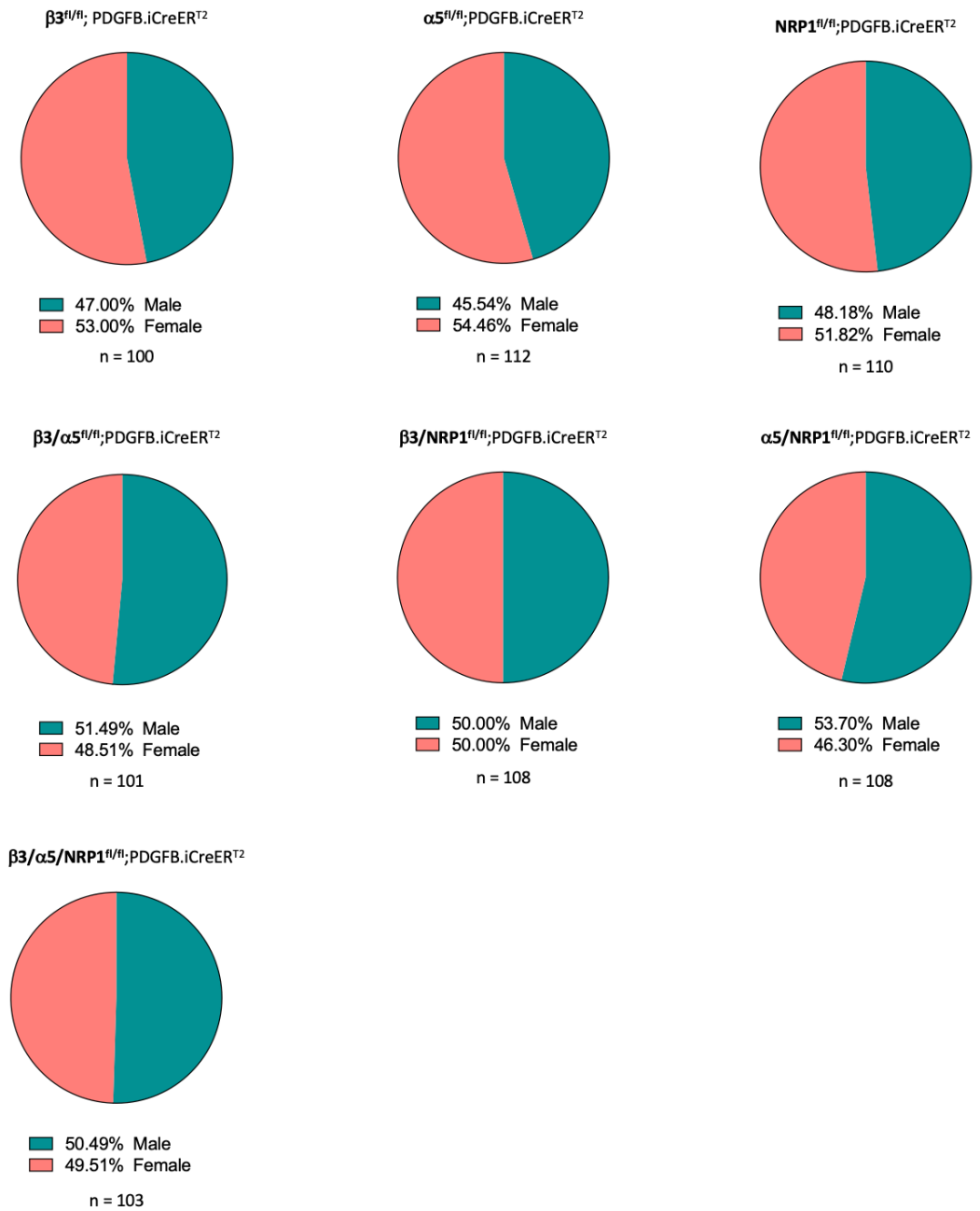


Figure 3.4 Gender ratios of progeny born in each genetically engineered mouse line. Progeny born in each floxed line were born at normal gender ratios. n = 100-112 mice per genotype.

3.2 Validating the Cre-*loxP* system as a suitable method by which to excise target genes in the postnatal mouse retina.

As discussed, the Cre-*loxP* system is widely used to induce targeted gene deletions and thereby study gene function *in vivo*. The spatiotemporal control it bestows is particularly useful to bypass developmental lethality. This relies on the CreER^{T2} system's sensitivity to tamoxifen (or its metabolite 4-hydroxytamoxifen), which induces its nuclear translocation and the subsequent recombination of floxed sequences. The potential side effects associated with tamoxifen administration are generally recognised and accounted for using tamoxifen-treated controls. Some publications, however, have also called for the use of Cre-positive controls that lack any floxed targets to account for the toxic effects of Cre-recombinase alone.

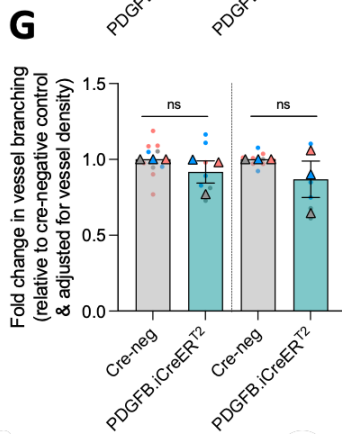
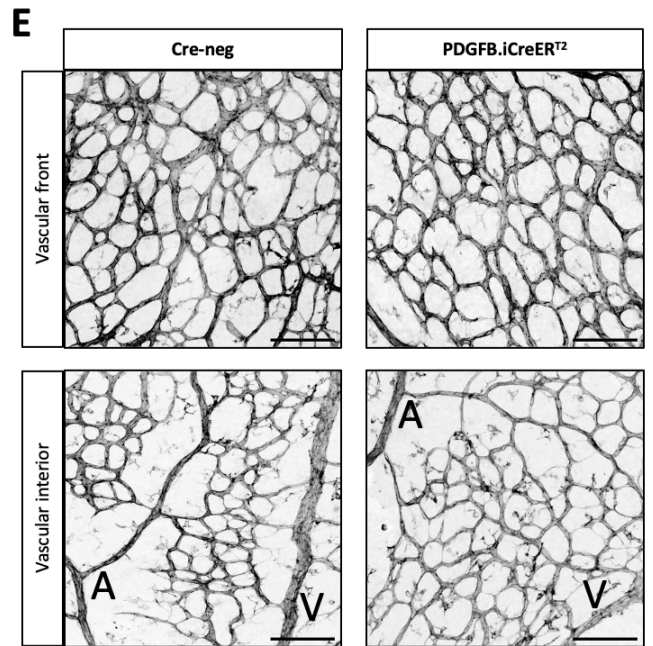
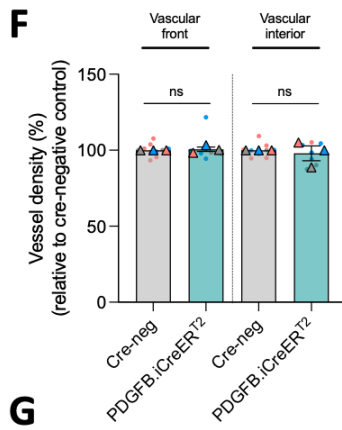
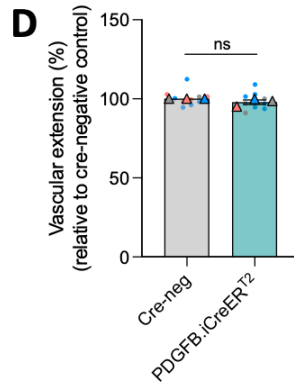
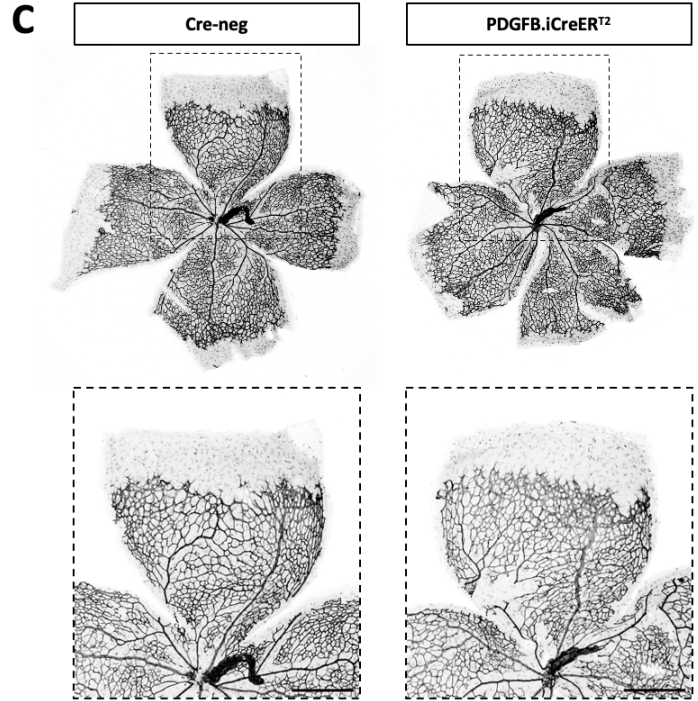
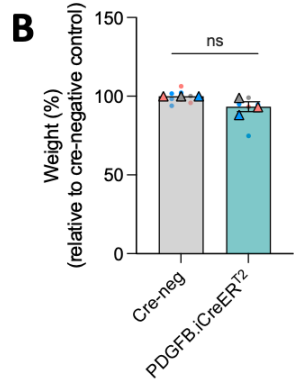
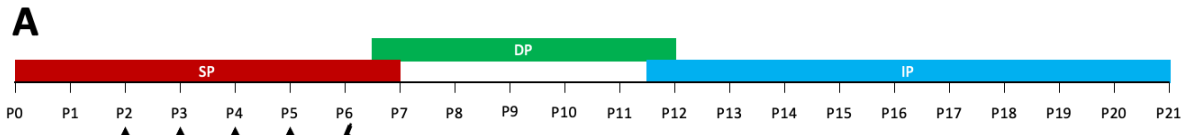
These effects have been attributed to its adulterous endonuclease activity, recognising and recombining pseudo- or cryptic-*loxP* sites within the mammalian genome. Whilst these sites are not exact copies of *loxP* sequences, they resemble them closely enough for Cre-recombinase to identify them and may occur as frequently as 1.2x per megabase (Mb) in the mouse genome (which is approximately 2588 Mb in length) (215). For example, Cre-toxicity has been associated with the α -myosin-heavy-chain and keratin 5 and 14 promoters of Cre, where its expression was associated with the development of dilated cardiomyopathy and the formation of tetraploid keratinocytes respectively (216, 217). More recently, this phenomenon made its way to the field of angiogenesis. Brash *et al* reported that both PDGFB and CDH5 driven CreER^{T2} could severely impede angiogenesis in the post-natal mouse retina in a tamoxifen dose-dependent manner (50-150 μ g) (218).

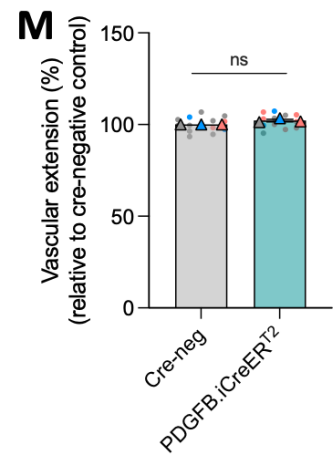
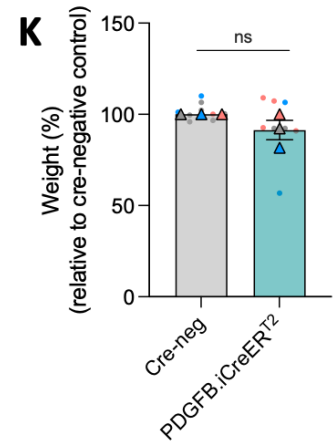
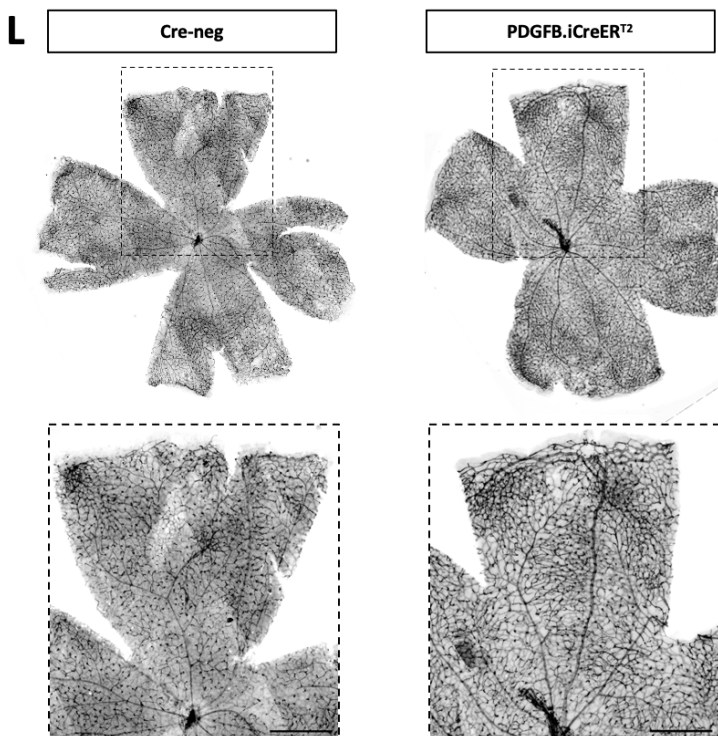
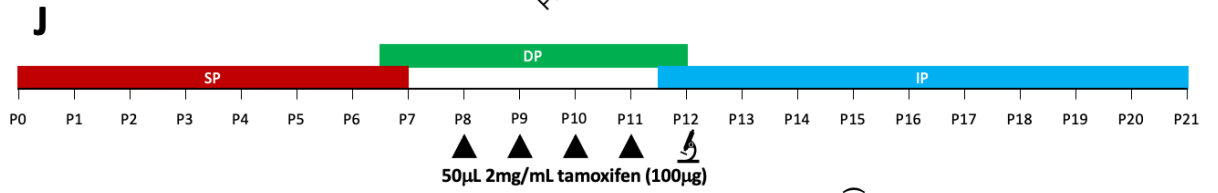
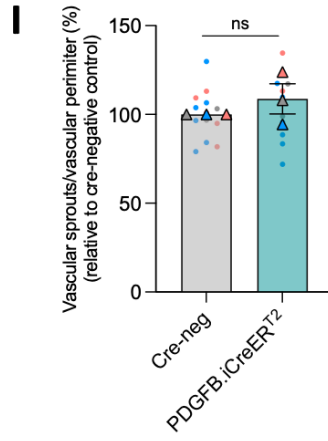
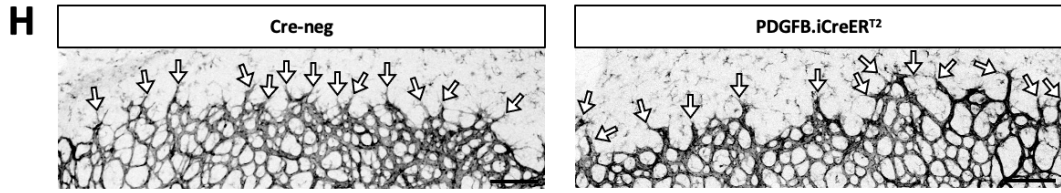
The murine retina is widely used in the field of sprouting angiogenesis due to its timely and stepwise vascular development. Briefly, preceded by astrocyte-mediated deposition of a fibronectin matrix, blood vessels sprout radially from the central retinal artery at the optic nerve head and follow a gradient of VEGF through the avascular space towards the retinal periphery, establishing a vascular monolayer termed the superficial plexus (SP) by post-natal day (P) 7. During its outgrowth the SP is divided into two vascular regions, its proliferative vascular front and remodelling vascular interior. These regions present different vascular characteristics, with the vascular interior possessing a lower density than that of the proliferative front due to ongoing remodelling acting to prune superfluous vessels. The veins within the SP then sprout downwards through the underlying

parenchyma in response to growing VEGF bioavailability in the neuronal layer to form the deep plexus (DP) by P12 (219). Akin with the SP, the DP expands radially towards the retinal periphery. By P21, the third and final monolayer termed the intermediate plexus (IP) is formed between the superficial and deep plexuses. An extensive period of vascular remodelling typified by a balance of both vessel regression and stabilisation then concludes vascularisation in each of these parallel, interconnected monolayers. In addition to its orderly vascularisation, which starkly contrasts the rather messy vascular systems associated with other organs, because of its transparency, the retina is particularly amenable to immunofluorescent imaging, establishing it as an ideal model for quantifying vascular growth (220, 221).

This thesis heavily relies on the retinal model to investigate the individual and combined angiogenic contributions of our three target receptors. As such, we sought to determine whether the Cre-toxicity reported by Brash *et al* could be replicated in our hands (218). Herein we aimed to provide a deep characterisation of retinal vascular development in PDGFB.iCreER^{T2} expressing mice that are devoid of any floxed genes. Notably, our tamoxifen administration regime differed from that used by Brash *et al*. Instead of copying their two doses at P2 and P4, we have replicated the regime used throughout this thesis, administering tamoxifen in corn oil (50µl, 2 mg/ml) via subcutaneous injection from P2 to P3 and interperitoneally from P4 to P5 before sacrificing animals on P6 (Fig 3.5 A). Notably, animal weight remained consistent between Cre-positive and Cre-negative pups, ruling out any broad developmental effects as a result of Cre-recombinase activity (Fig 3.5 B). We then quantified the extension of the growing SP as a measure of angiogenic aptitude and found that CreER^{T2} expression alone did not impair SP vascular growth (Fig 3.5 C-D). The vascular density of both the vascular interior, located towards the rear of the SP where vascular remodelling is beginning, and the vascular front, where sprouting angiogenesis is actively extending the monolayer towards the retinal periphery, were also unaffected (Fig 3.5 E-F). In our analysis of vascular branching, we have relativised the number of branching points to vascular density to account for any mirrored changes between the two. This also revealed no significant changes in either of the vascular zones discussed (Fig 3.5 G). Taking a closer look at the vascular front, we enumerated the number of sprouts protruding into the avascular space and made these values relative to their vascular perimeter, thereby accounting for any slight changes in available vascular surface area for sprouts to form. Again, we detected no difference between Cre-positive and Cre-negative littermates (Fig 3.5 H). We were therefore unable to detect Cre-induced vascular toxicity at this developmental time point.

We have also utilised a second tamoxifen administration regime at a later stage of retinal vascular development, the purpose for which will be discussed in the following chapter. To determine whether Cre-recombinase alone may cause any deleterious effects on retinal vasculature under this new regime, we repeated our investigation. Again, four tamoxifen doses (50 μ l, 2mg/mL) were administered but done so from P8 to P11 and each via an intraperitoneal injection before sacrificing animals at P12 (Fig 3.5 J). The first observation worth noting is the lack of change in overall animal weight, excluding the possibility of endothelial CreER^{T2} causing a general developmental delay, nor a developmental delay directly causing any vascular impediment (Fig 3.5 K). At P12 the SP should have long since vascularised, reaching the retinal periphery by P7. Indeed, there were no differences in this monolayer's vascular extension between Cre-negative and Cre-positive littermates (Fig 3.5 L-M), though a slight but significant reduction in its vascular density was detected (Fig 3.5 N-P). By P12 the DP should also have concluded its vascularisation meanwhile the IP should be just starting to form. Whilst the vascular density of the DP was unaffected, the IP saw slight hypervascularisation (Fig 3.5 N-P). Vascular branching in each of these three monolayers showed no change from their Cre-negative controls (Fig 3.5 Q), limiting Cre-induced vascular aberrations to the vascular density of the superficial and intermediate plexuses becoming hypo- and hypervascularised respectively. Where this thesis discusses retinal angiogenesis at P12 alongside this tamoxifen administration regime, these data will be included to avoid the misinterpretation of any vascular phenotypes attributed to the depletion of our target receptors.





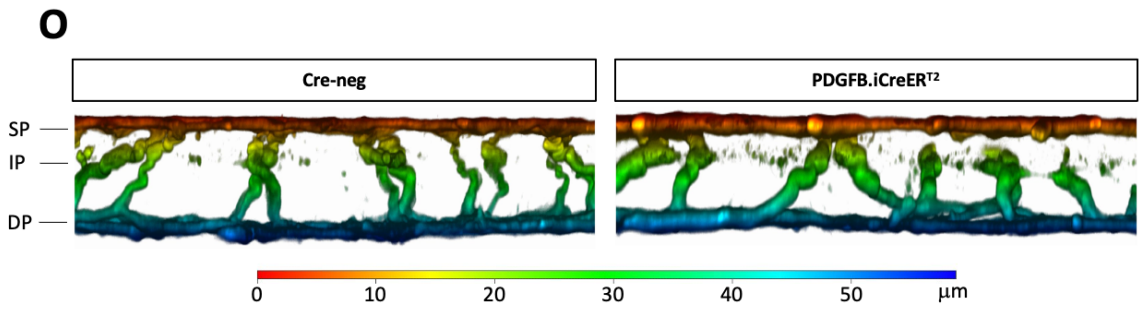
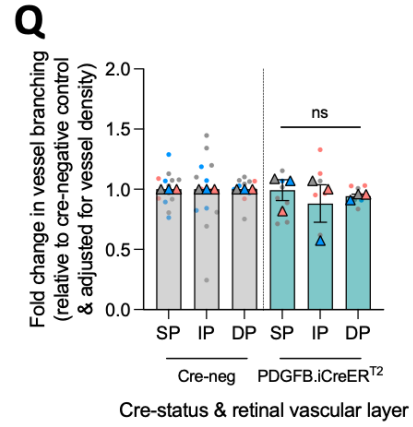
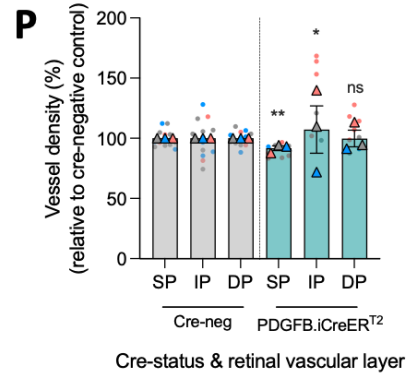
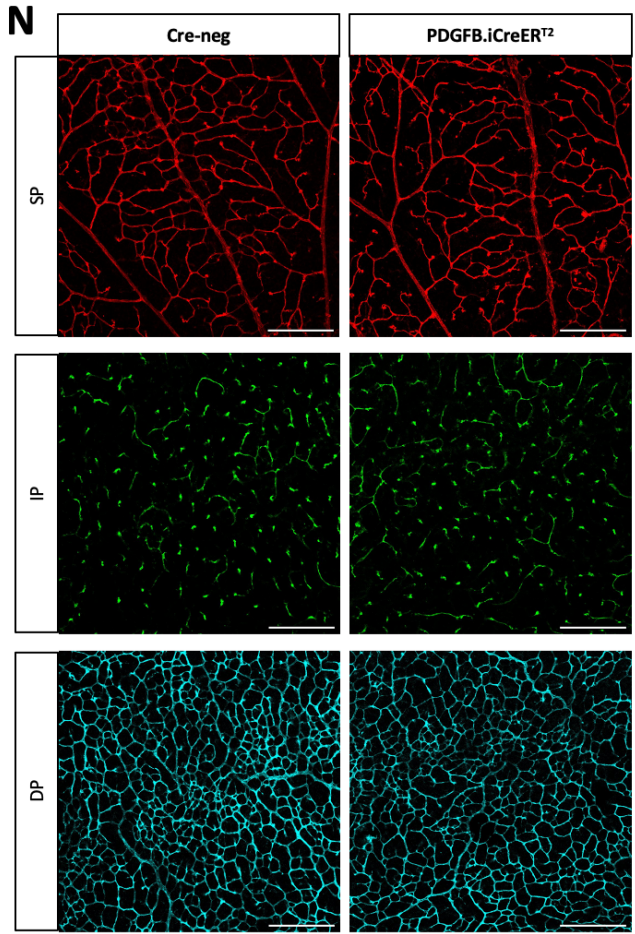


Figure 3.5 Characterization of vascular toxicity induced by PDGFB-driven Cre-recombinase in retinal vasculature at P6 and P12. **A)** Time-course schematic of retinal vascular development and tamoxifen administration. The SP vascularises from P0-P7, the DP from P6-P12, and the IP from P11-P21. Tamoxifen was administered (black triangles) via subcutaneous injection from P2-P3 and intraperitoneally from P4-P5 before sacrificing animals at P6. **B)** Quantification of animal weights recorded at P6, with Cre-positive weights presented as a percentage of the average weight of their Cre-negative littermates. Error bars displayed as mean \pm SEM. N = 3, n \geq 5 mice per group. **C)** Representative images of BS1-lectin labelled P6 SP retinal vasculature. Magnified image scale bar = 500 μ m. **D)** Quantification of P6 vascular extension presented as a percentage of the average vascular extension measured in Cre-negative littermates. Error bars displayed as mean \pm SEM. N = 3, n \geq 10 retinas per group. **E)** Representative images of BS1-lectin labelled P6 retinal vasculature at the vascular front and interior. A = artery, V = vein. Scale bar = 100 μ m. **F)** Quantification of vessel density in the vascular front and interior of P6 retinal vasculature, expressed as a percentage of the average vessel density measured in Cre-negative littermates. Error bars displayed as mean \pm SEM. N = 3, n \geq 7 retinas per group. **G)** Quantification of vessel branching, initially measured as a percentage of the average vessel branching in Cre-negative littermates before being expressed as a ratio of vessel branching to vessel density. Error bars displayed as mean \pm SEM. N = 3, n \geq 7 retinas per group. **H)** Representative images of BS1-lectin labelled retinal vascular peripheries. White/black arrows show vascular sprouts. Scale bar = 150 μ m. **I)** Quantification of vascular periphery sprouting. Enumerated vascular sprouts were divided by the perimeter of their leaflet's leading vascular edge before being expressed as a percentage of the average vascular sprouts per leaflet perimeter in Cre-negative littermates. Error bars displayed as mean \pm SEM. N = 3, n \geq 10 retinas per group. **J)** Time-course schematic of retinal vascular development and tamoxifen administration. Tamoxifen was administered (black triangles) via intraperitoneal injection from P8-P11 before sacrificing animals at P12. **K)** Quantification of animal weights recorded at P12, presented as a percentage of the average weight of Cre-negative littermates. Error bars displayed as mean \pm SEM. N = 3, n \geq 5 mice per group. **L)** Representative images of BS1-lectin labelled P12 SP retinal vasculature. Magnified image scale bar = 500 μ m. **M)** Quantification of P6 vascular extension presented as a percentage of the average vascular extension measured in Cre-negative littermates. Error bars displayed as mean \pm SEM. N = 3, n \geq 10 retinas per group. **N)** Representative images of BS1-lectin labelled P12 retinal SP (red), IP (green) and DP (blue) vasculature. Scale bar = 200 μ m. **O)** Colour depth-coded Z-stacks and scale bar. **P)** Quantification of vessel density in the SP, IP, and DP of P12 retinal vasculature, expressed as a percentage of the average vessel density measured in Cre-negative littermates. Error bars displayed as mean \pm SEM. N = 3, n \geq 10 retinas per group. **Q)** Quantification of SP, IP and DP vessel branching, initially measured as a percentage of the average vessel branching in Cre-negative littermates before being expressed as a ratio of vessel branching to vessel density. Error bars displayed as mean \pm SEM. N = 3, n \geq 10 retinas per group. Statistical significance was expressed and analysed as follows: *= $P < 0.05$, **= $P < 0.002$, unpaired students t-test (two-tailed)/one-way ANOVA.

3.3 Generation and validation of immortalised endothelial knockout cell lines derived from genetically engineered mouse models using TAT-Cre-recombinase.

To pick apart our proposed receptor network, we required endothelial cell lines for *in vitro* use. However, many of the assays to be performed required large numbers of endothelial cells which restricted our ability to use primary cultures due to their limited proliferative capacity. To overcome this, we have utilised a PyMT expressing retrovirus to immortalise endothelial cells isolated from mouse lung microvasculature and bypass their proliferative restrictions, thereby lessening the need for continuous primary cell line re-derivation (222). We and others have previously employed these cells and demonstrated their utility for modelling angiogenesis *in vitro* (161, 194, 223, 224, 225).

Using these immortalised cells, Dr Johnson first attempted individual and combinatorial siRNA-mediated knockdown of our three targets in each of their seven permutations, achieving ~60% knockdown of each receptor (211). However, this transient method of target depletion required endothelial nucleofection for each experiment which, across seven target combinations, was too laborious and costly. The transient nature of these depletions as well as the variability in the level of knockdown achieved was also of concern, as the angiogenic result of an experiment can be tied to the duration of target knockdown. In the case of β 3-integrin, we have shown that its acute endothelial depletion *in vivo* causes an anti-angiogenic effect that can preventatively inhibit tumour growth. Maintaining this inducible depletion long term however loses this benefit owing to a NRP1-dependent rescue mechanism (161, 195). Likewise, constitutive endothelial β 3-integrin depletion has no effect on overall tumour volume, whilst its global knockout enhanced angiogenesis and tumour growth due to upregulated VEGFR2 expression (155, 161). Transient depletions and variability in the level of knockdown achieved would therefore make it extremely difficult to robustly compare different knockdown combinations. CRISPR-Cas9 and the Dharmacon Edit-R system were subsequently employed to help generate cell lines with stable, long-term depletions of each of our target receptor combinations. Unfortunately, these systems demonstrated poor knockdown efficiency and transient depletions respectively, leaving neither system as a potential solution (211).

Dr Johnson next attempted isolating endothelial cells directly from the mouse lung of constitutively depleted mice ($\alpha 5^{fl/fl}; Tie1.Cre$), though failed to detect any target depletion *in vitro*. He therefore resorted to isolating lung endothelial cells from each floxed PDGFB.iCreER^{T2} mouse model and nucleofecting them twice with TAT-Cre recombinase following their PyMT-induced immortalisation to achieve target depletion. Importantly, a subpopulation of the isolated cells was not nucleofected, reserving a Cre-negative, principally WT, control line for each depleted line to be compared to. This approach delivered robust and long-lasting target depletion in each of the seven knockout combinations, even at later passages (Fig 3.6 A), enabling us to investigate the effects of long-lasting target depletion *in vitro* and determine whether our target receptors collectively regulate angiogenic processes (211). Having re-confirmed the knockout status of our cell lines, we sought further re-confirmation of their endothelial identity to ensure their phenotype had not drifted following routine passaging. Using lysates gathered at various passages we probed for a series of endothelial and lymphatic markers and found the endothelial expression profile of each cell line remained intact, expressing the endothelial markers VE-cadherin, PECAM-1, Endomucin, ERG and Claudin-5, whilst not expressing the lymphatic markers Prox-1 and Lyve-1 (Fig 3.6 B). Despite their demonstrated stability, these cell lines were not taken past P30 to avoid any potential target re-expression or endothelial phenotypic drifting.

Notably, throughout this thesis we have used 2D culture systems to model angiogenesis *in vitro*. Whilst this traditional method is widely used and has enabled reproducible, cost-effective investigations of vascular morphogenesis, they fail to re-capitulate the complexity of angiogenic micro-environments. Culture systems which allow for numerous matrix components to be organised as 3D supports such as hydrogels are becoming increasingly accessible. These more accurately mimic the native ECM scaffolding that surrounds capillaries. Furthermore, their composition, rigidity and incorporation of growth-factors are all tuneable. Angiogenesis is also directed by haemodynamic parameters such as shear stress, a further complexity that can be modelled *in vitro* through use of microfluidic models (226). The ability to co-culture endothelial cells with one or more cell types such as pericytes, fibroblasts and smooth muscle cells is a further advance that will help delineate the distinct roles of these cell types in the various phases of sprouting angiogenesis and, onward from this study, there would be merit in acquiring 3D- and co-culture systems to validate our *in vitro* findings, and to translate them more robustly with observations made *in vivo* (227).

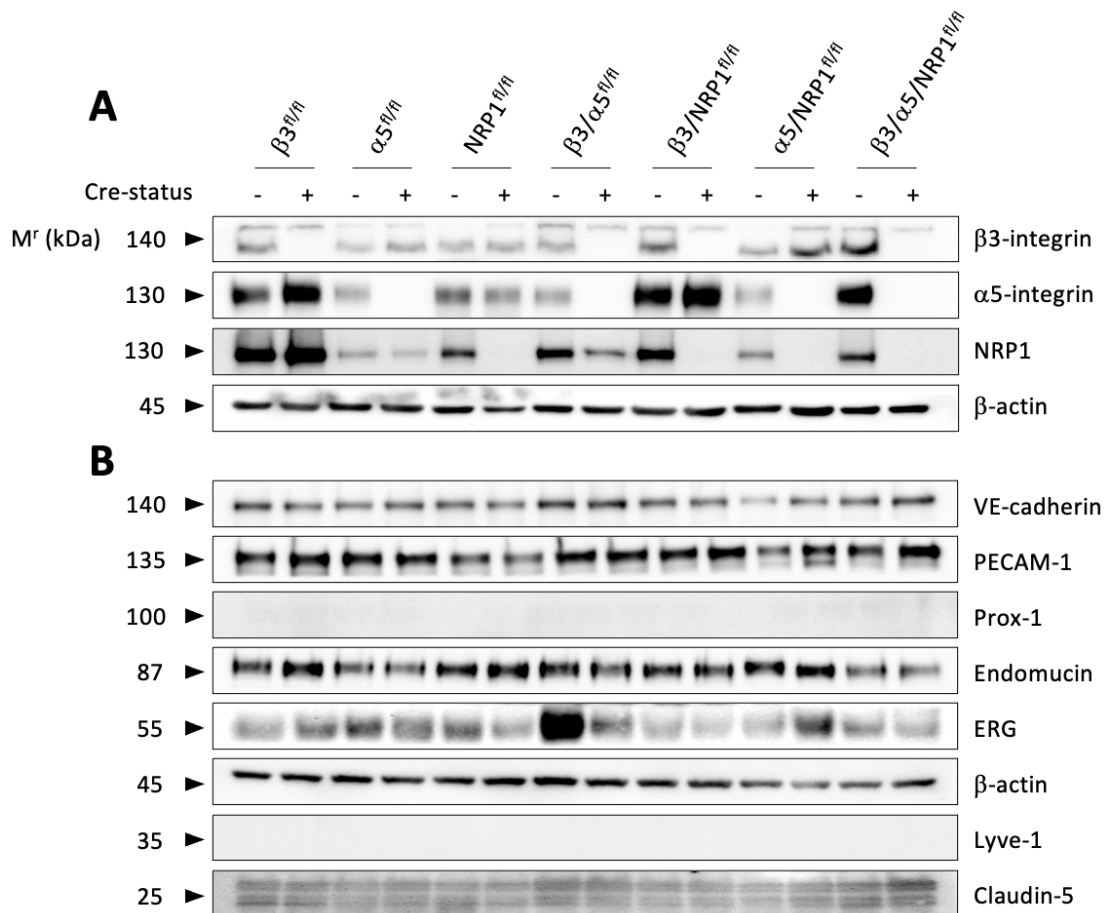


Figure 3.6 Nucleofection with TAT-Cre-recombinase was able to generate endothelial cells lines with long-lasting depletions of each target receptor. Endothelial cells isolated from the lung microvasculature of each genetically engineered mouse line were nucleofected twice with TAT-Cre-recombinase to induce the excision of floxed targets following their PyMT-induced immortalisation. **A)** Representative western blot of cell lysates obtained from endothelial cells in culture up until P30 for $\beta 3$ -integrin, $\alpha 5$ -integrin, NRP1, and β -actin as a loading control. **B)** Representative western blot of the same cell lysates probing for endothelial and lymphatic markers. β -actin was used as a loading control.

3.4 Endothelial responsiveness to VEGF is preserved following PyMT-induced immortalisation.

With our cell lines established and re-confirmed, we next sought to address any scepticism regarding our use of immortalised endothelial cells. We and others have shown that these cells are useful for modelling angiogenesis *in vitro*, though hesitance regarding the preservation of both their endothelial characteristics and behaviour following immortalisation has remained. To address this, Dr Benwell, a member of the lab investigating the role of NRP2 in angiogenesis, compared the expression profile of endothelial and lymphatic markers in our mLMECs before and after their PyMT-induced immortalisation. He found that their endothelial identity remained stable following transformation, maintaining strong expression of VE-cadherin, PECAM-1, ERG and claudin-5, whilst the lymphatic marker Prox-1 showed only limited expression (228). He went on to assess random migration speed and FA development on fibronectin matrices before and after transformation. FA size was measured using immunofluorescence for paxillin in fixed cells that were allowed to adhere for 90 minutes and 16 hours. Whilst no differences were detected at 90 minutes, immortalised cells showed significantly greater FA size at 16 hours which corresponded with their slower random migration speed over a 16-hour period. Dr Benwell postulated that their larger, more stable FAs were subject to slower turnover, limiting their disassembly at the rear of cell which would otherwise enable forward movement. These data contrast the aforementioned literature in which PyMT-induced transformation did not cause disparity between transformed and primary cultures in motility-dependent functions such as tube formation, scratch wound migration and responses to shear stress, even when assessed at extremely high passages (passage 69-81) (225).

Whilst some investigations therefore document the suitability of immortalised endothelial cells for the study of angiogenesis *in vitro*, we had yet to compare the VEGF-induced phosphorylation response of key angiogenic signalling pathways, particularly those pertinent to our target receptors, between primary endothelial cells and their immortalised counterparts. This seemed a necessary assessment considering how frequently we have utilised VEGF-challenge assays to investigate the signalling contributions of target molecules in immortalised cells (161, 195, 223, 229). For this comparison, three separate mouse endothelial lung preps were first isolated using the method described previously (methods – 2.7). When examining their endothelial identity, two of the three primary cultures demonstrated strong expression of PECAM-1, ERG and endomucin whilst showing no expression of the lymphatic markers Prox-1 and Lyve-1. This mirrored the endothelial profile of

the immortalised lines used for comparison, though low levels of Lyve-1 expression were detected. The third primary line had significantly weaker ERG expression and was therefore excluded from the following experiments (Fig 3.7 A).

Both primary and immortalised cells were adhered to fibronectin matrices before being starved in serum-free media for three hours and finally stimulated with VEGF over a 15-minute time course. We then assessed the VEGF-induced, acute phosphorylation response of VEGFR2 (Y1173), ERK1/2 (T202/Y204), Akt (T308), FAK (Y397), and Paxillin (Y118) (Fig 3.7 B). VEGFR2 Y1173 is recognised as a key autophosphorylation site, stimulating numerous downstream pathways including that of ERK1/2 at T202 and Y204 and Akt at T308 and S473. In turn, these signalling intermediaries are essential for endothelial migration, proliferation, and survival. The non-receptor tyrosine kinase FAK and its downstream substrate Paxillin are also fundamental for endothelial motility, enabling linkage between the plasma membrane and actin cytoskeleton following their recruitment to FAs. As one primary line was discounted from this analysis due to its unsatisfactory endothelial expression profile, only two technical replicates were performed. Statistical analysis could therefore not be performed, so we decided not to carry out densitometric analyses of the following blots but instead show a carefully chosen representative image. No obvious differences in either the total levels or the phosphorylation response of VEGFR2, Akt and ERK1/2 were observed between primary and immortalised cells. In addition, the phosphorylation response of FAK and Paxillin also mirrored that of PyMT-transformed cells, with VEGF treatment enhancing phosphorylation at the indicated residues. However, the total levels of both FAK and Paxillin reduced over the 15-minute VEGF exposure in primary endothelial cells, whilst remaining stable in their immortalised equivalents. The enhanced stability of these core focal adhesion proteins may help to explain why immortalised cells possess larger FAs and are less motile, but equally, this may also be an artefact of these larger adhesions rather than a cause. Despite this, the phosphorylation response of these proteins to VEGF appeared unchanged following PyMT-induced immortalisation.

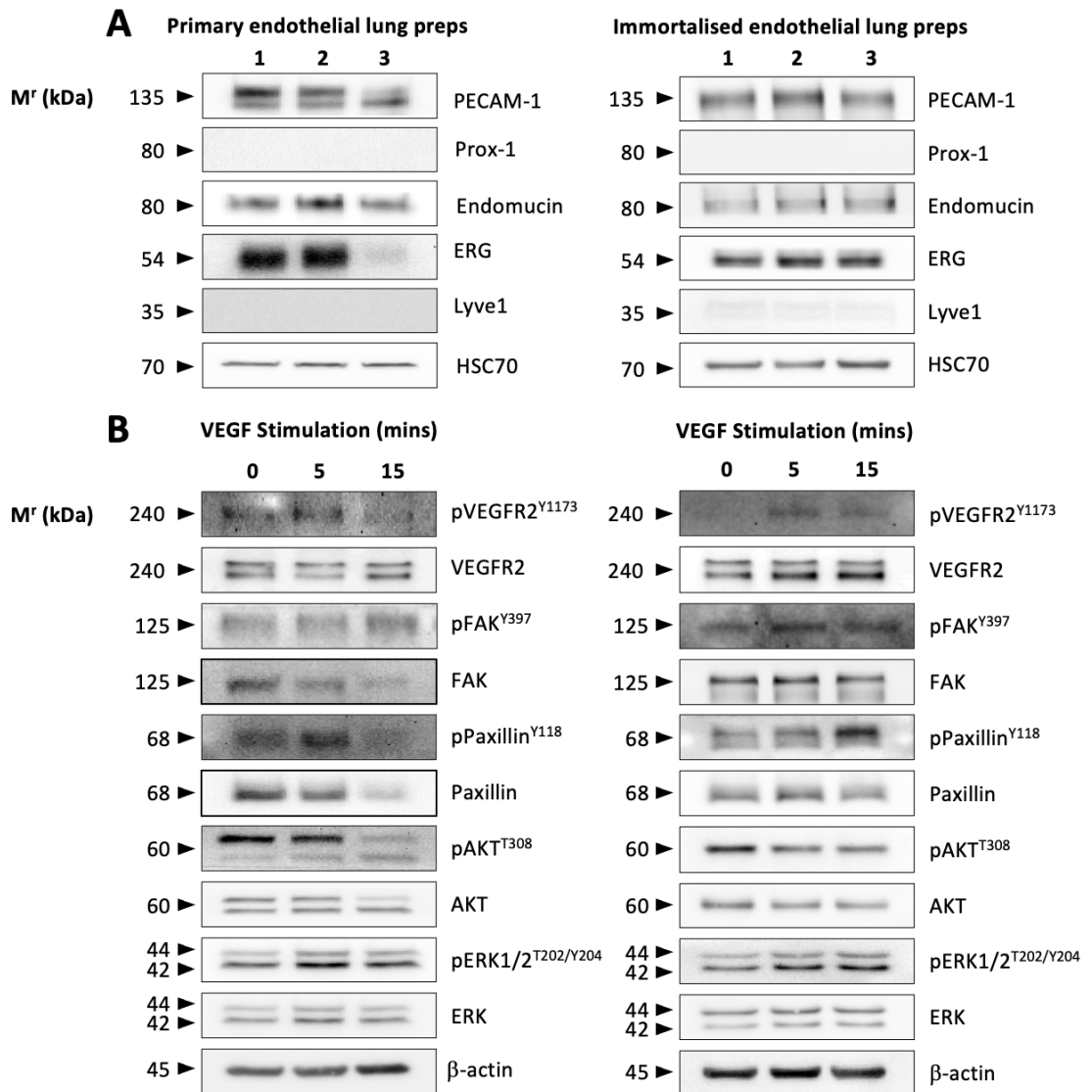


Figure 3.7 The VEGF phosphorylation response of key angiogenic signalling pathways is maintained following PyMT-induced immortalisation. A) Primary and immortalized endothelial cells were adhered to fibronectin overnight and lysed using ESB before their protein content was quantified using the DC protein assay. The representative western blot above displays the endothelial expression profile of each primary and immortalized line used for comparison. Endothelial markers used are PECAM-1 (CD31), endomucin and ERG, whilst the lymphatic markers are prox-1 and Lyve-1. Heat shock 70 (HSC70) was used as a loading control. N = 2. **B)** Primary and immortalized endothelial cells were adhered to fibronectin overnight, starved in serum-free media and then stimulated with VEGF for 0, 5 and 15 minutes. Following the allotted stimulation period, the cells were lysed using ESB, and protein content quantified using the DC protein assay. Samples were then analysed via western blot for phosphorylated and total expression of VEGFR2 (Y1173), FAK (Y397), Paxillin (Y118), Akt (T308), and ERK (T202/Y204). β-actin was used as a loading control. N = 2.

3.5 Discussion

To my benefit, using the PDGFB.iCreER^{T2} system and the mouse models individually floxed at β 3-integrin, α 5-integrin and neuropilin-1, Dr Johnson was able to generate each combinatorial knockout (β 3.EC^{KO}, α 5.EC^{KO}, NRP1.EC^{KO}, β 3/ α 5.EC^{KO}, β 3/NRP1.EC^{KO}, α 5/NRP1.EC^{KO}, and β 3/ α 5/NRP1.EC^{KO}) in an endothelial specific, tamoxifen-inducible model of target depletion. Furthermore, he was also able to isolate each of their corresponding endothelial cell lines for *in vitro* study, the identity of which we have re-confirmed at later passages. The protocol for breeding best practise that was passed down has maintained not only this colony but each of the GM colonies currently in use within the Robinson lab by enabling the rapid identification of any unintended modifications, ensuring their intended genetic identity is maintained. Using these tools, we could continue to explore how these three receptors regulate angiogenesis.

Where possible, we have validated our model systems to ensure any phenotypes observed throughout this thesis can be appropriately attributed to the absence or presence of our endothelial targets rather than the method used to induce target depletion. Whilst Brash *et al* reported tamoxifen dose-dependent Cre-toxicity in mouse retinal vasculature at P6, we were unable to detect any abnormal vascular phenotypes at this developmental time point despite doubling their frequency of tamoxifen injections in line with the administration regime used throughout this thesis (218). Later, at P12 however, we identified abnormal vascular density in the superficial and intermediate plexuses. To account for these Cre-induced effects these data will be included where relevant to avoid the misinterpretation of any vascular phenotypes observed. Brash *et al* also reported Cre-toxicity in the endothelial specific, tamoxifen-inducible CDH5.CreER^{T2} line, but not using Tie2.Cre, an endothelial specific but constitutively active Cre model. This begs the question, is the Cre-induced endothelial toxicity reported by Brash *et al* transient, and therefore able to be masked in a constitutively active model? If so, only an inducible model of Cre would reveal its toxicity, as any potential vascular recovery period could be circumvented by performing post-natal vascular analysis immediately after tamoxifen administration. Akin with the transient anti-angiogenic effects of acute β 3-integrin depletion, constitutive Cre activity or prolonged activity in an inducible model may enable recovery effects to hide Cre-induced toxicity (161, 218). Given that, in our hands, Cre-toxicity occurs at P12 rather than P6, it would be prudent to administer tamoxifen from P2-P5, mirroring our P6 investigation, and sacrifice animals at P12 to allow for any

recovery effects to take place. If the vascular density of the SP and IP normalises, it would confirm the transient nature of Cre-toxicity.

With regard to our immortalised knockout cell lines, we sought to further the body of evidence testifying to their utility *in vitro* by comparing the responsiveness of key angiogenic signalling pathways to VEGF in primary and immortalised cells. Whilst this revealed that FAK and Paxillin are more resistant to VEGF-induced downregulation in immortalised cells, the overall phosphorylation response of the receptor and signalling intermediaries shown were seemingly unchanged. As discussed previously, the preservation of FAK and Paxillin may help to explain why Dr Benwell saw elevated adhesion size and slower random migration speed in immortalised cells, though it is important to note that these experiments lacked VEGF stimulation and are therefore not directly comparable. In addition, we confirmed that the endothelial character of these endothelial cells is maintained post-immortalisation.

4 Interplay between $\alpha v\beta 3$ -integrin, $\alpha 5\beta 1$ -integrin and neuropilin-1 coordinates developmental angiogenesis in the postnatal mouse retina through autonomous and combined vascular-bed specific functions.

The post-natal mouse retina is a commonly used developmental model in the field of angiogenesis. Its stereotypic growth pattern, ease of experimental manipulation and amenability to immunofluorescent imaging make it an ideal investigative tool. As discussed in the previous chapter, tamoxifen was administered via four successive injections, though the timing of these administrations as well as that of retinal harvests have varied throughout this chapter and will be highlighted where relevant. Dr Johnson had previously determined that this tamoxifen administration regime effectively induced Cre-recombinase target gene recombination using tdTomato reporter mice. These mice possess a stop codon flanked by loxP sequences which, following its excision prompted by tamoxifen-activated Cre-recombinase activity, allowed expression of the red-fluorescent protein tdTomato to mark endothelial cells that had undergone recombination. Subsequent immunofluorescent imaging confirmed successful recombination across the retinal SP at P6 after administration of four tamoxifen doses (50 μ l, 2 mg/ml) from P2-5 by co-fluorescence of tdTomato with BS1-lectin-positive vasculature. Introducing this reporter line into each genetically engineered mouse model would have enabled continual confirmation of recombination, but we concluded that insertion of up to five transgenic genes would have been a time-consuming endeavour and likely have limited the overall progression of this project (211).

Here we have utilised the post-natal mouse retina to examine what individual and overlapping functions our three endothelial receptors of interest conduct as well as the longevity of these functions during developmental angiogenesis – are they required only transiently, or does their depletion alone and in combination instigate long-term angiogenic consequences that are unable to be compensated for by alternative mechanisms?

4.1 Neuropilin-1 is the principle driving force for sprouting angiogenesis in the postnatal mouse retina, but candidate interactions with and between β 3-integrin and α 5-integrin may be essential for the superficial plexus to fully vascularise.

Using the established floxed mouse lines discussed, Dr Johnson began investigating the effects of depleting our endothelial target receptors individually, in duplicate and in triplicate on developmental angiogenesis in the postnatal mouse retina. This experiment continued long into this project and is therefore presented here as a cumulative effort. Administering tamoxifen between P2-P5 and sacrificing animals at P6, we quantified the extension of the SP between the central retinal artery and sprouting vascular front (Fig 4.1 A). Importantly, Cre-positive animals were compared with their Cre-negative littermates to account for any variability in precise age. Whilst the genetic status of each experimental animal was confirmed via PCR analysis of tail biopsies, confirmation of target depletion had yet to be performed. Immunofluorescent confirmation was not possible due to the lack of suitable antibodies against β 3-integrin. Instead, lungs were taken upon tissue harvest for later confirmation via western blot as performed by others (230).

The vascular extension measured in the triple knockout (β 3/ α 5/NRP1.EC^{KO}) established the baseline level of outgrowth capable of occurring in the absence of each of our receptors together (Fig 4.1 B & C). From this baseline, the individual expression of β 3-integrin (α 5/NRP1.EC^{KO}) or α 5-integrin (β 3/NRP1.EC^{KO}) was unable to confer any pro-angiogenic benefit, with vascular extension remaining non-significantly different from the baseline established by the triple knockout (Fig 4.1 E). Expressing NRP1 alone (β 3/ α 5.EC^{KO}), however, was capable of driving angiogenesis closer to WT levels, though notably falling short of achieving the physiologically normal outgrowth of Cre-negative controls (Cre-neg). In agreement with literature then, NRP1 appeared to conduct discrete pro-angiogenic functions that are fundamental to early retinal vascularisation, backed-up here once more in that its individual depletion (NRP1.EC^{KO}) conferred an angiogenic impairment analogous to that observed when each of our targets were depleted together (β 3/ α 5/NRP1.EC^{KO}) (180, 181, 231). Nevertheless, alone, NRP1 failed to completely normalise SP vascular outgrowth (β 3/ α 5.EC^{KO}).

Before discussing these data further, it is worth noting that the depletion of β 3-integrin either individually or together with NRP1 (β 3.EC^{KO} and β 3/NRP1.EC^{KO}) caused a slight but significant reduction in overall animal weight (Fig 4.1 D). As this reduction was not significantly different

between these two genotypes, we could deduce that this was a β 3-integrin-dependent developmental effect. This therefore threw into question whether any retinal angiogenic defects observed in the absence of β 3-integrin could be attributed to its endothelial depletion, or a broader developmental delay in these mice. In an attempt to resolve this issue we found that omitting two β 3.EC^{KO} experiments in which the weight of Cre-positive pups was most substantially reduced relative to their Cre-negative controls saw animal weight restored to WT levels, whilst omitting the vascular extension values of the same experiments caused no effect to the overall vascular phenotype, leaving vascular extension significantly reduced relative to control retinas. Furthermore, if endothelial-specific depletion of β 3-integrin caused systemic developmental impairment, then it appeared the additional depletion of α 5-integrin and NRP1 individually or in combination (β 3/ α 5.EC^{KO}, α 5/NRP1.EC^{KO}, β 3/ α 5/NRP1.EC^{KO}) was enough to normalise animal weight. Considering our triple knockout displayed a more severe retinal angiogenic profile than that observed when β 3-integrin was targeted alone (β 3.EC^{KO}), we believed the reduced weight caused by β 3-integrin depletion was likely independent of its vascular effects in the retina. Nevertheless, it was impossible to rule this out, and therefore two possible receptor interactions could be theorised from these data.

The first assumed β 3-integrin depletion caused impairment to retinal vascular outgrowth irrespective of the reduction in overall animal weight. As stated previously, expression of β 3-integrin alone was unable to drive any angiogenic recovery from the baseline (α 5/NRP1.EC^{KO}), yet its individual depletion (β 3.EC^{KO}) conferred a significant impairment to vascular outgrowth (Fig 4.1 B & C). Although this conflicted with the normal retinal vascularisation of β 3-null mice, it agreed with therapeutic studies in which α v β 3-integrin antagonism inhibited choroidal and retinal neovascularisation, whilst additionally indicating that for β 3-integrin's pro-angiogenic contribution to take effect, α 5-integrin and/or NRP1 must also be expressed (Cre-neg, α 5.EC^{KO}, NRP1.EC^{KO}) (153, 232, 233, 234). As the detriment to vascular extension when β 3-integrin was depleted (β 3.EC^{KO}) was analogous to that when NRP1 was expressed alone (β 3/ α 5.EC^{KO}), and the co-expression of β 3-integrin and NRP1 was capable of driving a full angiogenic response (α 5.EC^{KO}), we hypothesized that β 3-integrin and NRP1 likely cooperate with one another in retinal vasculature to facilitate each other's full angiogenic potential (Fig 4.1 B & C). Meanwhile, lone depletion of α 5-integrin conferred no impairment to vascular outgrowth (α 5.EC^{KO}), no pro-angiogenic benefit when expressed alone (β 3/NRP1.EC^{KO}), and no cooperative enhancement of either β 3-integrin (NRP1.EC^{KO}) or NRP1 (β 3.EC^{KO}) relative to when these receptors were expressed individually (α 5/NRP1.EC^{KO} and

$\beta 3/\alpha 5.EC^{KO}$ respectively). This concurred with literature reporting no angiogenic detriment when $\alpha 5$ -integrin was conditionally depleted in endothelial cells (169).

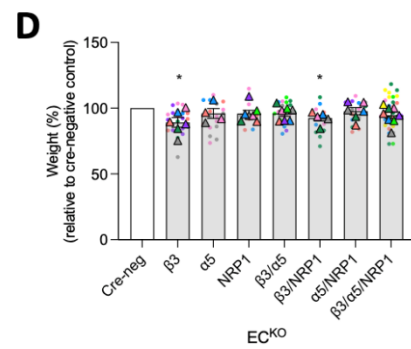
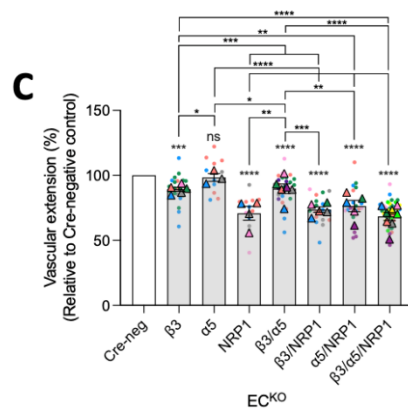
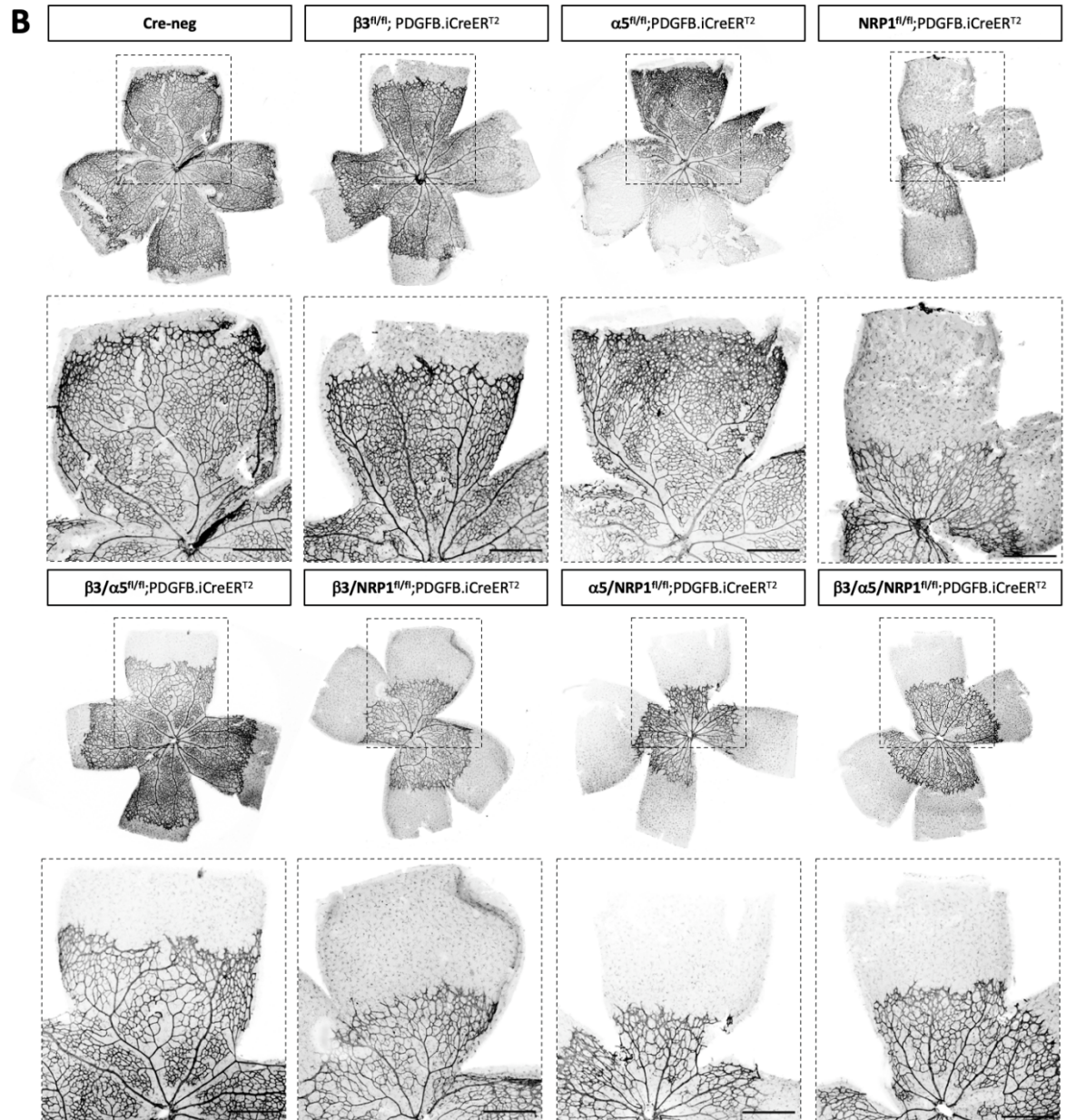
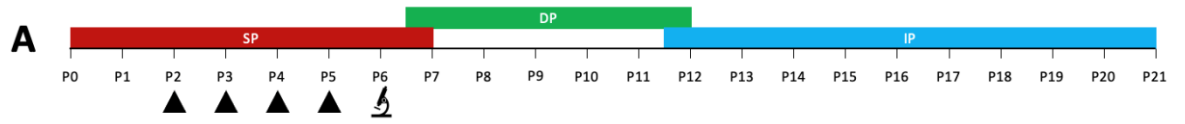
Alternatively, $\beta 3$ -integrin depletion may have caused a general developmental delay that was responsible for the impaired SP vascular outgrowth observed. Here we assumed targeting $\beta 3$ -integrin individually had no effect on retinal vascular extension. Nevertheless, the changes to vascular extension measured in each of our six other genotypes held true: $\beta 3$ - and $\alpha 5$ -integrin could not promote angiogenesis alone relative to our triple knockout ($\alpha 5/NRP1.EC^{KO}$, $\beta 3/NRP1.EC^{KO}$), NRP1 depletion conferred the most significant detriment to SP outgrowth ($NRP1.EC^{KO}$, $\beta 3/NRP1.EC^{KO}$, $\alpha 5/NRP1.EC^{KO}$, $\beta 3/\alpha 5/NRP1.EC^{KO}$), and expressing NRP1 alone drove angiogenesis beyond the baseline but fell short of achieving WT extension ($\beta 3/\alpha 5.EC^{KO}$). NRP1 therefore still required the co-expression of one or both of our integrin targets ($\beta 3.EC^{KO}$, $\alpha 5.EC^{KO}$, Cre-neg) to facilitate complete retinal vascular development. However, if we momentarily ignore NRP1, we noticed that whilst depleting either $\beta 3$ - or $\alpha 5$ -integrin alone ($\beta 3.EC^{KO}$, $\alpha 5.EC^{KO}$) had no vascular effect, co-targeting them saw a significant vascular impairment ($\beta 3/\alpha 5.EC^{KO}$). To explain this observation, we predicted these integrins likely compensated for one another, with each capable of driving angiogenesis in the absence of the other. Accordingly, only in their shared absence was an anti-angiogenic effect observed. From these data we therefore observed two potential receptor interactions contributing to retinal angiogenesis – the cooperation between $\beta 3$ -integrin and NRP1, and the compensation between $\beta 3$ - and $\alpha 5$ -integrin.

When looking at the vascular density of the SP, we split our analysis between the proliferative vascular front and the remodelling vascular interior. In doing so we gained an insight into the roles our receptors play in distinct phases of the angiogenic cascade, with endothelial proliferation, migration and tubulogenesis dominating in the vascular front, and mural cell recruitment, tightening of inter-cellular contacts, basement membrane deposition, and pruning of surplus vessels occurring towards the rear.

Looking first at the vascular front, changes in vascular density largely mirrored those seen in vascular extension, with $\beta 3$ -integrin and NRP1-dependent hypo-vascularisation ($\beta 3.EC^{KO}$, $NRP1.EC^{KO}$, $\beta 3/\alpha 5.EC^{KO}$, $\beta 3/NRP1.EC^{KO}$, $\alpha 5/NRP1.EC^{KO}$, $\beta 3/\alpha 5/NRP1.EC^{KO}$), and $\alpha 5$ -integrin appearing dispensable for normal vascular growth to proceed ($\alpha 5.EC^{KO}$) (Fig 4.1 F & G). As

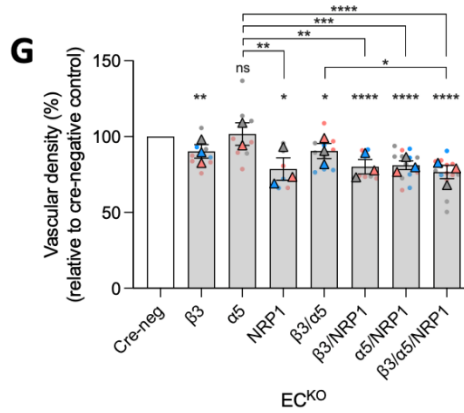
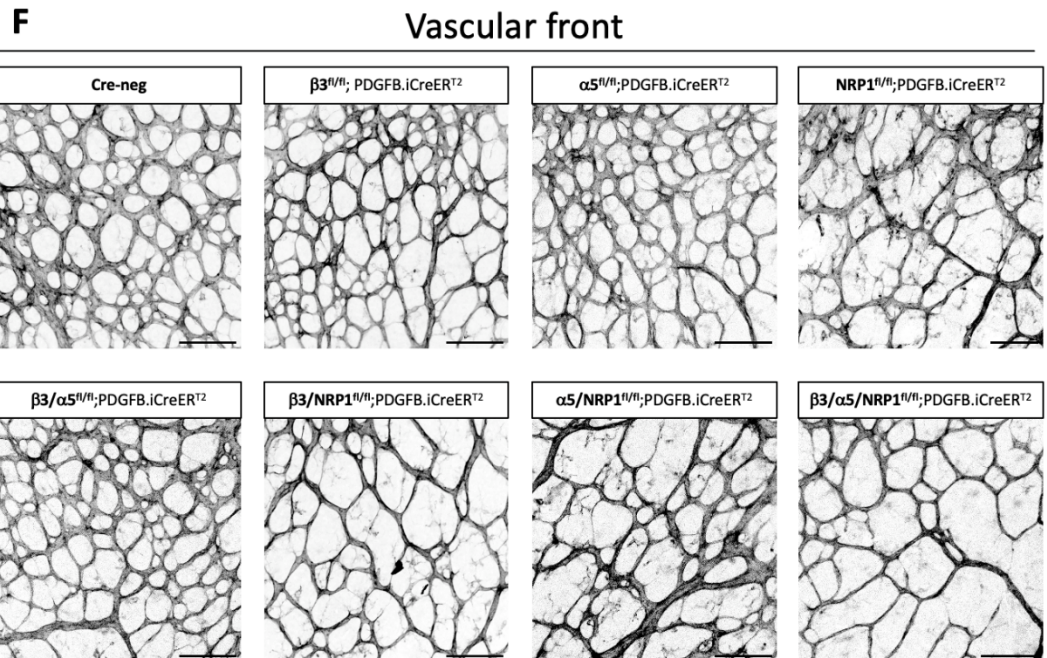
NRP1 has been shown not to influence endothelial proliferation, the hypo-vascularisation observed here was likely due to vascular instability causing excessive vessel regression (235). This phenotype was irrespective of its role as a VEGF co-receptor, as mice carrying a point mutation in its VEGF-binding domain to prevent NRP1-VEGF complex formation show no detriment to retinal vascular density at P9 (207). Integrins on the other hand are widely known to regulate endothelial proliferation (236). Pertinent to this study, Li *et al* reported that brain endothelial cells derived from $\beta 3$ -null mice displayed elevated $\alpha 5\beta 1$ -integrin expression that reciprocally drove endothelial proliferation beyond that of WT endothelial cells when plated on fibronectin matrices (173). Not only is the central retinal vasculature that we have analysed here also part of the central nervous system (CNS), but its vascular development follows a fibronectin-rich ECM scaffold deposited by astrocytes perinatally (171). Based on these factors, we would have predicted an $\alpha 5$ -integrin-dependent hyper-vascular response to $\beta 3$ -integrin depletion. However, in contradiction, others reported that $\beta 3$ -null endothelial cells displayed no compensatory changes to either cell surface or total levels of $\alpha 5\beta 1$ -integrin. Furthermore, as we have repeatedly stated, the method of target depletion used may be equally responsible for the vascular responses observed (154, 161). As we used a temporally controlled endothelial-specific model of target depletion, our observations may not necessarily concur with those previously reported in global knockout models.

Looking now at the vascular interior, the hypo-vascular effect of depleting $\beta 3$ -integrin alone or alongside $\alpha 5$ -integrin remained significantly different from Cre-negative controls, but nonetheless managed to progress slightly further towards WT levels such that the difference from their Cre-negative controls was negligible (Fig 4.1 H & I). This hinted that the vascular defects attributed to $\beta 3$ -integrin depletion alone or alongside $\alpha 5$ -integrin ($\beta 3.EC^{KO}$, $\beta 3/\alpha 5.EC^{KO}$) could be transient and may be accounted for over time. NRP1-depleted vascular interiors, however, remained hypo-vascularised with little to no recovery relative to their vascular fronts.



E

$\chi^{fl}.EC^{KO}$	$\beta 3$	$\alpha 5$	NRP1	$\beta 3/\alpha 5$	$\beta 3/NRP1$	$\alpha 5/NRP1$	$\beta 3/\alpha 5/NRP1$
$\beta 3$		0.0728 ns	0.0003 ***	>0.999 ns	0.0001 ***	0.0009 ***	<0.0001 ****
$\alpha 5$			<0.0001 ****	0.0751 ns	<0.0001 ****	<0.0001 ****	<0.0001 ****
NRP1				0.0003 ***	>0.9999 ns	0.9670 ns	>0.9999 ns
$\beta 3/\alpha 5$					0.0001 ***	0.0007 ***	<0.0001 ****
$\beta 3/NRP1$						0.9933 ns	0.9952 ns
$\alpha 5/NRP1$							0.7286 ns
$\beta 3/\alpha 5/NRP1$							



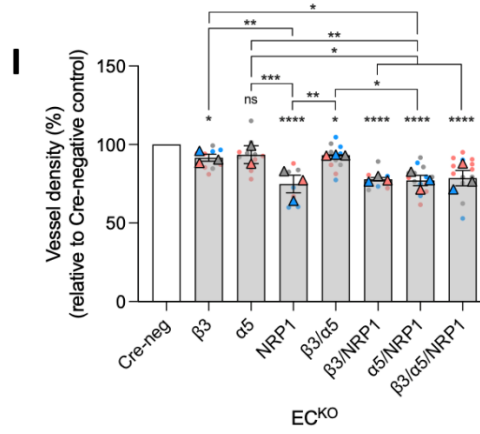
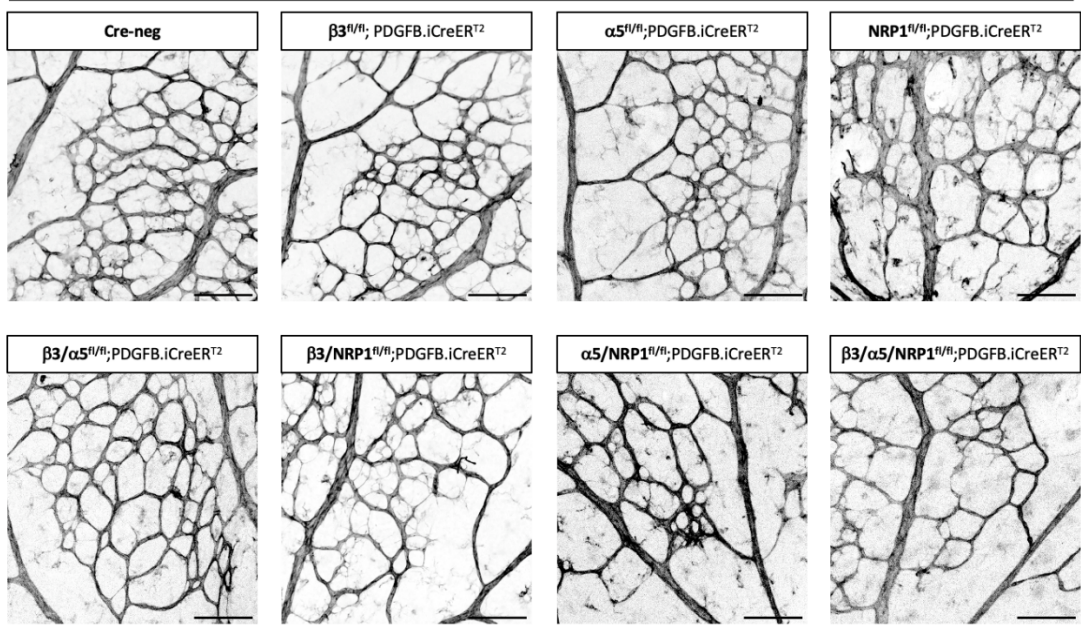
H**Vascular interior**

Figure 4.1 Neuropilin-1 is the principle driving force for sprouting angiogenesis in the postnatal mouse retina, but candidate interactions with and between β 3-integrin and α 5-integrin may be essential for the superficial plexus to fully vascularise. **A)** Time-course schematic of retinal vascular development and tamoxifen administration. Tamoxifen was administered (black triangles) via subcutaneous injection from P2-P3 and intraperitoneally from P4-P5 before sacrificing animals at P6. **B)** Representative images of BS1-lectin labelled P6 SP retinal vasculature. Magnified image scale bar = 500 μ m. **C)** Quantification of P6 vascular extension presented as a percentage of the average vascular extension measured in Cre-negative littermates. Error bars displayed as mean \pm SEM. $N \geq 3$, $n \geq 12$ retinas per group. **D)** Quantification of animal weights recorded at P6, with Cre-positive weights presented as a percentage of the average weight of their Cre-negative littermates. Error bars displayed as mean \pm SEM. $N \geq 3$, $n \geq 6$ mice per group. **E)** One-way ANOVA heatmap summary of P6 vascular extension between each Cre-positive knockout combination. Colour corresponds with statistical significance, with increasing significance correlating with darker shades of red. **F)** Representative 20X images of BS1-lectin labelled P6 retinal vascular fronts taken between an artery and a vein. Scale bar = 100 μ m. **G)** Quantification of vascular front vessel density, expressed as a percentage of the average vessel density measured in Cre-negative littermates. Error bars displayed as mean \pm SEM. $N \geq 2$, $n \geq 8$ retinas per group. **H)** Representative 20X images of BS1-lectin labelled P6 retinal vascular interiors taken between an artery and a vein. Scale bar = 100 μ m. **I)** Quantification of vascular interior vessel density, expressed as a percentage of the average vessel density measured in Cre-negative littermates. Error bars displayed as mean \pm SEM. $N \geq 2$, $n \geq 8$ retinas per group. Statistical significance was expressed and analysed as follows: *= $P < 0.05$, **= $P < 0.002$, ***= $P < 0.0002$, ****= $P < 0.0001$, unpaired students t-test (two-tailed)/one-way ANOVA.

4.2 Neuropilin-1 is critical to the timely vascularisation of the mouse retina.

We have previously shown that the consequences of target depletion can be influenced by the duration over which they are genetically targeted, and that previously observed vascular defects could be rescued by the upregulation of alternative angiogenic pathways (161, 195). To determine the longevity of the phenotypes observed at P6, we extended our analysis to a later developmental time point whilst maintaining our administration of tamoxifen from P2-P5 (Fig 4.2 A). At P18 the DP should have long since vascularised and the IP should be well on the way to completion too. Not only would analysis at this time point help us determine whether alternative pathways could offset the angiogenic impairments induced by individual and combinatorial target depletion at P6, but also whether any of our targets, or indeed the interactions between them, were involved in the vascularisation of the deep and intermediate plexuses.

Before looking at vascular growth in the P18 retina, we noticed that the individual or combined depletion of our targets had no effect on overall animal weight when compared with Cre-negative controls (Fig 4.2 B). The slight but significant drop in animal weight measured when β 3-integrin was depleted alone or alongside NRP1 at P6 (Fig 4.1 D) was therefore only an acute phenotype and able to be rescued over time. Similarly, vascular extension of the SP at P18 had normalised in each of our target knockout combinations (Fig 4.2 C & D). This provided yet further credence that alternative pathways could compensate for the loss of our targets if provided with sufficient time.

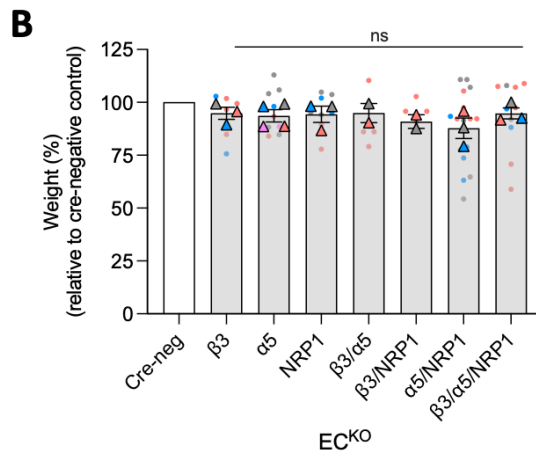
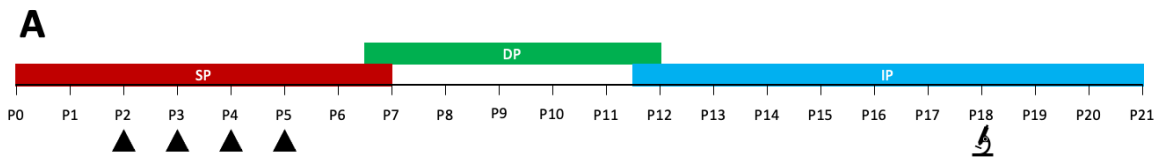
We next assessed the vascular density of the retina's three vascular layers to gain insight into the role our receptors play in the complete vascularisation of this organ. This revealed that the depletion of NRP1 either individually or alongside our integrin targets (NRP1.EC^{KO}, β 3/NRP1.EC^{KO}, α 5/NRP1.EC^{KO}, β 3/ α 5/NRP1.EC^{KO}) caused significant and largely analogous changes to each vascular plexus (Fig 4.2 E, F & G). The first observation to note is that despite its normalised vascular extension, the SP was hyper-vascularised relative to its Cre-negative controls in the absence of NRP1. This was in stark contrast with the hypo-vascularisation caused by NRP1 depletion at P6 (Fig 4.2 F-I) and indicated that the compensatory pathways upregulated to account for the loss of NRP1, whilst capable of progressing retinal vascular growth, may fail to appropriately resolve angiogenesis. The hyper-dense vascular network left behind the sprouting retinal front should normally undergo a significant period of remodelling typified by the regression of superfluous

vessels. Without refashioning these vessels into a mature network, it is unlikely that they would be able to function normally. NRP1 is therefore critical to producing a balanced angiogenic response at later developmental stages of retinal development. Crucially, the expression of both integrins without NRP1 (NRP1.EC^{KO}) conferred the same superficial hyper-vascular effect as the triple knockout ($\beta3/\alpha5/NRP1.EC^{KO}$), indicating this effect was irrespective of our integrin targets (Fig 4.2 E, F & G). However, whilst $\beta3$ -integrin did not contribute to this hyper-vascular effect when expressed alongside $\alpha5$ -integrin (NRP1.EC^{KO}), its individual expression ($\alpha5/NRP1.EC^{KO}$) was able to worsen hypervascularisation relative to the individual expression of $\alpha5$ -integrin ($\beta3/NRP1.EC^{KO}$). $\alpha5$ -integrin may have therefore performed an inhibitory function over $\beta3$ -integrin in certain circumstances, acting to limit its angiogenic involvement. Notably, this speculative interaction only occurred in the absence of NRP1, as $\alpha5$ -integrin depletion alone ($\alpha5.EC^{KO}$) did not result in $\beta3$ -integrin-dependent SP hypervascularisation.

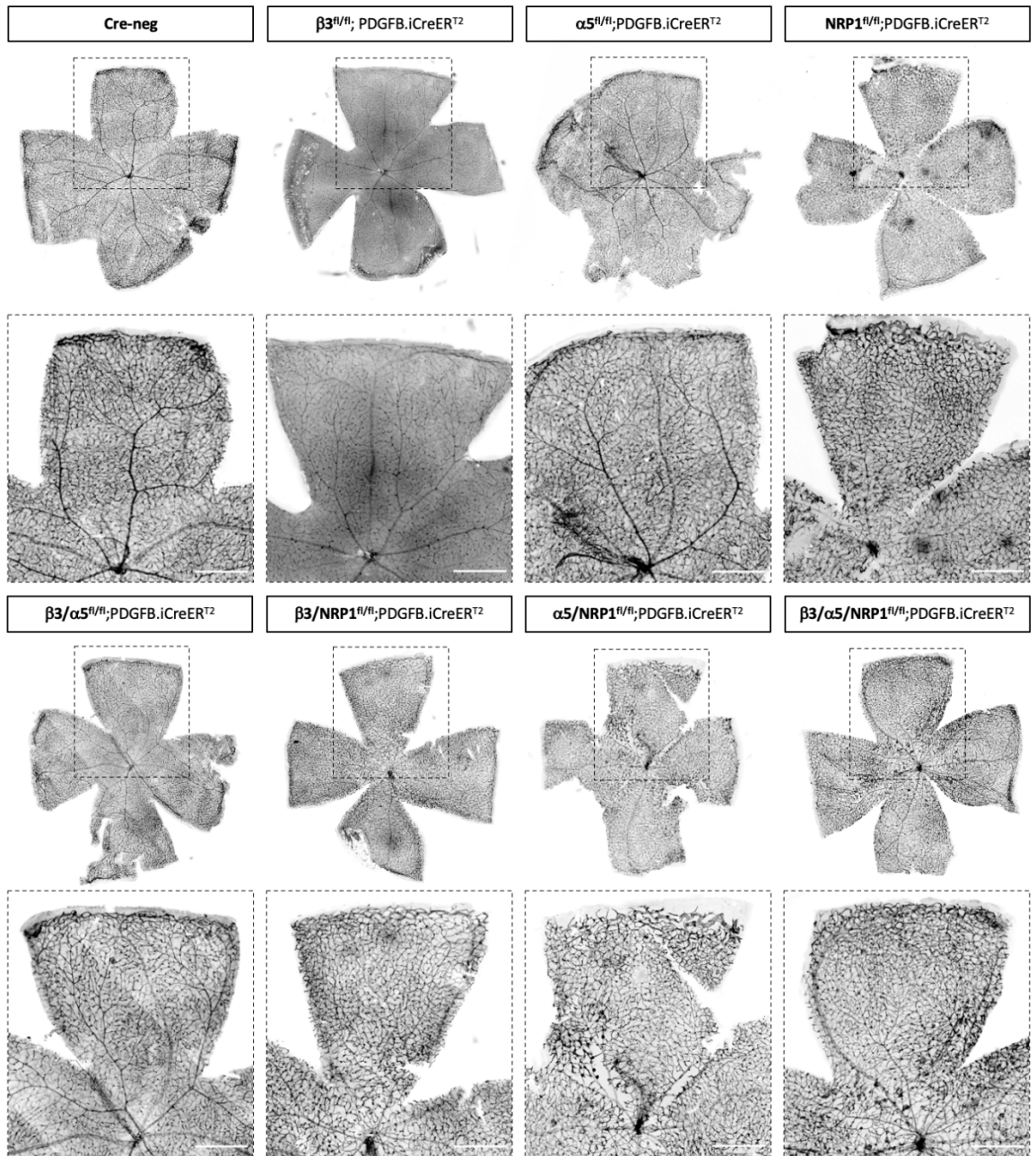
In contrast to the hyper-vascularisation of the SP, the DP was severely hypo-vascularised, again in a NRP1-dependent fashion, reaching less than half the vascular density of Cre-negative control retinas (Fig 4.2 E, F & G). NRP1 alone was therefore essential for the vascular development of this layer as reported previously (237, 238). Meanwhile the IP, whilst also hypo-vascularized, was significantly closer to its intended vascular density at P18. Considering the deep and intermediate plexuses begin their vascular development at P7 and P12 respectively, it was curious why the DP was more profoundly affected by NRP1 depletion than the IP given the additional developmental time it had to vascularise prior to tissue harvest. In light of this, we predicted that vascular development of the deep and intermediate plexuses would likely proceed in the absence of NRP1, albeit far more slowly, but the IP would conclude its vascularisation before that of the DP. If true, then the dogma of the retina's timely vascularisation appeared to be critically dependent on endothelial NRP1. This had already been partially answered by Fantin *et al* when investigating NRP1's VEGF-dependent functionality, though they did not comment on this phenomenon. They generated knock-in mice carrying a point mutation at Y297 (NRP1^{Y297/Y297}) such that VEGF was unable to bind with NRP1. Using the retinal angiogenesis model, they found that the DP remained more severely hypo-vascularised than the IP at P21. Unfortunately, this knock-in mouse model was hypomorphic for NRP1 expression, and thus these angiogenic defects could not be attributed to NRP1's VEGF-dependent functionality alone (180). Nevertheless, NRP1 represents a fundamental angiogenic driving force and regulator of retinal angiogenesis throughout its post-natal development.

Unlike the persistent vascular defects associated with NRP1 depletion, targeting β 3- or α 5-integrin (β 3.EC^{KO}, α 5.EC^{KO}) had no effect on the vascular density of any retinal vascular bed at P18, even when depleted together (β 3/ α 5.EC^{KO}). The absence of these integrins was likely offset by redundancy mechanisms capable of compensating for their function to drive a full angiogenic response at P18. NRP1 is a probable compensatory candidate. We have previously shown that NRP1 could coordinate endothelial migration in the long-term absence of β 3-integrin by facilitating paxillin activity in a VEGF-dependent manner. Furthermore, pathological angiogenesis also became reliant on NRP1 in this scenario such that its genetic depletion alongside β 3-integrin was able to compromise the growth of established tumours (195). We therefore hypothesized that, over time, NRP1 could offset the angiogenic detriment caused by integrin depletion at P6.

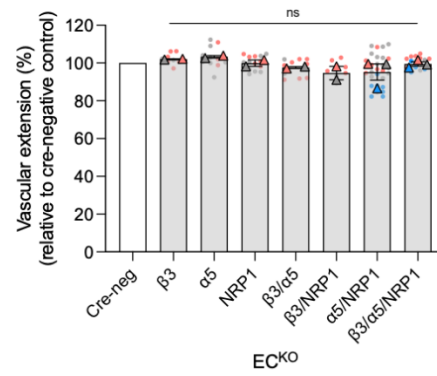
Our investigations at P18 also revealed other vascular malformations in NRP1-deficient vasculature, namely haemorrhages and large endothelial tufts (Fig 4.2 H). These abnormal vessel endings usually hang beneath the SP, unable to sprout downwards through the underlying retinal parenchyma, but may also sprout away from the retina and into the vitreous. Whilst the former positioning of retinal tufts may compromise intermediate and deep plexus vascularisation, vitreous tufts can cause bleeding and even tractional retinal detachment (220). Tuft malformations have been reported previously upon endothelial-specific NRP1 depletion in both retinal and subventricular hindbrain vasculature and their formation owed to inappropriate endothelial migration compromising vascular sprouting and tip cell guidance (180, 181). We also observed haemorrhages when dissecting these retinas. These were likely caused by vitreous tufts, as they have been previously reported to swell and eventually rupture (231). Figure 4.2-I displays a swollen tuft and its housed blood contents in triple knockout retinal vasculature. We had aimed to enumerate these retinal tufts to compare between our knockout combinations, but their considerable variation in size made their identification difficult. By eye, however, we know that these malformations were absent when β 3- and α 5-integrin were targeted alone or in combination (β 3.EC^{KO}, α 5.EC^{KO}, β 3/ α 5.EC^{KO}) (Fig 4.2 H).

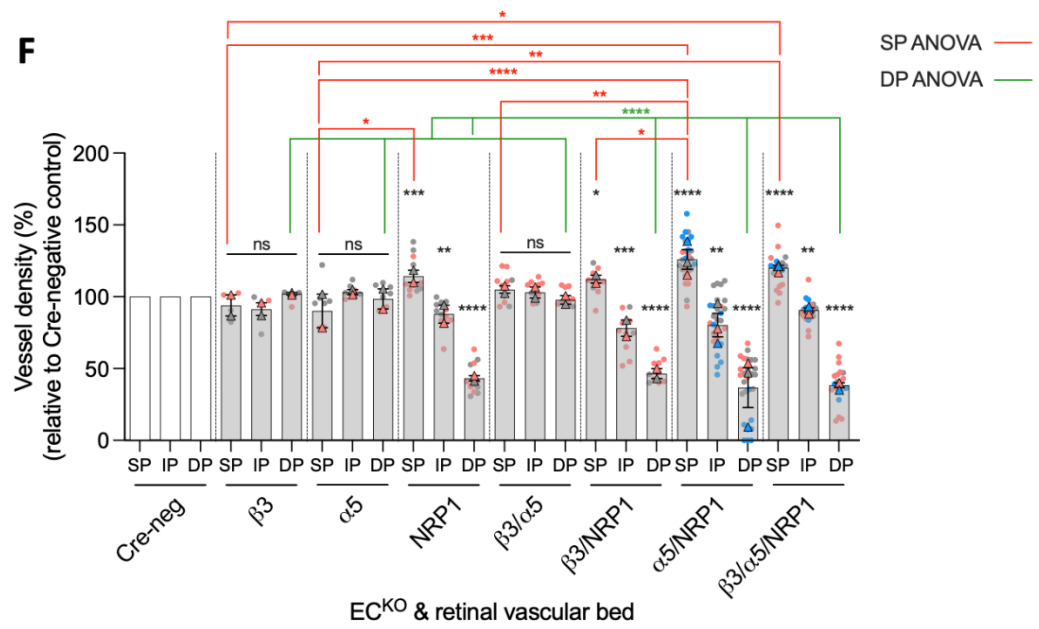
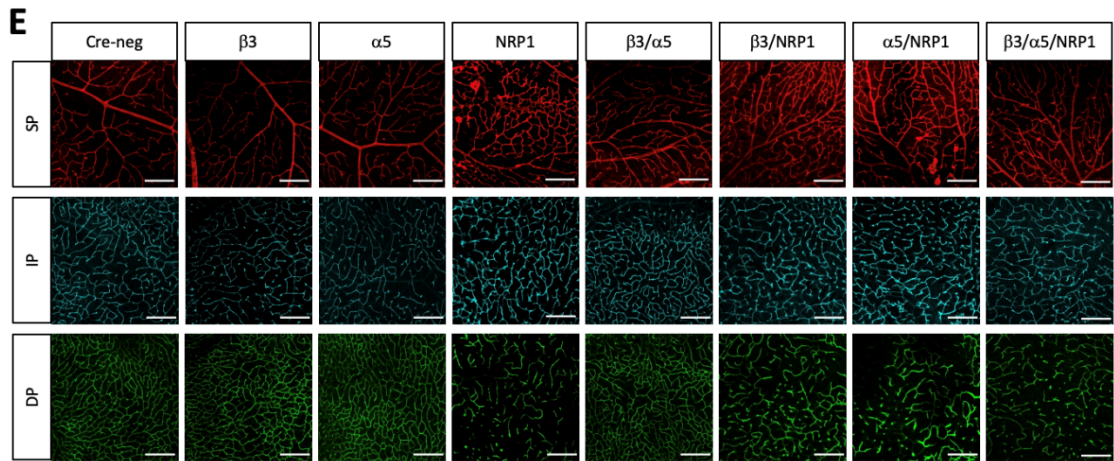


C



D



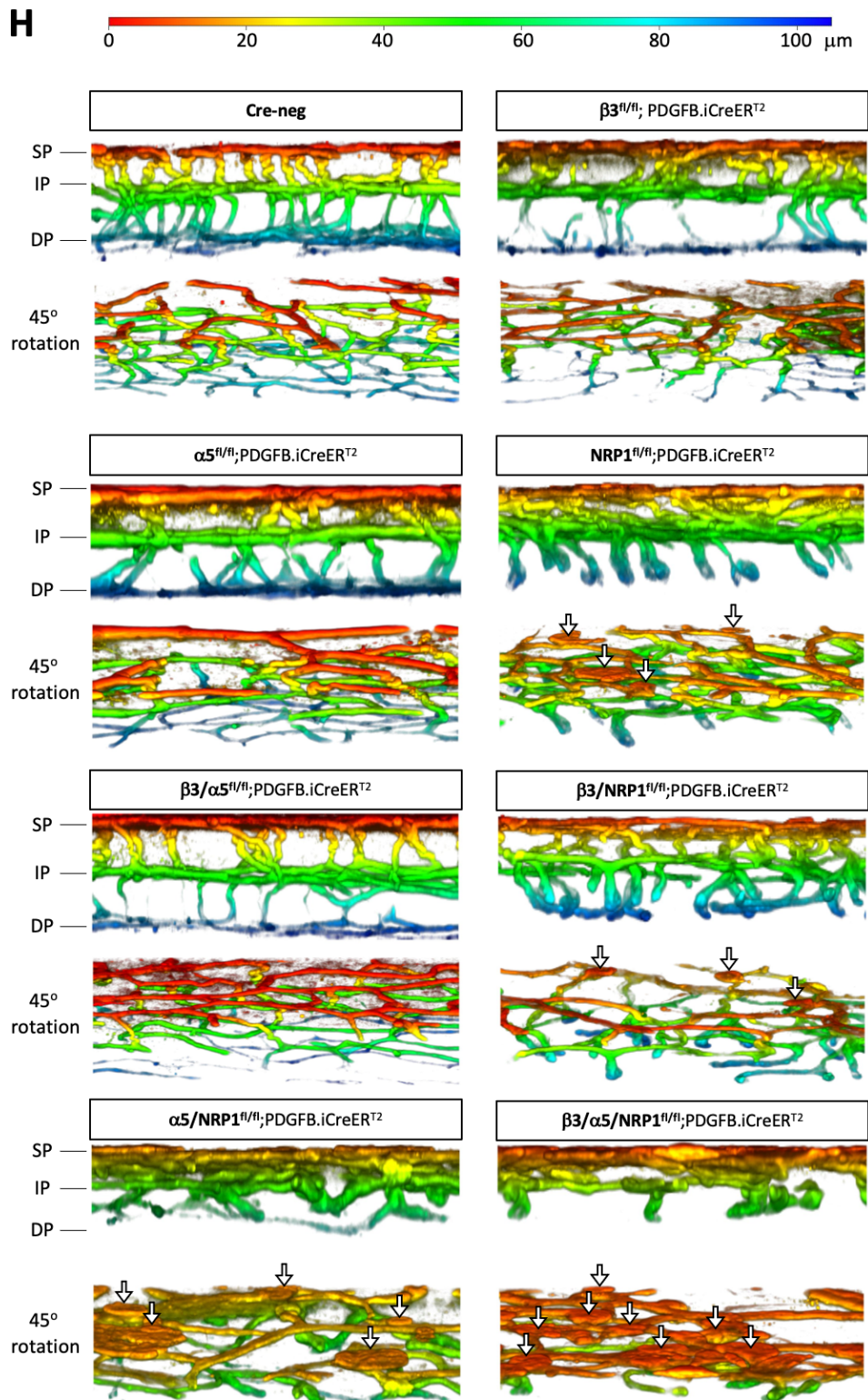


G

SP $\chi^{nfi}.EC^{KO}$	$\beta 3$	$\alpha 5$	NRP1	$\beta 3/\alpha 5$	$\beta 3/\text{NRP1}$	$\alpha 5/\text{NRP1}$	$\beta 3/\alpha 5/\text{NRP1}$
$\beta 3$		>0.9999 ns	0.1060 ns	0.6515 ns	0.3285 ns	0.0002 ***	0.0124 *
$\alpha 5$			0.0346 *	0.5339 ns	0.1903 ns	<0.0001 ****	0.0012 **
NRP1				0.7971 ns	0.9931 ns	0.1048 ns	0.9577 ns
$\beta 3/\alpha 5$					0.9928 ns	0.0014 **	0.1869 ns
$\beta 3/\text{NRP1}$						0.0203 *	0.6362 ns
$\alpha 5/\text{NRP1}$							0.4502 ns
$\beta 3/\alpha 5/\text{NRP1}$							

IP $\chi^{nfi}.EC^{KO}$	$\beta 3$	$\alpha 5$	NRP1	$\beta 3/\alpha 5$	$\beta 3/\text{NRP1}$	$\alpha 5/\text{NRP1}$	$\beta 3/\alpha 5/\text{NRP1}$
$\beta 3$		0.7288 ns	0.9954 ns	0.5583 ns	0.2755 ns	0.8750 ns	>0.9999 ns
$\alpha 5$			0.1249 ns	>0.9999 ns	0.0002 ***	0.0046 **	0.1736 ns
NRP1				0.0323 *	0.2060 ns	0.9421 ns	0.9995 ns
$\beta 3/\alpha 5$					<0.0001 ****	0.0002 ***	0.0417 *
$\beta 3/\text{NRP1}$						0.5423 ns	0.0472 *
$\alpha 5/\text{NRP1}$							0.5991 ns
$\beta 3/\alpha 5/\text{NRP1}$							

DP $\chi^{nfi}.EC^{KO}$	$\beta 3$	$\alpha 5$	NRP1	$\beta 3/\alpha 5$	$\beta 3/\text{NRP1}$	$\alpha 5/\text{NRP1}$	$\beta 3/\alpha 5/\text{NRP1}$
$\beta 3$		>0.9999 ns	<0.0001 ****	>0.9999 ns	<0.0001 ****	<0.0001 ****	<0.0001 ****
$\alpha 5$			<0.0001 ****	>0.9999 ns	<0.0001 ****	<0.0001 ****	<0.0001 ****
NRP1				<0.0001 ****	0.9808 ns	0.9114 ns	0.9852 ns
$\beta 3/\alpha 5$					<0.0001 ****	<0.0001 ****	<0.0001 ****
$\beta 3/\text{NRP1}$						0.3997 ns	0.6451 ns
$\alpha 5/\text{NRP1}$							0.9998 ns
$\beta 3/\alpha 5/\text{NRP1}$							



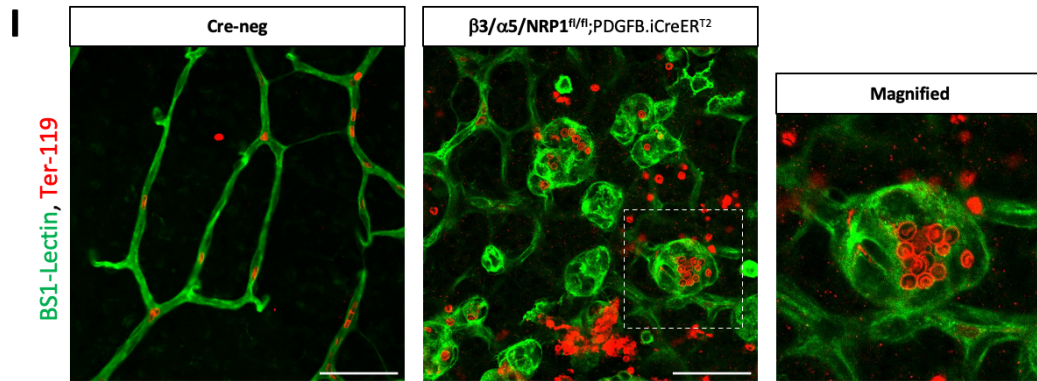


Figure 4.2 Neuropilin-1 is critical to the timely vascularization of the mouse retina. A) Time-course schematic of retinal vascular development and tamoxifen administration. Tamoxifen was administered (black triangles) via subcutaneous injection from P2-P3 and intraperitoneally from P4-P5 before sacrificing animals at P18. **B)** Quantification of animal weights recorded at P18, with Cre-positive weights presented as a percentage of the average weight of their Cre-negative littermates. Error bars displayed as mean \pm SEM. $N \geq 2$, $n \geq 5$ mice per group. **C)** Representative images of BS1-lectin labelled P18 SP retinal vasculature. Magnified image scale bar = 500 μ m. **D)** Quantification of P18 vascular extension presented as a percentage of the average vascular extension measured in Cre-negative littermates. Error bars displayed as mean \pm SEM. $N \geq 2$, $n \geq 8$ retinas per group. **E)** Representative images of BS1-lectin labelled P18 retinal vascular layers. SP (red), IP (blue) and DP (green). Scale bar = 200 μ m. **F)** Quantification of SP, IP, and DP vessel density in P18 retinal vasculature, expressed as a percentage of the average vessel density measured in Cre-negative littermates. Error bars displayed as mean \pm SEM. ANOVAs: red = SP, green = DP, IP was omitted for clarity. $N \geq 2$, $n \geq 8$ retinas per group. **G)** One-way ANOVA heatmap summary of SP, IP and DP vascular densities at P18, comparing statistical significance values between each Cre-positive knockout combination. Colour corresponds with statistical significance, with increasing significance correlating with darker shades of red. **H)** Colour depth-coded Z-stacks of retinal vascular layers taken at the midpoint between the optic nerve head and retinal periphery between an artery and a vein. Colour coded scale bar provided. Displayed under each genotype is a retinal side profile and the same image with a 45° tilt applied to reveal vascular tufts extending into the vitreous, denoted by the white and black arrows. Their flattened appearance was due to the process of retinal flat mounting. **I)** Representative images of the SP taken at the midpoint between the optic nerve head and retinal periphery between an artery and a vein in Cre-negative and $\beta 3/\alpha 5/NRP1^{fl/fl}; PDGFB.iCreER^{T2}$ P18 retinas, and co-stained for BS1-lectin and Ter-119. Magnified image displays a swollen vascular tuft protruding into the vitreous with housed erythrocyte contents. Scale bar = 50 μ m. Statistical significance was expressed and analysed as follows: *= $P < 0.05$, **= $P < 0.002$, ***= $P < 0.0002$, ****= $P < 0.0001$, unpaired students t-test (two-tailed)/one-way ANOVA.

4.3 Delaying target depletion to circumvent angiogenic compensation revealed the involvement of $\alpha 5$ -integrin in deep plexus vascularisation.

Though our analysis of P6 vascular density hinted that the angiogenic defects resultant of $\beta 3$ - and $\alpha 5$ -integrin depletion may only be transient, we remained surprised that the two major endothelial fibronectin-binding integrins, as well as the interactions between them, were unnecessary for retinal deep plexus formation at P18, particularly since this matrix component is essential for early retinal vascularisation and co-labels with deep plexus vasculature (239, 240). We hypothesised that alternative, NRP1-dependent angiogenic mechanisms were being employed to drive later stages of retinal angiogenesis in their absence. To determine whether this was the case, we delayed target depletion until P7 to remove any time allowance for retinal vasculature to adopt alternative angiogenic means for DP development and sacrificed animals at P12 (Fig 4.3 A). By this time point the DP should be concluding its vascular development.

Throughout each knockout combination animal weights remained non-significantly different from their Cre-negative controls (Fig 4.3 B). Each knockout line also displayed normal extension of the SP with the exception of our triple knockout ($\beta 3/\alpha 5/NRP1.EC^{KO}$) (Fig 4.3 C & D). This minor detriment to SP outgrowth likely arose because our first administration of tamoxifen caught the final stage of SP development at P7. The purpose for this was to deplete our targets at the earliest stages of DP formation, which incidentally coincided with the final stages of SP outgrowth. Testimony to the importance of co-expressing these three receptors for developmental angiogenesis, only in their shared absence could SP extension be halted when so close to completion.

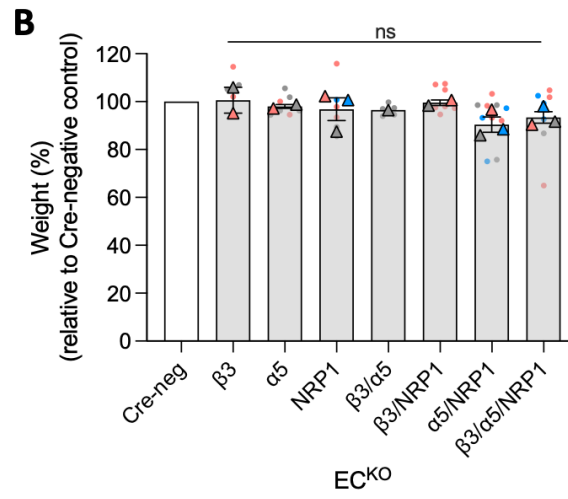
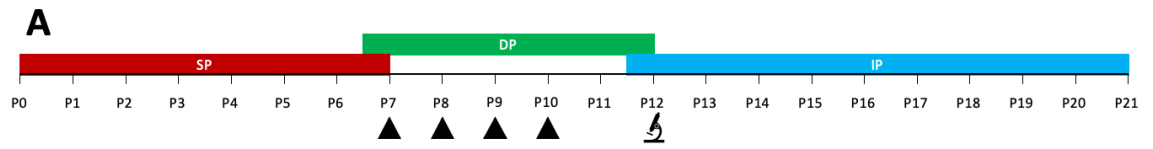
Looking next at the density of the retina's three vascular layers (Fig 4.3 E, F & G), the NRP1-dependent effects observed at P18 held true. In the absence of NRP1 ($NRP1.EC^{KO}$, $\beta 3/NRP1.EC^{KO}$, $\alpha 5/NRP1.EC^{KO}$, $\beta 3/\alpha 5/NRP1.EC^{KO}$) and seemingly ignorant of our integrin targets, the intermediate and deep plexuses became hypo-vascularised, with vascular sprouts failing to descend to the DP (Fig 4.3 H). Furthermore, in all but one of our NRP1 knockout combinations ($\beta 3/\alpha 5/NRP1.EC^{KO}$), the SP had hyper-vascularised, akin with that observed at P18. We surmised that this was due to impaired vessel regression rather than hyper-proliferation as this phenotype was restricted to the NRP1 knockouts that had fully extended their superficial vasculature ($NRP1.EC^{KO}$, $\beta 3/NRP1.EC^{KO}$, $\alpha 5/NRP1.EC^{KO}$) and entered the remodelling phase of their development before tamoxifen-induced

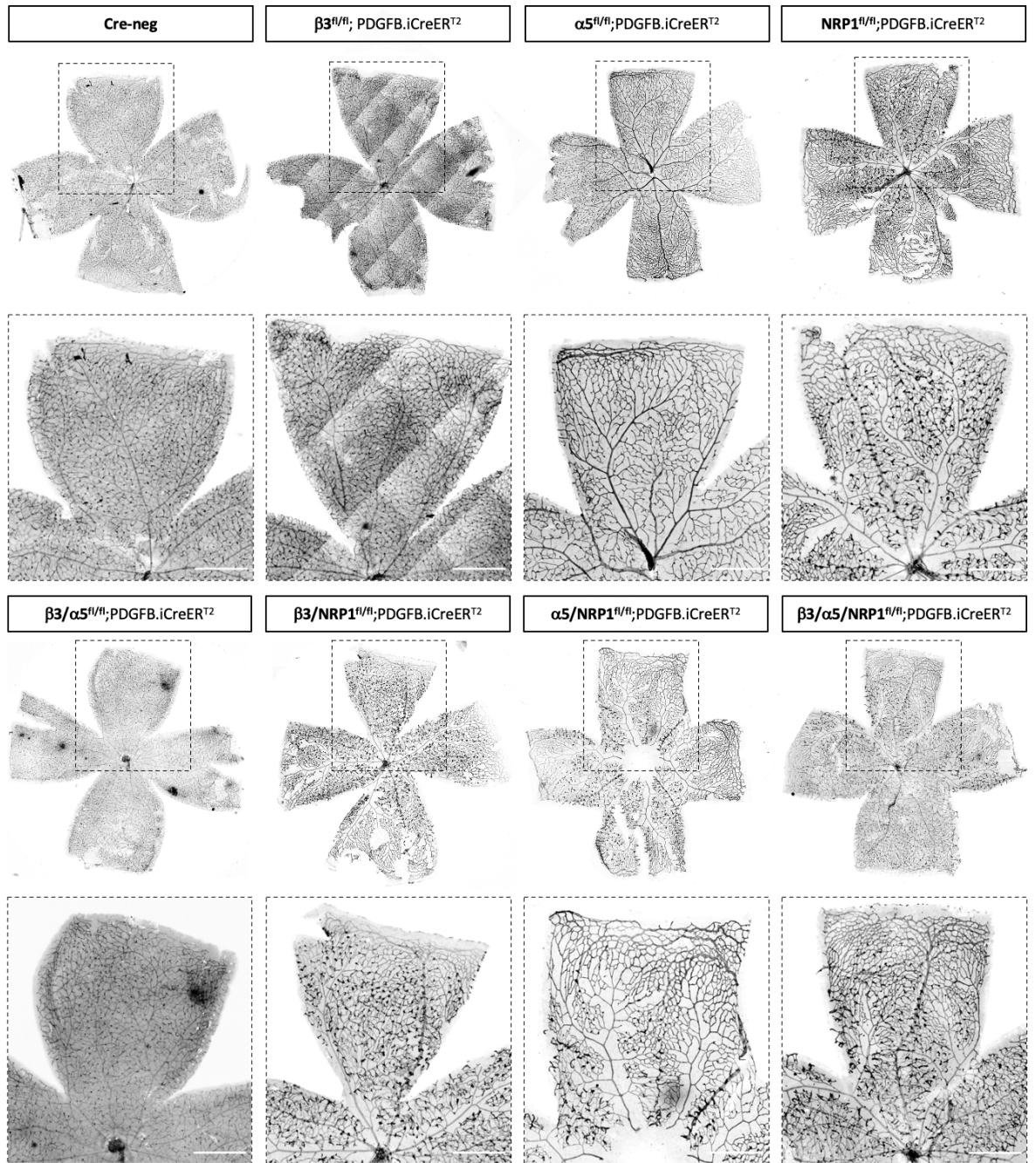
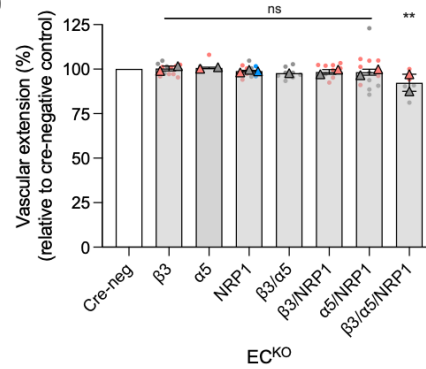
target depletion occurred. Once again, we observed that in the absence of NRP1 the IP was significantly more vascularised than the DP. Considering the IP had approximately 24 hours to develop prior to tissue harvest (Fig 4.3 A), NRP1 was likely less essential for the development of the intermediate layer, but altogether pivotal for the dogma of retinal vascular development in which the DP develops prior to the IP. Alternatively, this may have been an artefact of Cre-toxicity. We previously observed in PDGFB.iCreER^{T2} expressing mice that Cre-recombinase activity induced between P7-P10 caused slight hyper-vascularisation of the IP at P12 (Fig 4.3 E & F). This effect may have lessened the true angiogenic detriment caused by NRP1 depletion in this vascular bed, resulting in less severe hypo-vascularisation.

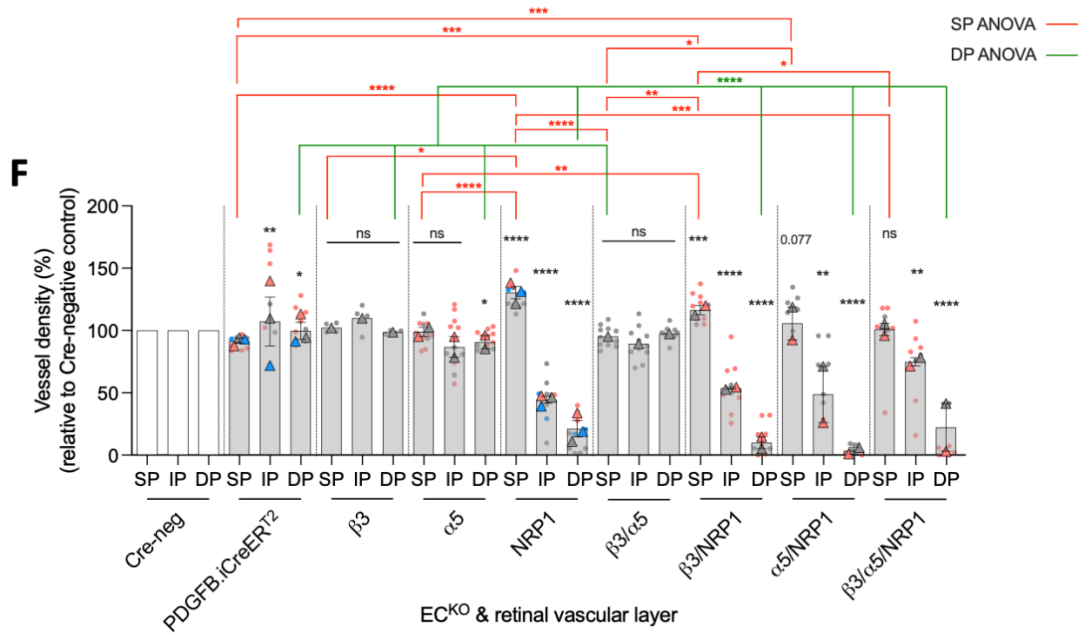
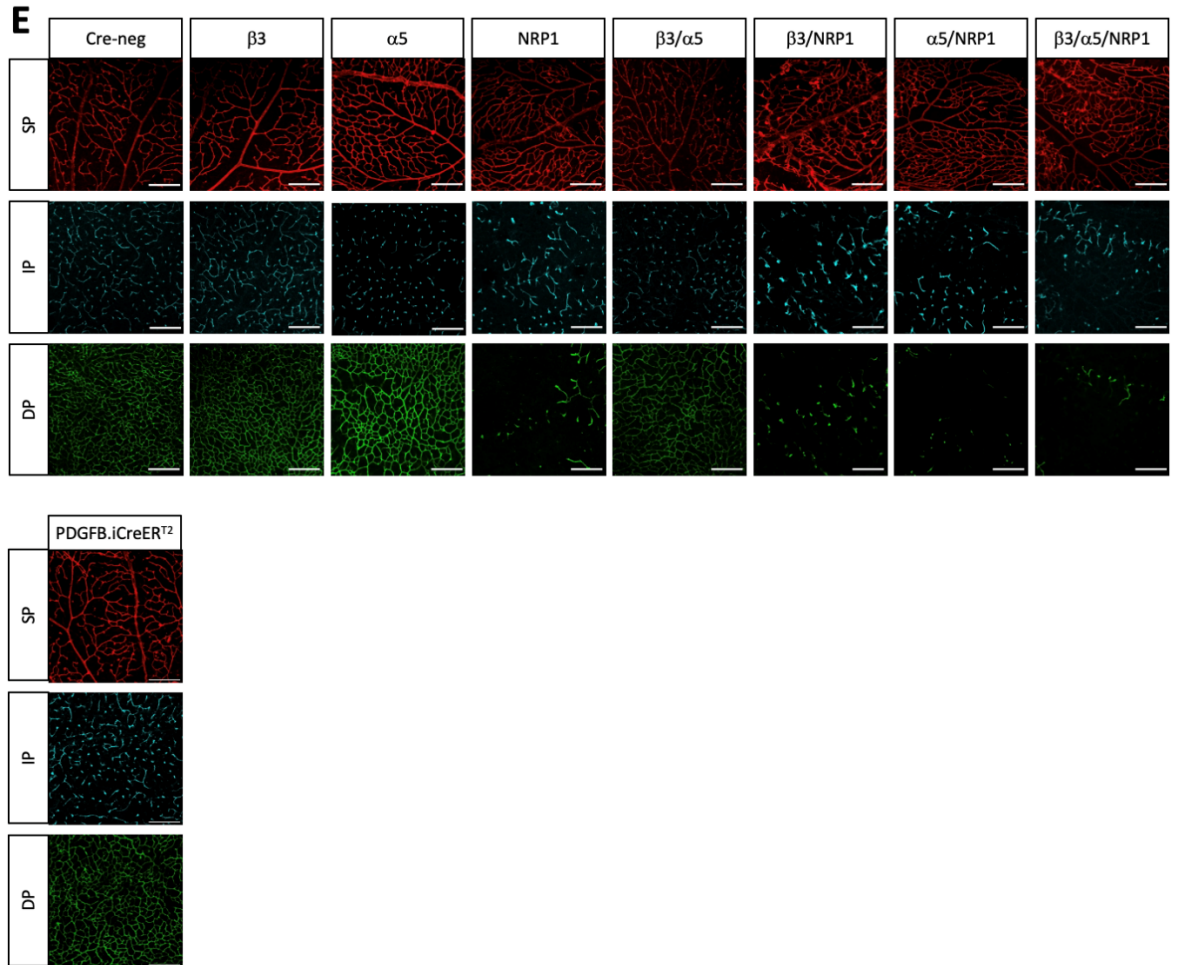
Our hypothesis that alternative angiogenic pathways were capable of sustaining vascular development in the absence of β 3- and α 5-integrin was based on former studies from the Robinson lab as well as our observations at P6 and P18, where the acute angiogenic detriment conferred by integrin depletion could be rescued over time (161, 194, 195). We postulated that by circumventing time-dependent recovery pathways we would reveal the true involvement of these integrin targets in later stages of retinal angiogenesis. In accordance with P6 data where α 5- and β 3-integrin were unable to drive angiogenesis beyond the baseline established by the triple knockout when expressed alone (β 3/NRP1.EC^{KO}, α 5/NRP1.EC^{KO}) (Fig 4.1 B & C), no angiogenic recovery in any vascular plexus was detected in the same genotypes at P12 (Fig 4.3 E & F). However, even when circumventing redundancy mechanisms such as that reported by Ellison *et al*, where NRP1 could compensate for the long-term absence of β 3-integrin, we detected no impairment in retinal vasculature at P12 when β 3-integrin was acutely depleted (β 3.EC^{KO}, β 3/ α 5.EC^{KO}) (Fig 4.3 E & F). NRP1-dependent compensatory mechanisms were therefore not responsible for the angiogenic recovery observed in β 3-integrin deficient vasculature at P18. Instead, β 3-integrin's pro-angiogenic contributions were restricted to superficial vasculature.

Unexpectedly, we found instead that the individual ablation of α 5-integrin (α 5.EC^{KO}) caused a slight but significant reduction in DP vascular density (Fig 4.3 E & F). This result conflicted with our findings at P6 where targeting α 5-integrin alone conferred no angiogenic detriment to SP extension or vascular density. Whilst the angiogenic perturbation observed here was extremely minor, it suggested α 5-integrin performed subtle pro-angiogenic functions exclusive to DP vasculature and, as this hypo-vascular effect was absent from our P18 data, was capable of being compensated for by other angiogenic pathways over time. We also noted that this slight angiogenic detriment

resultant of $\alpha 5$ -integrin depletion was lost following $\beta 3$ -integrin co-depletion ($\beta 3/\alpha 5.EC^{KO}$), though the deep plexus vascular density of these two knockout lines were non-significantly different (Fig 4.3 E, F & G). As the only remaining target being expressed when $\beta 3$ - and $\alpha 5$ -integrin were depleted together was NRP1, the vascular recovery observed could be dependent on this receptor, though this is purely speculative due to the lack of a significant change between the two genotypes. Furthermore, as WT levels of DP vascularisation were only achieved when $\beta 3$ -integrin was depleted ($\beta 3.EC^{KO}$, $\beta 3/\alpha 5.EC^{KO}$), or when each of our targets were expressed together (Cre-neg), we deduced that $\beta 3$ -integrin may be performing an anti-angiogenic role in the absence of $\alpha 5$ -integrin ($\alpha 5.EC^{KO}$) by limiting the pro-angiogenic functionality of NRP1. When all three receptors were expressed together (Cre-neg), $\alpha 5$ -integrin could restrict $\beta 3$ -integrin's inhibitory capacity. When $\alpha 5$ -integrin was depleted ($\alpha 5.EC^{KO}$), this inhibitory function could elicit a drop in DP vascular density that was subsequently rescued by the additional ablation of $\beta 3$ -integrin ($\beta 3/\alpha 5.EC^{KO}$). Only when these integrins were either dually depleted ($\beta 3/\alpha 5.EC^{KO}$) or expressed together (Cre-neg) could NRP1 engage its full angiogenic capacity in the DP.



C**D**



G

SP $\chi^{flfl}.EC^{KO}$	$\beta 3$	$\alpha 5$	NRP1	$\beta 3/\alpha 5$	$\beta 3/\text{NRP1}$	$\alpha 5/\text{NRP1}$	$\beta 3/\alpha 5/\text{NRP1}$
PDGFB.i CreER ^{T2}	0.7653 ns	0.8887 ns	<0.0001 ****	0.9855 ns	0.0004 ***	0.0077 ***	0.8839 ns
$\beta 3$		0.9985 ns	0.0366 *	0.9819 ns	0.4008 ns	0.7463 ns	0.9997 ns
$\alpha 5$			<0.0001 ****	0.9998 ns	0.0077 **	0.0978 ns	>0.9999 ns
NRP1				<0.0001 ****	0.8191 ns	0.5781 ns	0.0004 ***
$\beta 3/\alpha 5$					0.0025 **	0.0421 *	0.9994 ns
$\beta 3/\text{NRP1}$						0.9994 ns	0.0332 *
$\alpha 5/\text{NRP1}$							0.2106 ns
$\beta 3/\alpha 5/\text{NRP1}$							

IP $\chi^{flfl}.EC^{KO}$	$\beta 3$	$\alpha 5$	NRP1	$\beta 3/\alpha 5$	$\beta 3/\text{NRP1}$	$\alpha 5/\text{NRP1}$	$\beta 3/\alpha 5/\text{NRP1}$
PDGFB.i CreER ^{T2}	0.9243 ns	0.0168 *	<0.0001 ****	0.0196 *	<0.0001 ****	<0.0001 ****	<0.0001 ****
$\beta 3$		0.7989 ns	0.0023 **	0.8036 ns	0.0041 **	0.0204 *	0.1942 ns
$\alpha 5$			0.0117 *	>0.9999 ns	0.0187 *	0.1282 ns	0.7962 ns
NRP1				0.0141 *	0.9980 ns	0.9606 ns	0.4188 ns
$\beta 3/\alpha 5$					0.0235 *	0.1458 ns	0.8156 ns
$\beta 3/\text{NRP1}$						0.9995 ns	0.6839 ns
$\alpha 5/\text{NRP1}$							0.9481 ns
$\beta 3/\alpha 5/\text{NRP1}$							

DP $\chi^{flfl}.EC^{KO}$	$\beta 3$	$\alpha 5$	NRP1	$\beta 3/\alpha 5$	$\beta 3/\text{NRP1}$	$\alpha 5/\text{NRP1}$	$\beta 3/\alpha 5/\text{NRP1}$
PDGFB.i CreER ^{T2}	0.9549 ns	0.1414 ns	<0.0001 ****	0.6756 ns	<0.0001 ****	<0.0001 ****	0.8839 ****
$\beta 3$		0.9769 ns	<0.0001 ****	>0.9999 ns	<0.0001 ****	<0.0001 ****	<0.0001 ****
$\alpha 5$			<0.0001 ****	0.9661 ns	<0.0001 ****	<0.0001 ****	<0.0001 ****
NRP1				<0.0001 ****	0.9855 ns	0.2583 ns	0.9876 ns
$\beta 3/\alpha 5$					<0.0001 ****	<0.0001 ****	<0.0001 ****
$\beta 3/\text{NRP1}$						0.7726 ns	>0.9999 ns
$\alpha 5/\text{NRP1}$							0.8286 ns
$\beta 3/\alpha 5/\text{NRP1}$							

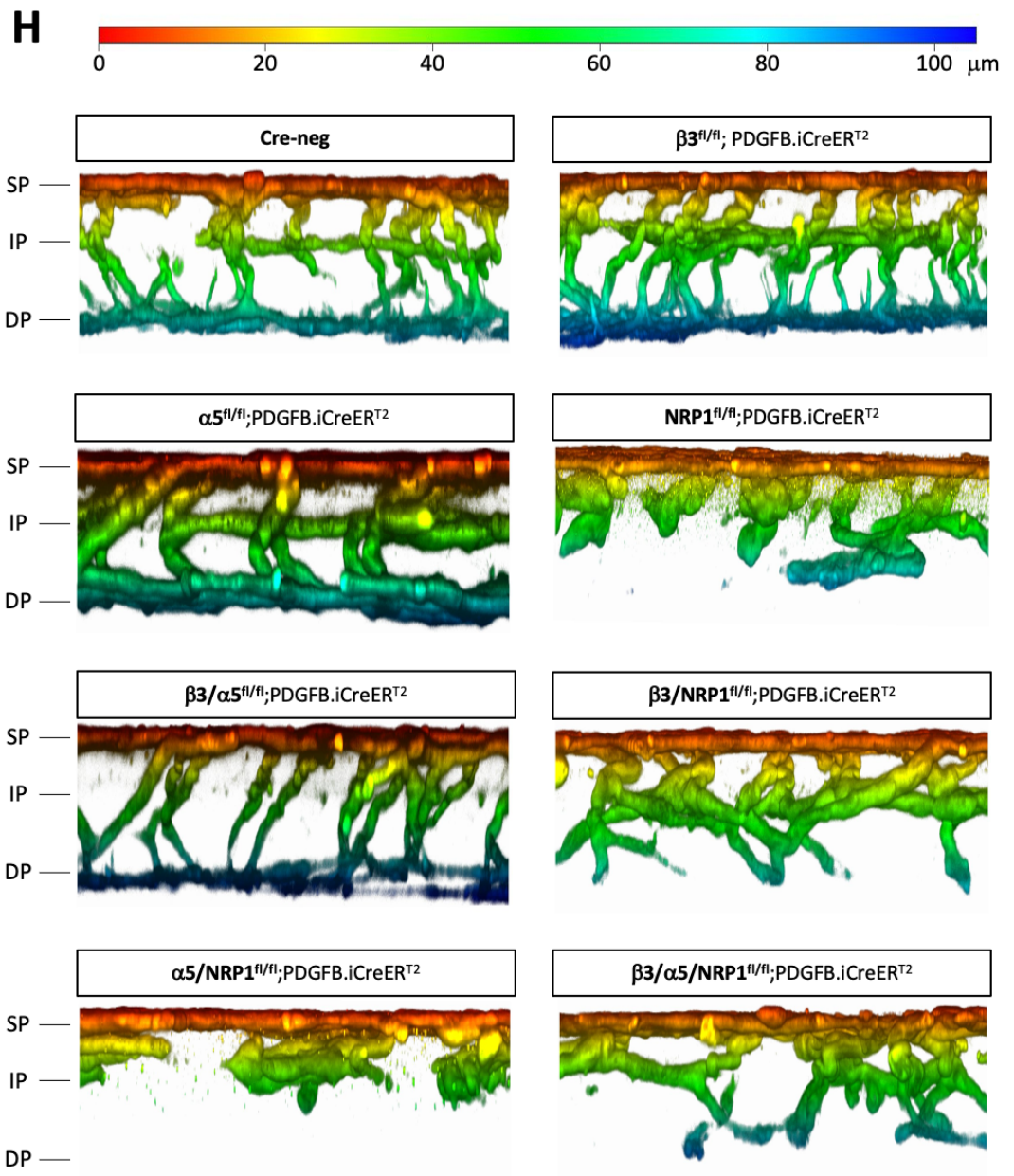


Figure 4.3 Delaying target depletion to circumvent angiogenic compensation reveals the involvement of $\alpha 5$ -integrin in deep plexus vascularisation. **A)** Time-course schematic of retinal vascular development and tamoxifen administration. Tamoxifen was administered (black triangles) via intraperitoneal injection from P7-P10 before sacrificing animals at P12. **B)** Quantification of animal weights recorded at P12, with Cre-positive weights presented as a percentage of the average weight of their Cre-negative littermates. Error bars displayed as mean \pm SEM. $N \geq 1$, $n \geq 4$ mice per group. **C)** Representative images of BS1-lectin labelled P12 SP retinal vasculature. Magnified image scale bar = 500 μm . **D)** Quantification of P12 vascular extension presented as a percentage of the average vascular extension measured in Cre-negative littermates. Error bars displayed as mean \pm SEM. $N \geq 1$, $n \geq 4$ retinas per group. **E)** Representative images of BS1-lectin labelled P12 retinal vascular layers. SP (red), IP (blue) and DP (green). Scale bar = 200 μm . **F)** Quantification of SP, IP and DP vessel density in P12 retinal vasculature, expressed as a percentage of the average vessel density measured in Cre-negative littermates. Error bars displayed as mean \pm SEM. $N \geq 1$, $n \geq 4$ retinas per group. **G)** ANOVA heatmap summary of SP, IP and DP vascular densities at P18, comparing statistical significance values between each Cre-positive knockout combination, including the PDGFB.iCreER^{T2} line. Colour corresponds with statistical significance, with increasing significance correlating with darker shades of red. **H)** Colour depth-coded Z-stack side-profile of retinal vascular layers taken at the midpoint between the optic nerve head and retinal periphery between an artery and a vein. Colour coded scale bar provided. Statistical significance was expressed and analysed as follows: *= $P < 0.05$, **= $P < 0.002$, ***= $P < 0.0002$, ****= $P < 0.0001$, unpaired students t-test (two-tailed)/one-way ANOVA.

4.4 Crosstalk between β 3-integrin, α 5-integrin and NRP1 is context-dependent.

We had originally predicted that the relationships between our three receptors of interest would be identifiable through macro analysis of retinal vasculature, a well-characterised and widely used model of angiogenesis. Whilst our studies thus far had revealed how individual receptors and certain interactions occurring between them were contributing to physiological angiogenesis, they appeared to be specific to the vascular plexus in question. This receptor network was therefore more complex than we had anticipated, with distinct and oft-times contradictory receptor interactions dominating at different developmental time points. Akin with that postulated by Robinson *et al* with regard to β 3-integrin, this receptor network appeared to adapt according to the angiogenic context in which it was present, making the identification of a consistent and testable series of interactions difficult (206).

To determine how these receptors interact with greater resolution, we would need to focus on a single developmental time point. This therefore bared the caveat that any findings may be transient and not necessarily hold true under angiogenic scenarios distinct from that in which they were identified. Our receptors of interest demonstrated the greatest combinatorial involvement in retinal angiogenesis at P6. Fortunately, at this time point the SP is still extending over its fibronectin-rich ECM in response to a gradient of VEGF, an *in vivo* scenario which, to varying extents, replicated the conditions under which our receptors have been documented to interact (179, 183, 194, 195). We therefore chose P6 as the developmental time point to investigate further.

4.5 Endothelial β 3-integrin and α 5-integrin are required for angiogenic sprout development *in vivo*.

The expansion of vascular networks begins with the formation of angiogenic sprouts in response to activating stimuli such as VEGF. Considering both β 3- and α 5-integrin are upregulated in activated endothelial cells and NRP1 is critical to the appropriate functioning of tip cells at the head of sprouts, these vascular protrusions seemed a likely point of functional convergence (31, 181, 241). Furthermore, the expression and function of VEGFR2 is a major determinant of endothelial tip cell selection, and each of our target receptors has been shown to interact with or modulate the function of this receptor (88, 147, 194, 242, 243). The forefront of the retinal SP is actively expanding in response to VEGF released from the surrounding hypoxic parenchyma. Following target depletion via tamoxifen administration between P2 and P4 and sacrificing mice at P6 (Fig 4.4 A), as described previously, we enumerated the number of vascular sprouts extending from the vascular front whilst accounting for the space available for these sprouts to form (the vascular perimeter). This provided an insight into the independent and overlapping roles our receptors play in the initiation of angiogenesis.

We first noted that the depletion of NRP1 either individually or in duplicate with β 3- or α 5-integrin (NRP1.EC^{KO}, β 3/NRP1.EC^{KO}, α 5/NRP1.EC^{KO}) caused a mirrored reduction in the number of retinal vascular sprouts relative to their Cre-negative controls (Fig 4.4 B & C). In light of our investigations into vascular extension and vascular density at P6, P12 and P18, this was likely a NRP1-dependent phenotype and independent of our integrin targets. Once again, endothelial depletion of α 5-integrin (α 5.EC^{KO}) prompted no change relative to controls at P6. Meanwhile, β 3-integrin deficient vasculature (β 3.EC^{KO}) demonstrated a significant decrease in sprouting. This concurred with that reported previously by Steri *et al* who documented a decrease in VEGF-dependent aortic ring sprouting *ex vivo* in the absence of endothelial β 3-integrin (161). Depleting these integrins together (β 3/ α 5.EC^{KO}), however, caused a reduction in retinal sprouting more profound than that caused by depleting β 3-integrin alone, leaving blunt-ended vasculature at the periphery of the SP. This even trended to be more severe than that measured in the absence of NRP1 (NRP1.EC^{KO}). β 3- and α 5-integrin were therefore collectively required for the appropriate initiation of angiogenesis in superficial retinal vasculature, and likely functioned synergistically to promote sprout formation. These data also suggested that in the absence of α 5-integrin (α 5.EC^{KO}) vascular sprout development

becomes reliant on β 3-integrin and is therefore sensitive to its co-depletion. Further still, whilst vascular sprouting in triple knockout retinal vasculature (β 3/ α 5/NRP1.EC^{KO}) was close to a significant reduction relative to its Cre-negative controls, generating a P value of 0.09, sprouting returned significantly closer to WT levels when compared with our double integrin knockout (β 3/ α 5.EC^{KO}). This suggested that the additional depletion of NRP1 may be able to partially rescue the compromised vascular sprouting observed when β 3- and α 5-integrin were co-depleted.

Our observed reduction in retinal sprouting when NRP1 was depleted juxtaposed that documented by Ellison *et al* who, also using the *ex vivo* aortic ring assay to model vascular sprouting, detected no change in sprouting following NRP1 depletion (195). One obvious difference between our experimentation was the environment in which our murine tissues were analysed. The retinal vasculature analysed here developed *in vivo* without any external alterations to its surrounding environment; the fibronectin-rich ECM was laid down by astrocytes and angiogenic stimuli were secreted from the broader retinal parenchyma to encourage vascular growth along its usual trajectory. *Ex vivo* environments such as that of the aortic ring assay, whilst providing useful insights into the endothelial-specific angiogenic contributions of target molecules in response to an administered growth factor or matrix substrate, are less easily extrapolated to more complex *in vivo* physiological or pathological scenarios. Whilst mural cells are retained in this *ex vivo* model, the host of other hetero-cellular contacts, the intricacies of the vasculature's ECM, and the wealth of soluble angiogenic cues that direct vascular growth are not recapitulated. Due to the number of factors at play, it was difficult to determine exactly why our observed sprouting reduction in the absence of NRP1 was not phenocopied *ex vivo*.

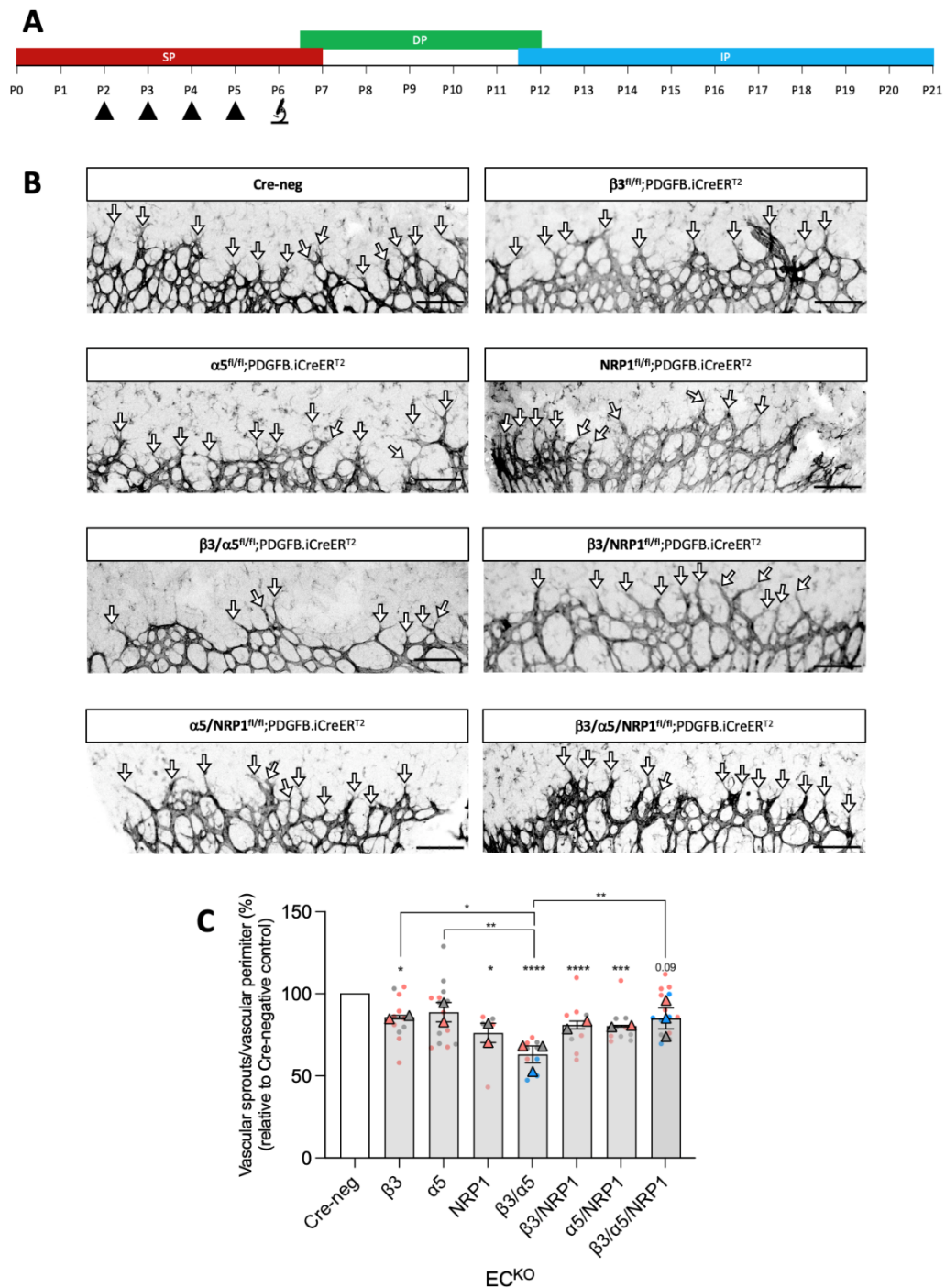


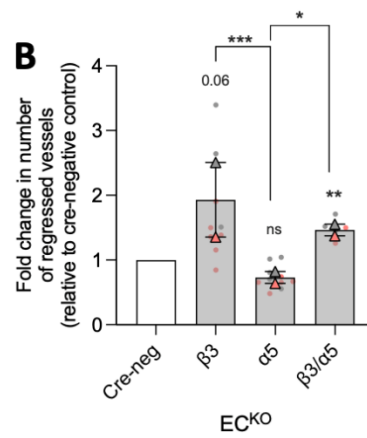
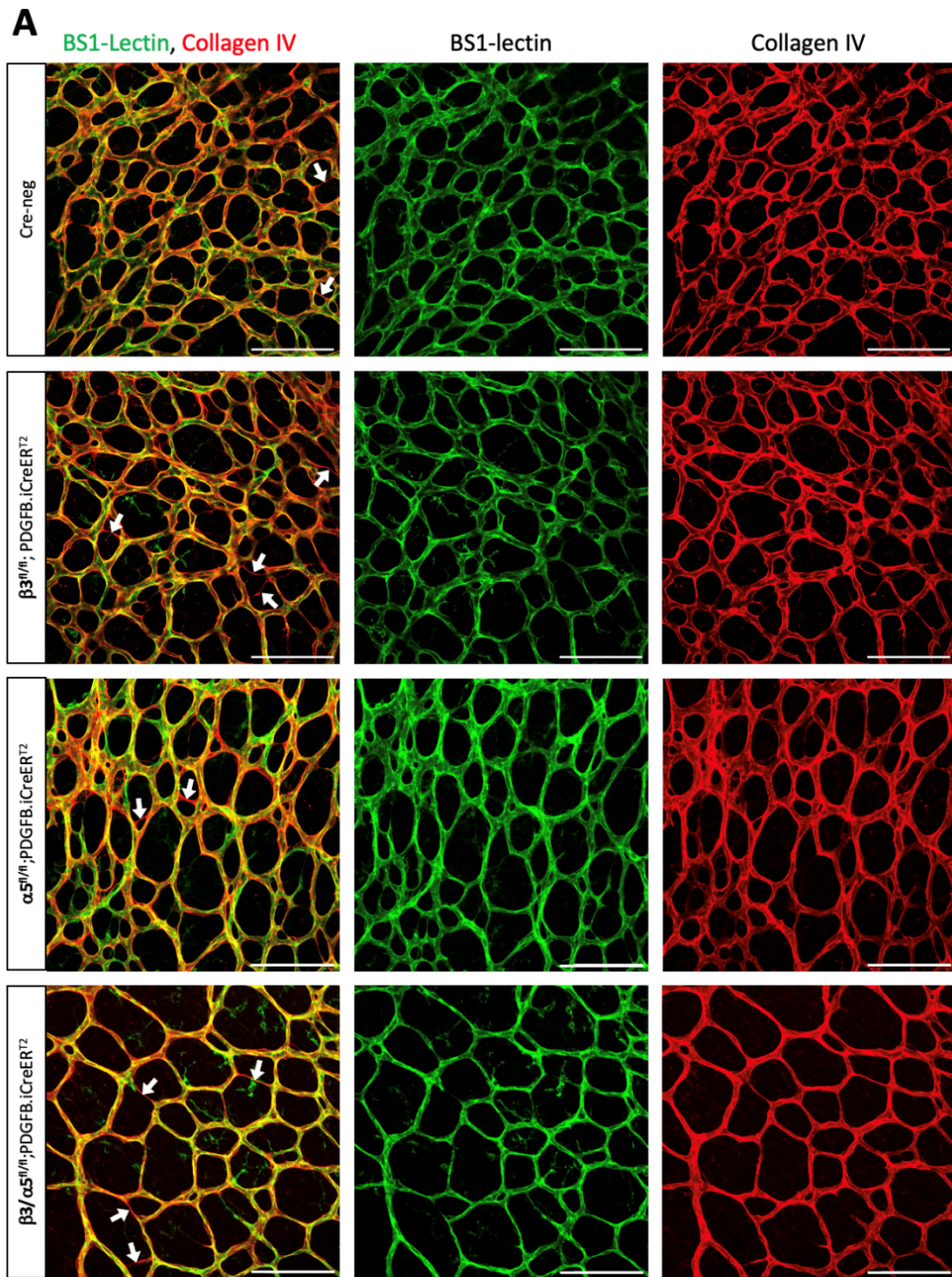
Figure 4.4 Endothelial $\beta 3$ -integrin and $\alpha 5$ -integrin are required for angiogenic sprout development *in vivo*. **A)** Time-course schematic of retinal vascular development and tamoxifen administration. Tamoxifen was administered (black triangles) via subcutaneous injection from P2-P3 and intraperitoneally from P4-P5 before sacrificing animals at P6. **B)** Representative images of BS1-lectin labelled P6 SP retinal vascular fronts. White arrows indicate vascular sprouts. Magnified image scale bar = 150 μ m. **C)** Quantification of vascular sprout enumeration normalized to vascular perimeter and made relative to their respective Cre-negative controls. Error bars displayed as mean \pm SEM. $N \geq 2$, $n \geq 5$ retinas per group. Statistical significance was expressed and analysed as follows: *= $P < 0.05$, **= $P < 0.002$, ***= $P < 0.0002$, ****= $P < 0.0001$, unpaired students t-test (two-tailed)/one-way ANOVA.

4.6 Endothelial β 3-integrin contributes to retinal vessel stability during vascular remodelling.

The effects of co-depleting β 3- and α 5-integrin on retinal vascular sprouting demonstrated their collective involvement in the appropriate initiation of angiogenesis. Generally, hyper- or hypo-sprouting at the vascular periphery translates to hyper- and hypo-dense retinal vascular interiors respectively (244, 245). We therefore presumed that the blunt-ended vasculature in our double integrin knockout (β 3/ α 5.EC^{KO}) would likewise be reflected in more severe hypo-vascularisation of the inner plexus relative to either single integrin knockout line. This, however, was evidently not the case as the vascular density observed at P6 revealed a significant but analogous drop in density when β 3-integrin was depleted individually (β 3.EC^{KO}) or in duplicate with α 5-integrin (β 3/ α 5.EC^{KO}) (Fig 4.1 F-I). The significantly worsened sprouting phenotype detected upon integrin co-depletion was therefore restricted to the vascular periphery. The β 3-integrin-dependent hypo-vascularisation detected could instead be the result of compromised vascular stability rather than impaired vessel sprouting.

As previously mentioned, superfluous vessels are selectively pruned during the normal remodelling process that follows the initial hyper-proliferative phases of angiogenesis. Once a vessel has regressed, its collagen-IV enriched basement membrane sleeve is left behind. By enumerating empty collagen-IV-positive and BS1 lectin-negative sleeves we could determine the propensity of vasculature to retract in the absence of our integrin targets. This revealed that β 3-integrin depletion either alone or alongside α 5-integrin (β 3.EC^{KO}, β 3/ α 5.EC^{KO}) caused a mirrored increase in the number of collagen-IV-positive regressed vessels (Fig 4.5 A & B). Meanwhile α 5-integrin depletion elicited no change relative to its Cre-negative controls (α 5.EC^{KO}), corresponding with normal SP vascular density. β 3-integrin was therefore essential for maintaining retinal vascular stability and the formation of mature vessels during remodelling but did so independently of α 5-integrin. Furthermore, the severe hypo-sprouting phenotype detected upon integrin co-depletion therefore appeared to be restricted to the vascular front. We speculated that β 3- and α 5-integrin may be preferentially expressed, and therefore most functionally relevant, at the retinal vascular front in angiogenic sprouts. Immunofluorescent analysis of α 5-integrin in WT retinal vasculature revealed this to be the case, with a clear increase in expression towards the vascular periphery of the SP at P6 (Fig 4.5 C), and still greater expression in protruding sprouts (Fig 4.5 D). Unfortunately, we were

unable to analyse the retinal vascular expression profile of β 3-integrin due to the lack of commercially available antibodies against this target.



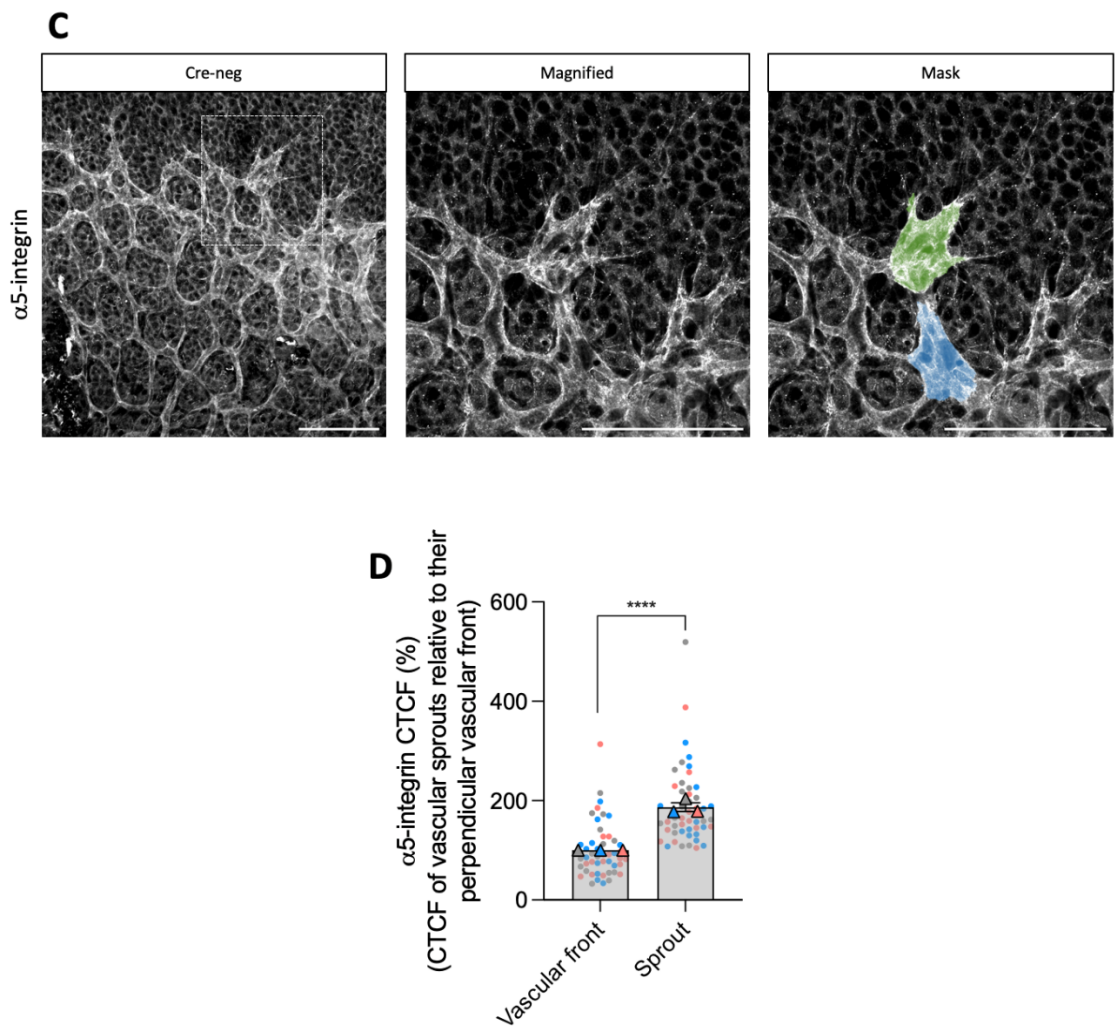


Figure 4.5 Endothelial β 3-integrin contributes to retinal vessel stability during vascular remodelling. **A)** Representative images of P6 retinal superficial vasculature taken 100 μ m from the vascular periphery between an artery and a vein co-stained for BS1-lectin and collagen IV. White arrows indicate regressed vessels. Scale bar = 100 μ m. **B)** Quantification of collagen IV-positive BS1-lectin-negative vessels expressed as a fold change relative to the average number of regressed vessels measured in Cre-negative controls. Error bars displayed as mean \pm SEM. N = 2, n \geq 5 retinas per group. **C)** Representative images of α 5-integrin-labelled retinal vascular periphery at P6 in a Cre-negative, WT retina. Mask image illustrates a false-coloured retinal sprout and its associated perpendicular vasculature used for CTCF analysis. Dashed box indicates the magnified image. Scale bars = 100 μ m. **D)** Quantification of α 5-integrin CTCF in retinal vascular sprouts expressed as a percentage relative to their connected perpendicular vasculature. Error bars displayed as mean \pm SEM. N = 1, n = 3 retinas per group (50 sprout/perpendicular vasculature measurements per group). Statistical significance was expressed and analysed as follows: * = P < 0.05, ** = P < 0.002, *** = P < 0.0002, **** = P < 0.0001, unpaired students t-test (two-tailed)/one-way ANOVA.

4.7 Endothelial β 3-integrin and α 5-integrin control filopodial dynamics.

During sprouting angiogenesis, polarised tip cells at the forefront of growing sprouts extend filopodia to sense their local environment and to direct their navigation through avascular spaces. Inactive integrins and other adhesion components are shuttled to the filopodium's tip during their development to initiate FA formation and anchorage to the ECM (246, 247). The linkage between the enclosed actin-filaments and extracellular substrates facilitated by these integrin-based macromolecular assemblies enables the translation of actin-polymerisation and retrograde flow into tractional, hepatotactic forward movement. Filopodial protrusions are therefore a key characteristic of endothelial tip cells and reliant on integrin-mediated adhesion to function appropriately. To determine whether β 3- and α 5-integrin conduct independent and/or overlapping filopodial functions that might cause or contribute to the sprouting defects observed previously, we examined several morphological parameters of filopodia extending from vascular sprouts at the periphery of superficial retinal vasculature at P6, once again following the same tamoxifen administration regime detailed previously.

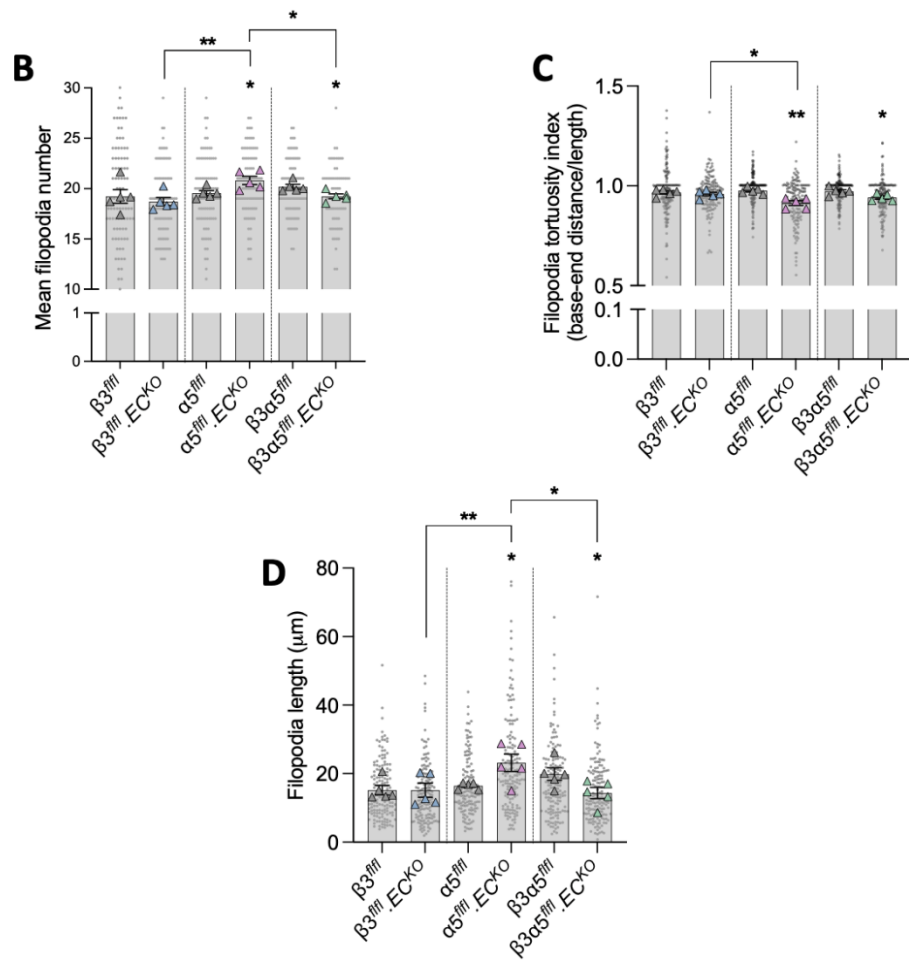
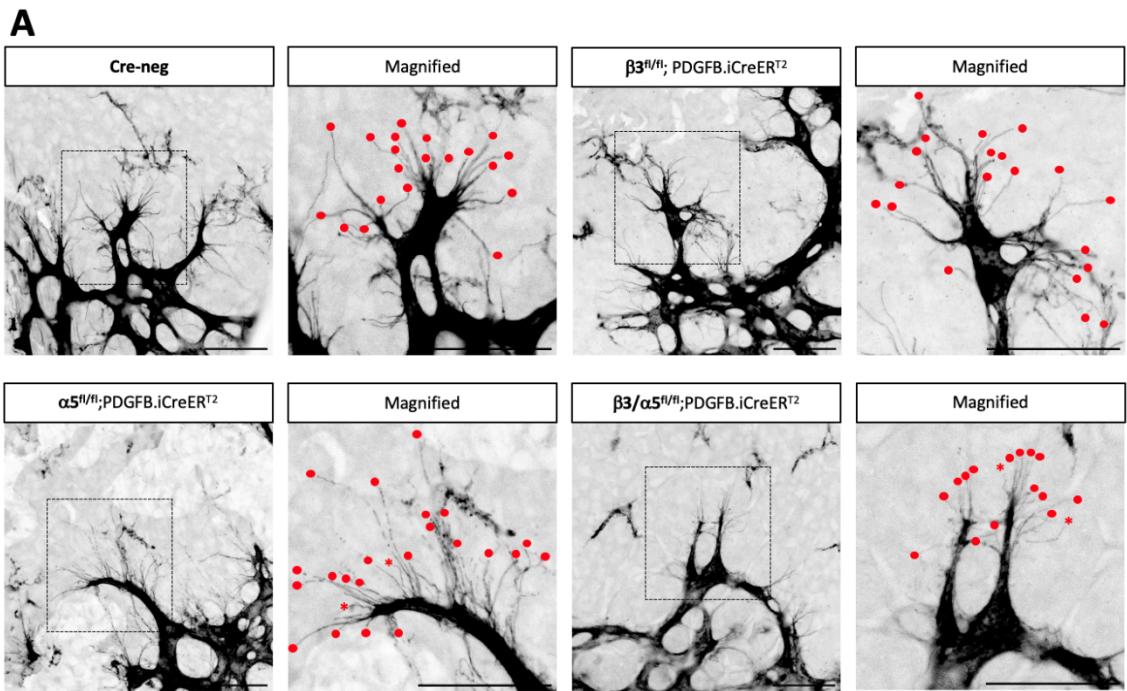
The depletion of β 3-integrin elicited no changes in the number, length, or tortuosity of filopodia extensions protruding from retinal sprouts (β 3.EC^{KO}) (Fig 4.6 A-D). This integrin was therefore likely dispensable for these filopodial attributes. Alternatively, its function could have been compensated for by α 5-integrin. Supporting this idea, of these two integrins α 5-integrin provides far stronger interactions with fibronectin matrices, with β 3-integrin instead mediating weaker links responsible for mechano-transduction (248, 249). Targeting α 5-integrin significantly increased each of these filopodial attributes (α 5.EC^{KO}). The elevated tortuosity observed here mirrored that reported by Stenzel *et al* who documented filopodial misalignment with astrocytic fibronectin following endothelial-specific α 5-integrin depletion (171). Increased filopodial number and length have also been reported previously in retinal endothelial cells upon endothelial depletion of β 1-integrin – α 5-integrin's heterodimeric partner. We inferred that the effects reported by Adams *et al* were likely attributed to specific ablation of α 5 β 1-integrin, but as β 1-integrin can heterodimerise with numerous endothelial α -subunits (α 1, α 2, α 3, α 4, α 6, α 9) we could not rule out the possibility that the absence of other endothelial β 1-integrin containing receptors may have contributed to their findings (135, 245). Whilst depleting our targets together maintained the elevated filopodial tortuosity triggered by α 5-integrin depletion, it reversed the associated increases in filopodial number and length, causing a marginal but significant reduction in both parameters (β 3/ α 5.EC^{KO}).

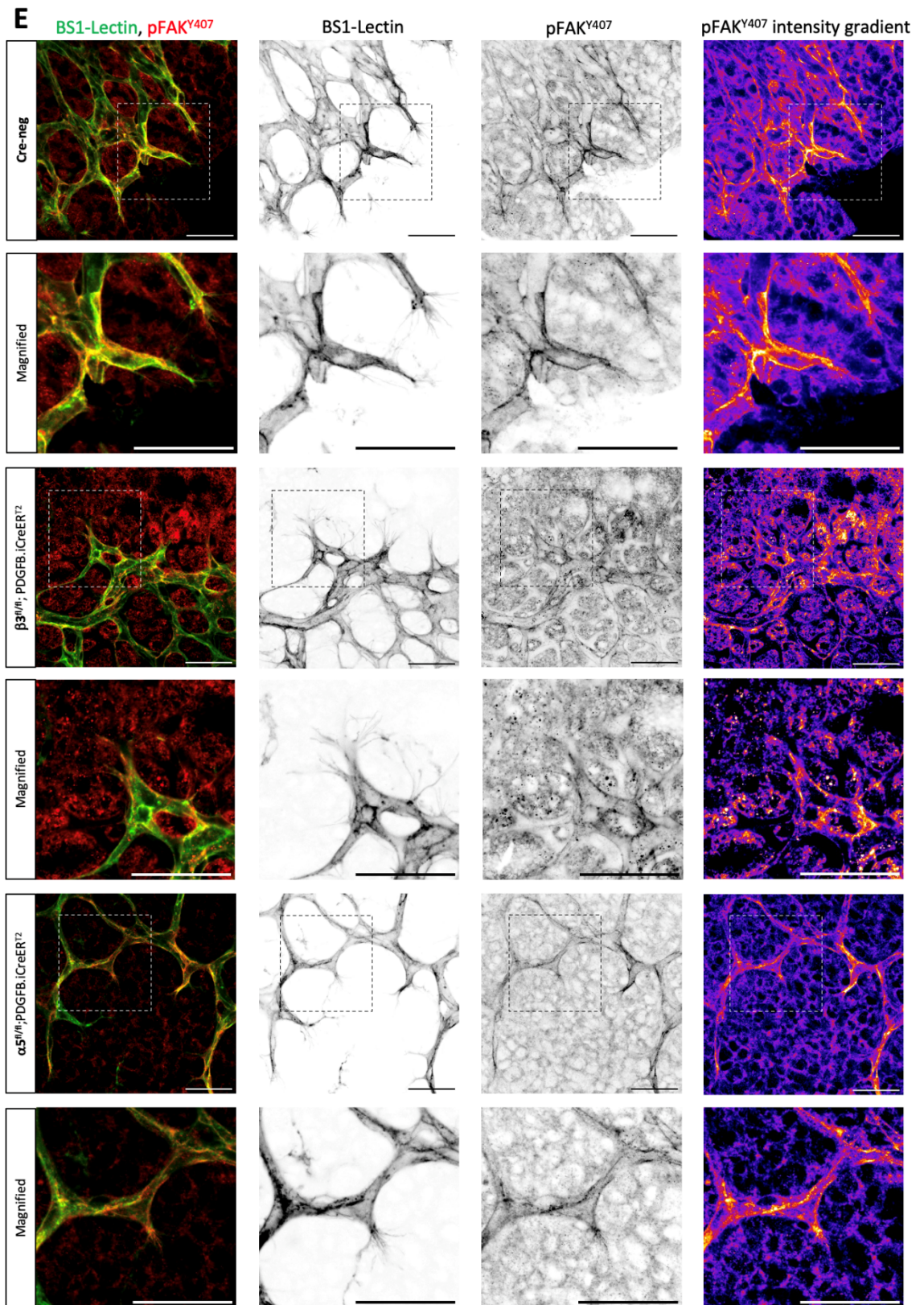
As tortuosity remained non-significantly different from that measured in the absence of $\alpha 5$ -integrin alone, we concluded that this effect was independent of $\beta 3$ -integrin, and that $\alpha 5$ -integrin was alone responsible for coordinating filopodial alignment to fibronectin-matrices in the SP. The reversal in filopodial number and length, however, only occurred upon co-depletion of our targets, indicating that the additional absence of $\beta 3$ -integrin could override the effect attributed to $\alpha 5$ -integrin's individual ablation. It has been recognised for some time now that αv -containing integrins can compensate for the absence of $\alpha 5\beta 1$ -integrin (250). Given its ability to mediate endothelial-fibronectin adhesion, $\alpha v\beta 3$ -integrin was the logical compensatory candidate. The weaker interactions it bestows with fibronectin likely enabled integrin co-depletion to exploit filopodial dependency on $\beta 3$ -integrin in the absence of $\alpha 5$ -integrin, leaving their number and length significantly reduced (248).

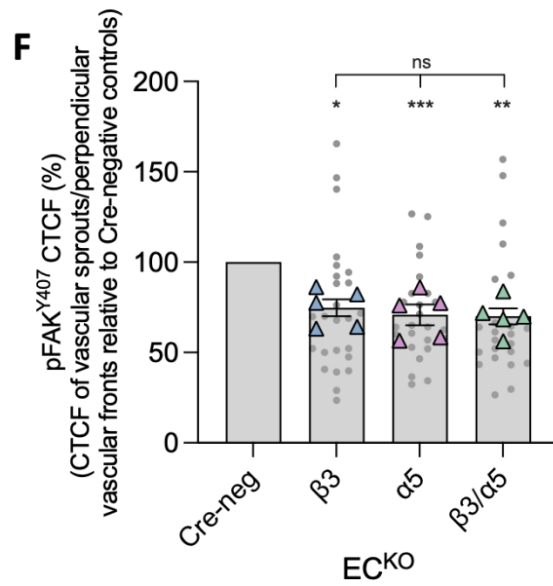
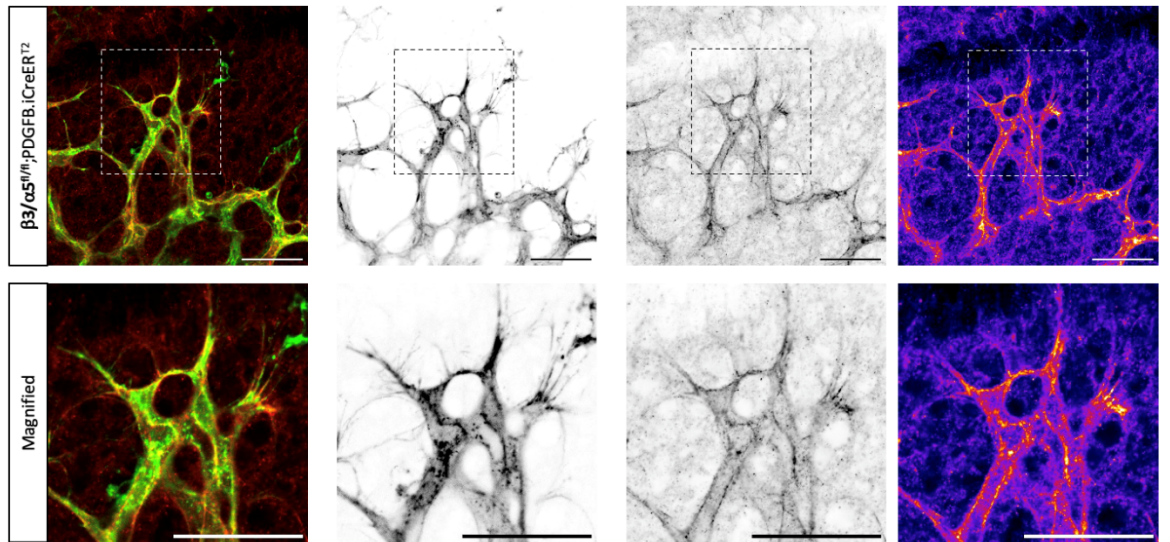
The non-receptor tyrosine kinase FAK is a core component of focal contacts and is activated downstream of growth factor receptors and activated integrins. Once activated, FAK hosts a range of activatable phospho-sites that are key to its signalling capabilities. It has also been widely recognised as a key contributor to FA development and turnover in polarised migration as, in its activated form, FAK is enriched in newly developing focal contacts whilst absent from those that are either stable or disassembling (251). FAK Y407 is one of several phosphorylation sites essential to endothelial migration in response to VEGF-induced integrin clustering (252). We utilised phospho-FAK Y407 as a measure of integrin-mediated endothelial adhesion and polarised migratory capacity in retinal endothelial sprouts. Corrected total cell fluorescence analysis of pFAK Y407 in retinal endothelial tip cells relative to their trailing stalk cells revealed markedly reduced phosphorylation when our integrin targets were depleted individually and in combination ($\beta 3.EC^{KO}$, $\alpha 5.EC^{KO}$, $\beta 3/\alpha 5.EC^{KO}$) (Fig 4.6 E & F). The scale of this reduction, however, was mirrored across our single and double integrin knockout lines indicating that whilst both $\beta 3$ - and $\alpha 5$ -integrin assisted in Y407 phosphorylation and FAK activation, they must do so independently of each other as a cumulative impairment to FAK phosphorylation was not observed following integrin co-depletion.

We also utilised the lung microvascular endothelial cell lines derived from our floxed mouse lines in an *in vitro* VEGF challenge assay to determine whether FAK's initial autophosphorylation site, Y397, and its main substrate, paxillin Y118, were influenced synergistically by our integrin targets. Whilst depletion of $\beta 3$ and $\alpha 5$ -integrin alone ($\beta 3^{fl/fl}.EC^{KO}$, $\alpha 5^{fl/fl}.EC^{KO}$) seemed to reduce FAK

phosphorylation at Y397, only through combinatorial integrin depletion ($\beta3/\alpha5^{fl/fl}.EC^{KO}$) was it significantly reduced (Fig 4.6 G & H). Only an N of 2 was achieved for our analysis of paxillin phosphorylation and therefore densitometric analysis was not performed, but a response similar to that at pFAK Y407 was observed by eye. Whilst individual integrin depletion caused impairment to paxillin Y118 phosphorylation, the most significant reduction occurred upon integrin co-depletion. Notably though, this genotype also demonstrated reduced total paxillin levels which may have been responsible for its reduced phosphorylation. These results only partially explain our previously observed filopodial defects. The cooperative reduction in both FAK and paxillin phosphorylation prompted by targeting both integrins together likely contributed to the measured reduction in filopodia length and number in this genotype, but the elevation in filopodial tortuosity induced by $\alpha5$ -integrin depletion individually was not reflected in FAK and downstream paxillin phosphorylation *in vitro*.







Increasing fluorescence intensity

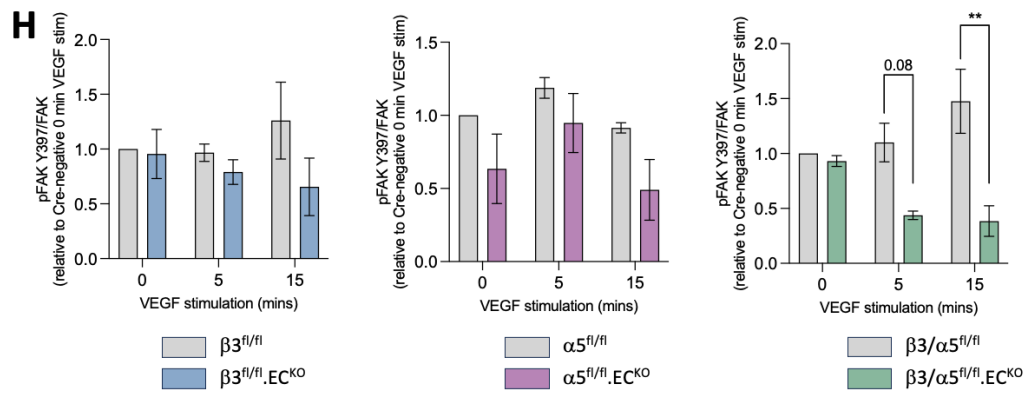
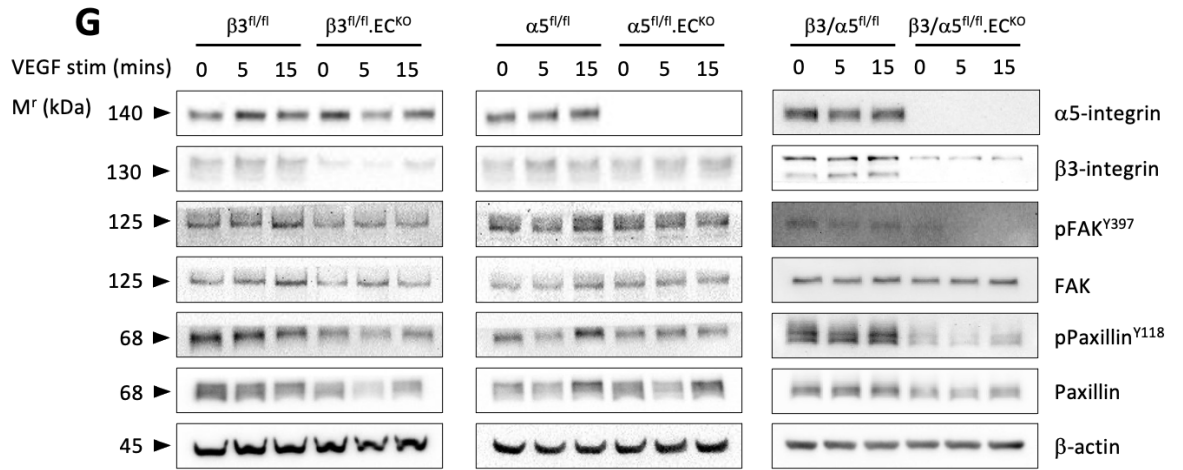


Figure 4.6 Endothelial β 3-integrin and α 5-integrin control filopodial dynamics. **A)** Representative BS1-lectin-labelled images of P6 retinal sprouts at the vascular front. Dashed boxes outline magnified images. Red dots indicate filopodial projections and red asterisks indicate tortuous filopodia. Scale bar = 50 μ m. **B)** Quantification of filopodia number per sprout at P6, presented as raw values alongside their respective Cre-negative controls. Error bars displayed as mean \pm SEM. n = 5 retinas per group measured across 3 technical replicates (20 sprouts per retina). **C & D)** Quantification of filopodial tortuosity index and length respectively, presented as raw values alongside their respective Cre-negative controls. Error bars displayed as mean \pm SEM. n = 5 retinas per group measured across 3 technical replicates (150 filopodial measurements per group). **E)** Representative images of retinal sprouts at the vascular front of the SP in P6 retinas co-labelled for BS1-lectin and pFAK Y407. The fire lut from FijiImageJTM was applied to visualize pFAK Y407 fluorescence intensity. Dashed boxes outline magnified images. Scale bars = 50 μ m. **F)** Quantification of pFAK Y407 CTCF in retinal vascular sprouts normalized to their associated perpendicular vasculature, expressed as a percentage relative to their respective Cre-negative controls. Error bars displayed as mean \pm SEM. n = 5 retinas per group measured across 3 technical replicates (5 sprouts per retina). **G)** Representative western blots of VEGF challenge assays in which Cre-negative and TAT-Cre-nucleofected endothelial cells were starved for 3 hours in serum-free media prior to stimulation with VEGF for 0, 5, and 15-minutes. Western blots show total levels of β 3- and α 5-integrin as well as phosphorylated and total levels of FAK (Y397) and paxillin (Y118). β -actin was used as a loading control. **H)** Densitometric quantification of pFAK Y397/total FAK relative to Cre-negative 0-minute VEGF stimulation obtained using FijiImageJTM. Error bars displayed as mean \pm SEM. N = 3. Statistical significance was expressed and analysed as follows: *=P<0.05, **=P<0.002, ***=P<0.0002, unpaired students t-test (two-tailed)/one-way ANOVA.

4.8 Discussion

From our analysis of vascular extension at P6 we deduced that neither β 3-integrin nor NRP1 could drive angiogenesis to physiologically normal levels without the co-expression of the other (Fig 4.1). Their pro-angiogenic functionality was therefore tied. This was particularly the case for β 3-integrin, which, unlike NRP1, was unable to contribute to vascular outgrowth when expressed alone. In the Robinson lab we have previously reported that the cytoplasmic tail of β 3-integrin performs negative regulatory functions over NRP1, limiting both its complexation with VEGFR2 and its activation of paxillin, thereby restricting its ability to drive endothelial motility (194, 195). Indeed, in the absence of just one allele encoding β 3-integrin, pathological angiogenesis becomes sensitive to the additional depletion of NRP1 (195). If these interactions held true in a developmental setting, we would have expected the endothelial depletion of β 3-integrin to release NRP1 from the aforementioned constraints and enable its pro-angiogenic capabilities to drive retinal vascular extension closer to WT levels. Instead, its failure to do so implied that this integrin was in fact required for NRP1 to reach its full pro-angiogenic capacity in this organ, or that β 3-integrin conducted essential, but NRP1-independent pro-angiogenic functions in mouse retinal vasculature.

Alternatively, if we consider the reduction in animal weight conferred by endothelial β 3-integrin depletion as directly responsible for the observed impairment in retinal vascular outgrowth, then β 3- and α 5-integrin may have engaged in reciprocal compensation whereby the absence of one could be offset by the activity of the other (Fig 4.1). Cooperative behaviour between these integrins has been previously documented. Neither integrin can form normal FAs on α 5 β 1-integrin selective substrates in the absence of the other, despite α v β 3-integrin being unable to engage with this extracellular substrate (169, 253). Of course, β 3-integrin can engage with the retinal fibronectin matrix *in vivo*, albeit more weakly than α 5-integrin, and can, to an extent, compensate for the absence of this integrin. These receptors may therefore control endothelial adhesion to fibronectin synergistically such that a significant impairment to SP outgrowth was only observed in their shared absence. A consistent theme to both proposed receptor interactions was the dispensability of α 5-integrin alone to SP extension. This conflicted with Stenzel *et al* who reported a minor impairment to retinal vascular outgrowth of 3-6% following this integrin's endothelial depletion (171). Notably, their depletion was achieved using the constitutive Tie2.Cre model. Prior work from the Robinson lab revealed that the method of target depletion used could alter the angiogenic response observed

and as such, Stenzel *et al*'s findings may not have been directly comparable to our observations (161).

Something we had yet to address in this chapter was whether the vessels formed in our various knockout combinations were functional. We observed that across each knockout line at P6, retinal arterioles maintained the appropriate avascular space in their immediate vicinity (Fig 4.1 B & H). These peri-arteriole capillary-free zones arise due to high blood oxygen content bestowing a vaso-inhibitory effect that induces selective capillary pruning. Meanwhile, venioles sit in a denser, proximal capillary network, though they maintain a narrow peri-veniole capillary-free zone (254). From these observations we could somewhat crudely deduce that arteriole and veniole perfusion were unaffected in the absence of our targets. Others have used microvascular diameter as a measure of capillary function, but as the flat-mounting process we use for retinal imaging compromised microvascular structure, we chose not to perform this analysis. One method of assessing vascular perfusion would be to stain vessels via intravenous administration of endothelial specific conjugated antibodies. Following tissue isolation only perfused vessels would be visible and could then be directly quantified.

Another consistent theme of this chapter was the functional dominance of NRP1 in our receptor network. Not only did NRP1 depletion cause the most significant impairment to SP outgrowth at P6 (Fig 4.1 B & C), but also the greatest hypo-vascularisation of the intermediate and deep plexuses at P12 (Fig 4.3 E, F & H) as well as the inducement of tuft malformations at P18 (Fig 4.2 H). Whilst the impairment to SP vascular outgrowth induced by NRP1 depletion mirrored that attributed to its function as a VEGF co-receptor, the generation of these vascular tufts is reportedly independent of its VEGF-dependent functionality as they are absent from retinal vasculature in mice harbouring a point mutation that disrupts NRP1-VEGF binding (207). The generation of these tufts may instead rely on NRP1's role in mediating endothelial adhesion, but considering NRP1 carries out this role by directing $\alpha 5\beta 1$ -integrin intracellular traffic to newly forming adhesive sites on fibronectin, it was curious why depletion of either integrin individually or in combination did not provoke tuft formation too (179). Instead, these tufts likely formed due to impaired endothelial receptiveness to semaphorin 3A or 3C, other NRP1 ligands demonstrated to prevent pathological neovascularisation in the retina when administered intravenously (255, 256).

Through our analysis of retinal angiogenesis at progressive developmental time points, we identified several autonomous and combined receptor functions. These functions appeared to be context specific, with functionality shifting depending on the precise developmental phase being investigated. At P6, $\alpha 5$ -integrin was dispensable for angiogenesis to proceed normally (Fig 4.1), yet at P12 its depletion conferred a significant reduction in DP vascularisation (Fig 4.3). Conversely, $\beta 3$ -integrin was required for SP formation but expendable for both IP and DP development at P12 and P18 (Fig 4.1, 4.2 & 4.3). Furthermore, the cooperative interplay between $\beta 3$ -integrin and NRP1 at P6 was reversed at P12, with $\beta 3$ -integrin instead appearing to limit the pro-angiogenic capacity of NRP1 when $\alpha 5$ -integrin was depleted. This function of $\beta 3$ -integrin more closely resembled that reported by Robinson *et al* (194). Furthermore, at P6 NRP1 depletion conferred a hypo-vascular effect in superficial vasculature, yet at P12 and P18 its absence caused hypervascularisation of the same plexus. Due to its lack of involvement in endothelial proliferation, NRP1 likely aided vessel stabilisation at P6 to prevent inappropriate vascular regression, whilst at later time points this function was reversed, instead encouraging the retraction of superfluous vessels to prevent the formation of hyper-dense vascular networks (180). We had therefore mapped how and when these three receptors contributed to developmental angiogenesis in this organ and revealed a series of contradictory functions. To resolve mechanistic interactions occurring between them, we required a single time point for further investigation to omit time-dependent functional variability from our analysis.

This revealed that $\beta 3$ - and $\alpha 5$ -integrin cooperate synergistically during vascular sprout development in the SP at P6 (Fig 4.4). Through filopodial analysis of these sprouts we revealed that $\beta 3$ -integrin could likely compensate for the loss of $\alpha 5$ -integrin such that integrin co-depletion exploited filopodial $\beta 3$ -integrin-dependency and reversed their enhanced number and length observed in the absence of $\alpha 5$ -integrin alone (Fig 4.5). This concurred with our enumeration of vascular sprouts, as depletion of $\alpha 5$ -integrin alone caused no significant defects. Furthermore, the only significant reduction in filopodial number and length occurred when our integrins were depleted together, which agrees with this genotype's hypo-sprouting severity. However, our filopodial observations failed to explain the hypo-sprouting phenotype caused by $\beta 3$ -integrin ablation as no measurable defects in filopodia morphology or frequency were detected. In addition, the relatively minor impairment in filopodial length, number and tortuosity seemed mismatched with the severely blunt-ended vasculature observed in our double integrin knockout. We therefore postulated that the substantial reduction in vascular sprouting caused by co-depletion of our

integrin targets was largely independent of filopodia adhesion and pathfinding. Also of note, retinal vascular abnormalities do not necessarily correspond with changes in vascular extension (244). This observation aligned with the elevated length and number of protruding filopodia detected in the absence of $\alpha 5$ -integrin, which did not elicit increased SP outgrowth relative to Cre-negative controls, nor did the severe hypo-sprouting phenotype detected in our double integrin knockout correspond with worsened vascular extension relative to the individual depletion of $\beta 3$ -integrin. Our analysis of retinal vascular extension, vascular sprouting at the retinal periphery, and the filopodial projections of these sprouts therefore appeared incongruent. We surmised that the cooperation between $\beta 3$ - and $\alpha 5$ -integrin in the development of retinal vascular sprouts was largely irrespective of their role in filopodial adhesion and pathfinding, and that other undetermined mechanisms were contributing to this phenotype.

5 Endothelial β 3-integrin, α 5-integrin and NRP1 control VEGFR2 dynamics via distinct mechanisms *in vitro*.

Much of our current analysis has focussed on retinal vascular development to capture the independent and overlapping contributions of our three endothelial receptors to angiogenesis. Among other vascular-bed specific functions, it revealed a critical involvement of both integrin targets in the appropriate development of retinal endothelial sprouts and their filopodial protrusions. VEGF/VEGFR signalling represents a key angiogenic driving force in the retina, prompting tip cell selection, filopodia-directed tip cell migration over astrocytic fibronectin as well as stalk cell proliferation (257, 258). Neurons also carefully titrate VEGF bioavailability beneath the SP to control development of deeper vascular beds in this organ (219). Akin with our endothelial receptors of interest then, endothelial VEGF-receptiveness is critical to angiogenic sprout development and the timely formation of the retina's tri-layered vascular network.

VEGF₁₆₄ is the dominant VEGF isoform expressed in the post-natal mouse retina, with VEGF₁₂₀, VEGF₁₄₄ and VEGF₁₈₈ being expressed to lesser degrees (257). It's major endothelial receptor, VEGFR2, is equally important for retinal vascular growth such that administration of antibodies directed against this receptor, or its endothelial specific depletion, significantly perturbed retinal endothelial sprouting (230, 259). Concentrated at the vascular front, VEGFR2 is highly expressed in tip cells and their associated filopodial extensions (257). β 3-integrin, α 5-integrin and NRP1 have each been documented to interact with this receptor and modulate its activity (88, 147, 194, 242, 243). We therefore sought to determine whether these receptors collectively influenced VEGFR2 activity.

5.1 β 3-integrin and NRP1 are essential for VEGFR2 signalling, but co-expression of β 3-integrin and α 5-integrin is required for VEGFR2 preservation.

To investigate the collective involvement of our receptor network on VEGF/VEGFR2 signalling, we utilised the endothelial cell lines isolated from our mouse models, the endothelial identity of which we confirmed previously (Fig 3.6). Once seeded on a fibronectin matrix these endothelial cells were starved in serum-free media and subsequently stimulated for up to 15 minutes with VEGF₁₆₄ before being lysed and analysed via western blotting for VEGFR2 phosphorylation at Y1173. Activation of this key autophosphorylation site induces transcriptional changes that encourage endothelial proliferation and migration (43). We additionally analysed Akt phosphorylation at T308, a residue essential to its catalytic activity. Akt is an important downstream effector of the VEGF/VEGFR2 signalling axis, stimulating endothelial proliferation, migration, and survival (260). Akt has additionally been shown to regulate the recycling of α v β 3- and α 5 β 1-integrins (261).

Looking first at our targets individually, we found that the absence of α 5-integrin (α 5^{fl/fl}.EC^{KO}) prompted no change in VEGFR2 or Akt phosphorylation relative to their total levels at the indicated residues (Fig 5.1 A). Although Stenzel *et al* assessed Akt activation in total retinal lysates rather than autonomously in endothelial cells, in support of our findings, they detected no change in Akt phosphorylation in mice lacking endothelial α 5-integrin relative to control retinas (171). Meanwhile, depletion of β 3-integrin (β 3^{fl/fl}.EC^{KO}) or NRP1 (NRP1^{fl/fl}.EC^{KO}) elicited a significant reduction in VEGF-induced VEGFR2 phosphorylation, though this impairment failed to significantly impact downstream Akt activation. It is worth noting however that phospho-Akt levels were very close to a significant reduction in the absence of β 3-integrin after VEGF stimulation for 15 minutes. Whilst some of these effects have been reported previously, contradicting these data, siRNA-driven NRP1 knockdown or peptide-blockade of NRP1-VEGF binding was reported to induce a marginal but significant decrease in Akt activation (161, 183, 262). Furthermore, the decrease in VEGFR2 phosphorylation measured here in the absence of NRP1 was far more substantial than that reported previously at Y1173 and should be borne in mind going forward.

Co-targeting of either β 3-integrin or α 5-integrin alongside NRP1 (β 3/NRP1^{fl/fl}.EC^{KO}, α 5/NRP1^{fl/fl}.EC^{KO}) mirrored the decreased VEGFR2 phosphorylation observed when NRP1 was targeted alone (NRP1^{fl/fl}.EC^{KO}), though was nearly capable of significantly prolonging this

impairment to 15 minutes (Fig 5.1 A). Looking downstream of VEGFR2, co-depleting α 5-integrin and NRP1 (α 5/NRP1^{fl/fl}.EC^{KO}) was, akin with the individual ablation of NRP1, unable to influence VEGF-induced Akt activation, but targeting NRP1 alongside β 3-integrin (β 3/NRP1^{fl/fl}.EC^{KO}) significantly reduced Akt phosphorylation after 15 minutes. The collective expression of β 3-integrin and NRP1 was therefore a requirement for suitable propagation of VEGF signalling to downstream Akt and reinforced our observations *in vivo* where co-expression of these two receptors was essential for retinal vascular growth to proceed normally (Fig 4.1 B & C). Looking now at our triple knockout cells (β 3/ α 5/NRP1^{fl/fl}.EC^{KO}), depletion of each receptor together conferred a significant reduction in VEGFR2 phosphorylation analogous to that observed in the absence of NRP1 or β 3-integrin alone, but additionally reduced its activation at 15 minutes (Fig 5.1 A). Furthermore, the reduced Akt activation observed when β 3-integrin and NRP1 were co-depleted (β 3/NRP1^{fl/fl}.EC^{KO}) was lost in these triple knockout cells (β 3/ α 5/NRP1^{fl/fl}.EC^{KO}). As many RTKs and G-protein coupled receptors (GPCRs) feed into Akt signalling pathways, and each of our receptor targets are known to crosstalk with growth factor receptors in addition to each other, deciphering the VEGF signalling responses observed proved challenging (163, 179, 194, 263, 264). Furthermore, commenting on the longevity of these phosphorylation impairments past the 5-minute time point through densitometric analysis was problematic. Though the individual depletion of β 3-integrin and NRP1 was statistically unable to prolong the impaired VEGFR2 activation detected at 5 minutes of VEGF stimulation, visual interpretation of the representative blots shown indicated that activation of this receptor remained severely impaired even after 15 minutes.

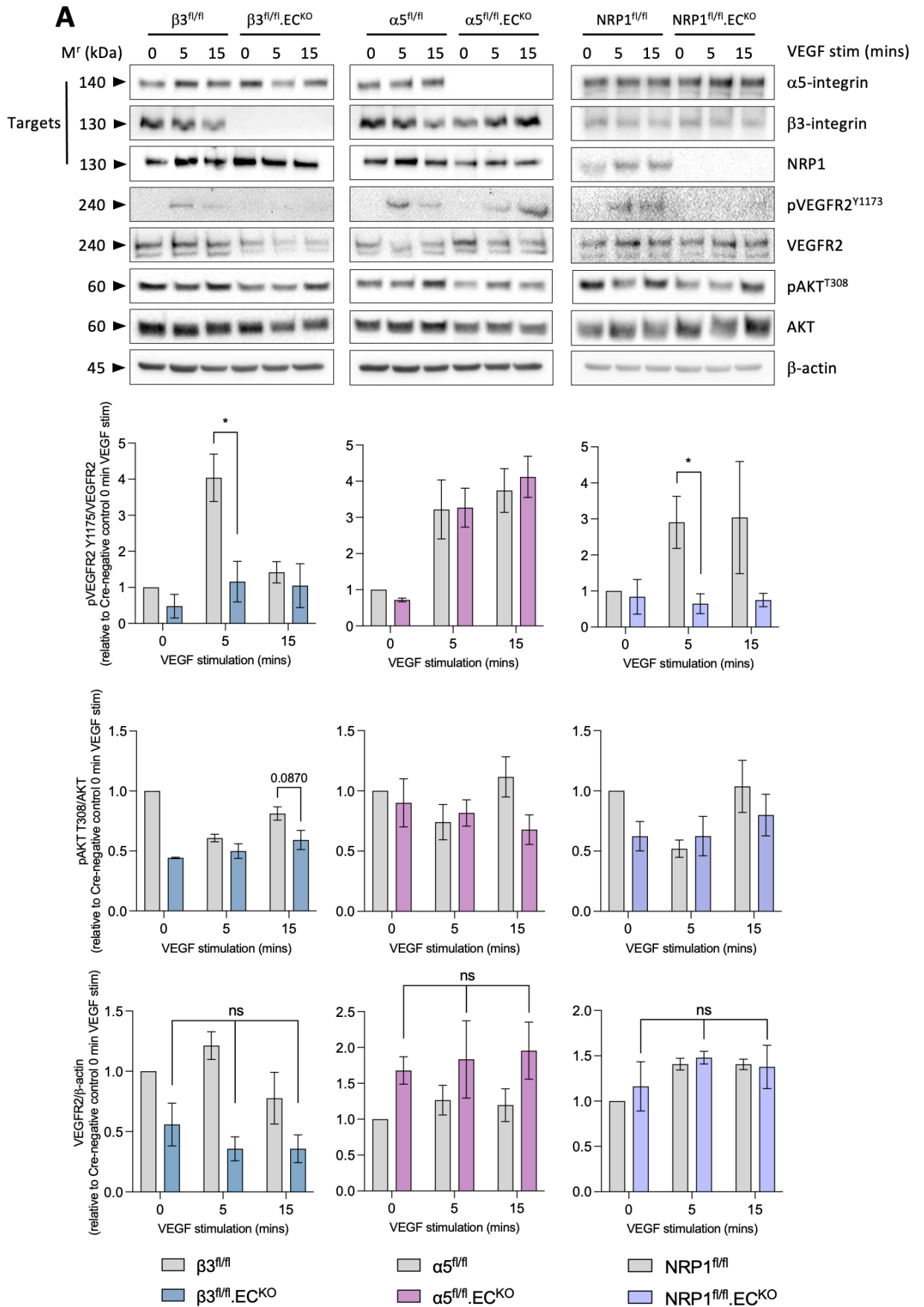
The densitometry of VEGFR2 and Akt phosphorylation discussed was made relative to the total expression of their respective protein to account for any variance in their expression. Whilst total levels of Akt appeared consistent throughout each knockout line relative to their controls, that of VEGFR2 varied significantly. We first compared the band intensity of VEGFR2 at each VEGF-stimulated time-point to its loading control before normalising these values to that of their respective Cre-negative control at 0-minutes of VEGF stimulation (Fig 5.1 A). This revealed that the changes in VEGFR2 expression across our knockout lines were independent of acute VEGF stimulation. We subsequently quantified VEGFR2 expression at 0 minutes of VEGF stimulation and made these values relative to that of their control cells at the same time point for comparison across each of our genotypes (Fig 5.1 B). This quantification revealed that the individual depletion of β 3-integrin (β 3^{fl/fl}.EC^{KO}) induced a slight but significant reduction in VEGFR2 total protein, a reduction that was substantially exaggerated by co-depletion of α 5-integrin (β 3/ α 5^{fl/fl}.EC^{KO}). In

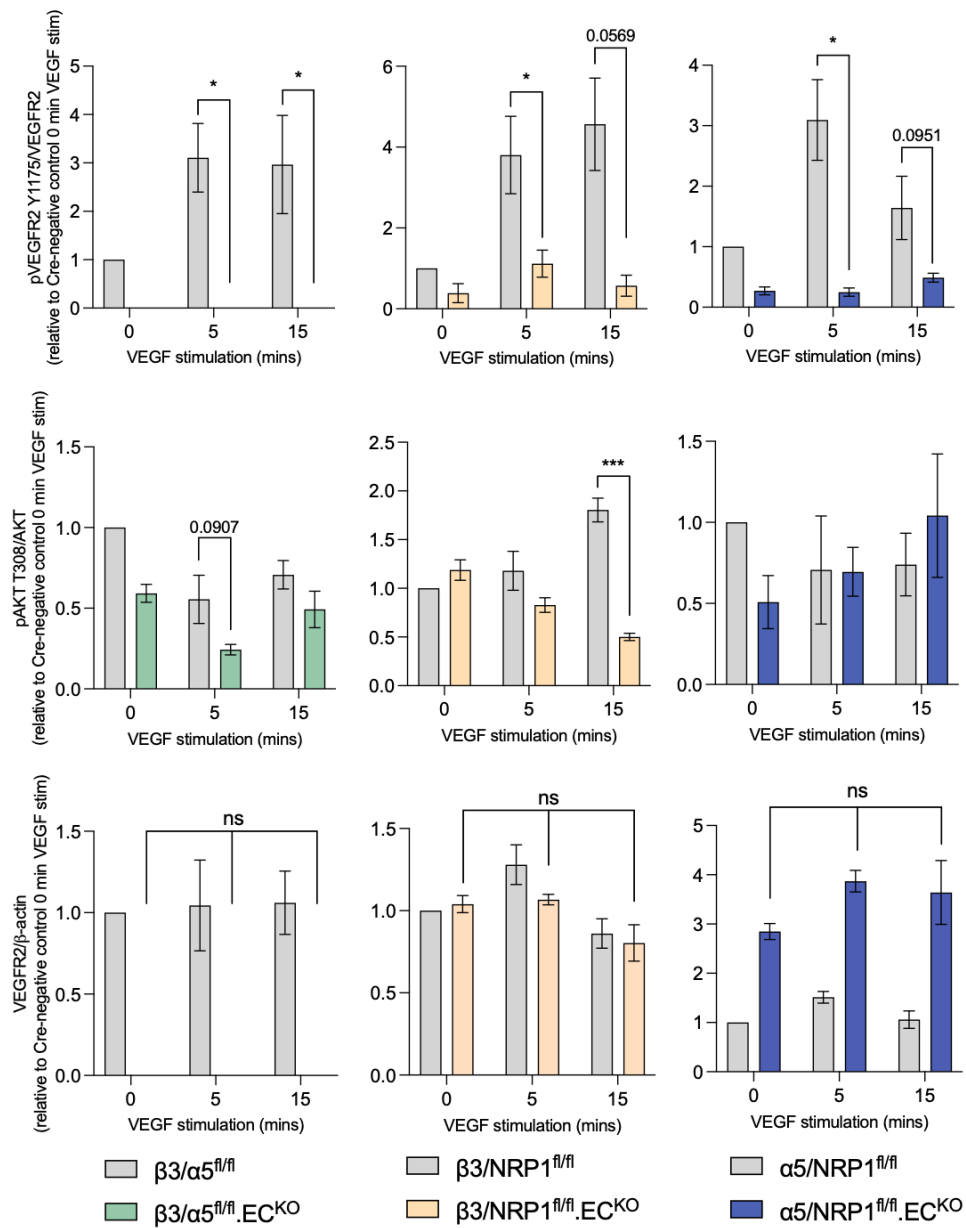
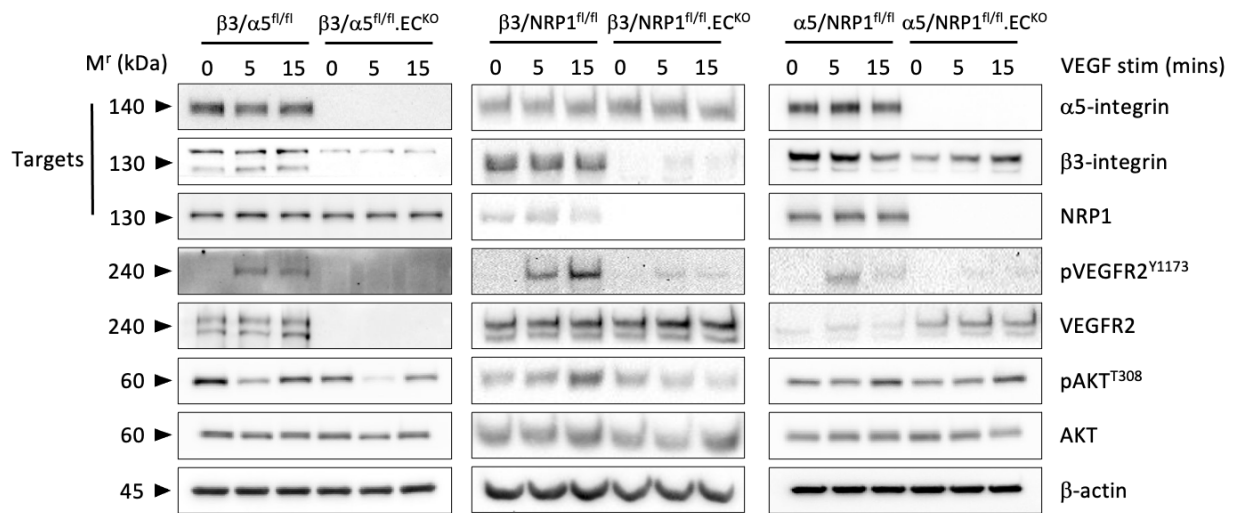
these co-depleted endothelial cells VEGFR2 was entirely absent. As such, the observed absence of VEGFR2 phosphorylation was caused by its reduction in total levels. Furthermore, as the elevated VEGFR2 expression triggered by individual ablation of $\alpha 5$ -integrin ($\alpha 5^{fl/fl}.EC^{KO}$) was mirrored by co-targeting of $\alpha 5$ -integrin and NRP1 together ($\alpha 5/NRP1^{fl/fl}.EC^{KO}$), we inferred that this effect was dependent on depletion of $\alpha 5$ -integrin alone. When $\beta 3$ -integrin and NRP1 were co-depleted ($\beta 3/NRP1^{fl/fl}.EC^{KO}$, $\beta 3/\alpha 5/NRP1^{fl/fl}.EC^{KO}$) VEGFR2 levels were rescued to WT levels.

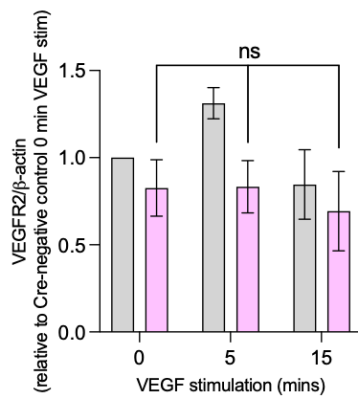
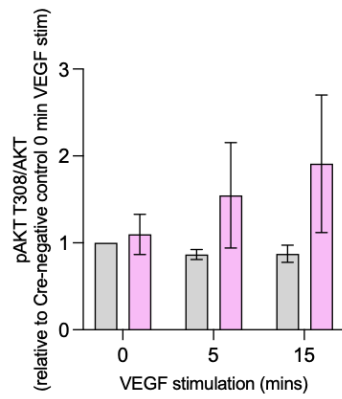
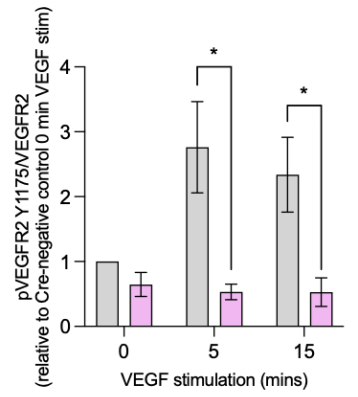
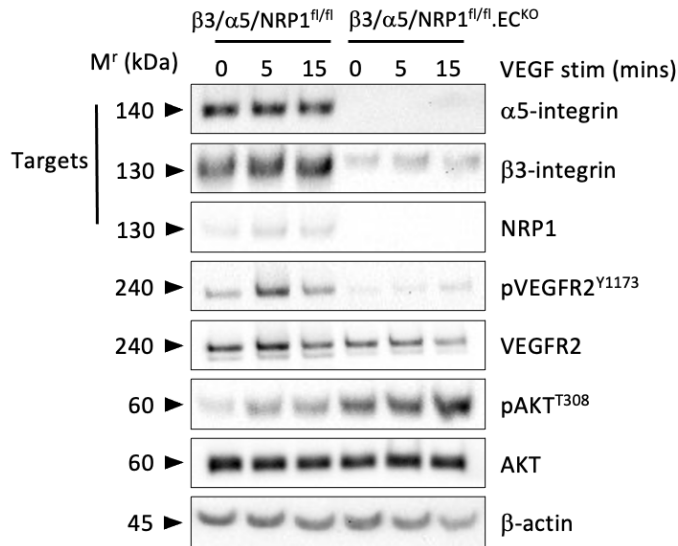
From these data we hypothesised several possible regulatory functions of our receptor network over VEGFR2 expression. As discussed above, the increase in VEGFR2 abundance induced by $\alpha 5$ -integrin depletion was irrespective of NRP1. Furthermore, as the elevated VEGFR2 expression detected when targeting $\alpha 5$ -integrin alone ($\alpha 5^{fl/fl}.EC^{KO}$) or alongside NRP1 ($\alpha 5/NRP1^{fl/fl}.EC^{KO}$) could be reduced to WT levels by the additional depletion of $\beta 3$ -integrin ($\beta 3/\alpha 5^{fl/fl}.EC^{KO}$, $\beta 3/\alpha 5/NRP1^{fl/fl}.EC^{KO}$), these elevations appeared $\beta 3$ -integrin-dependent. Both integrins therefore appeared to conduct distinct but inter-dependent regulatory functions over VEGFR2 abundance where $\beta 3$ -integrin drove its accumulation in the absence of $\alpha 5$ -integrin ($\alpha 5^{fl/fl}.EC^{KO}$, $\alpha 5/NRP1^{fl/fl}.EC^{KO}$), and $\alpha 5$ -integrin kept this pro-angiogenic function in check when co-expressed with $\beta 3$ -integrin (Cre-neg, $NRP1^{fl/fl}.EC^{KO}$). In addition, the reduction in VEGFR2 expression observed in the absence of $\beta 3$ -integrin alone or together with $\alpha 5$ -integrin ($\beta 3^{fl/fl}.EC^{KO}$, $\beta 3/\alpha 5^{fl/fl}.EC^{KO}$) could be reversed by the additional depletion of NRP1 ($\beta 3/NRP1^{fl/fl}.EC^{KO}$, $\beta 3/\alpha 5/NRP1^{fl/fl}.EC^{KO}$). NRP1 therefore also performed critical regulatory roles over this key angiogenic receptor, driving its downregulation in the absence of $\beta 3$ -integrin ($\beta 3^{fl/fl}.EC^{KO}$, $\beta 3/\alpha 5^{fl/fl}.EC^{KO}$).

The interactions of our receptors with VEGFR2 are well studied and we found several incongruences with existing literature. Conflicting with our results, global $\beta 3$ -integrin depletion induced enhanced tumour vascularisation and growth as a result of their elevated VEGFR2 expression (154, 155). When investigating the autonomous effects of endothelial $\beta 3$ -integrin to VEGF-induced angiogenesis however, Steri *et al* reported no change in the expression of VEGFR2 in lung microvascular endothelial cells isolated from $\beta 3^{fl/fl}.PDGFB.iCreER^{T2}$ mice, though its VEGF-induced phosphorylation at Y1173 was impaired in line with our observations here, a predictable response considering the known synergy between $\alpha v\beta 3$ -integrin and VEGFR2 (161). The increase in VEGFR2 expression prompted by global $\beta 3$ -integrin ablation was therefore likely the result of non-

endothelial β 3-integrin expressing cell types such as megakaryocytes, bone marrow-derived cells, platelets and pericytes (161, 206, 265). More recently, inducible genetic depletion or inhibition of pericyte β 3-integrin expression was found to significantly elevate both FAK and Akt phosphorylation. The associated increase in nuclear factor κ -B (NF κ B) transcriptional activity downstream of FAK and Akt activation enhanced the delivery of proliferative, but not migratory, paracrine signals to nearby tumour cells to augment their growth. Notably, unlike the increase in tumour angiogenesis induced by global β 3-integrin depletion, this effect was independent of changes in tumour vascular density (154, 266). There is, therefore, considerable evidence of the heterogeneous signalling and angiogenic outcomes resultant of targeting β 3-integrin in different cell types (266). Nevertheless, in our hands, genetic loss of endothelial β 3-integrin, α 5-integrin and NRP1 individually and in combination prompted significant changes in VEGFR2 expression indicating these receptors conduct discrete and cooperative functions as principal regulators of endothelial VEGFR2's lifecycle. Moving forward, we chose to focus our efforts on our two integrin receptors in an attempt to determine how they co-regulate VEGFR2.







$\beta3/\alpha5/NRP1^{fl/fl}$
 $\beta3/\alpha5/NRP1^{fl/fl}.EC^{KO}$

B

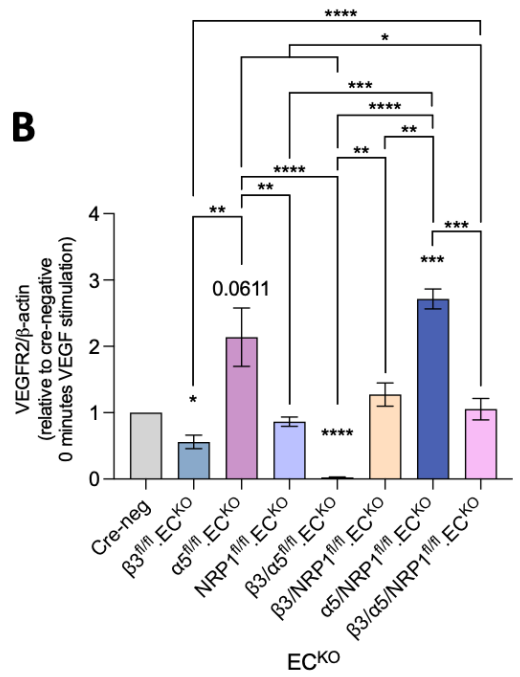


Figure 5.1 β 3-integrin and NRP1 are essential for VEGFR2 signalling, but β 3-integrin and α 5-integrin are collectively required for VEGFR2 preservation. **A)** Representative western blots of VEGF challenge assays in which Cre-negative and TAT-Cre-nucleofected endothelial cells seeded on fibronectin (10 μ g/ml) coated 10 cm dishes and left to adhere for 24 hours at 37°C were starved for 3 hours in serum-free media prior to stimulation with VEGF for 0, 5, and 15-minutes. Following their designated stimulation periods all dishes were placed on ice, lysed with ESB and their protein content quantified using the DC protein assay before prepping for western blot analysis. Western blots show total levels of β 3-integrin, α 5-integrin and NRP1, as well as total and phosphorylated levels of VEGFR2 (Y1173) and AKT (T308). β -actin was used as a loading control. Densitometric quantification of pVEGFR2 Y1173/total VEGFR2, pAKT T308/total AKT, and VEGFR2/ β -actin relative to Cre-negative 0-minute VEGF stimulation obtained using FijiImageJ™. Error bars displayed as means mean \pm SEM. N = 3. **B)** Densitometric quantification of VEGFR2/ β -actin at 0-minute VEGF stimulation relative to each genotype's respective Cre-negative control at 0-minute VEGF stimulation. Error bars displayed as mean \pm SEM. N = 3. Statistical significance was expressed and analysed as follows: *= P <0.05, **= P <0.002, unpaired students t-test (two-tailed)/one-way ANOVA.

5.2 β 3-integrin depletion enhanced VEGFR2 trafficking to degrading machinery.

Following its VEGF-induced stimulation, VEGFR2 undergoes clathrin-dependent endocytosis. Now housed in clathrin-coated vesicles the activated receptor is transported to early endosomes before proceeding through one of several possible trafficking pathways. Though VEGFR2 is initially activated by ligand binding at the cell's surface, its internalisation and endosomal trafficking are essential for the stimulation of its many downstream signalling pathways. Ultimately its journey is concluded via Rab4-dependent short-loop recycling back to the plasma membrane, Rab11-dependent long-loop recycling, or a Rab7-dependent pathway destined for degradation (43). VEGF is also known to regulate integrin trafficking. In particular, VEGF stimulation promotes α v β 3-integrin's Rab4-dependent recycling to the plasma membrane whilst also limiting its internalisation (267). Considering the depletion of our integrin receptors was evidently controlling VEGFR2 abundance, we hypothesised that β 3- and α 5-integrin were controlling aspects of VEGFR2 trafficking.

Firstly, to determine whether genetic targeting of β 3- and α 5-integrin influenced the surface expression of VEGFR2, we analysed its biotinylated surface levels in unstimulated target knockout endothelial cells (Fig 5.2 A). This revealed that changes in total VEGFR2 protein abundance translated to its surface expression, with β 3- and α 5-integrin depletion (β 3^{fl/fl}.EC^{KO}, α 5^{fl/fl}.EC^{KO}) prompting reduced and elevated VEGFR2 surface expression respectively, and their combined depletion (β 3/ α 5^{fl/fl}.EC^{KO}) ablating VEGFR2 surface expression entirely.

We postulated that these integrins could be directing VEGFR2 intracellular cargo, with β 3-integrin depletion prompting preferential traffic through degrading pathways, and α 5-integrin depletion protecting VEGFR2 by shuttling it away from these channels. Rab7 is the major GTPase regulating late endosomal traffic to lysosomes and proteasomes. We therefore performed a co-immunoprecipitation assay between Rab7 and VEGFR2 at 0 and 30 minutes of VEGF stimulation, though only in single knockout cells as VEGFR2 expression was virtually non-existent in our double integrin knockout line (Fig 5.2 B). The 30-minute VEGF-stimulated time point was used as a control, as VEGFR2 signalling is eventually concluded, at least in part, by receptor poly-ubiquitinylation and associated degradation. We therefore expected an increase in Rab7-VEGFR2 association in line with a reduction in total receptor expression at this time point in control cells. Indeed, in β 3^{fl/fl} and α 5^{fl/fl}

control endothelial cells VEGFR2 levels decreased following VEGF-stimulation, and this was additionally met by an elevated association with Rab7 relative to total VEGFR2 levels. In the absence of β 3- or α 5-integrin (β 3^{fl/fl}.EC^{KO}, α 5^{fl/fl}.EC^{KO}), VEGFR2 maintained a normal response to prolonged VEGF-stimulation, with its expression significantly reduced after 30 minutes in both conditions. At 0 minutes however, β 3-integrin depletion (β 3^{fl/fl}.EC^{KO}) prompted an increase in VEGFR2-Rab7 association relative to total receptor expression when compared with control cells at this time point. This indicated that under unstimulated conditions β 3-integrin protects VEGFR2 from excessive Rab7-directed degradation. In our α 5-integrin knockout endothelial cells (α 5^{fl/fl}.EC^{KO}) we expected reduced VEGFR2-Rab7 association to account for the accumulated levels of this receptor. Whilst their association was relatively less than that in control cells at 0-minutes of VEGF stimulation, it appeared less substantial than was required to account for the observed increase in VEGFR2 abundance.

Staining for VEGFR2 and Rab7 in permeabilised, unstimulated Cre-negative and TAT-Cre-nucleofected endothelial cells partially confirmed these findings, with VEGFR2-Rab7 co-localisation increasing in β 3-integrin depleted endothelial cells (β 3^{fl/fl}.EC^{KO}) relative to their Cre-negative counterparts (Fig 5.2 C & D). α 5-integrin depletion (α 5^{fl/fl}.EC^{KO}), however, prompted no measurable change in their co-localisation, further indicating that the upregulation of VEGFR2 detected in these cells was likely independent of changes in its Rab7-directed trafficking in unstimulated conditions.

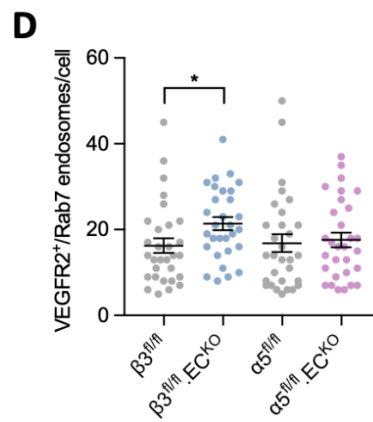
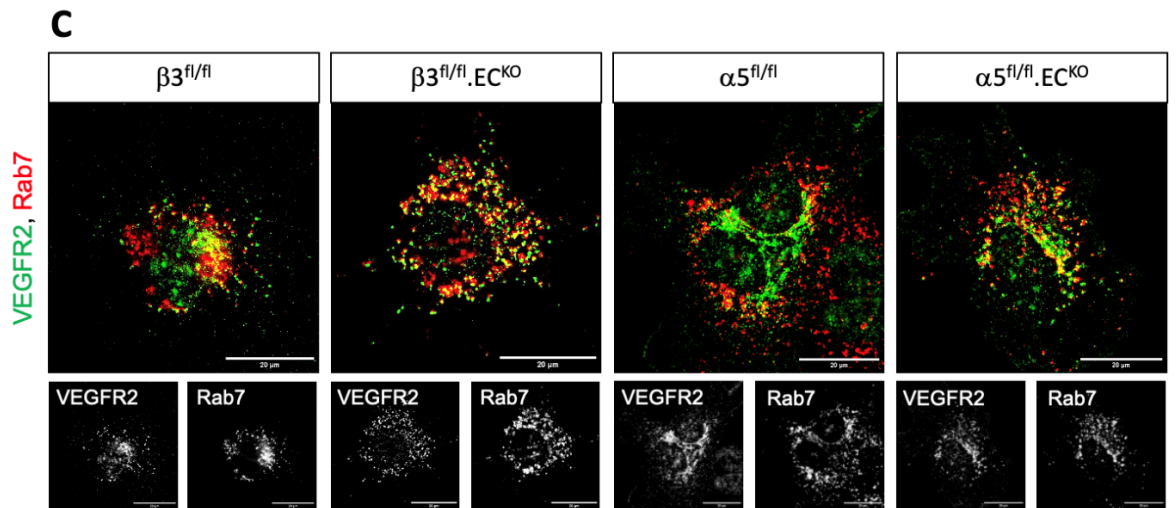
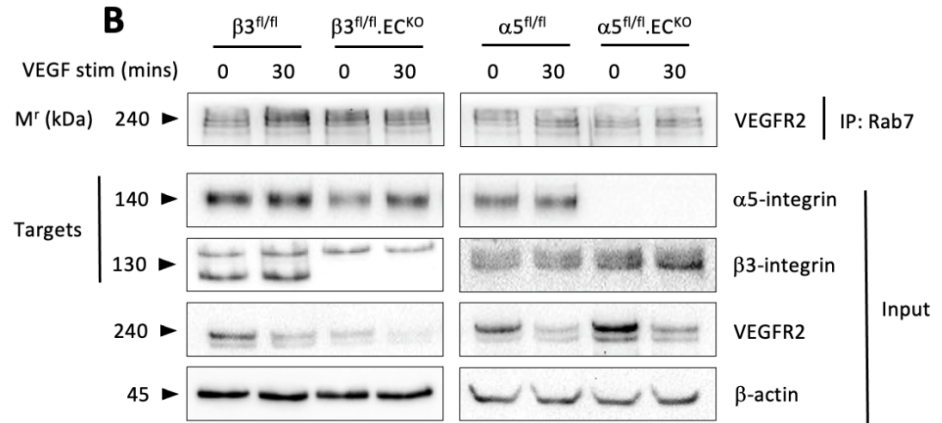
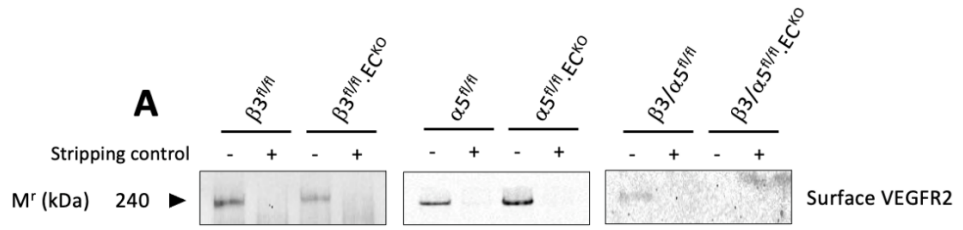


Figure 5.2 β 3-integrin depletion enhanced VEGFR2 trafficking to degrading machinery. **A)** Representative western blots show biotinylated cell surface VEGFR2 across each genotype as well as their respective MESNA-stripped negative controls. N=1. **B)** Cre-negative and TAT-Cre-nucleofected endothelial cells were seeded onto fibronectin-coated dishes (10 μ g/ml) and left to adhere for 24 hours at 37°C. These cells were starved in serum-free media prior to stimulation with VEGF for 0 and 30 minutes. Following completion of their designated stimulation periods, endothelial protein extracts were immunoprecipitated with protein-G Dynabeads® coupled with anti-Rab7 primary antibodies. Immunoprecipitated lysates were then subjected to western blot analysis alongside total cell lysates. Representative western blots show VEGFR2-Rab7 association as well as confirmation of target depletion and VEGFR2 input. β -actin was used as a loading control. β 3^{fl/fl}; β 3^{fl/fl}.EC^{KO} N = 2, α 5^{fl/fl}; α 5^{fl/fl}.EC^{KO} N = 1. **C)** Cre-negative and TAT-Cre-nucleofected endothelial cells were seeded at a low density onto acid-washed, oven-sterilised coverslips pre-coated with fibronectin (10 μ g/ml) for 3 hours after which they were fixed, blocked, permeabilized and incubated with anti-VEGFR2 and anti-Rab7 primary antibodies. The following day coverslips were incubated with the appropriate Alexa® fluor secondary antibodies diluted in PBS. The images shown are representative of VEGFR2 and Rab7 immuno-stained endothelial cells in the indicated genotypes. **D)** Quantification of the number of VEGFR2/Rab7-positive endosomes per cells. Error bars displayed as mean \pm SEM. N = 1, n = 30 cells. Statistical significance was expressed and analysed as follows: * = P < 0.05, unpaired students t-test (two-tailed).

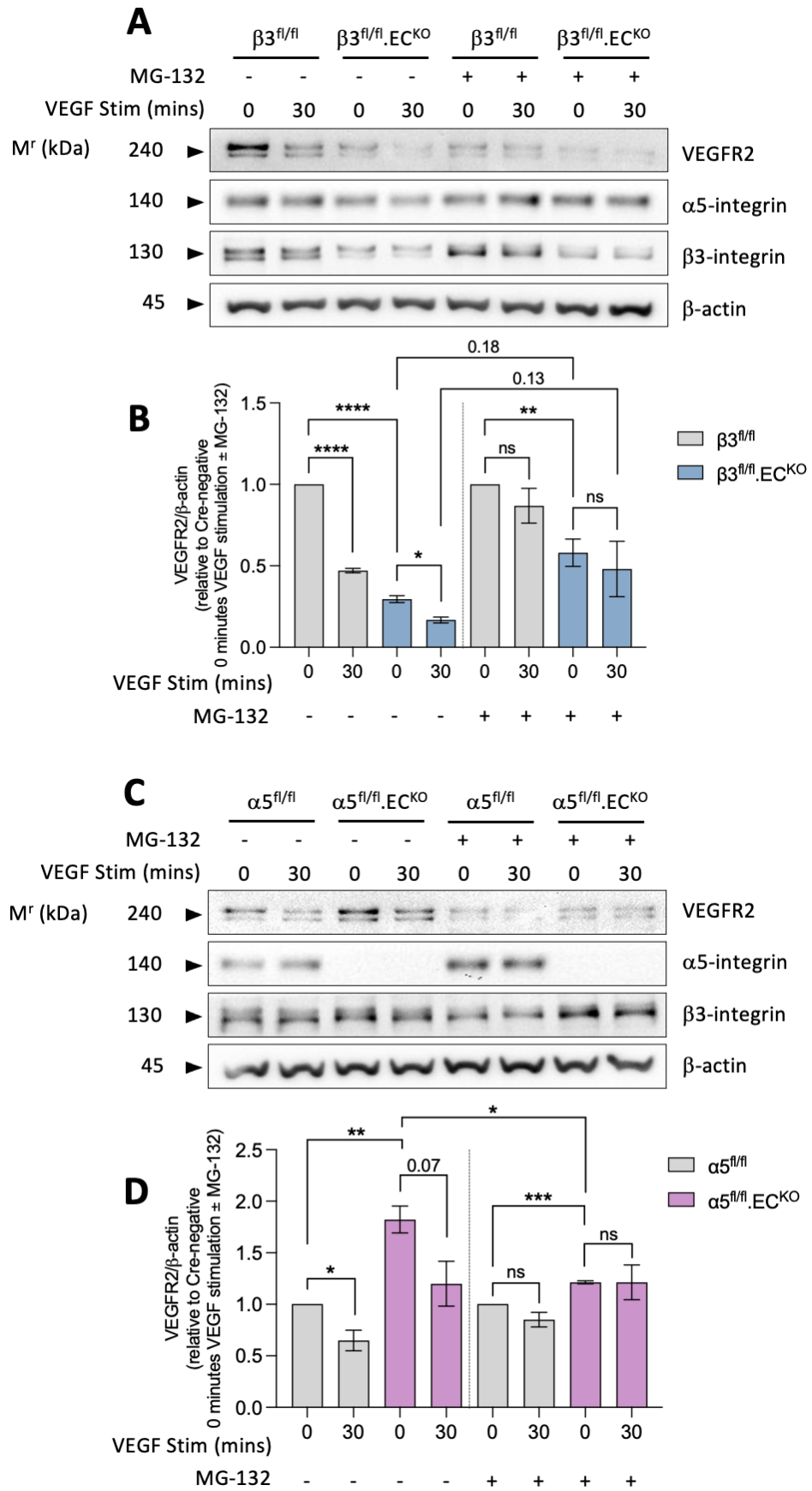
5.3 Lysosomal, but not proteasomal inhibition rescued the VEGFR2 downregulation induced by β 3-integrin depletion.

With VEGFR2 preferentially trafficking along Rab7-directed intracellular channels in the absence of β 3-integrin, we next hypothesized that inhibition of lysosomal and proteasomal machinery could restore VEGFR2 when β 3-integrin was depleted either individually or alongside α 5-integrin (β 3^{fl/fl}.EC^{KO}, β 3/ α 5^{fl/fl}.EC^{KO}). We additionally postulated this inhibition could elevate VEGFR2 expression further in α 5-integrin knockout cells (α 5^{fl/fl}.EC^{KO}). We and others have previously used MG-132 to potently inhibit the protease activity of the 26S proteasome complex (101, 268, 269, 270). Here, we repeated our 0- and 30-minute VEGF stimulation of control and integrin-knockout endothelial cells but supplemented their starvation in serum free media with MG-132. Once again, the 30-minute time point was used as a control to determine whether MG-132 was successfully blocking proteasome-mediated degradation of poly-ubiquitinated VEGFR2 during the normal resolution of VEGF-signalling.

Across our control and single-knockout cells (α 5^{fl/fl}.EC^{KO}, β 3^{fl/fl}.EC^{KO}), the reduction in VEGFR2 expression prompted by prolonged VEGF exposure was successfully inhibited in their MG-132 treated counterparts, confirming successful proteasomal inhibition (Fig 5.3 A-D). However, in the absence of β 3-integrin (β 3^{fl/fl}.EC^{KO}), MG-132 treatment failed to rescue VEGFR2 levels (Fig 5.3 A & B). Furthermore, contradicting our hypothesis, the increased VEGFR2 expression observed in our α 5-integrin knockout cells (α 5^{fl/fl}.EC^{KO}) returned to control levels following proteasome inhibition (Fig 5.3 C & D). We later discovered that MG-132 had been reported to suppress endothelial VEGFR2 transcription and significantly diminish the half-life of its mRNA, explaining why VEGFR2 expression was reduced even in unstimulated control cells (271). Unsurprisingly then, we saw no recovery of VEGFR2 expression in the absence of both integrins together (β 3/ α 5^{fl/fl}.EC^{KO}) (Fig 5.3 E).

To circumvent the unintended suppression of VEGFR2 synthesis whilst still inhibiting protein degradation, we instead used chloroquine, a well-established lysosome inhibitor (79, 244). Over a period of four hours chloroquine treatment elevated VEGFR2 expression in each control cell line, confirming its successful lysosomal inhibition (Fig 5.3 F-I). This elevation was also extended to β 3-integrin knockout endothelial cells (β 3^{fl/fl}.EC^{KO}), rescuing VEGFR2 to WT levels (Fig 5.3 F & G). Though this experiment was only performed once in α 5-integrin and double integrin knockout cells,

chloroquine treatment was able to further amplify the increased VEGFR2 abundance detected in the absence of α 5-integrin ($\alpha 5^{fl/fl}.EC^{KO}$) whilst no VEGFR2 restoration was detected in the absence of both integrins together ($\beta 3/\alpha 5^{fl/fl}.EC^{KO}$) (Fig 5.3 H & I). In agreement with prior data, the chloroquine-induced increase of VEGFR2 in α 5-integrin depleted cells indicated that, under baseline conditions, VEGFR2 intracellular cargo was still undergoing normal trafficking through Rab7-directed pathways to lysosomes for degradation. The elevated VEGFR2 protein levels detected in these cells may instead be due to enhanced VEGFR2 transcription. This could explain why the MG-132-induced transcriptional suppression of VEGFR2 had a greater effect on VEGFR2 levels in α 5-integrin-depleted cells relative to their Cre-negative counterparts. Likewise, the inability of lysosomal inhibition to prompt any VEGFR2 recovery in double integrin knockout cells also implied a transcriptional answer to this phenotype.



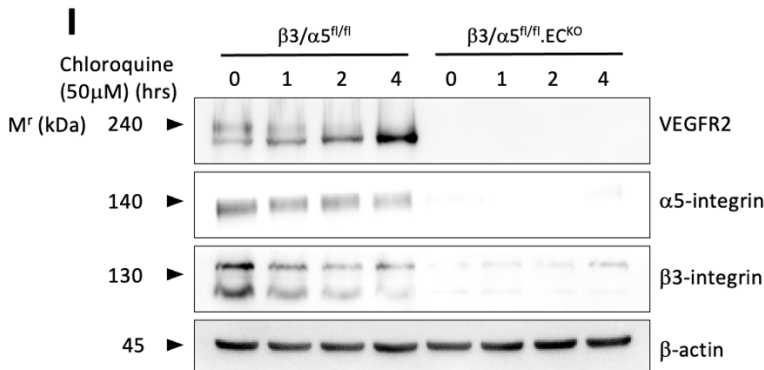
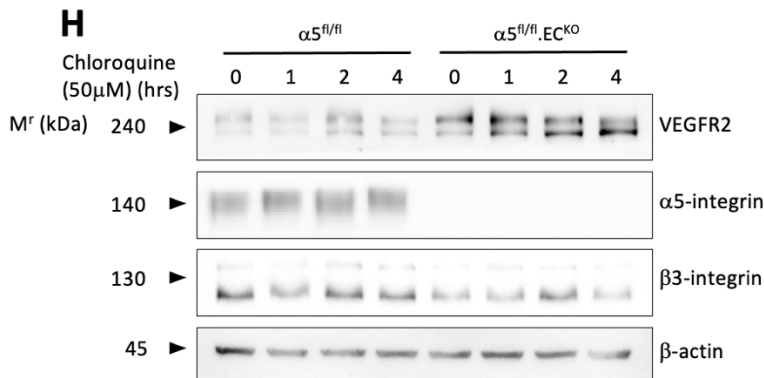
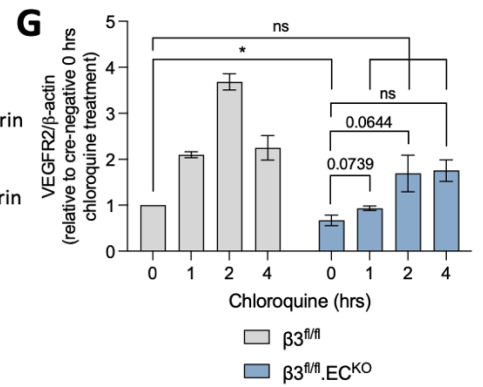
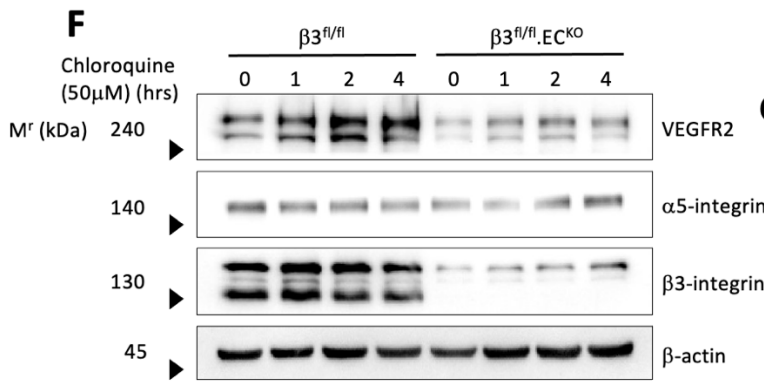
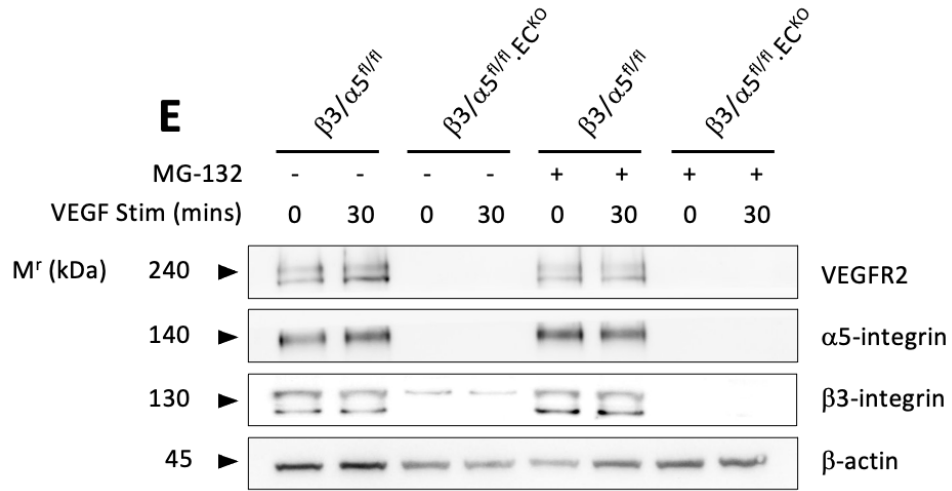


Figure 5.3 Lysosomal but not proteasomal inhibition rescued VEGFR2 downregulation induced by β 3-integrin depletion. Cre-negative and TAT-Cre-nucleofected endothelial cells were seeded onto 10 cm dishes pre-coated with fibronectin (10 μ g/ml) and left to adhere for 24 hours at 37°C. These cells were then starved for 3 hours in serum-free media \pm MG-132 (10 μ M) prior to stimulation with VEGF for 0- and 30-minutes. Following completion of their designated stimulation periods, all dishes were placed on ice, lysed in ESB, their protein content quantified using the DC protein assay and subsequently subjected to western blot analysis. **A, C & D)** Representative western blots of VEGFR2, β 3-integrin, α 5-intgrin and β -actin as a loading control across each single and double integrin knockout cell line. **B & D)** Densitometric quantification of VEGFR2/ β -actin relative to that of their Cre-negative control at 0-minute VEGF stimulation \pm MG-132 obtained using FijiImageJ™. Error bars displayed as mean \pm SEM. β 3^{fl/fl}/ β 3^{fl/fl}.EC^{KO} N = 3, α 5^{fl/fl}/ α 5^{fl/fl}.EC^{KO} N = 3, β 3/ α 5^{fl/fl}; β 3/ α 5^{fl/fl}.EC^{KO} N = 1. **F – I)** Cre-negative and TAT-Cre-nucleofected endothelial cells were seeded onto 10 cm dishes pre-coated with fibronectin (10 μ g/ml) and left to adhere for 24 hours at 37°C. These cells were then starved for the indicated time points in serum-free media \pm chloroquine (50 μ M). Following completion of their designated incubation periods, all dishes were placed on ice, lysed in ESB, their protein content quantified using the DC protein assay and subsequently subjected to western blot analysis. **F, H & I)** Representative western blots of VEGFR2, β 3-integrin, α 5-intgrin and β -actin as a loading control across each single and double integrin knockout cell line. **G)** Densitometric quantification of VEGFR2/ β -actin relative to their respective Cre-negative 0-hour time-point without chloroquine treatment in β 3^{fl/fl}/ β 3^{fl/fl}.EC^{KO} cells was obtained using FijiImageJ™. Error bars displayed as mean \pm SEM. β 3^{fl/fl}/ β 3^{fl/fl}.EC^{KO} N = 3, α 5^{fl/fl}/ α 5^{fl/fl}.EC^{KO} N = 1, β 3/ α 5^{fl/fl}; β 3/ α 5^{fl/fl}.EC^{KO} N = 1. Statistical significance was expressed and analysed as follows: *= P <0.05, **= P <0.002, ***= P <0.0002, ****= P <0.0001, unpaired students t-test (two-tailed)/one-way ANOVA.

5.4 Co-inhibition of $\alpha v\beta 3$ -integrin and $\alpha 5\beta 1$ -integrin reduced VEGFR2 protein levels without effecting its membrane shedding or endothelial adhesion to fibronectin.

The reduction in VEGFR2 prompted by co-depletion of our integrin targets *in vitro* was substantial. This effect was unlikely the result of off-target Cre-recombinase-induced recombination events since the effects of individual integrin-depletion on VEGFR2 expression were entirely different and the genes encoding $\beta 3$ -integrin, $\alpha 5$ -integrin and VEGFR2 reside on separate chromosomes. Nevertheless, we sought further confirmation of this observation by co-targeting $\beta 3$ - and $\alpha 5$ -integrin pharmacologically, thereby determining whether pharmacological antagonism could replicate the reduction in VEGFR2 produced through genetic silencing of both integrin receptors together. To accomplish this, we utilised ATN-161, a five amino-acid peptide (Ac-PHSCN-NH₂) that non-competitively targets the β -subunits of both $\alpha v\beta 3$ -integrin and $\alpha 5\beta 1$ -integrin. Derived from the synergy region of fibronectin, ATN-161 is not an RGD-peptide mimetic and does not influence cell adhesion to fibronectin *in vitro* (272).

Incubating WT, PyMT-immortalised endothelial cells in serum free media supplemented with ATN-161 at varying concentrations revealed that this dual-integrin inhibitor significantly reduced VEGFR2 protein levels when administered at a high concentration (10mM) (Fig 5.4 A & B). Notably, this decrease was independent of any up- or down-regulation of $\alpha v\beta 3$ - or $\alpha 5\beta 1$ -integrin monomeric subunits (Fig 5.4 A). We also confirmed that this concentration of ATN-161 did not influence endothelial adhesion to fibronectin whilst re-confirming the reduction in VEGFR2 in concurrently seeded cells (Fig 5.4 C & D). Antagonism of our integrin targets was therefore capable of significantly inhibiting VEGFR2 whilst leaving integrin mediated adhesion to fibronectin unimpaired. As discussed previously, internalised VEGFR2 may be destined for one of several possible trafficking channels. Its constitutive internalisation and rapid recycling back to the plasma membrane via Rab4-positive vesicles is reported to protect the receptor from excessive ectodomain cleavage. Blocking this trafficking route allows elevated receptor shedding from the plasma membrane leaving a 130 kDa cytoplasmic fragment (79). By over-exposing the representative blot shown this fragment was clearly observed and, akin with the mature 240 kDa fragment, demonstrated an equivalent drop in abundance (Fig 5.4 A). The observed reduction in mature VEGFR2 was therefore likely irrespective of changes in this pathway. Further studies are required to determine whether, upon co-inhibition of these integrin targets, VEGFR2 is

preferentially trafficked down degrading intracellular routes like in the absence of β 3-integrin alone, or whether its transcription is altered as suspected may be the case when α 5-integrin was genetically targeted alone or in combination with β 3-integrin.

ATN-453, the biotinylated form of ATN-161, is known to possess the same binding efficacy as its non-biotinylated counterpart. Khalili *et al*, however, demonstrated that its binding affinity could be additionally enhanced by supplementation with Mn^{2+} ($MnCl_2$) (272). Mechanistically, these ions induce a conformational shift towards the extended-open state of integrin heterodimers resulting in increased ligand affinity (273). We hypothesised that Mn^{2+} supplementation could enhance ATN-161-integrin binding and result in more effective VEGFR2 downregulation. Upon incubating the same WT, immortalised endothelial cells with lower concentrations of ATN-161 (0-100 μ M) in serum-free media alone or supplemented with $MnCl_2$, we observed that Mn^{2+} supplementation resulted in the significant downregulation of mature VEGFR2 when incubated with as a little as 1 μ M ATN-161 (Fig 5.4 E). Again, this downregulation was mirrored in VEGFR2's cytoplasmic fragment.

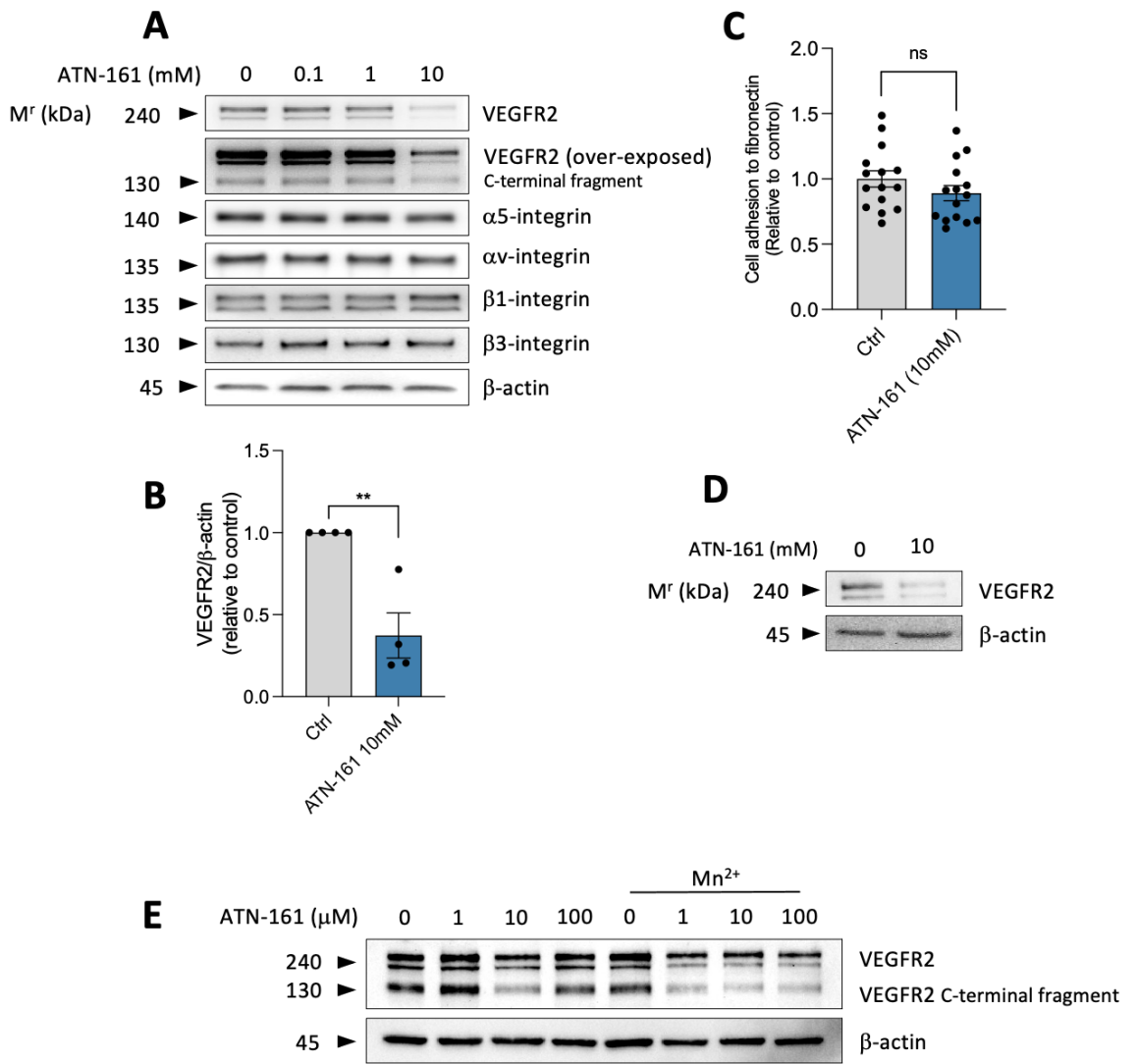


Figure 5.4 Co-inhibition of $\alpha v\beta 3$ -integrin and $\alpha 5\beta 1$ -integrin reduces VEGFR2 protein levels without effecting its membrane shedding or endothelial adhesion to fibronectin. WT endothelial cells were seeded onto 6 cm plates pre-coated with fibronectin and left to adhere for 24 hours at 37°C. These cells were then incubated in serum-free media containing various concentrations of ATN-161 for 1 hour at 37°C. Plates were put on ice following incubation and endothelial cells were lysed in ESB and their protein content was quantified using the DC protein assay before prepping for western blot analysis. **A)** Representative western blot showing total levels of VEGFR2, VEGFR2's C-terminal 130 kDa fragment, $\alpha 5$ -integrin, αv -integrin, $\beta 1$ -integrin and $\beta 3$ -integrin in endothelial cells incubated with ATN-161 (0-10 mM). β -actin was used as a loading control. **B)** Densitometric quantification of 10mM ATN-161 VEGFR2/b-actin relative to 0 mM ATN-161 control group obtained using FijiImageJ™. Error bars displayed as mean \pm SEM. N = 4. **C)** WT endothelial cells were seeded into 96-well plates that had been pre-coated with fibronectin in PBS (2 mg/ml) and blocked in 1% BSA/PBS for 1 hour. These cells were left to adhere for 3 hours in serum-free media supplemented with ATN-161 (10 mM). Following fixation and a series of PBS washes the adhered cells were stained with methylene blue before absorbance was read at 630 nm. The proportion of adhered cells after 3 hours was expressed relative to that of their non-treated controls. Error bar displayed as mean \pm SEM. N=1, n = 15 wells. **D)** Representative western blot of total VEGFR2 levels in WT endothelial cells seeded alongside the cell adhesion assay to confirm VEGFR2 downregulation. β -actin was used as a loading control. N = 1. **E)** Representative western blot showing total levels of VEGFR2 and its C-terminal 130 kDa fragment in endothelial cells incubated with ATN-161 (0-100 mM) \pm MnCl₂ (2 mM). β -actin was used as a loading control. N = 1. Statistical significance was expressed and analysed as follows: **=P<0.002, unpaired students t-test (two-tailed).

5.5 Investigating the contribution of β 3-integrin and α 5-integrin to pathological angiogenesis *in vivo*.

Tumour growth is initially restricted by its ability to recruit a blood vascular supply, with the failure to do so limiting tumour expansion to just a few millimeters in diameter. Tumour angiogenesis is therefore a key cancer hallmark (274). The involvement of integrins α v β 3 and α 5 β 1 in tumour angiogenesis is well documented. Since identifying its selective upregulation on angiogenic vasculature, α v β 3-integrin had been a major focus of anti-angiogenic drug development efforts, with pre-clinical studies showing potential (31, 139, 142, 145). However, the failure of Cilengitide, which had been assessed in almost 30 clinical trials for its potential use as a cancer treatment, slowed further efforts to utilise this integrin as an anti-angiogenic target (275, 276). Later studies revealed that its use at low concentrations could unexpectedly enhance pathological angiogenesis and tumour growth, a phenotype that was replicated in mice possessing a global depletion of β 3-integrin (160). Steri *et al* later revealed that short-term endothelial-specific β 3-integrin depletion could significantly reduce tumour angiogenesis and growth, but its depletion over longer periods provided no anti-angiogenic benefit (161). The recovery in tumour growth reported in the long-term absence of β 3-integrin was shown to rely on a NRP1-driven compensatory mechanism. As such, targeting both receptors in combination could reduce tumour growth more substantially than that achieved through their individual depletion (195). This therefore indicated that combinatorial targeting approaches could re-invigorate anti-angiogenic strategies.

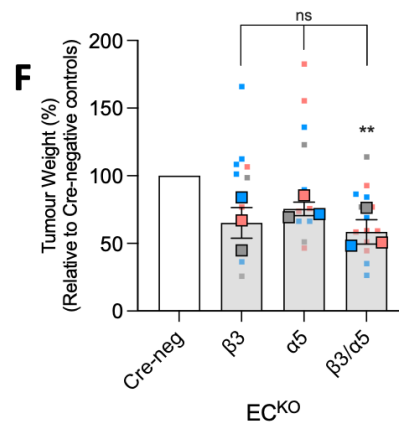
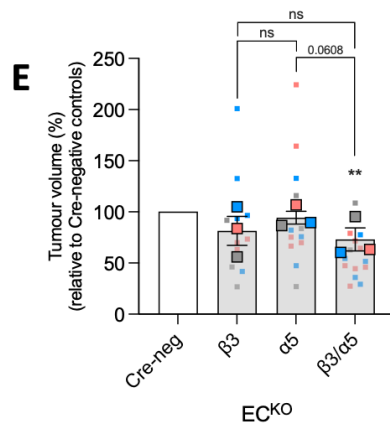
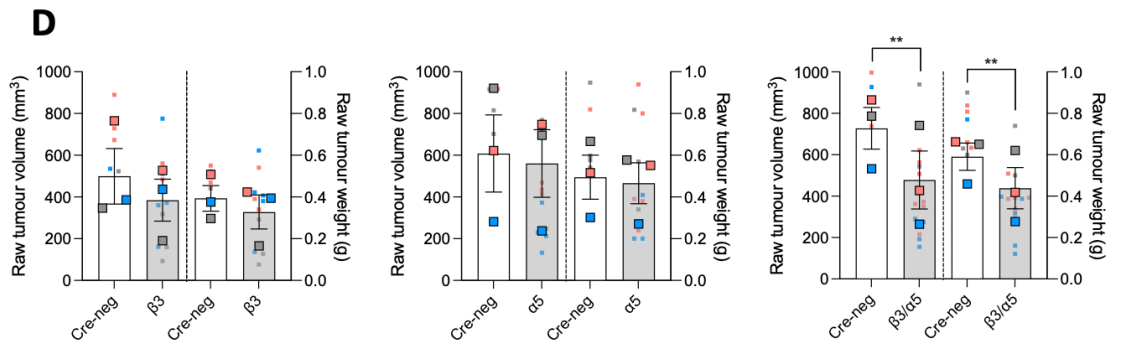
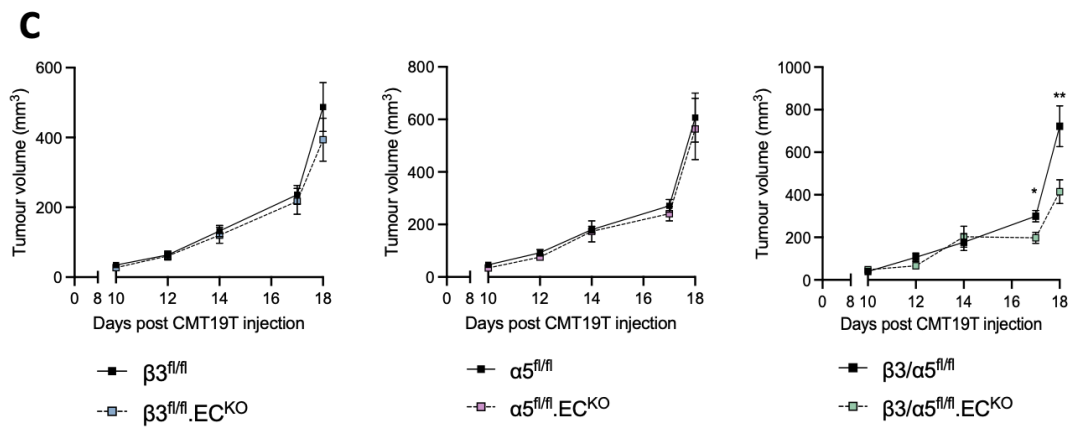
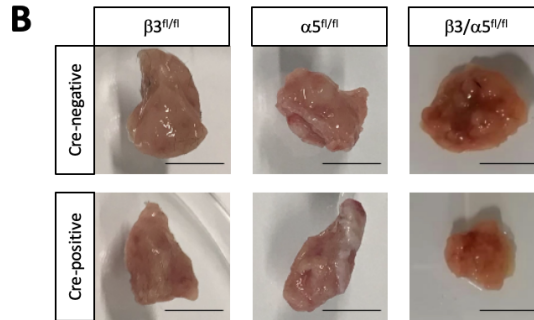
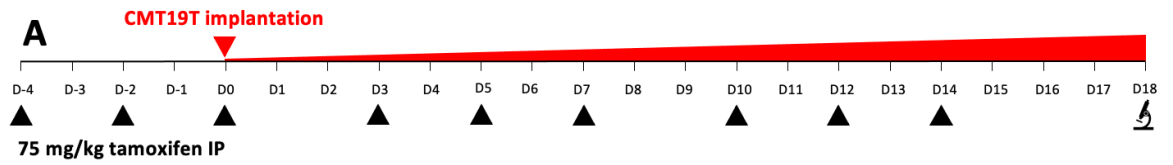
Like α v β 3-integrin, α 5 β 1-integrin is also upregulated on angiogenic vasculature, though, in contrast with its fibronectin-binding counterpart, its global depletion is embryonically lethal by virtue of severe mesodermal and vascular defects (167, 168, 277). Nevertheless, vascular development proceeded normally upon its endothelial-specific depletion (169). Non-endothelial α 5-integrin was found instead to be necessary for angiogenesis and tumour development, with antibody or peptide blockade of α 5 β 1-fibronectin interactions conveying an anti-angiogenic effect in both chick and murine models, and Kim *et al* demonstrating that function-blocking antibodies directed against this integrin could significantly reduce tumour growth and angiogenesis (163). Once again, its endothelial specific depletion was unable to replicate these findings (176). Considering these studies, Dr Johnson hypothesised that for tumorigenesis to be successfully inhibited, our endothelial receptors of interest would need to be targeted in combination.

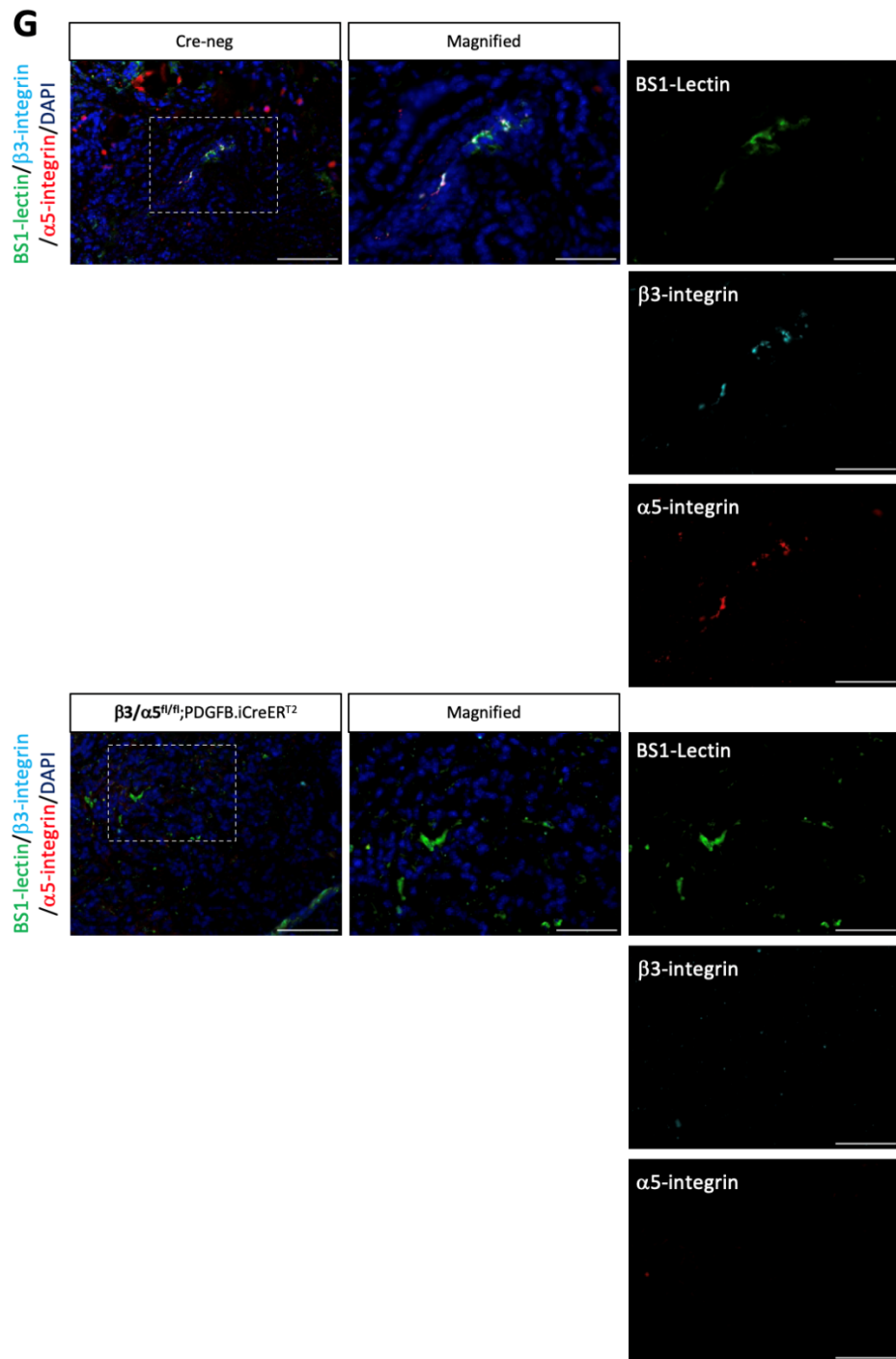
5.6 Co-targeting β 3-integrin and α 5-integrin prophylactically impaired tumorigenesis.

To investigate the involvement of our endothelial integrin targets in tumour growth, CMT19T mouse lung carcinoma cells were subcutaneously administered into the flanks of adult mice by Dr Johnson. These animals received tamoxifen (75 mg/kg) via intraperitoneal injection thrice weekly, with administration beginning four days prior to tumour cell implantation to ensure efficient target depletion. Hypothesising that short-term impairments in tumour growth could be rescued by the upregulation of compensatory mechanisms if provided with sufficient time, like that reported by Ellison *et al* where NRP1 could compensate for the long-term depletion of β 3-integrin, these tumours were allowed to grow for 18 days before tissue harvest (Fig 5.5 A & B) (195). During this time their progression was monitored using calliper measurements from 10 days post-implantation and are presented below as raw values (Fig 5.5 C). After 18 days the tumours were extracted, and their weight and volume were measured before being expressed as a percentage relative to that measured in their respective Cre-negative control littermates. Raw values of both tumour volume and weight at D18 are also shown for transparency (Fig 5.5 D-F).

Calliper measurements revealed no changes in the progressive growth of CMT19T tumours when β 3- or α 5-integrin were depleted individually (β 3.EC^{KO}, α 5.EC^{KO}), nor any changes in their weight or volume at day 18 when made relative to Cre-negative control littermates or expressed as raw values. These data agreed with previous studies reporting individual endothelial depletion of β 3- or α 5-integrin could not significantly alter tumour growth when modelled over an extended period, though failed to recapitulate the acute impairment to tumour growth observed by Steri *et al* in the absence of β 3-integrin at 12 days post-implantation (161, 169). One potential reason for this discrepancy could be the method of tamoxifen administration used. We have induced target deletion by a series of intraperitoneal tamoxifen injections, whilst Steri and colleagues utilised pellets that remain *in situ*, slowly releasing tamoxifen into the surrounding tissue (161). This is a more rigorous but also more costly method. Only in the absence of these integrins together (β 3/ α 5.EC^{KO}) was tumour growth significantly impaired. Calliper measurements recorded the first significant reduction in tumour volume at 17 days post-implantation, and analysis at day 18 revealed a significant reduction in relative tumour weight and volume of approximately 30% and 40% respectively (Fig 5.5 C, E & F). Immunofluorescent analysis of sections taken from these tumours revealed effective co-depletion of both integrins in BS1-lectin-positive tumour vasculature

(Fig 5.5 G). We had aimed to confirm target depletion in our single integrin knockout lines before the writing of this thesis, but this work remains to be done. We next assessed the effects of depleting our targets individually and in duplicate on tumour vascularity by enumerating endomucin-positive vessels in tumour sections and expressing these relative to their Cre-negative controls. Again, only when co-depleting β 3- and α 5-integrin could a significant reduction be observed, with tumour vascularity dropping by approximately 50% in their shared absence (Fig 5.5 H & I). The reduced tumour burden detected in the absence of both endothelial integrins together was therefore likely due to impaired vascular growth into the tumour. We suspected this anti-angiogenic effect was caused by downregulated endothelial VEGFR2 as shown previously through both genetic and pharmacological co-targeting of these integrins *in vitro*. By co-staining for VEGFR2 and endomucin we compared the number of VEGFR2-positive vessels with the total number of vessels across our integrin knockout genotypes (Fig 5.5 H & J). This revealed that, whilst β 3-integrin depletion (β 3.EC^{KO}) elicited a slight but significant reduction in the number of VEGFR2-positive vessels in line with that observed *in vitro*, integrin co-depletion only mirrored this effect (P=0.0545) (β 3/ α 5.EC^{KO}), failing to recapitulate the complete ablation of this receptor as observed *in vitro*. Other mechanisms must have accounted for the more severe anti-angiogenic effects observed by integrin co-depletion.





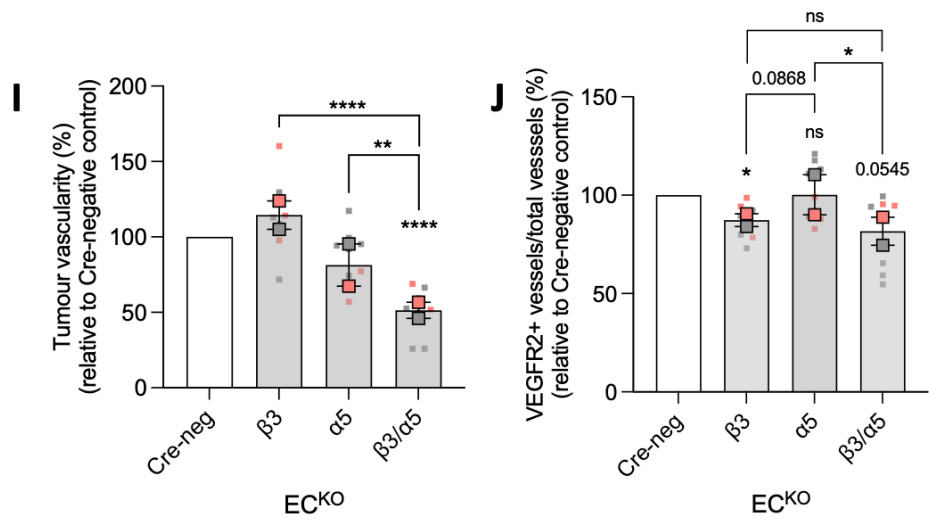
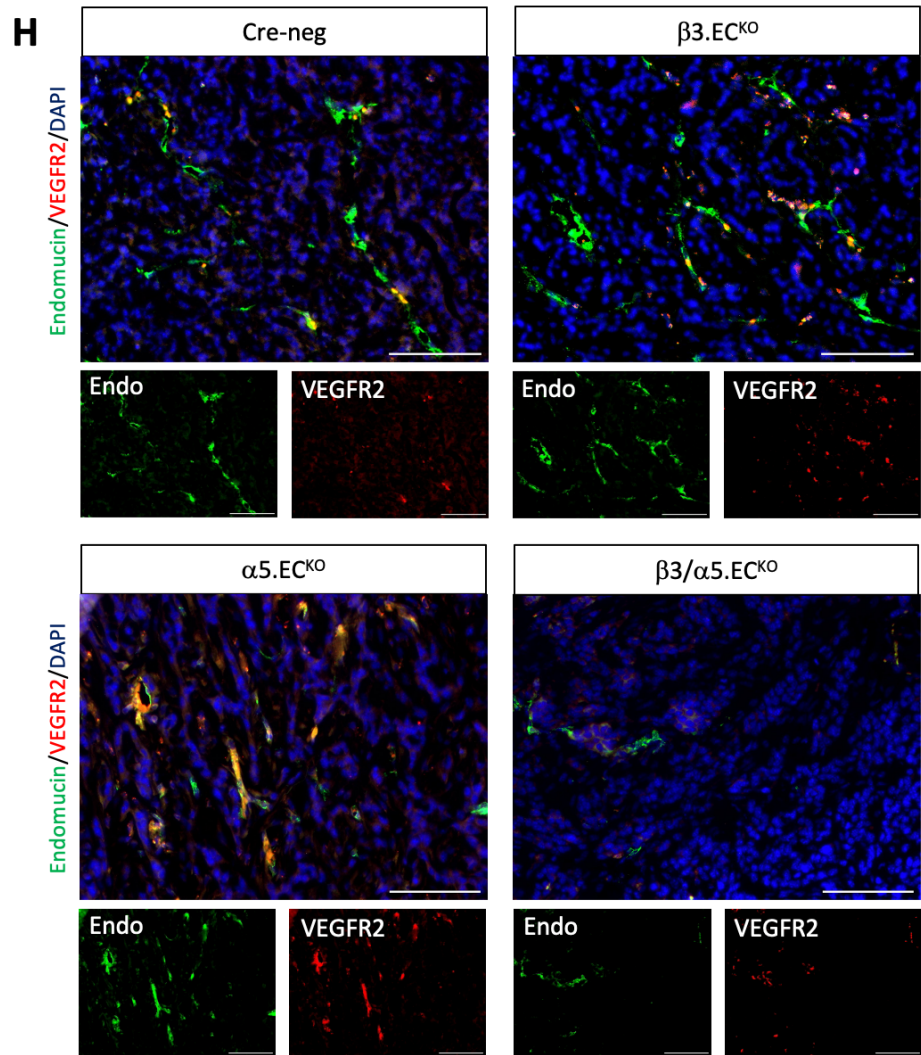


Figure 5.5 Co-targeting β 3-integrin and α 5-integrin could prophylactically impair tumorigenesis.

A) Time-course schematic of tamoxifen administration. Tamoxifen (75 mg/kg, 20 mg/ml stock) was administered (black triangles) via intraperitoneal injection thrice weekly (Monday, Wednesday, and Friday) beginning 4 days prior to subcutaneous CMT19T tumour cell implantation (D0 – red triangle) in both Cre-negative and Cre-positive littermates. Tumours were then allowed to grow for 18 days.

B) Representative images of CMT19T tumours removed from Cre-negative and Cre-positive littermates. Scale bar = 1 cm. **C)** Raw tumour volume (mm^3) kinetics acquired via caliper measurements of tumour bearing mice between D10-17 and the isolated tumours on D18. Tumour volume was calculated using the following formula: length x width² x 0.52. Error bars displayed as mean \pm SEM. N = 3, n \geq 11 tumours per group. **D)** Quantification of the raw tumour volume (mm^3) and raw tumour weight (g) of CMT19T tumours isolated on D18. Error bars displayed as mean \pm SEM. N = 3, n \geq 11 tumours per group. **E & F)** Quantification of tumour volume (E) and tumour weight (F) expressed as a percentage of the average volume and weight of their Cre-negative littermate controls. Error bars displayed as mean \pm SEM. N = 3, n \geq 11 mice per group. **G)** CMT19T tumour sections co-stained for β 3-integrin, α 5-integrin, and BS1-lectin. Scale bars = 100 μm . **H)** Representative images of CMT19T tumour sections co-stained for VEGFR2 and endomucin. Scale bar = 100 μm . **I)** Quantification of blood vessel density as the number of endomucin-positive vessels per tumour (calculated from 3 ROIs per tumour section across 2 sections per tumour) expressed as a percentage of the average number of vessels in their Cre-negative control littermates. Error bars displayed as mean \pm SEM. N = 2, n \geq 8 tumours per group. **J)** Quantification of VEGFR2/endomucin-positive tumour vessels relative to the total number of vessels and expressed as a percentage of the average VEGFR2-positive vessel density of Cre-negative controls. Error bars displayed as mean \pm SEM. N = 2, n \geq 8 tumours per group. Statistical significance was expressed and analysed as follows: *=P<0.05, **=P<0.002, ****=P<0.0001, unpaired students t-test (two-tailed)/one-way ANOVA.

5.7 Discussion

This chapter revealed that β 3-integrin, α 5-integrin and NRP1 form an endothelial regulatory network capable of controlling VEGFR2 dynamics *in vitro*. Previous studies reported that low concentrations of the RGD-mimetic α v β 3-integrin inhibitor Cilengitide could promote co-trafficking of α v β 3-integrin and VEGFR2 through Rab4A-positive vesicles. Though VEGFR2 internalisation remained unaffected, their preferential trafficking through this endosomal pathway carried VEGFR2 back to the plasma membrane and therefore limited its lysosomal degradation. α v β 3-integrin inhibition therefore had the protective effect of reducing VEGFR2's degradation. This mechanism also enhanced VEGF-induced angiogenesis *ex vivo* and the recruitment of functional vasculature in tumours (160). These studies further strengthened existing literature detailing the enhanced tumour vascularisation, VEGF-induced permeability and normal developmental phenotype of β 3-integrin knockout mice owed to their elevated expression of VEGFR2 (153, 154, 155, 278).

In contradiction, we found that endothelial β 3-integrin depletion alone induced a slight but significant reduction in VEGFR2 expression. Its downregulation was due to preferential trafficking through Rab7-positive late endosomes to degrading lysosomes. This anti-angiogenic effect prompted by targeting endothelial β 3-integrin additionally correlated with our previous observations where its depletion induced a significant impairment to developmental angiogenesis in the retina, though confirmation of VEGFR2 downregulation in retinal vasculature upon β 3-integrin depletion remains to be performed. Our *in vitro* results also indicated that α 5-integrin performed an anti-angiogenic role by limiting β 3-integrin's upregulation of VEGFR2. As such, when this integrin was depleted (α 5^{fl/fl}.EC^{KO}, α 5/NRP1^{fl/fl}.EC^{KO}) VEGFR2 saw a 2-3-fold increase in expression that could be ablated entirely by the additional depletion of β 3-integrin (β 3/ α 5^{fl/fl}.EC^{KO}). Alongside its anti-angiogenic role then, α 5-integrin must conduct some pro-angiogenic functions to sustain the partial VEGFR2 expression detected in the absence of β 3-integrin alone (β 3^{fl/fl}.EC^{KO}). We subsequently noted that the severe VEGFR2 phenotype prompted by dual integrin depletion could then be rescued by depleting our targets in triplicate (β 3/ α 5/NRP1^{fl/fl}.EC^{KO}). NRP1 was therefore at least somewhat responsible for severe reduction in VEGFR2 prompted by depleting our integrins in duplicate.

We additionally found that the changes in VEGFR2 expression observed in our integrin knockout lines ($\beta 3^{fl/fl}.EC^{KO}$, $\alpha 5^{fl/fl}.EC^{KO}$, $\beta 3/\alpha 5^{fl/fl}.EC^{KO}$) reflected their surface expression. Steri and colleagues reported that whilst the elevated VEGFR2 expression of $\beta 3^{fl/fl}.Tie1.Cre$ -positive lung microvascular endothelial cells reflected in its increased surface expression, neither total nor surface levels of this receptor were affected in their $\beta 3^{fl/fl}.PDGFB.Cre$ -positive lung microvascular counterparts. One notable difference between our study and that performed by Steri *et al* was the degree to which $\beta 3$ -integrin was depleted. Here we have completely abolished endothelial $\beta 3$ -integrin expression, whilst Steri *et al* reduced it by approximately 60% (161). Knowing that slight alterations in $\beta 3$ -integrin expression can influence VEGFR2 expression, these differences may have accounted for the observed discrepancies (195).

We and others have documented the angiogenic consequences of individually depleting our target integrins on tumorigenesis and revealed only transient beneficial effects (161, 176). Re-confirming this, tumour growth and vascularity was only influenced upon co-depletion of $\beta 3$ - and $\alpha 5$ -integrin, but extending our analysis to 18 days post-implantation enabled us to determine the longevity of these effects. Of note, the contribution of our integrin targets to pathological and developmental angiogenesis differed. In pathological scenarios their shared absence was required to prompt measurable reductions in tumour vascularity and growth, whilst in the retina the individual depletion of $\beta 3$ -integrin was enough to significantly perturb vascular outgrowth of the superficial plexus. Their dual expression was instead required for angiogenic sprout development in this organ. It is also worth noting that not all our *in vitro* findings correlated with our *in vivo* observations. Should $\alpha 5$ -integrin depletion lead to VEGFR2 upregulation we would have expected hyper-sprouting at the retinal vascular front as well as enhanced neovascularisation and tumour growth in pathological models as observed following global $\beta 3$ -integrin depletion (155). Moreover, the ablation of VEGFR2 in $\beta 3/\alpha 5^{fl/fl}.EC^{KO}$ cells failed to translate to a more severe retinal angiogenic phenotype in line with that caused by endothelial VEGFR2 genetic depletion (230). As we know to be the case for $\alpha 5$ -integrin, our integrin targets could be most highly expressed, and therefore most functionality relevant, in angiogenic sprouts protruding from the vascular periphery. The vascular effects resulting from their endothelial co-depletion could therefore be most concentrated in this region to cause selective inhibition of endothelial sprouting at the vascular front whilst leaving that occurring in the inner remodelling plexus less affected.

Continuing this theme of incongruencies, though ATN-161 treatment could significantly and reproducibly downregulate VEGFR2 *in vitro*, the scale of the reduction was more analogous to that seen in the individual absence of β 3-integrin rather than both integrin targets together. Furthermore, another co-inhibitor of α v β 3- and α 5 β 1-integrin, AXT-107, has been reported to reduce VEGFR2 expression in cultured endothelial cells by promoting its poly-ubiquitination and associated degradation, a mechanism dependent on Rab7-directed vesicular trafficking which we have shown here becomes enhanced in the individual absence of β 3-integrin. Further studies are required to determine exactly how ATN-161 orchestrated the VEGFR2 downregulation observed (279). It would also be prudent to determine how this antagonist influences the expression of VEGFR2 in mural cells that co-express these integrins such as pericytes to gain a broader insight into the effects of dual integrin inhibition on microvascular growth (266).

6 Final discussion

The involvement of fibronectin and its endothelial receptors in the coordination of angiogenesis has been the subject of continued debate, with clinical trials aiming to derive anti-angiogenic benefit from selective receptor targeting falling short of the promising results predicted in pre-clinical studies (157, 158, 161, 163, 176, 195, 276). Studies have since documented crosstalk mechanisms linking endothelial fibronectin receptors that likely contribute to treatment resistance by providing compensatory angiogenic recovery pathways upon individual receptor targeting. Only when such pathways were additionally targeted could prolonged anti-angiogenic and anti-tumorigenic effects be achieved (161, 195). We hypothesised that the three endothelial fibronectin receptors $\alpha v\beta 3$ -integrin, $\alpha 5\beta 1$ -integrin and NRP1 could engage in complex crosstalk mechanisms involving cooperative, competitive, and compensatory interactions to regulate angiogenesis. To examine these interactions, we utilised seven genetically engineered mouse lines in which the endothelial depletion of our target receptors was temporally controlled via tamoxifen administration using the PDGFB.iCreER^{T2} system. Crucially, each knockout line was compared to its own Cre-negative control line, establishing 14 lines in total. Cultured endothelial cell lines derived from these mice were used to continue our investigations *in vitro*. Using these tools, we explored the discrete and interlinked angiogenic functions of these endothelial fibronectin receptors.

Using the post-natal mouse retina as a model of developmental angiogenesis we were able to determine the short- and long-term involvement of our receptors in the vascularisation of this organ. This revealed a series of individual, cooperative, contradictory and vascular-bed specific functions.

From P6 through to our most prolonged analysis at P18, NRP1 was the overwhelmingly dominant pro-angiogenic player within our receptor network. Its depletion conferred the most substantial vascular impairments to each of the retina's three vascular beds, and even appeared to control the well-established checkpoints that orchestrate its timely vascular growth, with angiogenic development of IP proceeding before that of the DP in NRP1-depleted retinas. This directly contradicted the dogma of retinal vascular development (280, 281). Nevertheless, retinal vascular growth persisted in its absence and would likely have reached completion if provided with sufficient time. At P6 however, NRP1 was unable to drive a full vascular response when expressed alone. Only

in the additional presence of one or both our integrin targets could the SP reach WT levels of vascular outgrowth. This cooperative effect was between β 3-integrin and NRP1, meanwhile vascular extension at this developmental time-point was independent of α 5-integrin as reported previously (169). Knowing that the vascular defects resultant of acute β 3-integrin depletion are transient due to upregulation of NRP1-driven compensatory pathways, we hypothesised that the vascular recovery observed in the absence of β 3-integrin at P18 could be overcome by delaying its depletion until directly prior to tissue harvest, thereby circumventing the upregulation of compensatory mechanisms (161, 195). However, this revealed no vascular impediment in any retinal vascular bed upon β 3-integrin depletion. Instead, a minor pro-angiogenic, vascular bed-specific function of α 5-integrin in DP vascularisation was revealed. This indicated that the pro-angiogenic function of α 5-integrin, and not that of β 3-integrin, was being compensated for by alternative angiogenic pathways at P18 to shroud its true, albeit subtle, involvement in retinal DP development.

Since these receptors showed greatest functional overlap at P6, we focussed our attention at this developmental time-point. We found that the depletion of α 5-integrin alongside β 3-integrin (β 3/ α 5.ECKO) resulted in retinal hypo-sprouting at the vascular periphery that was significantly more severe than when either integrin was targeted alone. Their phenotype even matched and trended on being more severe than that measured in NRP1-depleted retinas which had consistently displayed the most substantial vascular impairments. Such a phenotype could theoretically be accounted for by the abolishment of endothelial VEGFR2 expression as detected *in vitro* in the absence of both integrin targets. However, not all of the evidence aligned. The hypo-sprouting prompted by integrin co-depletion did not reflect in a more stunted SP nor a more hypo-vascularised inner plexus, with vascular extension and density in this genetic line mirroring that detected in the individual absence of β 3-integrin. Perhaps then, given one of our integrin targets was preferentially expressed in sprout structures, this phenotype was localised to protruding angiogenic sprouts at the vascular front and irrespective of overall vascular outgrowth. After all, others have reported previously that retinal hyper-sprouting driven by elevated endothelial VEGFR2 expression at the vascular front did not correspond with any associated increase in retinal vascular extension relative to controls (244). However, further incongruencies kept this hyper-sprouting phenotype in question even with the aforementioned caveat that sprouting and extension do not necessarily go hand-in-hand. Should downregulated VEGFR2 at the vascular front convey localised hypo-sprouting in the absence of both integrins, then the elevation in VEGFR2

expression detected in the absence of $\alpha 5$ -integrin *in vitro* should have reflected in retinal hyper-sprouting. Instead, vascular sprouting was normal. We attempted to visualise VEGFR2 in the retina, trialling numerous antibodies, but ultimately failed to achieve a usable stain. If our *in vitro* findings directly translated *in vivo* we would have expected a complete ablation of VEGFR2 following dual integrin depletion and with it an even more severe sprouting profile in line with that documented following endothelial depletion of VEGFR2 or $\beta 1$ -integrin (230, 245). We hypothesize that the remaining sprouts observed in the absence of both $\beta 3$ - and $\alpha 5$ -integrin were those that failed to undergo tamoxifen-induced recombination and therefore still expressed VEGFR2. At the time of writing this thesis we had begun inserting the tdTomato reporter gene into $\beta 3/\alpha 5$.PDGFB.iCreER^{T2} mice to assess target recombination in retinal endothelial sprouts of $\beta 3/\alpha 5$.EC^{KO} retinas and were even in the final stages of its generation, but unfortunately this experiment remained unfinished. This hypothesis is clearly reliant on the aforementioned changes in VEGFR2 expression translating to retinal vasculature in our integrin knockout lines, and specifically to the retinal vascular periphery. Although we failed to successfully stain for VEGFR2 in the retina, a logical next step would be to additionally stain for VEGFR1 and VEGFR3 to determine whether these receptors were likewise influenced by our integrin targets.

We had yet to investigate vascular function in the presence and absence of our three receptors, with any comments made being purely speculative. We observed that retinal arterioles and venules in each knockout combination retained their associated capillary free zones, a gauge of vessel perfusion and lumen formation, but such rudimentary analysis was clearly limited. Additional immunofluorescent analysis of fibrinogen in the retina, a serum protein and indicator of damaged inter-endothelial junctions within the blood-retinal-barrier when found extravasated from vasculature, would have provided a more robust indication of vascular permeability in our various knockout combinations (282).

From a pathological perspective, when assessing how $\beta 3$ - and $\alpha 5$ -integrin contribute to angiogenesis in tumour models, we found that tumorigenesis could be successfully inhibited only in their shared absence. Whilst this was an encouraging result, its therapeutic relevance was limited due to the method of tamoxifen administration employed in which our targets were depleted prior to tumour cell implantation. In the future we plan to deplete our integrin targets once the implanted tumour cells form a palpable mass to recapitulate a clinical scenario more accurately. The reduction in tumour volume induced by dual integrin depletion was associated with a

significant reduction in tumour vascularity that was absent when either integrin was targeted alone. Again, whilst promising, the contribution of these integrins to pathological and physiological angiogenesis differed, as lone depletion of $\beta 3$ -integrin was sufficient to hinder overall vascular expansion in the retina. The pathological observations more closely matched the hypo-sprouting vascular periphery of $\beta 3/\alpha 5.EC^{KO}$ retinas, a phenotype we postulated may be due to selective VEGFR2 ablation in sprouting vessels. However, we found the number of VEGFR2-positive tumour vessels was significantly reduced in a $\beta 3$ -integrin dependent manner, with no additional downregulation prompted by combinatorial integrin depletion. This indicated that: 1) the dramatic reduction in VEGFR2 protein levels observed *in vitro* upon integrin co-depletion failed to translate to *in vivo* pathological vasculature, and 2) endothelial $\beta 3$ -integrin depletion conferred a slight reduction in vascular VEGFR2 levels *in vivo*, though this failed to provide any anti-angiogenic benefit. The preferential trafficking of VEGFR2 through Rab7-positive endosomal routes to degrading lysosomes enabled by $\beta 3$ -integrin depletion may therefore hold true under pathological and physiological settings, though the lack of any anti-angiogenic advantage brought by depleting this receptor and inducing VEGFR2 downregulation remains unexplained. Akin with our studies of retinal vasculature, endothelial cells escaping target recombination could be a plausible reason why our *in vivo* and *in vitro* results were not mirrored.

In summary, endothelial $\alpha v\beta 3$ -integrin, $\alpha 5\beta 1$ -integrin and NRP1 conduct discrete and overlapping functions to coordinate angiogenesis. Using seven genotypes in which our targets were able to be depleted individually and in combination, this thesis was able to identify specific angiogenic settings in which our receptors performed complex interactions, though the functional consequences of these interactions differed depending on the context in which they were present. The differences observed between physiological and pathological angiogenesis *in vivo*, as well as those between *in vitro* and *in vivo* settings, could have resulted from endothelial heterogeneity in which various redundancy mechanisms involving receptors different from those focussed on in this thesis may have been utilised to recover normal angiogenic processes in our different receptor knockout combinations, thereby muddying the water and making interpretation of gene-depletion induced vascular defects more difficult. Despite this, our methods have documented some of the complex and contradictory vascular outcomes resulting from individual and combinatorial endothelial target depletion.

Abbreviations

4-OHT – 4-hydroxytamoxifen

Ab - Antibody

ADAM – A disintegrin and metalloproteinase

ANG1/2 – Angiopoietin-1/2

Anxa2 – Annexin A2

AWERB - Animal welfare and ethical review board

Bp – Base pair

BP – Breeding pair

BSA – bovine serum albumin

Cas9 – CRISPR associated protein 9

Cdc42 – Cell division control protein 42

CHO – Chinese hamster ovary

CNS – Central nervous system

CRISPR – Clustered regularly interspaced palindromic repeat

CSB – Cell surface biotinylation

CTCF – Corrected total cell fluorescence

DAG – Diacylglycerol

DAPI – 4'6-diamidino-2-phenylindole

DEP1 – Density enhanced phosphatase-1

dH₂O – Distilled water

Dll4 – Delta-like ligand 4

DP – Deep plexus

E – Embryonic day

EC^{KO} – Endothelial cell knockout

ECL – Enhanced chemiluminescence

ECM – Extracellular matrix

ECS – Endothelial cell sorting

EDTA – Ethylenediaminetetraacetic acid

EGTA – Ethylene glycol tetra-acetic acid

ER – Endoplasmic reticulum

ERG – ETS related gene

ERK – Extracellular regulated kinase

ESB – Electrophoresis sample buffer

EtOH – Ethanol

FA – Focal adhesion

FAK – Focal adhesion kinase

FGF – Fibroblast growth factor

Floxed – flanked by loxP sites

Flt-1 – Fms-like tyrosine kinase-1

FOXO1 – Forkhead box protein 01

GIPC1 – GIAP interacting protein C-terminus, member 1

GM – Genetically modified

GPCR – G protein coupled receptor

Grb2 – Growth factor receptor bound protein 2

HCl – Hydrochloric acid

Het - Heterozygous

HIF – Hypoxia inducible factor

HRP – Horseradish peroxidase

HSC70 – Heat shock cognate 70

HSP90 – Heat shock protein 90

HSPG – Heparin sulphate proteoglycan

IAC – Integrin adhesion complex

ICAM-2 – Intracellular adhesion molecule 2

IF – Immunofluorescence

Ig - Immunoglobulin

IP - Immunoprecipitation

IP – intermediate plexus

IP₃ – Inositol 1, 4, 5-triphosphate

MACS - Magnetically activated cell sorting

MAPK – Mitogen-activated protein kinase

Mb - Megabase

MEK – Mitogen-activated protein kinase kinase

MeOH – Methanol

MESNA – Sodium 2-mercaptoethane sulfonate

MMP – Matrix metalloproteinase

NFAT – Nuclear factor of activated T-cell

NFκB – Nuclear factor κB

NICD – Notch intracellular domain

NIP1 – Neuropilin-interacting protein-1

NO – Nitric oxide

NRP1/2 – Neuropilin-1/2

P – Postnatal day

p130Cas – p130 CRK-associated substrate

p38 MAPK – p38 mitogen-activated protein kinase

PAGE – poly-acrylamide gel electrophoresis

PAI-1 – Plasminogen activator inhibitor-1

PBS – Phosphate buffered saline

PCR – Polymerase chain reaction

PDGF β - Platelet derived growth factor β

PDZ – PSD-95/Dlg/ZO-1 domain

PECAM1 – Platelet and endothelial adhesion molecule 1

PFA – Paraformaldehyde

PI3K – Phosphoinositide 3-kinase

PIP₂ – Phosphatidylinositol 4, 5-bisphosphate

PIP₃ – Phosphatidylinositol 3, 4, 5-triphosphate

PKA – Protein kinase A

PKB/Akt – Protein kinase B

PKC – Protein kinase C

PKC – Protein kinase C

PLC γ – Phospholipase C γ

PLGF – Platelet-like growth factor

PTEN – Phosphatase and tensin homolog

PTP1B – Protein tyrosine phosphatase 1B

PyMT – Polyomavirus middle T antigen

R26 – Rosa 26 locus

Rac1 – Ras-related C3 botulinum toxin substrate 1

Rcc2 – Regulator of chromosome condensation 2

RGD – Arginine-Glycine-Aspartic acid

RIAM – Rap1-GTP-interacting adaptor molecule

ROI – Region of interest

RT – Room temperature

RTK – Receptor tyrosine kinase

SBS - Soerensen buffer

SDS – Sodium dodecyl sulphate

SEA – Serine-Glutamic acid-Alanine

SEM – Standard error of the mean

SH2 – Src homology domain 2

SH3 – Src homology domain 3

SP – Superficial plexus

Src – Proto-oncogene tyrosine protein kinase

sVEGFR – soluble vascular endothelial growth factor

TE – Tris-HCl-EDTA

TGF β – Transforming growth factor β

Tie2 – Tyrosine protein kinase receptor 2

TIMP – Tissue inhibitor of metalloproteinase

TM - Transmembrane

TNF α – Tumour necrosis factor α

TSAd – T-cell specific adaptor protein

VASP – Vasodilator stimulator phosphoprotein

VE-PTP – Vascular endothelial-protein tyrosine phosphatase

VEGF – Vascular endothelial growth factor

VEGFR1/2/3 – Vascular endothelial growth factor receptor 1/2/3

VSMC – Vascular smooth muscle cell

WB – western blot

WT – Wild-type

References

1. Flamme I, Frolich T, Risau W. Molecular mechanisms of vasculogenesis and embryonic angiogenesis. *J Cell Physiol.* 1997;173(2):206-10.
2. Dudley AC, Griffioen AW. Pathological angiogenesis: mechanisms and therapeutic strategies. *Angiogenesis.* 2023;26(3):313-47.
3. Monahan-Earley R, Dvorak AM, Aird WC. Evolutionary origins of the blood vascular system and endothelium. *J Thromb Haemost.* 2013;11 Suppl 1:46-66.
4. Pugsley MK, Tabrizchi R. The vascular system. An overview of structure and function. *J Pharmacol Toxicol Methods.* 2000;44(2):333-40.
5. Poelmann RE, Gittenberger-de Groot AC, Hierck BP. The development of the heart and microcirculation: role of shear stress. *Med Biol Eng Comput.* 2008;46(5):479-84.
6. Westcott EB, Segal SS. Perivascular innervation: a multiplicity of roles in vasomotor control and myoendothelial signaling. *Microcirculation.* 2013;20(3):217-38.
7. Potente M, Makinen T. Vascular heterogeneity and specialization in development and disease. *Nat Rev Mol Cell Biol.* 2017;18(8):477-94.
8. Wagenseil JE, Mecham RP. Vascular extracellular matrix and arterial mechanics. *Physiol Rev.* 2009;89(3):957-89.
9. Aird WC. Phenotypic heterogeneity of the endothelium: I. Structure, function, and mechanisms. *Circ Res.* 2007;100(2):158-73.
10. Jambusaria A, Hong Z, Zhang L, Srivastava S, Jana A, Toth PT, et al. Endothelial heterogeneity across distinct vascular beds during homeostasis and inflammation. *Elife.* 2020;9.
11. Marcu R, Choi YJ, Xue J, Fortin CL, Wang Y, Nagao RJ, et al. Human Organ-Specific Endothelial Cell Heterogeneity. *iScience.* 2018;4:20-35.
12. Neve A, Cantatore FP, Maruotti N, Corrado A, Ribatti D. Extracellular matrix modulates angiogenesis in physiological and pathological conditions. *Biomed Res Int.* 2014;2014:756078.
13. Carmeliet P, Jain RK. Molecular mechanisms and clinical applications of angiogenesis. *Nature.* 2011;473(7347):298-307.
14. Dalton CJ, Lemmon CA. Fibronectin: Molecular Structure, Fibrillar Structure and Mechanochemical Signaling. *Cells.* 2021;10(9).
15. George EL, Baldwin HS, Hynes RO. Fibronectins are essential for heart and blood vessel morphogenesis but are dispensable for initial specification of precursor cells. *Blood.* 1997;90(8):3073-81.
16. Milner R, Hung S, Erokwu B, Dore-Duffy P, LaManna JC, del Zoppo GJ. Increased expression of fibronectin and the alpha 5 beta 1 integrin in angiogenic cerebral blood vessels of mice subject to hypobaric hypoxia. *Mol Cell Neurosci.* 2008;38(1):43-52.
17. Huang H, Huang Q, Wang F, Milner R, Li L. Cerebral ischemia-induced angiogenesis is dependent on tumor necrosis factor receptor 1-mediated upregulation of alpha5beta1 and alphaVbeta3 integrins. *J Neuroinflammation.* 2016;13(1):227.
18. Carmeliet P, Ferreira V, Breier G, Pollefeyt S, Kieckens L, Gertsenstein M, et al. Abnormal blood vessel development and lethality in embryos lacking a single VEGF allele. *Nature.* 1996;380(6573):435-9.
19. Ferrara N, Carver-Moore K, Chen H, Dowd M, Lu L, O'Shea KS, et al. Heterozygous embryonic lethality induced by targeted inactivation of the VEGF gene. *Nature.* 1996;380(6573):439-42.
20. Shalaby F, Rossant J, Yamaguchi TP, Gertsenstein M, Wu XF, Breitman ML, et al. Failure of blood-island formation and vasculogenesis in Flk-1-deficient mice. *Nature.* 1995;376(6535):62-6.
21. Carmeliet P. Angiogenesis in health and disease. *Nat Med.* 2003;9(6):653-60.
22. Patan S. Vasculogenesis and angiogenesis as mechanisms of vascular network formation, growth and remodeling. *J Neurooncol.* 2000;50(1-2):1-15.
23. Swift MR, Weinstein BM. Arterial-venous specification during development. *Circ Res.* 2009;104(5):576-88.

24. Mentzer SJ, Konerding MA. Intussusceptive angiogenesis: expansion and remodeling of microvascular networks. *Angiogenesis*. 2014;17(3):499-509.
25. De Smet F, Segura I, De Bock K, Hohensinner PJ, Carmeliet P. Mechanisms of vessel branching: filopodia on endothelial tip cells lead the way. *Arterioscler Thromb Vasc Biol*. 2009;29(5):639-49.
26. Chung AS, Ferrara N. Developmental and pathological angiogenesis. *Annu Rev Cell Dev Biol*. 2011;27:563-84.
27. Blancas AA, Wong LE, Glaser DE, McCloskey KE. Specialized tip/stalk-like and phalanx-like endothelial cells from embryonic stem cells. *Stem Cells Dev*. 2013;22(9):1398-407.
28. Murakami M, Nguyen LT, Zhuang ZW, Moodie KL, Carmeliet P, Stan RV, et al. The FGF system has a key role in regulating vascular integrity. *J Clin Invest*. 2008;118(10):3355-66.
29. Krock BL, Skuli N, Simon MC. Hypoxia-induced angiogenesis: good and evil. *Genes Cancer*. 2011;2(12):1117-33.
30. Chen L, Endler A, Shibasaki F. Hypoxia and angiogenesis: regulation of hypoxia-inducible factors via novel binding factors. *Exp Mol Med*. 2009;41(12):849-57.
31. Brooks PC, Clark RA, Cheresh DA. Requirement of vascular integrin alpha v beta 3 for angiogenesis. *Science*. 1994;264(5158):569-71.
32. Schweisguth F. Regulation of notch signaling activity. *Curr Biol*. 2004;14(3):R129-38.
33. Harrington LS, Sainson RC, Williams CK, Taylor JM, Shi W, Li JL, et al. Regulation of multiple angiogenic pathways by Dll4 and Notch in human umbilical vein endothelial cells. *Microvasc Res*. 2008;75(2):144-54.
34. Benedito R, Roca C, Sorensen I, Adams S, Gossler A, Fruttiger M, et al. The notch ligands Dll4 and Jagged1 have opposing effects on angiogenesis. *Cell*. 2009;137(6):1124-35.
35. Hellstrom M, Phng LK, Hofmann JJ, Wallgard E, Coultas L, Lindblom P, et al. Dll4 signalling through Notch1 regulates formation of tip cells during angiogenesis. *Nature*. 2007;445(7129):776-80.
36. Jakobsson L, Franco CA, Bentley K, Collins RT, Ponsioen B, Aspalter IM, et al. Endothelial cells dynamically compete for the tip cell position during angiogenic sprouting. *Nat Cell Biol*. 2010;12(10):943-53.
37. Costa G, Harrington KI, Lovegrove HE, Page DJ, Chakravartula S, Bentley K, et al. Asymmetric division coordinates collective cell migration in angiogenesis. *Nat Cell Biol*. 2016;18(12):1292-301.
38. Nesmith JE, Chappell JC, Cluceru JG, Bautch VL. Blood vessel anastomosis is spatially regulated by Flt1 during angiogenesis. *Development*. 2017;144(5):889-96.
39. Fantin A, Vieira JM, Gestri G, Denti L, Schwarz Q, Prykhodzhiy S, et al. Tissue macrophages act as cellular chaperones for vascular anastomosis downstream of VEGF-mediated endothelial tip cell induction. *Blood*. 2010;116(5):829-40.
40. Potente M, Gerhardt H, Carmeliet P. Basic and therapeutic aspects of angiogenesis. *Cell*. 2011;146(6):873-87.
41. Davis GE, Saunders WB. Molecular balance of capillary tube formation versus regression in wound repair: role of matrix metalloproteinases and their inhibitors. *J Invest Dermatol Symp Proc*. 2006;11(1):44-56.
42. Bergers G, Song S. The role of pericytes in blood-vessel formation and maintenance. *Neuro Oncol*. 2005;7(4):452-64.
43. Simons M, Gordon E, Claesson-Welsh L. Mechanisms and regulation of endothelial VEGF receptor signalling. *Nat Rev Mol Cell Biol*. 2016;17(10):611-25.
44. Robinson CJ, Stringer SE. The splice variants of vascular endothelial growth factor (VEGF) and their receptors. *J Cell Sci*. 2001;114(Pt 5):853-65.
45. Shalaby F, Ho J, Stanford WL, Fischer KD, Schuh AC, Schwartz L, et al. A requirement for Flk1 in primitive and definitive hematopoiesis and vasculogenesis. *Cell*. 1997;89(6):981-90.

46. Fong GH, Rossant J, Gertsenstein M, Breitman ML. Role of the Flt-1 receptor tyrosine kinase in regulating the assembly of vascular endothelium. *Nature*. 1995;376(6535):66-70.
47. Tischer E, Mitchell R, Hartman T, Silva M, Gospodarowicz D, Fiddes JC, et al. The human gene for vascular endothelial growth factor. Multiple protein forms are encoded through alternative exon splicing. *J Biol Chem*. 1991;266(18):11947-54.
48. Ferrara N. Binding to the extracellular matrix and proteolytic processing: two key mechanisms regulating vascular endothelial growth factor action. *Mol Biol Cell*. 2010;21(5):687-90.
49. Mamer SB, Wittenkeller A, Imoukhuede PI. VEGF-A splice variants bind VEGFRs with differential affinities. *Sci Rep*. 2020;10(1):14413.
50. Dardente H, English WR, Valluru MK, Kanthou C, Simpson D. Debunking the Myth of the Endogenous Antiangiogenic Vegfxxx transcripts. *Trends Endocrinol Metab*. 2020;31(6):398-409.
51. Whitaker GB, Limberg BJ, Rosenbaum JS. Vascular endothelial growth factor receptor-2 and neuropilin-1 form a receptor complex that is responsible for the differential signaling potency of VEGF(165) and VEGF(121). *J Biol Chem*. 2001;276(27):25520-31.
52. Perez-Gutierrez L, Ferrara N. Biology and therapeutic targeting of vascular endothelial growth factor A. *Nat Rev Mol Cell Biol*. 2023.
53. Lee S, Chen TT, Barber CL, Jordan MC, Murdock J, Desai S, et al. Autocrine VEGF signaling is required for vascular homeostasis. *Cell*. 2007;130(4):691-703.
54. Ruhrberg C, Gerhardt H, Golding M, Watson R, Ioannidou S, Fujisawa H, et al. Spatially restricted patterning cues provided by heparin-binding VEGF-A control blood vessel branching morphogenesis. *Genes Dev*. 2002;16(20):2684-98.
55. Carmeliet P, Ng YS, Nuyens D, Theilmeier G, Brusselmans K, Cornelissen I, et al. Impaired myocardial angiogenesis and ischemic cardiomyopathy in mice lacking the vascular endothelial growth factor isoforms VEGF164 and VEGF188. *Nat Med*. 1999;5(5):495-502.
56. Bellomo D, Headrick JP, Silins GU, Paterson CA, Thomas PS, Gartside M, et al. Mice lacking the vascular endothelial growth factor-B gene (*Vegfb*) have smaller hearts, dysfunctional coronary vasculature, and impaired recovery from cardiac ischemia. *Circ Res*. 2000;86(2):E29-35.
57. Aase K, von Euler G, Li X, Ponten A, Thoren P, Cao R, et al. Vascular endothelial growth factor-B-deficient mice display an atrial conduction defect. *Circulation*. 2001;104(3):358-64.
58. Haiko P, Makinen T, Keskkitalo S, Taipale J, Karkkainen MJ, Baldwin ME, et al. Deletion of vascular endothelial growth factor C (VEGF-C) and VEGF-D is not equivalent to VEGF receptor 3 deletion in mouse embryos. *Mol Cell Biol*. 2008;28(15):4843-50.
59. Maharaj AS, Saint-Geniez M, Maldonado AE, D'Amore PA. Vascular endothelial growth factor localization in the adult. *Am J Pathol*. 2006;168(2):639-48.
60. Yamamoto H, Rundqvist H, Branco C, Johnson RS. Autocrine VEGF Isoforms Differentially Regulate Endothelial Cell Behavior. *Front Cell Dev Biol*. 2016;4:99.
61. Koch S, Tugues S, Li X, Gualandi L, Claesson-Welsh L. Signal transduction by vascular endothelial growth factor receptors. *Biochem J*. 2011;437(2):169-83.
62. Dumont DJ, Fong GH, Puri MC, Gradwohl G, Alitalo K, Breitman ML. Vascularization of the mouse embryo: a study of *flk-1*, *tek*, *tie*, and vascular endothelial growth factor expression during development. *Dev Dyn*. 1995;203(1):80-92.
63. Waltenberger J, Claesson-Welsh L, Siegbahn A, Shibuya M, Heldin CH. Different signal transduction properties of KDR and Flt1, two receptors for vascular endothelial growth factor. *J Biol Chem*. 1994;269(43):26988-95.
64. Kendall RL, Thomas KA. Inhibition of vascular endothelial cell growth factor activity by an endogenously encoded soluble receptor. *Proc Natl Acad Sci U S A*. 1993;90(22):10705-9.
65. Hiratsuka S, Nakao K, Nakamura K, Katsuki M, Maru Y, Shibuya M. Membrane fixation of vascular endothelial growth factor receptor 1 ligand-binding domain is important for vasculogenesis and angiogenesis in mice. *Mol Cell Biol*. 2005;25(1):346-54.

66. Hiratsuka S, Minowa O, Kuno J, Noda T, Shibuya M. Flt-1 lacking the tyrosine kinase domain is sufficient for normal development and angiogenesis in mice. *Proc Natl Acad Sci U S A*. 1998;95(16):9349-54.
67. Patten IS, Rana S, Shahul S, Rowe GC, Jang C, Liu L, et al. Cardiac angiogenic imbalance leads to peripartum cardiomyopathy. *Nature*. 2012;485(7398):333-8.
68. Zeisler H, Llurba E, Chantraine F, Vatish M, Staff AC, Sennstrom M, et al. Predictive Value of the sFlt-1:PlGF Ratio in Women with Suspected Preeclampsia. *N Engl J Med*. 2016;374(1):13-22.
69. Dumont DJ, Jussila L, Taipale J, Lymboussaki A, Mustonen T, Pajusola K, et al. Cardiovascular failure in mouse embryos deficient in VEGF receptor-3. *Science*. 1998;282(5390):946-9.
70. Heinolainen K, Karaman S, D'Amico G, Tammela T, Sormunen R, Eklund L, et al. VEGFR3 Modulates Vascular Permeability by Controlling VEGF/VEGFR2 Signaling. *Circ Res*. 2017;120(9):1414-25.
71. Tammela T, Zarkada G, Nurmi H, Jakobsson L, Heinolainen K, Tvorogov D, et al. VEGFR-3 controls tip to stalk conversion at vessel fusion sites by reinforcing Notch signalling. *Nat Cell Biol*. 2011;13(10):1202-13.
72. Zarkada G, Heinolainen K, Makinen T, Kubota Y, Alitalo K. VEGFR3 does not sustain retinal angiogenesis without VEGFR2. *Proc Natl Acad Sci U S A*. 2015;112(3):761-6.
73. Albuquerque RJ, Hayashi T, Cho WG, Kleinman ME, Dridi S, Takeda A, et al. Alternatively spliced vascular endothelial growth factor receptor-2 is an essential endogenous inhibitor of lymphatic vessel growth. *Nat Med*. 2009;15(9):1023-30.
74. Sarabipour S, Ballmer-Hofer K, Hristova K. VEGFR-2 conformational switch in response to ligand binding. *Elife*. 2016;5:e13876.
75. Sakurai Y, Ohgimoto K, Kataoka Y, Yoshida N, Shibuya M. Essential role of Flk-1 (VEGF receptor 2) tyrosine residue 1173 in vasculogenesis in mice. *Proc Natl Acad Sci U S A*. 2005;102(4):1076-81.
76. Basagiannis D, Zografou S, Murphy C, Fotsis T, Morbidelli L, Ziche M, et al. VEGF induces signalling and angiogenesis by directing VEGFR2 internalisation through macropinocytosis. *J Cell Sci*. 2016;129(21):4091-104.
77. Gampel A, Moss L, Jones MC, Brunton V, Norman JC, Mellor H. VEGF regulates the mobilization of VEGFR2/KDR from an intracellular endothelial storage compartment. *Blood*. 2006;108(8):2624-31.
78. Stenmark H. Rab GTPases as coordinators of vesicle traffic. *Nat Rev Mol Cell Biol*. 2009;10(8):513-25.
79. Basagiannis D, Christoforidis S. Constitutive Endocytosis of VEGFR2 Protects the Receptor against Shedding. *J Biol Chem*. 2016;291(32):16892-903.
80. Ballmer-Hofer K, Andersson AE, Ratcliffe LE, Berger P. Neuropilin-1 promotes VEGFR-2 trafficking through Rab11 vesicles thereby specifying signal output. *Blood*. 2011;118(3):816-26.
81. Cebe-Suarez S, Zehnder-Fjallman A, Ballmer-Hofer K. The role of VEGF receptors in angiogenesis; complex partnerships. *Cell Mol Life Sci*. 2006;63(5):601-15.
82. Song YY, Liang D, Liu DK, Lin L, Zhang L, Yang WQ. The role of the ERK signaling pathway in promoting angiogenesis for treating ischemic diseases. *Front Cell Dev Biol*. 2023;11:1164166.
83. Srivastava RK, Unterman TG, Shankar S. FOXO transcription factors and VEGF neutralizing antibody enhance antiangiogenic effects of resveratrol. *Mol Cell Biochem*. 2010;337(1-2):201-12.
84. Takagi S, Tsuji T, Amagai T, Takamatsu T, Fujisawa H. Specific cell surface labels in the visual centers of *Xenopus laevis* tadpole identified using monoclonal antibodies. *Dev Biol*. 1987;122(1):90-100.
85. Takagi S, Hirata T, Agata K, Mochii M, Eguchi G, Fujisawa H. The A5 antigen, a candidate for the neuronal recognition molecule, has homologies to complement components and coagulation factors. *Neuron*. 1991;7(2):295-307.

86. Kolodkin AL, Levengood DV, Rowe EG, Tai YT, Giger RJ, Ginty DD. Neuropilin is a semaphorin III receptor. *Cell*. 1997;90(4):753-62.
87. Soker S, Fidler IJ, Neufeld G, Klagsbrun M. Characterization of novel vascular endothelial growth factor (VEGF) receptors on tumor cells that bind VEGF165 via its exon 7-encoded domain. *J Biol Chem*. 1996;271(10):5761-7.
88. Soker S, Takashima S, Miao HQ, Neufeld G, Klagsbrun M. Neuropilin-1 is expressed by endothelial and tumor cells as an isoform-specific receptor for vascular endothelial growth factor. *Cell*. 1998;92(6):735-45.
89. Carmeliet P, Tessier-Lavigne M. Common mechanisms of nerve and blood vessel wiring. *Nature*. 2005;436(7048):193-200.
90. Parker MW, Guo HF, Li X, Linkugel AD, Vander Kooi CW. Function of members of the neuropilin family as essential pleiotropic cell surface receptors. *Biochemistry*. 2012;51(47):9437-46.
91. Schwarz Q, Ruhrberg C. Neuropilin, you gotta let me know: should I stay or should I go? *Cell Adh Migr*. 2010;4(1):61-6.
92. Cai H, Reed RR. Cloning and characterization of neuropilin-1-interacting protein: a PSD-95/Dlg/ZO-1 domain-containing protein that interacts with the cytoplasmic domain of neuropilin-1. *J Neurosci*. 1999;19(15):6519-27.
93. Panigrahy D, Adini I, Mamluk R, Levonyak N, Bruns CJ, D'Amore PA, et al. Regulation of soluble neuropilin 1, an endogenous angiogenesis inhibitor, in liver development and regeneration. *Pathology*. 2014;46(5):416-23.
94. Cackowski FC, Xu L, Hu B, Cheng SY. Identification of two novel alternatively spliced Neuropilin-1 isoforms. *Genomics*. 2004;84(1):82-94.
95. Gagnon ML, Bielenberg DR, Gechtman Z, Miao HQ, Takashima S, Soker S, et al. Identification of a natural soluble neuropilin-1 that binds vascular endothelial growth factor: In vivo expression and antitumor activity. *Proc Natl Acad Sci U S A*. 2000;97(6):2573-8.
96. Chen H, Bagri A, Zupicich JA, Zou Y, Stoeckli E, Pleasure SJ, et al. Neuropilin-2 regulates the development of selective cranial and sensory nerves and hippocampal mossy fiber projections. *Neuron*. 2000;25(1):43-56.
97. Kitsukawa T, Shimono A, Kawakami A, Kondoh H, Fujisawa H. Overexpression of a membrane protein, neuropilin, in chimeric mice causes anomalies in the cardiovascular system, nervous system and limbs. *Development*. 1995;121(12):4309-18.
98. Kawasaki T, Kitsukawa T, Bekku Y, Matsuda Y, Sanbo M, Yagi T, et al. A requirement for neuropilin-1 in embryonic vessel formation. *Development*. 1999;126(21):4895-902.
99. Gu C, Rodriguez ER, Reimert DV, Shu T, Fritzsche B, Richards LJ, et al. Neuropilin-1 conveys semaphorin and VEGF signaling during neural and cardiovascular development. *Dev Cell*. 2003;5(1):45-57.
100. Takashima S, Kitakaze M, Asakura M, Asanuma H, Sanada S, Tashiro F, et al. Targeting of both mouse neuropilin-1 and neuropilin-2 genes severely impairs developmental yolk sac and embryonic angiogenesis. *Proc Natl Acad Sci U S A*. 2002;99(6):3657-62.
101. Benwell CJ, Johnson RT, Taylor J, Price CA, Robinson SD. Endothelial VEGFR Coreceptors Neuropilin-1 and Neuropilin-2 Are Essential for Tumor Angiogenesis. *Cancer Res Commun*. 2022;2(12):1626-40.
102. Pan Q, Chathery Y, Wu Y, Rathore N, Tong RK, Peale F, et al. Neuropilin-1 binds to VEGF121 and regulates endothelial cell migration and sprouting. *J Biol Chem*. 2007;282(33):24049-56.
103. Parker MW, Xu P, Li X, Vander Kooi CW. Structural basis for selective vascular endothelial growth factor-A (VEGF-A) binding to neuropilin-1. *J Biol Chem*. 2012;287(14):11082-9.
104. Soker S, Miao HQ, Nomi M, Takashima S, Klagsbrun M. VEGF165 mediates formation of complexes containing VEGFR-2 and neuropilin-1 that enhance VEGF165-receptor binding. *J Cell Biochem*. 2002;85(2):357-68.

105. Prahst C, Heroult M, Lanahan AA, Uziel N, Kessler O, Shraga-Heled N, et al. Neuropilin-1-VEGFR-2 complexing requires the PDZ-binding domain of neuropilin-1. *J Biol Chem.* 2008;283(37):25110-4.
106. Lanahan A, Zhang X, Fantin A, Zhuang Z, Rivera-Molina F, Speichinger K, et al. The neuropilin 1 cytoplasmic domain is required for VEGF-A-dependent arteriogenesis. *Dev Cell.* 2013;25(2):156-68.
107. Morin E, Sjoberg E, Tjomsland V, Testini C, Lindskog C, Franklin O, et al. VEGF receptor-2/neuropilin 1 trans-complex formation between endothelial and tumor cells is an independent predictor of pancreatic cancer survival. *J Pathol.* 2018;246(3):311-22.
108. Pellet-Many C, Frankel P, Jia H, Zachary I. Neuropilins: structure, function and role in disease. *Biochem J.* 2008;411(2):211-26.
109. Hynes RO. Integrins: bidirectional, allosteric signaling machines. *Cell.* 2002;110(6):673-87.
110. Tamkun JW, DeSimone DW, Fonda D, Patel RS, Buck C, Horwitz AF, et al. Structure of integrin, a glycoprotein involved in the transmembrane linkage between fibronectin and actin. *Cell.* 1986;46(2):271-82.
111. Sonnenberg A. Integrins and their ligands. *Curr Top Microbiol Immunol.* 1993;184:7-35.
112. Campbell ID, Humphries MJ. Integrin structure, activation, and interactions. *Cold Spring Harb Perspect Biol.* 2011;3(3).
113. King N, Hittinger CT, Carroll SB. Evolution of key cell signaling and adhesion protein families predates animal origins. *Science.* 2003;301(5631):361-3.
114. Plow EF, Haas TA, Zhang L, Loftus J, Smith JW. Ligand binding to integrins. *J Biol Chem.* 2000;275(29):21785-8.
115. Plow EF, Meller J, Byzova TV. Integrin function in vascular biology: a view from 2013. *Curr Opin Hematol.* 2014;21(3):241-7.
116. Sun G, Guillon E, Holley SA. Integrin intra-heterodimer affinity inversely correlates with integrin activatability. *Cell Rep.* 2021;35(10):109230.
117. Kanchanawong P, Calderwood DA. Organization, dynamics and mechanoregulation of integrin-mediated cell-ECM adhesions. *Nat Rev Mol Cell Biol.* 2023;24(2):142-61.
118. Buskermolen ABC, Kurniawan NA, Bouten CVC. An automated quantitative analysis of cell, nucleus and focal adhesion morphology. *PLoS One.* 2018;13(3):e0195201.
119. Sun Z, Costell M, Fassler R. Integrin activation by talin, kindlin and mechanical forces. *Nat Cell Biol.* 2019;21(1):25-31.
120. Zamir E, Katz M, Posen Y, Erez N, Yamada KM, Katz BZ, et al. Dynamics and segregation of cell-matrix adhesions in cultured fibroblasts. *Nat Cell Biol.* 2000;2(4):191-6.
121. Scales TM, Parsons M. Spatial and temporal regulation of integrin signalling during cell migration. *Curr Opin Cell Biol.* 2011;23(5):562-8.
122. Gudzenko T, Franz CM. Studying early stages of fibronectin fibrillogenesis in living cells by atomic force microscopy. *Mol Biol Cell.* 2015;26(18):3190-204.
123. Lu Q, Rounds S. Focal adhesion kinase and endothelial cell apoptosis. *Microvasc Res.* 2012;83(1):56-63.
124. Jacamo RO, Rozengurt E. A truncated FAK lacking the FERM domain displays high catalytic activity but retains responsiveness to adhesion-mediated signals. *Biochem Biophys Res Commun.* 2005;334(4):1299-304.
125. Calalb MB, Polte TR, Hanks SK. Tyrosine phosphorylation of focal adhesion kinase at sites in the catalytic domain regulates kinase activity: a role for Src family kinases. *Mol Cell Biol.* 1995;15(2):954-63.
126. Parsons JT. Focal adhesion kinase: the first ten years. *J Cell Sci.* 2003;116(Pt 8):1409-16.
127. Bolos V, Gasent JM, Lopez-Tarruella S, Grande E. The dual kinase complex FAK-Src as a promising therapeutic target in cancer. *Onco Targets Ther.* 2010;3:83-97.
128. Chang F, Lemmon CA, Park D, Romer LH. FAK potentiates Rac1 activation and localization to matrix adhesion sites: a role for betaPIX. *Mol Biol Cell.* 2007;18(1):253-64.

129. Ilic D, Kovacic B, McDonagh S, Jin F, Baumbusch C, Gardner DG, et al. Focal adhesion kinase is required for blood vessel morphogenesis. *Circ Res.* 2003;92(3):300-7.
130. Mostafavi-Pour Z, Askari JA, Parkinson SJ, Parker PJ, Ng TT, Humphries MJ. Integrin-specific signaling pathways controlling focal adhesion formation and cell migration. *J Cell Biol.* 2003;161(1):155-67.
131. Ivaska J. Unanchoring integrins in focal adhesions. *Nat Cell Biol.* 2012;14(10):981-3.
132. Stupack DG, Cheresh DA. Get a ligand, get a life: integrins, signaling and cell survival. *J Cell Sci.* 2002;115(Pt 19):3729-38.
133. Stupack DG, Puente XS, Boutsaboualoy S, Storgard CM, Cheresh DA. Apoptosis of adherent cells by recruitment of caspase-8 to unligated integrins. *J Cell Biol.* 2001;155(3):459-70.
134. Frisch SM, Francis H. Disruption of epithelial cell-matrix interactions induces apoptosis. *J Cell Biol.* 1994;124(4):619-26.
135. Silva R, D'Amico G, Hodivala-Dilke KM, Reynolds LE. Integrins: the keys to unlocking angiogenesis. *Arterioscler Thromb Vasc Biol.* 2008;28(10):1703-13.
136. Avraamides CJ, Garmy-Susini B, Varner JA. Integrins in angiogenesis and lymphangiogenesis. *Nat Rev Cancer.* 2008;8(8):604-17.
137. Zhou X, Rowe RG, Hiraoka N, George JP, Wirtz D, Mosher DF, et al. Fibronectin fibrillogenesis regulates three-dimensional neovessel formation. *Genes Dev.* 2008;22(9):1231-43.
138. Wang J, Milner R. Fibronectin promotes brain capillary endothelial cell survival and proliferation through alpha5beta1 and alphavbeta3 integrins via MAP kinase signalling. *J Neurochem.* 2006;96(1):148-59.
139. Brooks PC, Montgomery AM, Rosenfeld M, Reisfeld RA, Hu T, Klier G, et al. Integrin alpha v beta 3 antagonists promote tumor regression by inducing apoptosis of angiogenic blood vessels. *Cell.* 1994;79(7):1157-64.
140. McCarty JH, Barry M, Crowley D, Bronson RT, Lacy-Hulbert A, Hynes RO. Genetic ablation of alphav integrins in epithelial cells of the eyelid skin and conjunctiva leads to squamous cell carcinoma. *Am J Pathol.* 2008;172(6):1740-7.
141. Bader BL, Rayburn H, Crowley D, Hynes RO. Extensive vasculogenesis, angiogenesis, and organogenesis precede lethality in mice lacking all alpha v integrins. *Cell.* 1998;95(4):507-19.
142. Brooks PC, Stromblad S, Klemke R, Visscher D, Sarkar FH, Cheresh DA. Antiintegrin alpha v beta 3 blocks human breast cancer growth and angiogenesis in human skin. *J Clin Invest.* 1995;96(4):1815-22.
143. Gladson CL. Expression of integrin alpha v beta 3 in small blood vessels of glioblastoma tumors. *J Neuropathol Exp Neurol.* 1996;55(11):1143-9.
144. Friedlander M, Theesfeld CL, Sugita M, Fruttiger M, Thomas MA, Chang S, et al. Involvement of integrins alpha v beta 3 and alpha v beta 5 in ocular neovascular diseases. *Proc Natl Acad Sci U S A.* 1996;93(18):9764-9.
145. Wilkinson-Berka JL, Jones D, Taylor G, Jaworski K, Kelly DJ, Ludbrook SB, et al. SB-267268, a nonpeptidic antagonist of alpha(v)beta3 and alpha(v)beta5 integrins, reduces angiogenesis and VEGF expression in a mouse model of retinopathy of prematurity. *Invest Ophthalmol Vis Sci.* 2006;47(4):1600-5.
146. Vasudev NS, Reynolds AR. Anti-angiogenic therapy for cancer: current progress, unresolved questions and future directions. *Angiogenesis.* 2014;17(3):471-94.
147. Soldi R, Mitola S, Strasly M, Defilippi P, Tarone G, Bussolino F. Role of alphavbeta3 integrin in the activation of vascular endothelial growth factor receptor-2. *EMBO J.* 1999;18(4):882-92.
148. Masson-Gadais B, Houle F, Laferriere J, Huot J. Integrin alphavbeta3, requirement for VEGFR2-mediated activation of SAPK2/p38 and for Hsp90-dependent phosphorylation of focal adhesion kinase in endothelial cells activated by VEGF. *Cell Stress Chaperones.* 2003;8(1):37-52.
149. Mahabeleshwar GH, Feng W, Phillips DR, Byzova TV. Integrin signaling is critical for pathological angiogenesis. *J Exp Med.* 2006;203(11):2495-507.

150. Mahabeleshwar GH, Feng W, Reddy K, Plow EF, Byzova TV. Mechanisms of integrin-vascular endothelial growth factor receptor cross-activation in angiogenesis. *Circ Res.* 2007;101(6):570-80.
151. Tucci M, Stucci S, Silvestris F. Does cilengitide deserve another chance? *Lancet Oncol.* 2014;15(13):e584-e5.
152. Stupp R, Hegi ME, Gorlia T, Erridge SC, Perry J, Hong YK, et al. Cilengitide combined with standard treatment for patients with newly diagnosed glioblastoma with methylated MGMT promoter (CENTRIC EORTC 26071-22072 study): a multicentre, randomised, open-label, phase 3 trial. *Lancet Oncol.* 2014;15(10):1100-8.
153. Hodivala-Dilke KM, McHugh KP, Tsakiris DA, Rayburn H, Crowley D, Ullman-Cullere M, et al. Beta3-integrin-deficient mice are a model for Glanzmann thrombasthenia showing placental defects and reduced survival. *J Clin Invest.* 1999;103(2):229-38.
154. Reynolds LE, Wyder L, Lively JC, Taverna D, Robinson SD, Huang X, et al. Enhanced pathological angiogenesis in mice lacking beta3 integrin or beta3 and beta5 integrins. *Nat Med.* 2002;8(1):27-34.
155. Reynolds AR, Reynolds LE, Nagel TE, Lively JC, Robinson SD, Hicklin DJ, et al. Elevated Flk1 (vascular endothelial growth factor receptor 2) signaling mediates enhanced angiogenesis in beta3-integrin-deficient mice. *Cancer Res.* 2004;64(23):8643-50.
156. Strieth S, Eichhorn ME, Sutter A, Jonczyk A, Berghaus A, Dellian M. Antiangiogenic combination tumor therapy blocking alpha(v)-integrins and VEGF-receptor-2 increases therapeutic effects in vivo. *Int J Cancer.* 2006;119(2):423-31.
157. Atkinson SJ, Gontarczyk AM, Alghamdi AA, Ellison TS, Johnson RT, Fowler WJ, et al. The beta3-integrin endothelial adhesome regulates microtubule-dependent cell migration. *EMBO Rep.* 2018;19(7).
158. D'Amico G, Robinson SD, Germain M, Reynolds LE, Thomas GJ, Elia G, et al. Endothelial-Rac1 is not required for tumor angiogenesis unless alphavbeta3-integrin is absent. *PLoS One.* 2010;5(3):e9766.
159. Worth DC, Hodivala-Dilke K, Robinson SD, King SJ, Morton PE, Gertler FB, et al. Alpha v beta3 integrin spatially regulates VASP and RIAM to control adhesion dynamics and migration. *J Cell Biol.* 2010;189(2):369-83.
160. Reynolds AR, Hart IR, Watson AR, Welte JC, Silva RG, Robinson SD, et al. Stimulation of tumor growth and angiogenesis by low concentrations of RGD-mimetic integrin inhibitors. *Nat Med.* 2009;15(4):392-400.
161. Steri V, Ellison TS, Gontarczyk AM, Weilbaeher K, Schneider JG, Edwards D, et al. Acute depletion of endothelial beta3-integrin transiently inhibits tumor growth and angiogenesis in mice. *Circ Res.* 2014;114(1):79-91.
162. Somanath PR, Malinin NL, Byzova TV. Cooperation between integrin alphavbeta3 and VEGFR2 in angiogenesis. *Angiogenesis.* 2009;12(2):177-85.
163. Kim S, Bell K, Mousa SA, Varner JA. Regulation of angiogenesis in vivo by ligation of integrin alpha5beta1 with the central cell-binding domain of fibronectin. *Am J Pathol.* 2000;156(4):1345-62.
164. Li L, Liu F, Welser-Alves JV, McCullough LD, Milner R. Upregulation of fibronectin and the alpha5beta1 and alphavbeta3 integrins on blood vessels within the cerebral ischemic penumbra. *Exp Neurol.* 2012;233(1):283-91.
165. Stephens LE, Sutherland AE, Klimanskaya IV, Andrieux A, Meneses J, Pedersen RA, et al. Deletion of beta 1 integrins in mice results in inner cell mass failure and peri-implantation lethality. *Genes Dev.* 1995;9(15):1883-95.
166. Fassler R, Meyer M. Consequences of lack of beta 1 integrin gene expression in mice. *Genes Dev.* 1995;9(15):1896-908.
167. Yang JT, Rayburn H, Hynes RO. Embryonic mesodermal defects in alpha 5 integrin-deficient mice. *Development.* 1993;119(4):1093-105.

168. Francis SE, Goh KL, Hodivala-Dilke K, Bader BL, Stark M, Davidson D, et al. Central roles of alpha5beta1 integrin and fibronectin in vascular development in mouse embryos and embryoid bodies. *Arterioscler Thromb Vasc Biol.* 2002;22(6):927-33.
169. van der Flier A, Badu-Nkansah K, Whittaker CA, Crowley D, Bronson RT, Lacy-Hulbert A, et al. Endothelial alpha5 and alphav integrins cooperate in remodeling of the vasculature during development. *Development.* 2010;137(14):2439-49.
170. Lei L, Liu D, Huang Y, Jovin I, Shai SY, Kyriakides T, et al. Endothelial expression of beta1 integrin is required for embryonic vascular patterning and postnatal vascular remodeling. *Mol Cell Biol.* 2008;28(2):794-802.
171. Stenzel D, Lundkvist A, Sauvaget D, Busse M, Graupera M, van der Flier A, et al. Integrin-dependent and -independent functions of astrocytic fibronectin in retinal angiogenesis. *Development.* 2011;138(20):4451-63.
172. Milner R, Campbell IL. Developmental regulation of beta1 integrins during angiogenesis in the central nervous system. *Mol Cell Neurosci.* 2002;20(4):616-26.
173. Li L, Welser JV, Milner R. Absence of the alpha v beta 3 integrin dictates the time-course of angiogenesis in the hypoxic central nervous system: accelerated endothelial proliferation correlates with compensatory increases in alpha 5 beta 1 integrin expression. *J Cereb Blood Flow Metab.* 2010;30(5):1031-43.
174. Bourdoulous S, Orend G, MacKenna DA, Pasqualini R, Ruoslahti E. Fibronectin matrix regulates activation of RHO and CDC42 GTPases and cell cycle progression. *J Cell Biol.* 1998;143(1):267-76.
175. Li L, Welser-Alves J, van der Flier A, Boroujerdi A, Hynes RO, Milner R. An angiogenic role for the alpha5beta1 integrin in promoting endothelial cell proliferation during cerebral hypoxia. *Exp Neurol.* 2012;237(1):46-54.
176. Murphy PA, Begum S, Hynes RO. Tumor angiogenesis in the absence of fibronectin or its cognate integrin receptors. *PLoS One.* 2015;10(3):e0120872.
177. Takagi S, Kasuya Y, Shimizu M, Matsuura T, Tsuboi M, Kawakami A, et al. Expression of a cell adhesion molecule, neuropilin, in the developing chick nervous system. *Dev Biol.* 1995;170(1):207-22.
178. Murga M, Fernandez-Capetillo O, Tosato G. Neuropilin-1 regulates attachment in human endothelial cells independently of vascular endothelial growth factor receptor-2. *Blood.* 2005;105(5):1992-9.
179. Valdembri D, Caswell PT, Anderson KI, Schwarz JP, Konig I, Astanina E, et al. Neuropilin-1/GIPC1 signaling regulates alpha5beta1 integrin traffic and function in endothelial cells. *PLoS Biol.* 2009;7(1):e25.
180. Fantin A, Herzog B, Mahmoud M, Yamaji M, Plein A, Denti L, et al. Neuropilin 1 (NRP1) hypomorphism combined with defective VEGF-A binding reveals novel roles for NRP1 in developmental and pathological angiogenesis. *Development.* 2014;141(3):556-62.
181. Fantin A, Vieira JM, Plein A, Denti L, Fruttiger M, Pollard JW, et al. NRP1 acts cell autonomously in endothelium to promote tip cell function during sprouting angiogenesis. *Blood.* 2013;121(12):2352-62.
182. Fantin A, Lampropoulou A, Gestri G, Raimondi C, Senatore V, Zachary I, et al. NRP1 Regulates CDC42 Activation to Promote Filopodia Formation in Endothelial Tip Cells. *Cell Rep.* 2015;11(10):1577-90.
183. Raimondi C, Fantin A, Lampropoulou A, Denti L, Chikh A, Ruhrberg C. Imatinib inhibits VEGF-independent angiogenesis by targeting neuropilin 1-dependent ABL1 activation in endothelial cells. *J Exp Med.* 2014;211(6):1167-83.
184. Gonzalez AM, Bhattacharya R, deHart GW, Jones JC. Transdominant regulation of integrin function: mechanisms of crosstalk. *Cell Signal.* 2010;22(4):578-83.
185. Eliceiri BP, Cheresh DA. The role of alphav integrins during angiogenesis: insights into potential mechanisms of action and clinical development. *J Clin Invest.* 1999;103(9):1227-30.

186. Blystone SD, Graham IL, Lindberg FP, Brown EJ. Integrin alpha v beta 3 differentially regulates adhesive and phagocytic functions of the fibronectin receptor alpha 5 beta 1. *J Cell Biol.* 1994;127(4):1129-37.
187. Blystone SD, Lindberg FP, LaFlamme SE, Brown EJ. Integrin beta 3 cytoplasmic tail is necessary and sufficient for regulation of alpha 5 beta 1 phagocytosis by alpha v beta 3 and integrin-associated protein. *J Cell Biol.* 1995;130(3):745-54.
188. Blystone SD, Slater SE, Williams MP, Crow MT, Brown EJ. A molecular mechanism of integrin crosstalk: alphavbeta3 suppression of calcium/calmodulin-dependent protein kinase II regulates alpha5beta1 function. *J Cell Biol.* 1999;145(4):889-97.
189. Simon KO, Nutt EM, Abraham DG, Rodan GA, Duong LT. The alphavbeta3 integrin regulates alpha5beta1-mediated cell migration toward fibronectin. *J Biol Chem.* 1997;272(46):29380-9.
190. Ly DP, Zazzali KM, Corbett SA. De novo expression of the integrin alpha5beta1 regulates alphavbeta3-mediated adhesion and migration on fibrinogen. *J Biol Chem.* 2003;278(24):21878-85.
191. Kim S, Harris M, Varner JA. Regulation of integrin alpha v beta 3-mediated endothelial cell migration and angiogenesis by integrin alpha5beta1 and protein kinase A. *J Biol Chem.* 2000;275(43):33920-8.
192. Kim S, Bakre M, Yin H, Varner JA. Inhibition of endothelial cell survival and angiogenesis by protein kinase A. *J Clin Invest.* 2002;110(7):933-41.
193. Diaz C, Neubauer S, Rechenmacher F, Kessler H, Missirlis D. Recruitment of alpha(nu)beta(3) integrin to alpha(5)beta(1) integrin-induced clusters enables focal adhesion maturation and cell spreading. *J Cell Sci.* 2020;133(1).
194. Robinson SD, Reynolds LE, Kostourou V, Reynolds AR, da Silva RG, Tavora B, et al. Alphav beta3 integrin limits the contribution of neuropilin-1 to vascular endothelial growth factor-induced angiogenesis. *J Biol Chem.* 2009;284(49):33966-81.
195. Ellison TS, Atkinson SJ, Steri V, Kirkup BM, Preedy ME, Johnson RT, et al. Suppression of beta3-integrin in mice triggers a neuropilin-1-dependent change in focal adhesion remodelling that can be targeted to block pathological angiogenesis. *Dis Model Mech.* 2015;8(9):1105-19.
196. Naik A, Al-Yahyaee A, Abdullah N, Sam JE, Al-Zeheimi N, Yaish MW, et al. Neuropilin-1 promotes the oncogenic Tenascin-C/integrin beta3 pathway and modulates chemoresistance in breast cancer cells. *BMC Cancer.* 2018;18(1):533.
197. Fukasawa M, Matsushita A, Korc M. Neuropilin-1 interacts with integrin beta1 and modulates pancreatic cancer cell growth, survival and invasion. *Cancer Biol Ther.* 2007;6(8):1173-80.
198. Fantin A, Schwarz Q, Davidson K, Normando EM, Denti L, Ruhrberg C. The cytoplasmic domain of neuropilin 1 is dispensable for angiogenesis, but promotes the spatial separation of retinal arteries and veins. *Development.* 2011;138(19):4185-91.
199. Claxton S, Kostourou V, Jadeja S, Chambon P, Hodivala-Dilke K, Fruttiger M. Efficient, inducible Cre-recombinase activation in vascular endothelium. *Genesis.* 2008;46(2):74-80.
200. Morgan EA, Schneider JG, Baroni TE, Uluckan O, Heller E, Hurchla MA, et al. Dissection of platelet and myeloid cell defects by conditional targeting of the beta3-integrin subunit. *FASEB J.* 2010;24(4):1117-27.
201. Zudaire E, Gambardella L, Kurcz C, Vermeren S. A computational tool for quantitative analysis of vascular networks. *PLoS One.* 2011;6(11):e27385.
202. Reynolds LE, Hodivala-Dilke KM. Primary mouse endothelial cell culture for assays of angiogenesis. *Methods Mol Med.* 2006;120:503-9.
203. Krilleke D, DeErkenez A, Schubert W, Giri I, Robinson GS, Ng YS, et al. Molecular mapping and functional characterization of the VEGF164 heparin-binding domain. *J Biol Chem.* 2007;282(38):28045-56.

204. Tomayko MM, Reynolds CP. Determination of subcutaneous tumor size in athymic (nude) mice. *Cancer Chemother Pharmacol.* 1989;24(3):148-54.
205. Lord SJ, Velle KB, Mullins RD, Fritz-Laylin LK. SuperPlots: Communicating reproducibility and variability in cell biology. *J Cell Biol.* 2020;219(6).
206. Robinson SD, Hodivala-Dilke KM. The role of beta3-integrins in tumor angiogenesis: context is everything. *Curr Opin Cell Biol.* 2011;23(5):630-7.
207. Gelfand MV, Hagan N, Tata A, Oh WJ, Lacoste B, Kang KT, et al. Neuropilin-1 functions as a VEGFR2 co-receptor to guide developmental angiogenesis independent of ligand binding. *Elife.* 2014;3:e03720.
208. Payne S, De Val S, Neal A. Endothelial-Specific Cre Mouse Models. *Arterioscler Thromb Vasc Biol.* 2018;38(11):2550-61.
209. Yang X, Chitalia SV, Matsuura S, Ravid K. Integrins and their role in megakaryocyte development and function. *Exp Hematol.* 2022;106:31-9.
210. Ohsaka A, Hirota-Komatsu S, Araki M, Komatsu N. Platelet-derived growth factor receptors form complexes with neuropilin-1 during megakaryocytic differentiation of thrombopoietin-dependent UT-7/TPO cells. *Biochem Biophys Res Commun.* 2015;459(3):443-9.
211. Johnson R. Deciphering the Angiogenic Regulatory Network: How endothelial fibronectin receptors interact to regulate vascular formation. : University of East Anglia; 2019.
212. Song AJ, Palmiter RD. Detecting and Avoiding Problems When Using the Cre-lox System. *Trends Genet.* 2018;34(5):333-40.
213. Walz A, Rodriguez I, Mombaerts P. Aberrant sensory innervation of the olfactory bulb in neuropilin-2 mutant mice. *J Neurosci.* 2002;22(10):4025-35.
214. Kim H, Kim M, Im SK, Fang S. Mouse Cre-LoxP system: general principles to determine tissue-specific roles of target genes. *Lab Anim Res.* 2018;34(4):147-59.
215. Semprini S, Troup TJ, Kotelevtseva N, King K, Davis JR, Mullins LJ, et al. Cryptic loxP sites in mammalian genomes: genome-wide distribution and relevance for the efficiency of BAC/PAC recombineering techniques. *Nucleic Acids Res.* 2007;35(5):1402-10.
216. Buerger A, Rozhitskaya O, Sherwood MC, Dorfman AL, Bisping E, Abel ED, et al. Dilated cardiomyopathy resulting from high-level myocardial expression of Cre-recombinase. *J Card Fail.* 2006;12(5):392-8.
217. Jimeno D, Feiner L, Lillo C, Teofilo K, Goldstein LS, Pierce EA, et al. Analysis of kinesin-2 function in photoreceptor cells using synchronous Cre-loxP knockout of Kif3a with RHO-Cre. *Invest Ophthalmol Vis Sci.* 2006;47(11):5039-46.
218. Brash JT, Bolton RL, Rashbrook VS, Denti L, Kubota Y, Ruhrberg C. Tamoxifen-Activated CreERT Impairs Retinal Angiogenesis Independently of Gene Deletion. *Circ Res.* 2020;127(6):849-50.
219. Okabe K, Kobayashi S, Yamada T, Kurihara T, Tai-Nagara I, Miyamoto T, et al. Neurons limit angiogenesis by titrating VEGF in retina. *Cell.* 2014;159(3):584-96.
220. Stahl A, Connor KM, Sapieha P, Chen J, Dennison RJ, Krah NM, et al. The mouse retina as an angiogenesis model. *Invest Ophthalmol Vis Sci.* 2010;51(6):2813-26.
221. Selvam S, Kumar T, Fruttiger M. Retinal vasculature development in health and disease. *Prog Retin Eye Res.* 2018;63:1-19.
222. Taylor J, Benwell CJ, Robinson SD. Using Immortalized Endothelial Cells to Study the Roles of Adhesion Molecules in VEGF-Induced Signaling. *Methods Mol Biol.* 2022;2475:133-41.
223. Alghamdi AAA, Benwell CJ, Atkinson SJ, Lambert J, Johnson RT, Robinson SD. NRP2 as an Emerging Angiogenic Player; Promoting Endothelial Cell Adhesion and Migration by Regulating Recycling of alpha5 Integrin. *Front Cell Dev Biol.* 2020;8:395.
224. Tavora B, Reynolds LE, Batista S, Demircioglu F, Fernandez I, Lechertier T, et al. Endothelial-cell FAK targeting sensitizes tumours to DNA-damaging therapy. *Nature.* 2014;514(7520):112-6.

225. Ni CW, Kumar S, Ankeny CJ, Jo H. Development of immortalized mouse aortic endothelial cell lines. *Vasc Cell*. 2014;6(1):7.
226. Buchanan CF, Verbridge SS, Vlachos PP, Rylander MN. Flow shear stress regulates endothelial barrier function and expression of angiogenic factors in a 3D microfluidic tumor vascular model. *Cell Adh Migr*. 2014;8(5):517-24.
227. Zucchelli E, Majid QA, Foldes G. New artery of knowledge: 3D models of angiogenesis. *Vasc Biol*. 2019;1(1):H135-H43.
228. Benwell C. Neuropilin-2 as a Novel Angiogenic Player: deciphering the contributions of neuropilin-2 during developmental and pathological angiogenesis: University of East Anglia; 2022 30 Jan 2023.
229. Benwell CJ, Taylor J, Robinson SD. Endothelial neuropilin-2 influences angiogenesis by regulating actin pattern development and alpha5-integrin-p-FAK complex recruitment to assembling adhesion sites. *FASEB J*. 2021;35(8):e21679.
230. Karaman S, Paavonsalo S, Heinolainen K, Lackman MH, Ranta A, Hemanthakumar KA, et al. Interplay of vascular endothelial growth factor receptors in organ-specific vessel maintenance. *J Exp Med*. 2022;219(3).
231. Gerhardt H, Ruhrberg C, Abramsson A, Fujisawa H, Shima D, Betsholtz C. Neuropilin-1 is required for endothelial tip cell guidance in the developing central nervous system. *Dev Dyn*. 2004;231(3):503-9.
232. Yoshida T, Gong J, Xu Z, Wei Y, Duh EJ. Inhibition of pathological retinal angiogenesis by the integrin alphavbeta3 antagonist tetraiodothyroacetic acid (tetrac). *Exp Eye Res*. 2012;94(1):41-8.
233. Hammes HP, Brownlee M, Jonczyk A, Sutter A, Preissner KT. Subcutaneous injection of a cyclic peptide antagonist of vitronectin receptor-type integrins inhibits retinal neovascularization. *Nat Med*. 1996;2(5):529-33.
234. Kamizuru H, Kimura H, Yasukawa T, Tabata Y, Honda Y, Ogura Y. Monoclonal antibody-mediated drug targeting to choroidal neovascularization in the rat. *Invest Ophthalmol Vis Sci*. 2001;42(11):2664-72.
235. Jones EA, Yuan L, Breant C, Watts RJ, Eichmann A. Separating genetic and hemodynamic defects in neuropilin 1 knockout embryos. *Development*. 2008;135(14):2479-88.
236. Schwartz MA, Assoian RK. Integrins and cell proliferation: regulation of cyclin-dependent kinases via cytoplasmic signaling pathways. *J Cell Sci*. 2001;114(Pt 14):2553-60.
237. Pan Q, Chanthery Y, Liang WC, Stawicki S, Mak J, Rathore N, et al. Blocking neuropilin-1 function has an additive effect with anti-VEGF to inhibit tumor growth. *Cancer Cell*. 2007;11(1):53-67.
238. Raimondi C, Brash JT, Fantin A, Ruhrberg C. NRP1 function and targeting in neurovascular development and eye disease. *Prog Retin Eye Res*. 2016;52:64-83.
239. Jiang B, Liou GI, Behzadian MA, Caldwell RB. Astrocytes modulate retinal vasculogenesis: effects on fibronectin expression. *J Cell Sci*. 1994;107 (Pt 9):2499-508.
240. Corliss BA, Ray HC, Doty RW, Mathews C, Sheybani N, Fitzgerald K, et al. Pericyte Bridges in Homeostasis and Hyperglycemia. *Diabetes*. 2020;69(7):1503-17.
241. Schaffner F, Ray AM, Dontenwill M. Integrin alpha5beta1, the Fibronectin Receptor, as a Pertinent Therapeutic Target in Solid Tumors. *Cancers (Basel)*. 2013;5(1):27-47.
242. Chen TT, Luque A, Lee S, Anderson SM, Segura T, Iruela-Arispe ML. Anchorage of VEGF to the extracellular matrix conveys differential signaling responses to endothelial cells. *J Cell Biol*. 2010;188(4):595-609.
243. Njah K, Chakraborty S, Qiu B, Arumugam S, Raju A, Pobbati AV, et al. A Role of Agrin in Maintaining the Stability of Vascular Endothelial Growth Factor Receptor-2 during Tumor Angiogenesis. *Cell Rep*. 2019;28(4):949-65 e7.
244. Kwak EA, Pan CC, Ramonett A, Kumar S, Cruz-Flores P, Ahmed T, et al. beta(IV)-spectrin as a stalk cell-intrinsic regulator of VEGF signaling. *Nat Commun*. 2022;13(1):1326.

245. Yamamoto H, Ehling M, Kato K, Kanai K, van Lessen M, Frye M, et al. Integrin beta1 controls VE-cadherin localization and blood vessel stability. *Nat Commun.* 2015;6:6429.
246. He K, Sakai T, Tsukasaki Y, Watanabe TM, Ikebe M. Myosin X is recruited to nascent focal adhesions at the leading edge and induces multi-cycle filopodial elongation. *Sci Rep.* 2017;7(1):13685.
247. Fischer RS, Lam PY, Huttenlocher A, Waterman CM. Filopodia and focal adhesions: An integrated system driving branching morphogenesis in neuronal pathfinding and angiogenesis. *Dev Biol.* 2019;451(1):86-95.
248. Roca-Cusachs P, Gauthier NC, Del Rio A, Sheetz MP. Clustering of alpha(5)beta(1) integrins determines adhesion strength whereas alpha(v)beta(3) and talin enable mechanotransduction. *Proc Natl Acad Sci U S A.* 2009;106(38):16245-50.
249. Lin GL, Cohen DM, Desai RA, Breckenridge MT, Gao L, Humphries MJ, et al. Activation of beta 1 but not beta 3 integrin increases cell traction forces. *FEBS Lett.* 2013;587(6):763-9.
250. Yang JT, Hynes RO. Fibronectin receptor functions in embryonic cells deficient in alpha 5 beta 1 integrin can be replaced by alpha V integrins. *Mol Biol Cell.* 1996;7(11):1737-48.
251. Papusheva E, Mello de Queiroz F, Dalous J, Han Y, Esposito A, Jares-Erijmanxa EA, et al. Dynamic conformational changes in the FERM domain of FAK are involved in focal-adhesion behavior during cell spreading and motility. *J Cell Sci.* 2009;122(Pt 5):656-66.
252. Le Boeuf F, Houle F, Sussman M, Huot J. Phosphorylation of focal adhesion kinase (FAK) on Ser732 is induced by rho-dependent kinase and is essential for proline-rich tyrosine kinase-2-mediated phosphorylation of FAK on Tyr407 in response to vascular endothelial growth factor. *Mol Biol Cell.* 2006;17(8):3508-20.
253. Schaufler V, Czichos-Medda H, Hirschfeld-Warnecken V, Neubauer S, Rechenmacher F, Medda R, et al. Selective binding and lateral clustering of alpha5beta1 and alphavbeta3 integrins: Unraveling the spatial requirements for cell spreading and focal adhesion assembly. *Cell Adh Migr.* 2016;10(5):505-15.
254. Arthur E, Elsner AE, Sapoznik KA, Papay JA, Muller MS, Burns SA. Distances From Capillaries to Arterioles or Venues Measured Using OCTA and AOSLO. *Invest Ophthalmol Vis Sci.* 2019;60(6):1833-44.
255. Yang WJ, Hu J, Uemura A, Tetzlaff F, Augustin HG, Fischer A. Semaphorin-3C signals through Neuropilin-1 and PlexinD1 receptors to inhibit pathological angiogenesis. *EMBO Mol Med.* 2015;7(10):1267-84.
256. Yu W, Bai Y, Han N, Wang F, Zhao M, Huang L, et al. Inhibition of pathological retinal neovascularization by semaphorin 3A. *Mol Vis.* 2013;19:1397-405.
257. Gerhardt H, Golding M, Fruttiger M, Ruhrberg C, Lundkvist A, Abramsson A, et al. VEGF guides angiogenic sprouting utilizing endothelial tip cell filopodia. *J Cell Biol.* 2003;161(6):1163-77.
258. Rocha SF, Schiller M, Jing D, Li H, Butz S, Vestweber D, et al. Esm1 modulates endothelial tip cell behavior and vascular permeability by enhancing VEGF bioavailability. *Circ Res.* 2014;115(6):581-90.
259. Benedito R, Rocha SF, Woeste M, Zamykal M, Radtke F, Casanovas O, et al. Notch-dependent VEGFR3 upregulation allows angiogenesis without VEGF-VEGFR2 signalling. *Nature.* 2012;484(7392):110-4.
260. Zhou W, Li W, Wang S, Salovska B, Hu Z, Tao B, et al. An optogenetic-phosphoproteomic study reveals dynamic Akt1 signaling profiles in endothelial cells. *Nat Commun.* 2023;14(1):3803.
261. Roberts MS, Woods AJ, Dale TC, Van Der Sluijs P, Norman JC. Protein kinase B/Akt acts via glycogen synthase kinase 3 to regulate recycling of alpha v beta 3 and alpha 5 beta 1 integrins. *Mol Cell Biol.* 2004;24(4):1505-15.
262. Jia H, Bagherzadeh A, Hartzoulakis B, Jarvis A, Lohr M, Shaikh S, et al. Characterization of a bicyclic peptide neuropilin-1 (NP-1) antagonist (EG3287) reveals importance of vascular endothelial growth factor exon 8 for NP-1 binding and role of NP-1 in KDR signaling. *J Biol Chem.* 2006;281(19):13493-502.

263. Vanhaesebroeck B, Guillermet-Guibert J, Graupera M, Bilanges B. The emerging mechanisms of isoform-specific PI3K signalling. *Nat Rev Mol Cell Biol.* 2010;11(5):329-41.
264. Eliceiri BP. Integrin and growth factor receptor crosstalk. *Circ Res.* 2001;89(12):1104-10.
265. Watson AR, Pitchford SC, Reynolds LE, Direkze N, Brittan M, Alison MR, et al. Deficiency of bone marrow beta3-integrin enhances non-functional neovascularization. *J Pathol.* 2010;220(4):435-45.
266. Wong PP, Munoz-Felix JM, Hijazi M, Kim H, Robinson SD, De Luxan-Delgado B, et al. Cancer Burden Is Controlled by Mural Cell-beta3-Integrin Regulated Crosstalk with Tumor Cells. *Cell.* 2020;181(6):1346-63 e21.
267. di Blasio L, Droetto S, Norman J, Bussolino F, Primo L. Protein kinase D1 regulates VEGF-A-induced alphavbeta3 integrin trafficking and endothelial cell migration. *Traffic.* 2010;11(8):1107-18.
268. Zhang L, Hu JJ, Gong F. MG132 inhibition of proteasome blocks apoptosis induced by severe DNA damage. *Cell Cycle.* 2011;10(20):3515-8.
269. Zhang L, Tang H, Kou Y, Li R, Zheng Y, Wang Q, et al. MG132-mediated inhibition of the ubiquitin-proteasome pathway ameliorates cancer cachexia. *J Cancer Res Clin Oncol.* 2013;139(7):1105-15.
270. Jin F, Xiao D, Zhao T, Yu M. Proteasome inhibitor MG132 suppresses pancreatic ductal adenocarcinoma-cell migration by increasing ESE3 expression. *Oncol Lett.* 2020;19(1):858-68.
271. Meissner M, Reichenbach G, Stein M, Hrgovic I, Kaufmann R, Gille J. Down-regulation of vascular endothelial growth factor receptor 2 is a major molecular determinant of proteasome inhibitor-mediated antiangiogenic action in endothelial cells. *Cancer Res.* 2009;69(5):1976-84.
272. Khalili P, Arakelian A, Chen G, Plunkett ML, Beck I, Parry GC, et al. A non-RGD-based integrin binding peptide (ATN-161) blocks breast cancer growth and metastasis in vivo. *Mol Cancer Ther.* 2006;5(9):2271-80.
273. Anderson JM, Li J, Springer TA. Regulation of integrin alpha5beta1 conformational states and intrinsic affinities by metal ions and the ADMIDAS. *Mol Biol Cell.* 2022;33(6):ar56.
274. Saman H, Raza SS, Uddin S, Rasul K. Inducing Angiogenesis, a Key Step in Cancer Vascularization, and Treatment Approaches. *Cancers (Basel).* 2020;12(5).
275. Gu Y, Dong B, He X, Qiu Z, Zhang J, Zhang M, et al. The challenges and opportunities of alphavbeta3-based therapeutics in cancer: From bench to clinical trials. *Pharmacol Res.* 2023;189:106694.
276. Mason WP. End of the road: confounding results of the CORE trial terminate the arduous journey of cilengitide for glioblastoma. *Neuro Oncol.* 2015;17(5):634-5.
277. Goh KL, Yang JT, Hynes RO. Mesodermal defects and cranial neural crest apoptosis in alpha5 integrin-null embryos. *Development.* 1997;124(21):4309-19.
278. Robinson SD, Reynolds LE, Wyder L, Hicklin DJ, Hodivala-Dilke KM. Beta3-integrin regulates vascular endothelial growth factor-A-dependent permeability. *Arterioscler Thromb Vasc Biol.* 2004;24(11):2108-14.
279. Silva RLE, Kanan Y, Mirando AC, Kim J, Shmueli RB, Lorenc VE, et al. Tyrosine kinase blocking collagen IV-derived peptide suppresses ocular neovascularization and vascular leakage. *Sci Transl Med.* 2017;9(373).
280. Fruttiger M. Development of the mouse retinal vasculature: angiogenesis versus vasculogenesis. *Invest Ophthalmol Vis Sci.* 2002;43(2):522-7.
281. Ruhrberg C, Bautch VL. Neurovascular development and links to disease. *Cell Mol Life Sci.* 2013;70(10):1675-84.
282. Murata T, Ishibashi T, Inomata H. Immunohistochemical detection of extravasated fibrinogen (fibrin) in human diabetic retina. *Graefes Arch Clin Exp Ophthalmol.* 1992;230(5):428-31.